Order Number 9029910

Diagenesis and related petrophysical characteristics of Ellenburger Group carbonates (Lower Ordovician), West Texas and southeastern New Mexico

Amthor, Joachim Emil, Ph.D.

City University of New York, 1990

U·M·I
300 N. Zeeb Rd.
Ann Arbor, MI 48106

DIAGENESIS AND RELATED PETROPHYSICAL CHARACTERISTICS OF ELLENBURGER GROUP CARBONATES (LOWER ORDOVICIAN), WEST TEXAS AND SOUTHEASTERN NEW MEXICO.

by

JOACHIM E. AMTHOR

A dissertation submitted to the Graduate Faculty in Earth and Environmental Sciences in partial fulfillment of the requirements for the degree of Doctor of Philosophy, The City University of New York.

1990

This manuscript has been read and accepted for the Graduate Faculty in Earth and Environmental Sciences in satisfaction of the dissertation requirement for the degree of Doctor of Philosophy.

4/24/90

Date

Prof. Gerald M. Friedman
Chair of Examining Committee

4/24/90

Date

Prof. Daniel Habib
Executive Officer

Prof. Somdev Bhattacharji

Dr. Robert G. Loucks

Prof. David Thurber

Supervisory Committee

THE CITY UNIVERSITY OF NEW YORK

ABSTRACT

DIAGENESIS AND RELATED PETROPHYSICAL CHARACTERISTICS OF ELLENBURGER GROUP CARBONATES (LOWER ORDOVICIAN), WEST TEXAS AND SOUTHEASTERN NEW MEXICO.

by

Joachim E. Amthor

Advisor: Professor Gerald M. Friedman

The distribution of major rock types and lithofacies in Ellenburger Group (Lower Ordovician) carbonate rocks from the deep subsurface (1.5 to 6.4 km) of West Texas and southeastern New Mexico indicate deposition as epicontinental platform carbonates, ranging from mixed clastic-carbonate deposits during an early marine phase to shallow subtidal to supratidal deposits during late stages of Ellenburger deposition.

Petrographic studies and X-ray analyses indicate that 90% of the studied samples were pervasively dolomitized. Seven dolomite- rock textures have been recognized and classified according to crystal-size distribution (unimodal or polymodal) and crystal- boundary shape (planar or nonplanar). Paragenetic relationships of the dolomite-rock textures indicate that Ellenburger carbonate rocks were subjected to a complex diagenetic history ranging from early shallow-subtidal dolomitization to late-diagenetic deep-burial dolomitization.

Electron-microprobe analyses of the dolomite-rock textures reveal characteristic differences in the distribution of major and minor elements. There was an increasing incorporation of iron and manganese into the lattice during progressive dolomitization. The geochemistry of the dolomite-rock textures correlates with the petrography: different dolomite-rock textures are also geochemically distinct.

Ellenburger dolostones were strongly modified during the post- Ellenburger unconformity by karst - related brecciation. Breccia types and associated deposits indicate a

karst-related origin for most of the brecciation and fracturing observed in the Ellenburger cores. Karstification and dolomitization are closely related. Porosity and permeability pathways created by karst dissolution seem to have been of prime importance for the distribution of different dolomite types.

The integration of petrographic and geochemical data with petrophysical measurements obtained by high-pressure mercury porosimetry leads to recognition of nature and extent of micro-scale heterogeneity within the complex Ellenburger reservoir rocks. Dolomitization, leaching, and secondary porosity development are intimately associated in the Ellenburger carbonates.

Examination of various petrophysical parameters such as recovery efficiency, permeability, porosity, pore-throat size, and surface area reveal no simple relationships. Rocks of the karst lithofacies were modified more strongly during diagenesis than were rocks from the mottled dolomudstone/wackestone and the peloid - ooid - intraclast dolopackstone/ grainstone lithofacies. Rocks from the latter lithofacies are characterized by petrophysical parameters which indicate that these rocks are good candidates for enhanced-oil recovery projects.

Using petrophysical parameters such as median throat-size, pore-throat size at 20% Hg-saturation, normalized pore-throat size, effective porosity, and minimum recovery efficiency, the petrophysical characteristics of the karst facies were examined. The results reflect the highly variable processes and diagenetic modifications that generated this facies, resulting in its heterogeneous nature.

To my wife Eva.

ACKNOWLEDGEMENTS

I wish to acknowledge and thank my supervisor, Professor Gerald M. Friedman, for his support throughout this study. My thanks are extended to the members of the thesis committee: Prof. Somdev Bhattacharji, Brooklyn College, Dr. Robert G. Loucks, ARCO Oil and Gas Company, and Prof. David Thurber, Queens College. Their help and guidance is greatly appreciated.

Many thanks also to the following people who contributed their expertise and time to this undertaking: David Kopaska - Merkel for his help in the porosimeter lab and helpful reviews of this part of the study, Dave Wark (RPI) for instruction on the microprobe, Ashraf Wali for his assistance in the darkroom, and Charlotte Schreiber for her advice and moral support.

Thanks to students and faculty of the City University who made this time a wonderful experience: Prof. J. Chamberlain, Jr., Prof. D. Habib, Lillian Hess, Peter Hofmann, Ali Kaya, Prof. A. Ludman, Prof. C. Nehru , Prof. A. Ohan, Guy Reed, Golam Sarwar, Prof. B.C. Schreiber, Prof. E. Schreiber, and Ashraf Wali.

Financial support was provided by the following sources: Department of Energy (# DOE DE FG 02-85 ER 1322) to Prof. Gerald M. Friedman, German Academic Exchange Service (DAAD), Germanistic Society of America and International Institute of Education, ARCO Fellowships Funds, City University of New York Graduate School, and Brooklyn College. My sincere thanks for this support. Thanks are extended to Shell Oil Company for providing the core material, and to the Northeastern Science Foundation and its treasurer Sue T. Friedman for funds and support.

I would like to say thank you to my wife Eva. Her love, and her patience and understanding during the long and difficult months of seperation made this effort possible.

After spending more than three years in the United States I am more than ever grateful to my family for their love, and the good education I did receive.

TABLE OF CONTENTS

LIST OF TABLES

LIST OF ILLUSTRATIONS

INTRODUCTION

The Lower Ordovician Ellenburger Group, a sequence of extensive shallow-water platform carbonates, contains numerous prolific hydrocarbon reservoirs with a cumulative production of 3.58 Bbbl of oil equivalent through 1987 (Kerans et al., 1989).

Most recent studies stressed the relative importance of karstification and tectonic-induced fracturing for porosity development in the Ellenburger, which is commonly referred to as "fractured dolomite" (Galloway et al., 1983). Ijirigho and Schreiber (1986, 1988) ascribed at least 95% of fractures, which contribute to production, to a tectonic origin, with as much as four tectonic epochs recognizable in some wells. Other workers (e.g. Lucia, 1968, 1970, 1988; Loucks and Anderson, 1980, 1985; Tobin, 1985; Kerans, 1988 a,b) strongly favored a karst-related origin for these post- depositional features, with tectonic-induced fracturing and brecciation to be of local importance. Relatively little work, however, has been done on the role of dolomitization in the generation of secondary porosity in the Ellenburger dolomite (e.g. Folk, 1959; Loucks and Anderson, 1980, 1985; Lee and Friedman, 1987, 1988; Kupecz and Kerans, 1987; Kupecz et al., 1988; Kupecz, 1989). There is especially a dearth of detailed petrographic, geochemical and petrophysical studies on Ellenburger dolomites from the deep Tobosa Basin (present-day Delaware and Val Verde Basins).

Ellenburger reservoirs from the deep Tobosa Basin account for 61% of total Ellenburger hydrocarbon, or 2.2 Bbbl oil equivalent (Kerans et al. 1989). Despite their importance these deep reservoirs received relatively little attention. Recent discoveries of deep gas in the Arbuckle Group of the Arkoma Basin of Oklahoma, an age equivalent to the Ellenburger in West Texas, have generated new interest in these deep reservoirs.

PURPOSE

The purpose of this study is to provide detailed petrographic, geochemical and petrophysical information on Ellenburger carbonate rocks from the deep subsurface of the Permian Basin. This approach includes a discussion of the origin of Ellenburger dolomites, and the integration and synthesis of petrographic and geochemical data with petrophysical measurements to gain a better understanding of the importance of geologic heterogeneity within these complex reservoir rocks.

MATERIALS AND ANALYTICAL METHODS

MATERIALS

Samples from five different wells from the Lower Ordovician Ellenburger Group in the deep Permian basin of West Texas and southern New Mexico were examined for this study (Figure 1) (Table 1). The wells extend from Lea County, southeastern New Mexico, to Edwards County, southeast Texas. Wells 1 to 4 are located in the Delaware Basin, well 5 in the Val Verde Basin. Well 4, J.E. Phillips Puckett No. 1, is situated at the transition of Delaware Basin to the Val Verde Basin. The wells represent present-day burial depths, ranging from 5,000 ft to more than 22,000 ft (1,500 to 6,700 m) and different paleogeographic positions.

Cored intervals of Ellenburger strata were logged and samples for petrographic and geochemical analysis were taken from core slabs. In addition to the slabbed cores and polished core slabs, 270 polished thin sections have been examined using a petrographic microscope. Selected thin sections have been studied under the luminoscope and, for chemical spot analysis, using an electron microprobe.

For petrophysical analysis closely spaced (1-3 ft)(.3-1 m) core plugs have been collected. Thin sections and core plugs were taken as closely spaced as possible, usually not more then a foot apart.

ANALYTICAL METHODS

Petrography

Thin sections were prepared from samples collected at 1-5 feet intervals from the five cores. Standard carbonate staining methods were employed for the identification of calcite and dolomite, and to test for the presence of Fe^{2+} ions (Friedman, 1959). Twohundredseventy polished thin sections were studied using a Leitz Wetzlar Ortholux microscope, equipped with a Leitz Orthomat automatic camera system for high-resolution photography.

Cathodoluminescence

Cathodoluminescent properties of selected polished thin sections were examined using a Nuclide Luminoscope, Model ELM-2. Operating conditions for cathodoluminescence petrography and photography were a beam voltage of 12 to 15 kV and a beam current of .4 to .6 mA in a 40 - 60 mtorr vacuum under an air atmosphere.

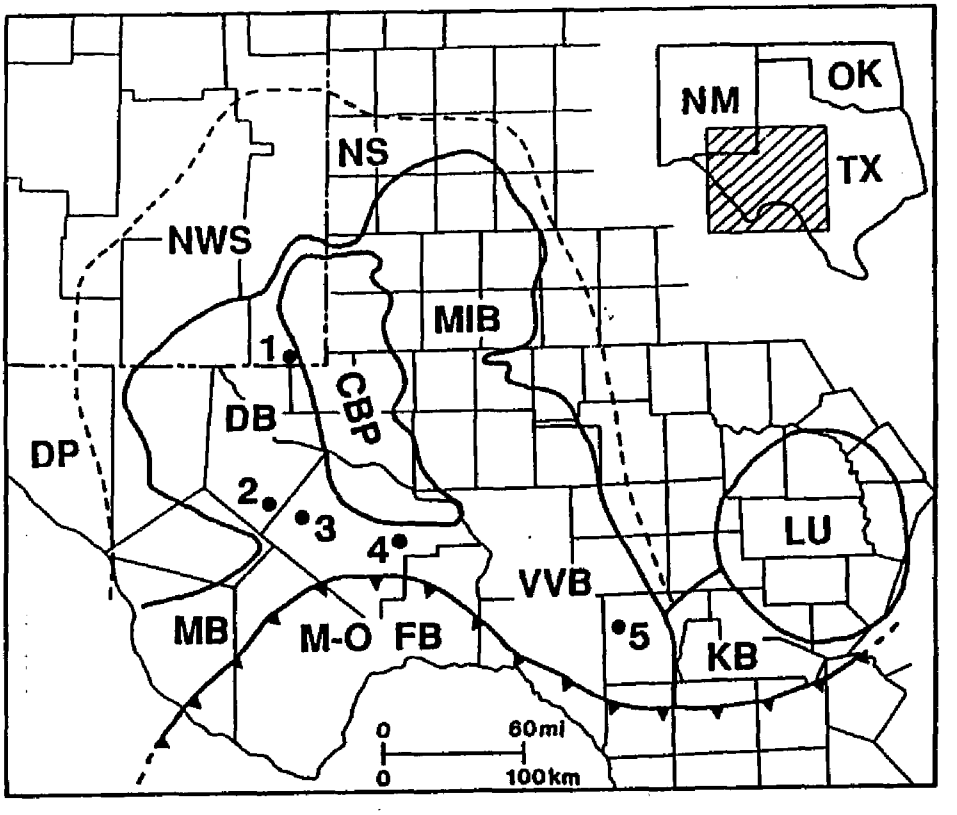

Figure 1. -- Location map showing major geological divisions of the Permian Basin of West Texas and southeastern New Mexico; position of Paleozoic Tobosa Basin is shown by dashed line. Numbers relate to approximate location of wells from which core samples were studied, with depth ranges in parentheses: 1 = Continental State #1, Lea County, NM (12,060 - 12,161 ft, 3,676 - 3,707 m). 2 = Terrill State Unit #1, Reeves County, TX (20,929 - 21,280 ft, 6,379 - 6,386 m). 3 = M.C. Mendel "A", Pecos County, TX (22,607 - 22,636 ft, 6,891 - 6,951 m). 4 = Phillips Puckett No. 1, Pecos County, TX, (13,311 - 14,848 ft, 4,057 - 4,526 m). 5 = J.E. Phillips #1, Edwards County, TX, (5,104 - 5,306 ft, 1,556 - 1,617 m).

DB = Delaware Basin; MIB = Midland Basin; VVB = Val Verde Basin; MB = Marfa Basin; KB = Kerr Basin; CBP = Central Basin Platform; M-O FB = Marathon-Ouachita Fold Belt; LU = Llano Uplift; NWS = Northwestern Shelf; NS = Northern Shelf; ES = Eastern Shelf.

Table 1: Data on Cores and Samples Studied.

Well 1: Continental State #1 Field : State Line Ellenburger
County: Lea, NM Company: Standard Oil Company of Texas
Location: 660' FNL, 1980'FEL; Sec. 5; Twp. 24-S; Rge 38-E
Cored interval studied: 12060 - 12072 ft (3676 - 3680 m)
12076 - 12112 ft (3681 - 3692 m)
12119 - 12161 ft (3694 - 3707 m)

Well 2: Terrill State Unit #1 Field : Wildcat
County: Reeves, TX Company: Sun Oil Company
Location: Sec. 272, BLK. 13; 1960' FSL, 660 FEL
Cored interval studied: 20929 - 20953 ft (6379 - 6386 m)
21142 - 21216 ft (6444 - 6467 m)
21218 - 21280 ft (6467 - 6486 m)

Well 3: M.C. Mendel "A", #1 Field : Wildcat (Ellenburger)
County: Pecos, TX Company: Forest Oil Company
Location: 1980' from N & WL; Sec. 11, BLK 49; TWP 9
Cored interval studied: 22607 - 22636 ft (6891 - 6900 m)
22698 - 22725 ft (6918 - 6927 m)
22800 - 22805 ft (6949 - 6951 m)

Well 4: Puckett No. 1 Field : Puckett
County: Pecos, TX Company: Phillips Petroleum Company
Location: 660' FSL 660' FEL Sec. 42; BLK 101 TC
Cored interval studied: 13311 ft (4057 m)
13376 - 13391 ft (4077 - 4082 m)
13480 ft (4109 m)
13487 - 13490 ft (4111 - 4112 m)
14532 - 14540 ft (4429 - 4432 m)
14590 - 14600 ft (4447 - 4450 m)
14833 ft (4521 m)
14846 - 14848 ft (4525 - 4526 m)

Well 5: J.E. Phillips #1 Field : Wildcat
County: Edwards Company: The Texas Company
Location: 660' S & W lns. of T.C. RR Co.; Sur. #4, A-2647
Cored interval studied: 5104 - 5148 ft (1556 - 1569 m)
5179 - 5215 ft (1579 - 1590 m)
5220 - 5306 ft (1591 - 1617 m)

X-Ray Diffraction

A Phillips x-ray diffractometer with Cu K-alpha radiation was used for qualitative and semi-quantitative analysis of carbonate samples. Finely ground powders were sieved through a 62 micron mesh and packed into a sample holder and examined for their dolomite concentration using Cu K-alpha radiation at 40 kV and 20 mA. The relative proportion of calcite to dolomite in individual samples was determined by taking the ratio of the heights of the (104) calcite peak and the (104) dolomite peak, where % Dol = [Dol/(Cal+Dol)] (Royse et al., 1971; Sperber et al., 1984).

Electron Microprobe

Polished thin sections were analyzed using a fully automated JEOL 733 electron microprobe, equipped with 5 wavelength dispersive spectrometers with 2 analyzing crystals each, backscattered electron detectors and energy dispersive X-ray analysis capabilities. Operating conditions for the microprobe were 15 kV accelerating voltage, 25 nA beam current, approximately 10 micron beam diameter and maximum counting times of 60 seconds. Spots were analyzed for Ca, Mg, Fe, Mn, and Sr, employing Bence-Albee corrections (Bence and Albee, 1968; Albee and Ray, 1970) and using standards provided by the Smithsonian Institute (Jarosewich & Macintyre, 1983) and by the Harvard Museum. Detections limits for Fe, Mn, and Sr were 0.03, 0.03, and 0.02 weight-percent respectively, with a 97% confidence level.

Capillary-Pressure Analysis

A study of petrophysical characteristics was made using standard cylindrical core plugs. These are 13 mm in diameter and 10-25 mm in height, drilled from core slabs using a drill press and diamond bit. Samples were taken at intervals ranging from 1 to 10 ft (.3 to 3 m), averaging 3 feet (1 m), and spaced to ensure coverage of all lithologies and facies.

The core plugs were soaked for 48 hours in a 50/50 solution of toluene and acetone, followed by 24 hours in a 60° C oven. Particularly dirty samples were soaked for additional 24 hours in fresh acetone before drying.

Rock samples were analyzed for capillary-pressure data in Micromeritics Pore Sizer 9305. Equipped with two low-pressure ports and one high-pressure port the pore sizer allows pore throats to 0.006 microns to be measured.

Samples were evacuated to a pressure of 10 to 20 microns of mercury, the sample chamber filled with mercury, and then pressurized incrementally, allowing equilibration at each

increment. With each increment of pressure smaller pore throats became available to mercury invasion. Ellenburger rock samples were pressurized to 15,000 PSIA (Hg-air). The imbibition (withdrawal or extrusion) curve was obtained by releasing pressure incrementally and taking readings at successively lower pressures. Thus, intrusion curves covered a pressure range of 1.5 to 15,000 PSIA (Hg-air), whereas extrusion curves covered the range from 15,000 to 14 PSIA (Hg-air).

The results of capillary-pressure analyses were displayed as graphs of capillary pressure versus cumulative mercury intrusion or throat size. The plots were made using the BASIC program RUN9305.BAS supplied by the Micromeritics Corporation.

Detailed experimental procedures had been outlined in Micromeritics Manual (1983), Kopaska-Merkel et al., (1987), and Kopaska-Merkel and Amthor (1988).

Geophysical Wireline-Logs

Geophysical well-logs available for this study included sonic, gamma-ray, resistivity, spontaneous potential and density logs in various combinations. These logs were used to correlate the different wells, and log-derived geophysical data were keyed to the data obtained by capillary-pressure analysis, petrographic and geochemical analysis.

GEOLOGIC AND STRATIGRAPHIC SETTING

PREVIOUS WORK

Earliest investigations on the Ellenburger date back to 1912, when Plage (1912) first studied "Ellenburger Limestone". The name is derived from outcrops of dolomite and limestones in the Ellenburger Hills of southeastern San Saba region, Texas.

Cloud and Barnes (1948) measured outcrops of Ellenburger and equivalent rocks in Central Texas and the Franklin Mountains of West Texas and defined intervals , units and subunits. Lower Ordovician rocks of the Franklin Mountains belong to the El Paso Group and represent the outcropping equivalents to the Ellenburger Group, which are rocks of Lower Ordovician age in the subsurface of West Texas and southeastern New Mexico.

The general stratigraphy of the Ellenburger rocks is discussed by Cloud and Barnes (1948, p. 30-35) and Barnes et al. (1959). In outcrops in Central Texas, the Ellenburger Group consists of interbedded limestones and dolostones, in the subsurface mostly of dolostones. Barnes et al. (1959) used a number of physical, chemical and palaeontologic approaches to correlate pre-Simpson (that is upper Cambrian and Lower Ordovician) rocks in outcrops with units in the subsurface. Their two-volume summary report gives a detailed account of the difficulties involved in regional correlation of subsurface Ellenburger data. The studies by Cloud and Barnes (1948) and Barnes et al. (1959) form still much of the sources for stratigraphic and (generally meager) biostratigraphic data on Ellenburger subsurface rocks.

Subsequent published studies on the Ellenburger focused mainly on its role as a major oil and gas producer in the Permian Basin of West Texas (e.g. Kvenvolden and Squires, 1967; Neustaedter, 1968; Holmquist, 1965; Smith, 1979).

Facies and depositional studies were covered in papers by Lucia (1968, 1970) and Toomey (1970). They studied outcropping Ellenburger equivalents in the El Paso Group of West Texas and southeastern New Mexico , recognizing several periods of subaerial exposure during deposition of Ellenburger equivalents as indicated by numerous zones of solution and solution-collapse breccias. Loucks and Anderson (1980, 1985), studying cores from the Puckett Field, Pecos County, inferred deposition of the Ellenburger in an alluvial fan/sabkha environment (Lower Ellenburger) and a subtidal to supratidal environment (Middle to Upper Ellenburger). They also recognized subaerial exposure periods, indicated by zones of solution-collapse breccias and paleosoils.

Ijirigho (1981) discussed nature and cause of secondary porosity within Ellenburger rocks

from the Delaware and Val Verde basins. He concluded that the development of excellent secondary porosity occurred during Late Pennsylvanian to Early Permian times, a period, which also represents the most mobile stage for hydrocarbon migration into already existing reservoirs. In a later study, Ijirigho (1985) presented geochemical analyses that showed that the Ellenburger is capable of generating its own hydrocarbons.

Recent studies stressed the relative importance of dolomitization, karstification, and tectonic-induced fracturing for porosity development in the Ellenburger, which is commonly referred to as "fractured dolomite" (Galloway et al., 1983). Ijirigho and Schreiber (1986, 1988) ascribed at least 95% of fractures, which contribute to production, to a tectonic origin, with as much as four tectonic epochs recognizable in some wells. Other workers (e.g. Lucia, 1968, 1970, 1988; Tobin, 1985; Kerans, 1988 a,b) strongly favored a karst-related origin for these post- depositional features, with tectonic-induced fracturing and brecciation to be of local importance. Episodic subaerial exposure and karstification, which created vuggy, cavern, solution-channel, moldic, breccia and fracture porosity are thought to be responsible for reservoir compartmentalization within the Ellenburger (Tobin, 1985, Kerans, 1988).

The role of dolomitization in the generation of secondary porosity in the Ellenburger dolomite has been discussed by Lee and Friedman (1987) and Kupecz and Kerans (1987).

Previous discussions of dolomitization of Ellenburger carbonates focused on the role of burial in the formation of dolomites. Lee and Friedman (1987, 1988) concluded that Ellenburger dolomites are of deep-burial origin, where as Kupecz et al., (1988) argued, that burial depth was not the dominant factor controlling the formation of late-stage dolomite. Alternative mechanisms, such as the availability of conduits to transport warm reactive fluids, may better explain the distribution of the various kinds of dolomites in the Ellenburger rocks.

In a recent study, Kupecz (1989) subdivided dolomites within the Ellenburger into two groups: early-stage (pre-Middle Ordovician) replacement dolomites, and late-stage (post-Lower Ordovician) replacement dolomites and cements. Early-stage dolomites comprise the most extensive and volumetrically abundant type, replacing originally mud-supported facies. They are interpreted as a stabilization phase of an even earlier dolomite generation (Kupecz, 1989). Late-stage dolomite is comprised of a "precursor", and three major generations, with the volumetrically most abundant type replacing the grainstone facies. The paragenetic sequence established by Kupecz (1989) indicates a complex history for Ellenburger dolomites, ranging from early-diagenetic to late-stage dolomitization.

A research seminar was held on May 17, 1989 by the PBS-SEPM, which was devoted to Lower Paleozoic rocks of West Texas and southern New Mexico (Cunningham and Cromwell, 1989). Ten papers given at the conference dealt with Ellenburger and El Paso Group

stratigraphy, diagenesis, reservoir heterogeneity and hydrocarbon accumulation. Clemons (1989) discussed the Ellenburger - El Paso connection. He described the sedimentology and petrography of El Paso members and emphasized the lithostratigraphic correlation of the El Paso Group (?formation) with the Ellenburger. Kerans and Lucia (1989) introduced second, third and fourth/fifth order scales of cyclicity in the El Paso Group and their relation to genesis and architecture of Ellenburger reservoirs. They were also able to correlate third-order cycles in the El Paso Group with third-order relative sea-level cycles from the Appalachians, suggesting a eustatic driving mechanism for the third-order cycles. Amthor and Friedman (1989 b) presented petrographic and geochemical evidence for multistage dolomitization in Ellenburger carbonates. They defined seven dolomite-rock textures, which are also distinct geochemically. Mazzullo (1989) evaluated the procedure and reliability of subdividing the Ellenburger in the subsurface of the Midland basin on the basis of lithology and insoluble residue. Three formations and various zones of regional mappable distribution can be distinguished. Amthor and Friedman (1989 c) illustrated how petrophysical data obtained from capillary-pressure analysis can help in understanding vertical heterogeneity within Ellenburger karst facies. Depositional setting and porosity development of the Ellenburger in the Langley Field, Lea County, New Mexico, were described by Verseput (1989). He recognized four lithofacies characteristic of deposition in a supratidal/intertidal environment. How structural evolution is related to secondary porosity development, hydrocarbon formation and migration in the Ellenburger Group was shown by Ijirigho (1989), using the Coyanosa and Brown-Bassett fields as case histories. Mear (1989) discussed Ellenburger reservoir development at Midland Farms and Inez Fields, Andrews County, Texas, and explained why the reservoirs contain effective porosity not accurately measurable by electric logs. Kerans, Holtz and Tyler (1989) introduced three distinct groups of Ellenburger reservoirs and associated production characteristics (Group A to C reservoirs).

STRATIGRAPHY

The general stratigraphy of the Lower Ordovician Ellenburger Group is discussed by Dake and Bridge (1932), Cloud and Barnes (1948, p. 30-35), and Barnes et al. (1959, p. 34-42), and Barnes and Bell (1977).

Cloud and Barnes (1948) elevated the Ellenburger to Group status and divided it, in ascending order, into Tanyard, Gorman, Honeycut Formations and post Honeycut beds (Figures 2, 3). This subdivision was based on outcrop studies of Ellenburger type sections in Central Texas (Llano region). The Tanyard formation consists of a thinner lower member, the Threadgill (average 243 ft), and a thicker upper member, the Staendebach (average 359 ft). Each member is composed of interbedded limestones and dolostones, with dolostones dominating in the subsurface. The Gorman formation of the Llano region averages 463 ft in thickness and is a "mostly microgranular and very fine-grained dolomite" (Barnes et al., 1959). Grain-size is the chief criterion of distinguishing the Gorman from the underlying Tanyard formation. The Honeycut formation, 679 ft thick in its type section, consists either of interbedded limestones and dolostones or of dolostones. Cloud and Barnes (1948) and Barnes et al. (1959) recognized that the Honeycut and part of the Gorman formation are truncated by an unconformity. To the east post-Honeycut beds are present which have been designated unit B2a, B2b, and C by Cloud and Barnes (1948) for outcropping strata in the Beach and Franklin Mountains, equivalent units in the subsurface have been designated with a prime mark (e.g. B2a').

Barnes et al., (1959), in a continuation of the work on the Ellenburger in Central Texas, studied Ellenburger and equivalent rocks in the subsurface of Texas and southeast New Mexico. Their report gives a summary of the difficulties associated with the regional correlation of Ellenburger type sections with equivalent strata in the subsurface and in outcrops in West Texas, and these difficulties still exist today. In several studies attempts have been made to subdivide the Ellenburger Group in the subsurface and on outcrops into various zones on the basis of insoluble residue in order to facilitate regional correlation (e.g. Hendricks, 1940, 1952; Cole, 1942; Crowley and Hendricks, 1945; Barnes and Dixon, 1959; Umphress, 1977; Mazzullo, 1989).

Ellenburger carbonate rocks are continuous to the west with the El Paso Group. The lithostratigraphic and biostratigraphic correlation of El Paso and Ellenburger strata are discussed by several workers (e.g. Cloud and Barnes, 1948; Barnes et al., 1959; Toomey, 1970; Clemons, 1989) (Figures 3, 4).

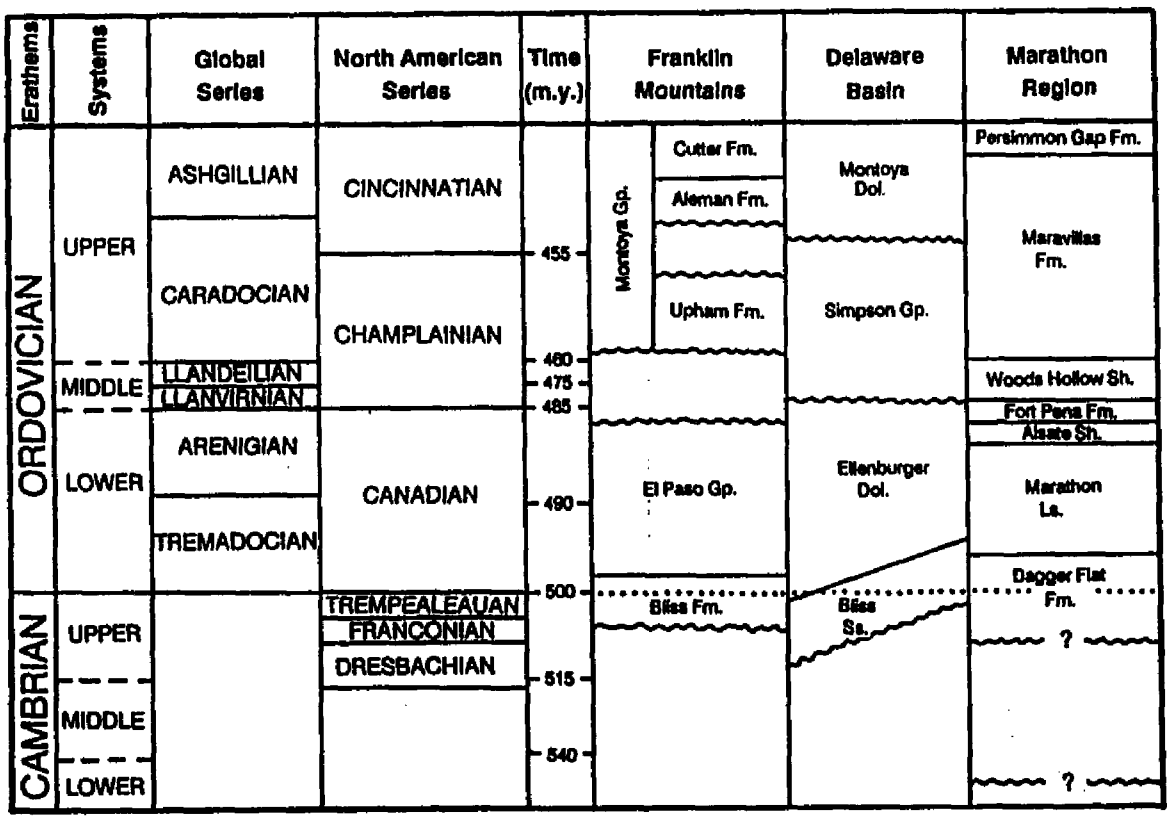

Figure 2. - - Stratigraphic correlation chart of Lower Ordovician strata in Texas, showing the Ellenburger Dolomite and the age-equivalent El Paso Group (Franklin Mountains), and Marathon Limestone (Marathon Region). (From COSUNA, 1983).

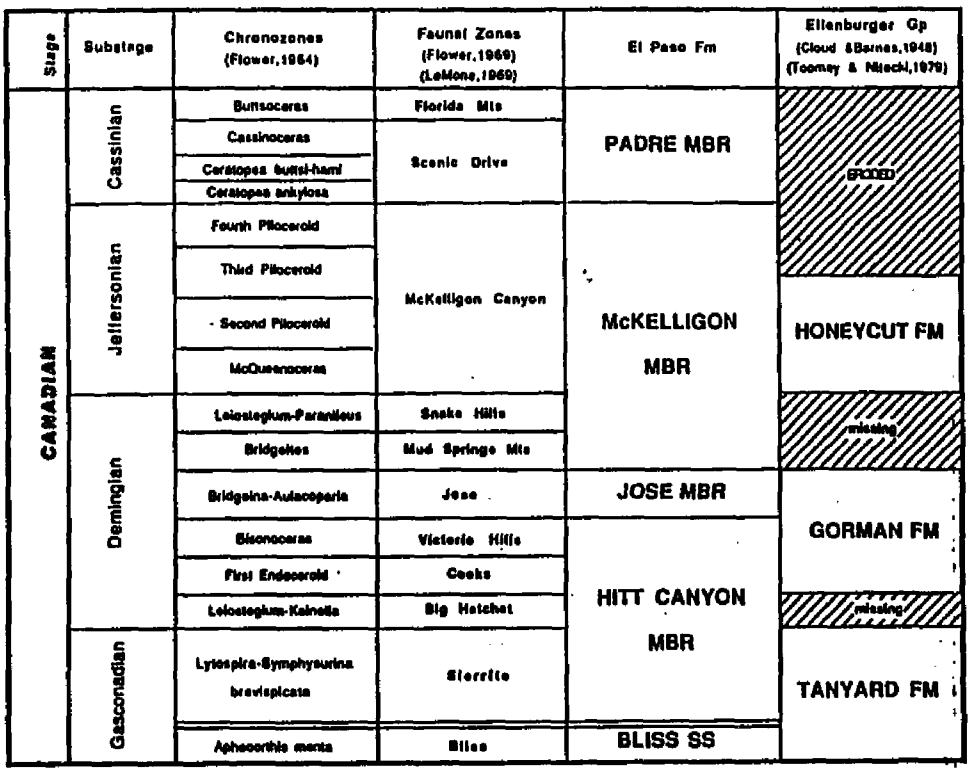

Figure 3. - - Biostratigraphic correlation chart of the exposed El Paso Formation, and the subsurface Ellenburger Group. (From Clemons, 1989; see there for references).

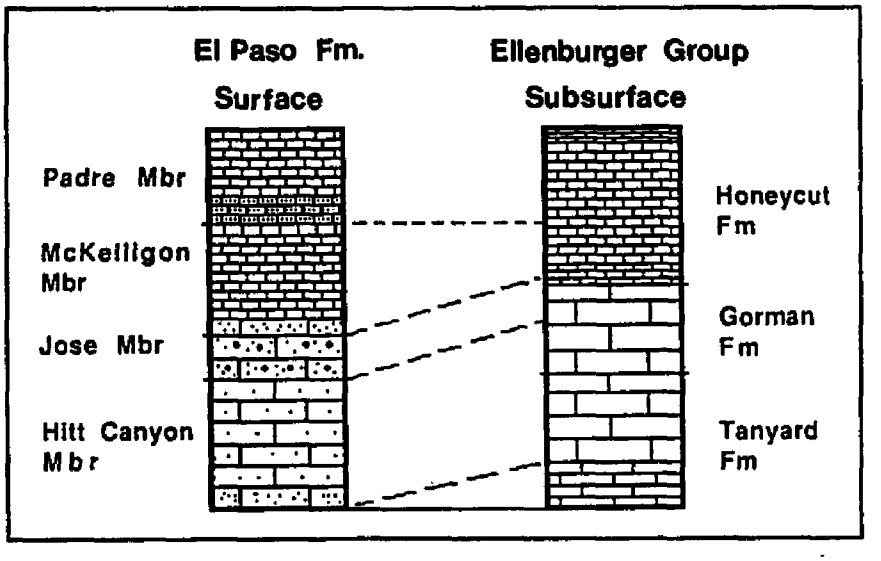

Figure 4. - - Lithostratigraphic correlation of the exposed El Paso Formation and the subsurface Ellenburger Group. (From Clemons, 1989).

In the study area Ellenburger rocks overlay conformably Cambrian rocks (Bliss sandstone), are unconformably overlain by the Middle Ordovician Simpson Group limestones and shales (Figure 2) (Barnes et al., 1959), and reach a thickness of 500-1600 ft (150-490 m). Wells in West Texas which have penetrated the Ellenburger indicate the section to be primarily dolostones. The thickest sequence of pre-Simpson Paleozoic rocks in the subsurface of West Texas has been encountered in the Puckett Field, Pecos County. The Phillips Petroleum Company No. 1 Glenna and No. 1 Puckett wells provide 1700 feet (520 m) of cored section from the Precambrian basement to the top of the Ellenburger (Barnes et al., 1959; Loucks & Anderson, 1980, 1985). In this section the Ellenburger attains a thickness of 1600 feet (490 m). Loucks & Anderson (1980, 1985) subdivided the Ellenburger in the Puckett Field area into a lower, middle and upper Ellenburger, based on predominant facies types. This subdivision does not correlate with the lithostratigraphic nomenclature established by Cloud and Barnes (1948), and Barnes et al. (1959).

It should be emphasized, that considerable differences exist in stratigraphic terminology and interpretation between workers (e.g. Cunningham and Cromwell, 1989). For example, is the El Paso lithostratigraphic unit a formation or a group? Similar problems exist for the Ellenburger, where the subdivision into three formations, as established by Cloud and Barnes (1948), was based largely on differences in grain size, sand content and color. These criteria are not very reliable in defining formations in the pervasively dolomitized Ellenburger rocks. The studied samples could not unequivocally be assigned to a certain formation using these criteria. For the remainder of this study the informal usage of Ellenburger dolomite was preferred rather than the formal designation of the Ellenburger as a group. Wherever possible a designation of the studied cores in lower, middle or upper Ellenburger following the terminology of Loucks and Anderson (1980, 1985) was attempted.

GEOLOGIC SETTING

The term Permian Basin was originally applied to the large basin in the central part of the U.S., occupied by the Permian sea at the end of the Paleozoic. It is now applied in a more geographic sense to those parts of the "Permian Basin" that were occupied by the Permian seas of West Texas and eastern New Mexico (Elam, 1984).

The Delaware and the Val Verde basins were subdivisions of the Permian Basin and successors of an ancestral basin, the Tobosa, which was in existence from the latest Precambrian to middle Paleozoic (Galley, 1958; Adams, 1965; Hills, 1972, 1984). The separation of the Tobosa Basin into its subdivisions (Delaware, Midland, Val Verde, Marfa and Kerr basin) began in the late Paleozoic during which the previous stable West Texas craton experienced increasing amounts of tectonic disturbance (Wuellner et al., 1986).

Available information concerning the Precambrian history of West Texas suggests that two prominent trends of crustal weakness influenced subsequent Paleozoic and depositional events (Hills, 1972, 1984; Walper, 1977; Wuellner et al., 1986). Hills (1984) argued that north-northwest trending zones of crustal weakness were created by a left lateral transform fault and associated triple junction. Walper (1977) ascribed much of the tectonic activity in the Delaware basin to the development of a failed arm in the Late Precambrian (Delaware aulacogen). Wuellner et al. (1986) reported on structural elements with a general east-west orientation.

These two prominent trends of crustal weakness in West Texas may be linked to a single Late Precambrian-Early Cambrian rifting event which shaped the southern margin of the lower and middle Paleozoic North American continent (Hills, 1972, 1984; Wuellner et al., 1986). The nature of this rifting event was discussed by King (1975), Cebull et al. (1976) and Thomas (1983).

Following this rifting event, a stable passive margin (Tobosa basin) developed along the southern terminus of the North American craton. Wuellner et al. (1986, their figures 2 and 4) distinguished a passive margin shelf facies (shallow water carbonates and siliciclastics deposited on a largely stable craton) and a passive margin slope/basin facies (organic-rich mudrocks, cherts, carbonates, minor amount of sandstones, gravity-flow deposits, deposited on slowly subsiding transitional to oceanic crust). Late Precambrian to Middle Mississippian rocks of the Delaware and Val Verde basin were represented by the passive margin facies, rocks of the Marathon region by the passive margin slope/basin facies (Wuellner et al., 1986, their figure 2).

Rocks of the passive margin shelf facies of the Tobosa basin included Late Cambrian sandstones, Early Ordovician carbonates (Ellenburger), Middle Ordovician limestones and

shales of the Simpson Group, Late Ordovician to Devonian carbonates and Late Devonian black shales (Woodford shale).

The Late Paleozoic was a time of great change in sedimentation on the formerly, primarily stable West Texas craton (Hills, 1984; Wuellner et al., 1986). In the Early Mississippian the Tobosa basin began to deepen on either side of a paleohigh, the position of which correlates with the modern central basin platform (Hills, 1972, 1984). By Late Mississippian, the former Tobosa basin was divided into two basins, now known as the Delaware (western basin) and the Midland (eastern basin) basins (Nicholas and Rozendal, 1975), separated by the Central Basin platform which continued to rise throughout the Pennsylvanian. The southern parts of the Tobosa basin, Kerr and Val Verde basins, subsided rapidly as foredeeps, probably in response to increasing tectonism along the Ouachita front, which was caused by a continent-continent collision along the southern margin of North America (Kluth and Coney, 1981; Wuellner et al., 1986).

After the breakup of the Tobosa basin in its subdivision, the deeper parts of the Delaware, Val Verde, and Midland basins continued to receive large amount of sands and shales, whereas the shelf edges were vast areas of limestone deposition until the end of the Paleozoic.

Ellenburger carbonates (Lower Ordovician)

In West Texas, the Ellenburger consisted of interbedded limestones and dolostones in surface exposures, in the subsurface it was mostly dolostones. The deposition of the Ellenburger shallow water carbonates and the underlying Bliss Sandstone (Cambrian) occurred as a part of an Early to Middle Paleozoic passive margin shelf facies of the Tobosa basin during a major Late Cambrian/Early Ordovician marine transgression over Precambrian basement rocks (Barnes et al., 1959; Ross, 1976; Hills, 1984; Wuellner et al., 1986).

Isopach data in Barnes et al. (1959) showed onlap of Cambrian and Ordovician strata (Ellenburger) on Precambrian rocks from the southeast to the northwest. An isopach map (Figure 5) of the Ellenburger is showing a gradual thickening of the Ellenburger platform carbonates towards the east, south and southeast, documenting the onlap of Ellenburger deposits towards the northwest. Exceptions from this trend is local thinning along the axis of the Central Basin Platform due to Mississippian/Pennsylvanian uplift.

Previous studies (e.g. Barnes et al., 1959; Lucia, 1968; Ross, 1976; Kerans, 1988 a) showed, that the facies distribution of the Ellenburger follows this general trend, with more open marine conditions prevailing in the southeast near the shelf break of the Tobosa Basin and more restricted inner shelf conditions towards the northwest.

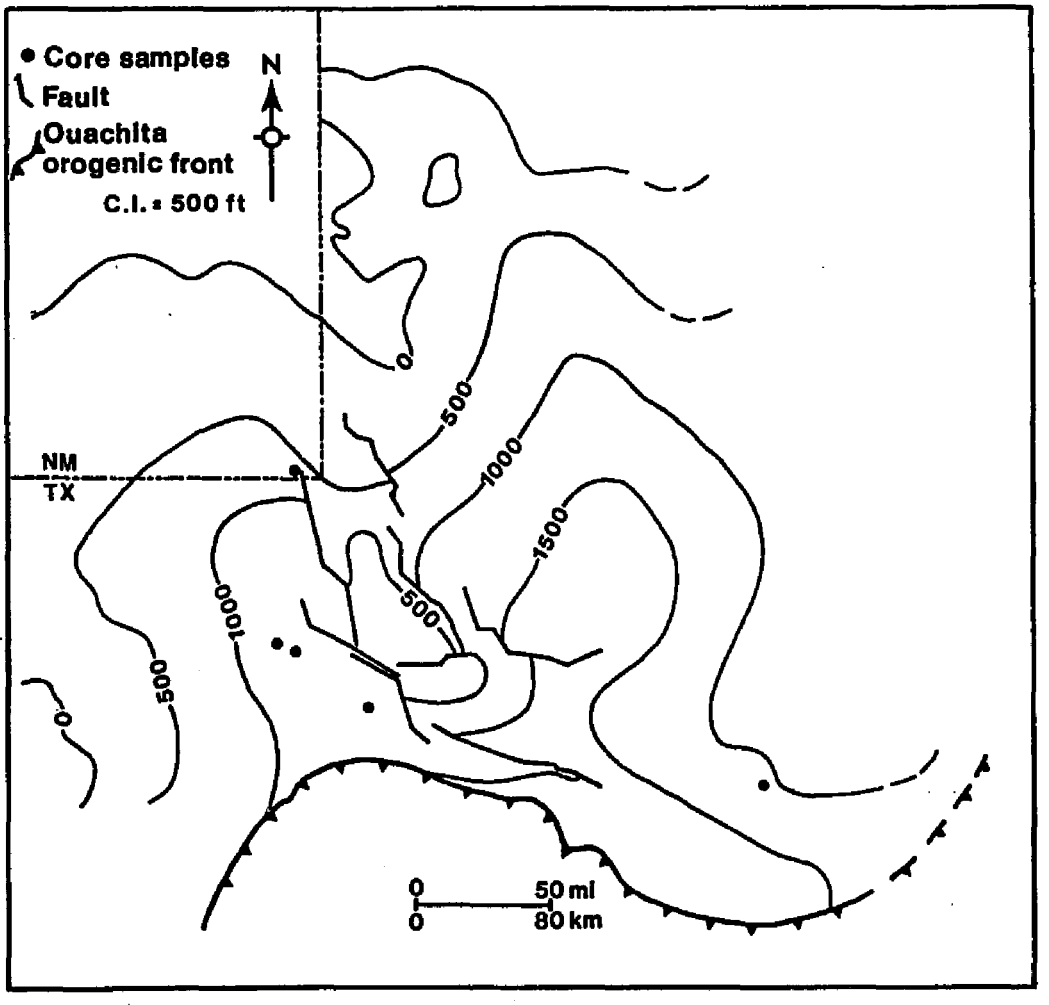

Figure 5. - - Isopach map of Ellenburger Group platform carbonates in Texas and New Mexico, showing thickening towards the east, south, and southeast in direction of the inferred shelf edge of the Paleozoic Tobosa Basin. (Modified from Galloway et al., 1983).

DEPOSITIONAL ENVIRONMENTS AND FACIES

Because a carbonate reservoir is formed in an original body of sediment which often underwent a long and complex history, a double study (deposition and diagenesis) is always necessary (Wilson, 1980). Knowledge of the depositional setting and facies architecture is invaluable in the deduction of the diagenetic history. The correct identification of the environments of deposition and the diagenetic history are the key to the analysis of heterogeneity (Weber, 1986).

An examination of the initial depositional environments of the Ellenburger rocks establishes the framework for studies of the subsequent diagenetic changes that modified the Ellenburger rocks.

Description and determination of original depositional environments is based on handspecimen description and petrographic examination of thin sections. Because of pervasive dolomitization original depositional environments were inferred based on the presence or absence of carbonate particles (oolds, peloids, intraclasts, skeletal grains) and preserved original depositional textures (lamination, crossbedding).

Three distinct rock types are present in the studied cores (Figure 6): Limestones, dolostones, and clastic rocks.

Dolostones are volumetrically the most important types accounting for 90% of the studied cores. Cores 1 to 4 were completely dolomitized, core 5 consists of interbedded limestones/ dolostones. Clastic rocks occur at the base of core 4 near the transition between Cambrian sandstones to Ellenburger dolostones.

Despite pervasive dolomitization primary depositional textures were preserved and the carbonate rocks are subdivided according to their depositional textures (Dunham, 1962) into five lithofacies:

Lithofacies 1: Laminated dolomudstones/wackestones, including algal laminated and planar laminated dolomud- stones.

Lithofacies 2: (Dolo)mudstones/wackestones.

Lithofacies 3: Mottled dolomudstones/wackestones.

Lithofacies 4: Peloid-ooid-intraclast (dolo)packstones/grainstones

Lithofacies 5: Sandy dolostones

As a post-depositional (diagenetic) facies present in cores 1, 4, and 5:

Lithofacies 6: Karst Facies.

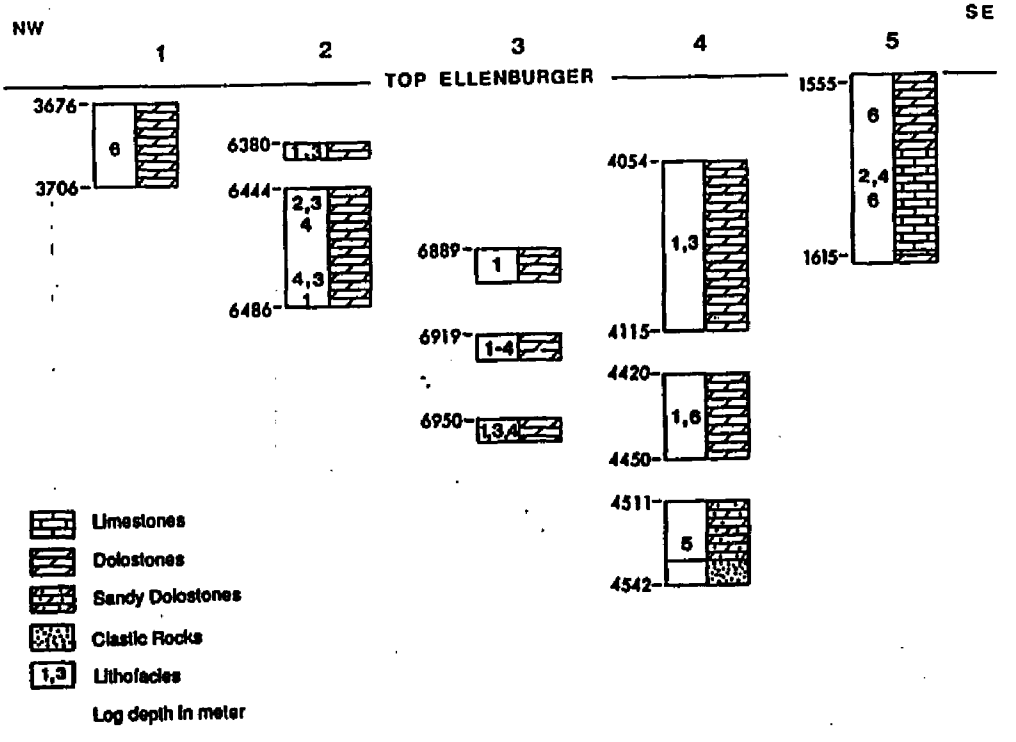

Figure 6. - - Schematic well-logs illustrating stratigraphic distribution of lithology and lithofacies within the studied Ellenburger cores (numbers 1 to 5). Lithofacies are as follows: 1 = laminated (dolo)mudstones/wackestones (lithofacies 1), 2 = (dolo)mudstones/ wackestones (lithofacies 2), 3 = burrowed (dolo)mudstones/wackestones (lithofacies 3), 4 = peloid - ooid - intraclast (dolo)packstones/grainstones (lithofacies 4), 5 = sandy dolostones (lithofacies 5), 6 = karst facies.

LIMESTONES

Limestones are found only in well 5, where they are interbedded with dolostones. Two lithofacies are distinguished:

- Mudstone/wackestone facies (lithofacies 2).
- Peloid-ooid-intraclast packstone/grainstone facies (lithofacies 4).

Mudstone/wackestone facies (lithofacies 3).

This facies comprises dense, light-gray to gray structureless mudstones and wackestones. For most parts they are nonfossiliferous, but in places skeletal fragments (brachiopods, trilobites, gastropods, echinoderms) are encountered. Common to this facies is disseminated pyrite. Rarely observed were bioturbated intervals and algal-laminated (stromatolitic) structures. The mud/wackestone lithofacies attains a thickness of 2-5 ft (0.6-1.5 m).

Peloid-ooid-intraclast packstone/grainstone facies (lithofacies 4).

This facies is the most commonly observed limestone facies. Peloids, ooids and intraclasts in various proportions are the most abundant constituents (Figure 7 A). Intraclasts are either micritic and/or peloidal clasts, usually rounded to subrounded, and have the typical discoidal shape of rip-up clasts. Ooids, ranging from 80 - 400 microns, exhibit a radial structure or were superficial ooids. Ooids commonly occur in packstones with varying amounts of mud, and show point, sutured, and concavo-convex contacts (Figure 7 A) (Bhattacharyya and Friedman, 1984). In these packstones bivalve shells still retain their original shell structure. Compaction features are ubiquitous, indicating a correlation of high lime-mud content and low degree of early cementation. In peloidal grainstones the particles show isopachous rim cements followed by blocky calcite (Figure 7 B), and bivalve and gastropod shells were replaced and filled by a coarse calcite.

The peloid-ooid-intraclast pack/grainstone facies is up to 30 ft (10 m) thick. Very common is the association of this facies with the mudstone/wackestone facies. 15-20 mm thick peloid-ooid- rich layers are found to alternate with thin mudstone layers (Figure 8 A). The lower contact commonly is erosive with small (1-2 cm) intraclasts at the base of the grainstone layer. Rare escape structures and burrows indicate a rather sudden deposition of the grainstone layers (events).

Flat-pebble conglomerates are associated with both facies types (Figure 8 B). Thin (mostly less then 5 mm), round to subrounded clasts, a few mm up to 5 cm long with typical discoidal shapes make up thin layers (characteristically up to 10 cm) in both facies. The clasts

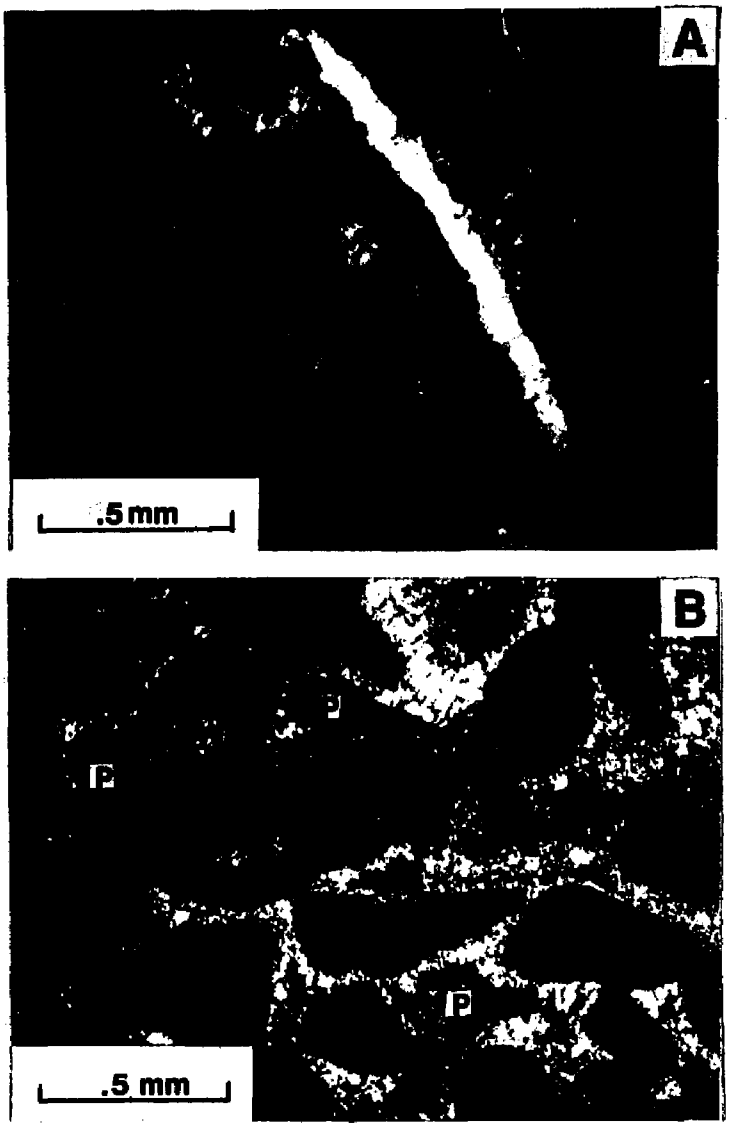

Figure 7. -- Thin-section photomicrographs of packstone/ grainstone lithofacies. A) Photomicrograph of peloid-ooid packstone. Note sutured (concavo-convex) contacts between radial ooids, breakage of shell fragment, and deformed ooids, all of which indicates compaction and lack of early cementation. Sample from 5,267 ft (1,605 m), well 5. B) Photomicrograph of peloidal grainstone of lithofacies 4 (peloid-ooid-intraclast packstone/ grainstone facies). Isopachous rim cements coat grains, followed by later sparry calcite, which only partly occludes pore spaces resulting in interparticle porosity (P). Plane polarized light. Sample from 5,267 ft (1,605 m), well 5.

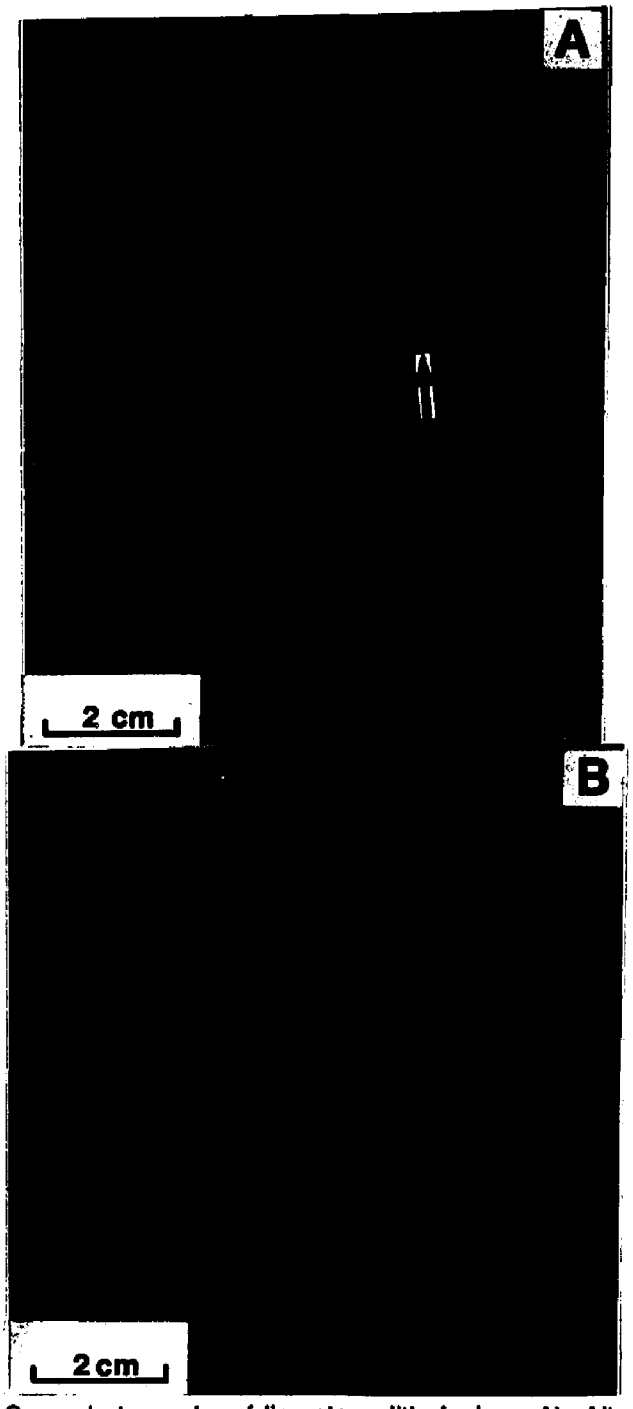

Figure 8. - - Core photographs of limestone lithofacies. A) Alternation of mudstone/ wackestone layers (light gray) with peloid- ooid rich layers (dark gray). Note sharp erosive lower contact of peloid-ooid layer, enhanced by solution seam (arrow). Vertical structures are interpreted to represent escape structures. Sample from 5,266 ft (1,605 m), well 5. B) Flat-pebble conglomerate associated with limestone facies. Shape and arrangement of intraclasts indicate that they must have been at least semi-lithified at the time of deposition. Sample from 5,244 ft (1,598 m), well 5.

are identical in composition to the surrounding limestones (micritic and/or peloidal limestones). Shape and arrangement of the clasts indicate that they must have been at least semi-lithified at the time of deposition.

Interpretation. -- Both limestone lithofacies are only found in the upper Ellenburger (Honeycut Formation, using the nomenclature of Barnes et al., 1959) in the J.E. Phillips #1 core, Edwards County, Texas (well 5). They are interpreted to represent shallow subtidal to lower intertidal, open marine deposits. The presence of brachiopods and gastropods indicates more open, less restricted marine conditions, if compared to strata in the western part of the study area. Features commonly associated with tidal-flat deposits (birdseye structures, desiccation cracks, tidal channels) (e.g. Matter, 1967; Roehl, 1967; Ginsburg, 1975; Shinn, 1983) are largely absent. Laminated and burrowed limestones are observed in places, but they are always associated with subtidal mud/wackestones. The alternation of peloid-ooid rich layers with mud/wackestone layers also indicates deposition in an shallow subtidal to low intertidal setting (Ashton, 1981). The peloid-rich layers represent mechanically deposited layers and represent higher energy periods in an otherwise low-energy setting. Lloyd et al. (1987) described ooid formation by wind-generated waves and currents, suggesting the possibility of ooid formation far away from steep ramps or shelf margins and high energy intertidal settings. Thus ooids could form on subtidal shoals in open marine settings of shallow epeiric seas, where the only water energy within extensive regions would be that generated by local winds (Hallam, 1981, p. 91).

Flat-pebble conglomerates associated with the limestones facies also indicate low intertidal to shallow subtidal deposition. They could represent subaerial desiccation flakes, but considering the relative scarcity of desiccation features they most likely represent clasts of early submarine cemented limestones that have been ripped-off and redeposited by storms or other erosional events (Sepkoski, 1982).

Besides sedimentary criteria, the paleogeographic position of well 5 (see Figure 5) also supports a more open marine setting for the limestone lithofacies. Barnes et al., (1959, Figure 15) showed, that limestones increase relative to dolostones eastward, accompanied by an increase in traces of evaporites westward.

The mudstone/wackestone facies (lithofacies 2) and the peloid- ooid-intraclast packstone/grainstone facies (lithofacies 4) are comparable to the gastropod-intraclast grainstone facies assemblage described by Kerans (1988 a). He ascribed this facies assemblage to a less restricted, more basinward shelf setting and interpreted it as part of an aggradational sequence ending Ellenburger deposition.

The limestone facies were subsequently modified by pre-Simpson erosion and

karstification. This diagenetic modification is discussed later in the section on Diagenesis.

DOLOSTONES

Dolostones make up 90% of the studied cores and despite pervasive dolomitization there are sufficient primary structures and textures preserved that allow recognition of the following lithofacies (Figure 6):

Lithofacies 1: Laminated dolomudstones/wackestones.

Lithofacies 2: Dolomudstones/wackestones.

Lithofacies 3: Mottled dolomudstone/wackestones.

Lithofacies 4: Ooid-peloid-intraclast dolopackstones/grainstones.

Lithofacies 5: Sandy dolostones.

Laminated dolomudstone/wackestone facies (lithofacies 1).

This facies includes algal laminated and planar laminated dolomudstones. These types are taken together as one lithofacies because, dolomitization allows only in rare cases a unequivocal distinction between algal and nonalgal lamination and the different types are usually closely related.

Laminated dolomudstones attain a thickness of 10-30 ft (3-10 m), are dark-colored and typically finely laminated (Figure 9 A). Very common as a faint parallel lamination, associated with thin (<.5 cm) laminae of rounded to subangular quartz and feldspar grains (Figure 9 A). The detrital quartz grains show in part a bimodal distribution, with very-fine to fine-grained rounded grains and coarse - grained subrounded to subangular grains. An absence of fossils, and disseminated pyrite is characteristic. Thin sections reveal very-fine to fine crystalline mosaics of planar-s (subhedral) dolomite exhibiting a common alternation of dark, very-fine crystalline dolomite with clear, fine crystalline dolomite. Bioturbation is only rarely observed in this lithofacies.

Planar laminated dolomudstones are thinly-bedded (< 1 cm), even to wavy laminated, consisting of alternating smooth dark (muddy) and light (silty) layers (Figure 9 C). In places, small-scale cross stratification and convolute bedding indicate a higher energy setting (current-laminated units).

Locally algal-laminated dolostones are intercalated, forming algal laminae or small biostromal structures. Features indicative of desiccation suggest supratidal deposition.

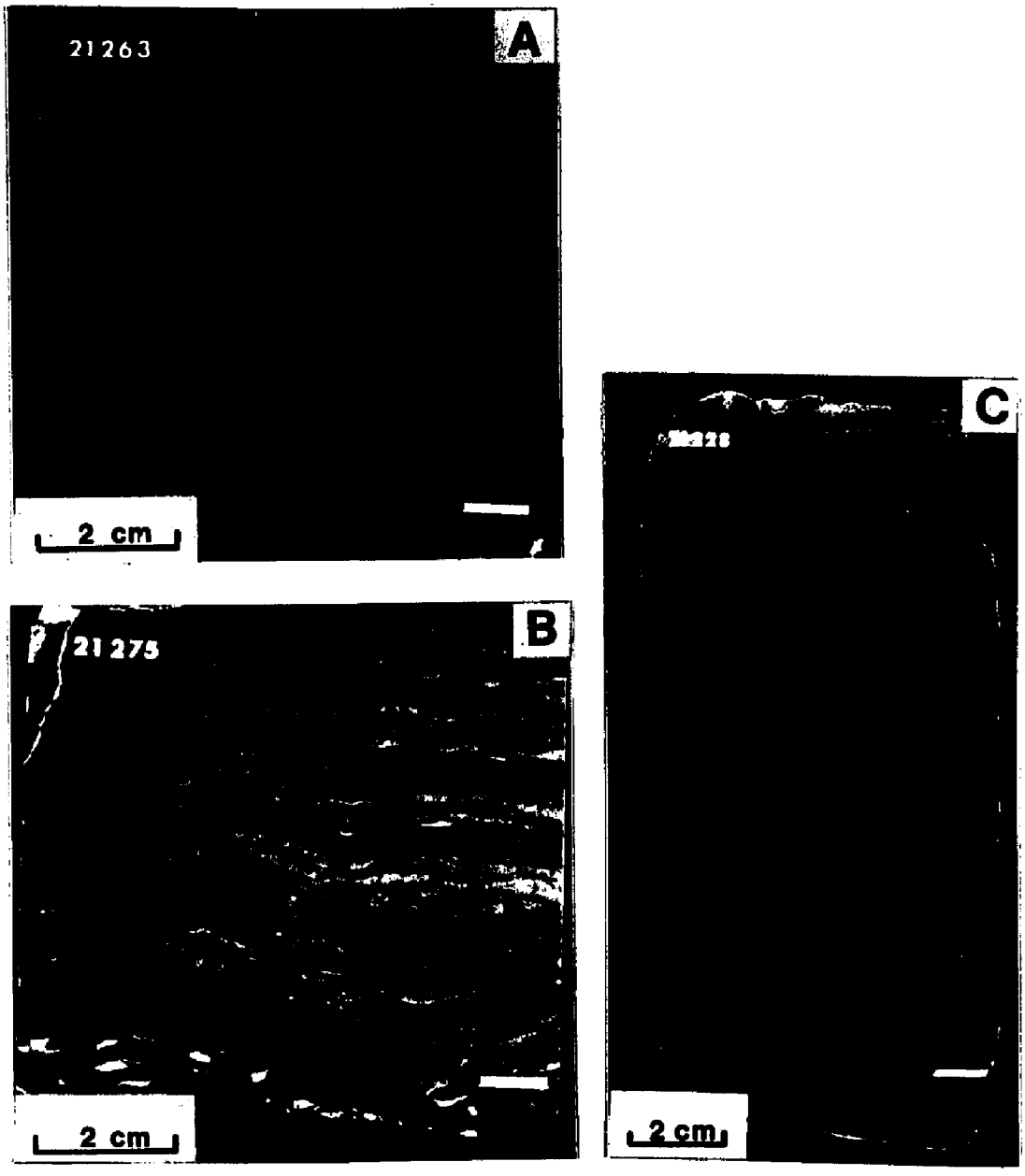

Figure 9. - - Core photographs of laminated dolomudstone lithofacies. A) Laminated dolomudstone with intercalated quartz- rich layers, representing intertidal to supratidal deposition. Sample from 21,263 ft (6,481 m), well 2. B) Algal laminated dolomudstone of the laminated dolomudstone facies. Sample from 21,273 ft (6,484 m), well 2. C) Planar laminated dolomudstone with alternating muddy (dark) and silty layers (light). Small-scale cross-stratification and truncation of layers indicate higher energy setting (current laminated units). Sample from 21,247 ft (6,476 m), well 2.

Interpretation. -- The absence of fossils and bioturbation, the dark to very dark color of the rocks, the fine lamination with locally small biostromal structures, and desiccation features are indicative of a restricted, low intertidal to supratidal setting (e.g. Roehl, 1967; Shinn, 1983).

Characteristic for this setting are intercalations of thin laminae of detrital quartz and feldspar with laminated dolomudstones. The fine-grained sand usually is rounded, while the larger grains are often subangular and show pitted surfaces. The detrital quartz is interpreted to be of aeolian origin. The presence of these detrital grains indicates the proximity of a continental setting to the inferred intertidal to supratidal setting. Clemons (1989) described similar cryptalgal laminates from the lower Padre member of the El Paso Group, Lucia (1970) included such cryptalgal laminates in his Cindy Formation, a tidal flat unit.

The planar laminated dolomudstone are interpreted as current- laminated deposits of more silty material during or after storms.

Dolomudstone/wackestone facies (lithofacies 2).

Dolomudstones/wackestones form up to 25 ft (8 m) thick units, that are composed of dark, dense, structureless dolomudstones and fossiliferous dolowackestones (Figure 10 A). Besides whole fossils (e.g. gastropods) and fossil fragments, peloids are the most common constituents encountered. Soft sediment deformation is observed locally. A nodular appearance (fitted fabric) is characteristic for some intervals. Flat-pebble conglomerates (Figure 10 B) and grainstone layers are commonly intercalated; some bioturbated zones are also present within this lithofacies. The presence of whole fossils and the low degree of reworking of fossil shells generally indicate a low-energy setting.

In thin sections this facies is characterized by dark, dense mosaics of very-fine to fine crystalline planar-s (subhedral) dolomite. Fossils, if present, are nonmimically replaced by a medium-crystalline clear dolomite.

Mottled dolomudstone/wackestone facies (lithofacies 3).

Bioturbated (mottled) dolomudstones/wackestones comprise a prominent facies within the studied cores and formed intervals of up to 30 ft (10 m). The bioturbated character of this facies is visible in core slabs due to the color differences between the burrowed (light) and nonburrowed (dark) parts (Figure 11). Thin sections show dense mosaics of planar-s (subhedral) dolomite in the non-mottled areas, and planar-s (subhedral) and planar-e (euhedral) mosaics in the mottled parts, with intercrystalline and solution-enlarged intercrystalline porosity (up to 10% effective porosity).

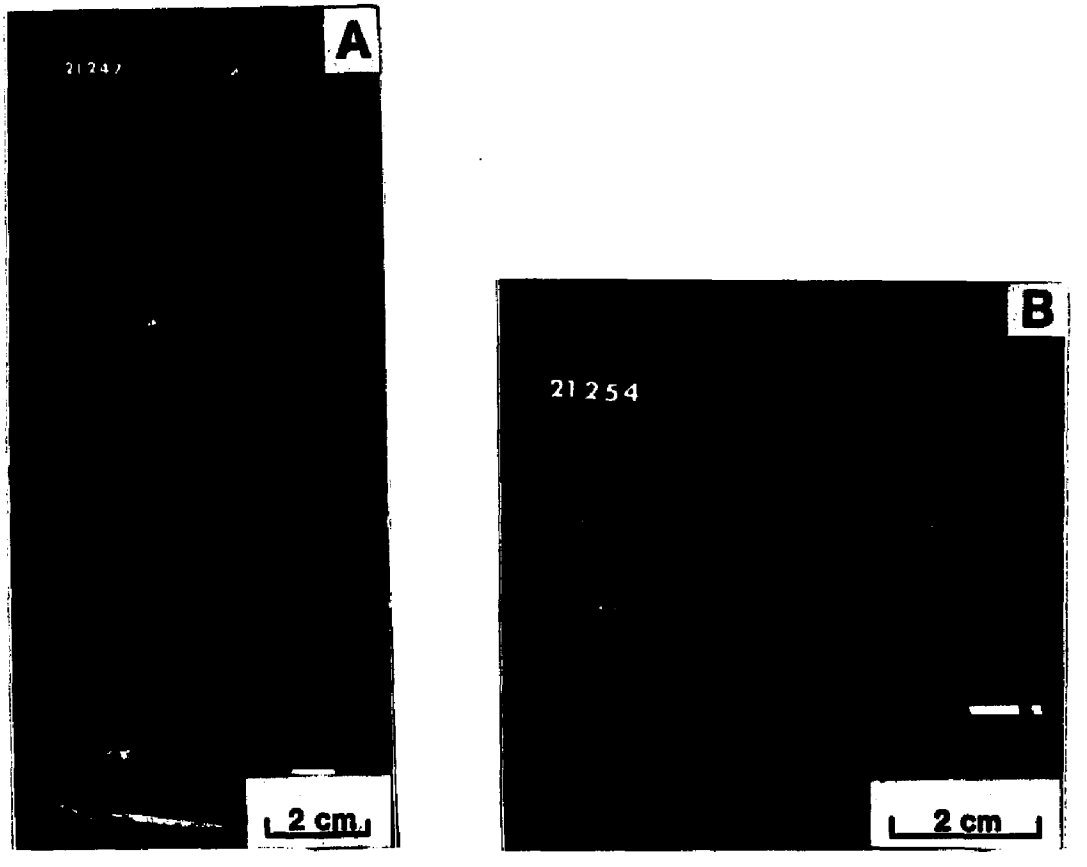

Figure 10. -- Core photographs of dolomudstone/wackestone lithofacies. A) Fossiliferous dolowackestone with well-preserved gastropods in otherwise dense and structureless dolowackestone. Sample from 21,247 ft (6,476 m), well 2. B) Flat-pebble conglomerate, associated with the dolomudstone/wackestone lithofacies. Sample from 21,254 ft (6,478 m), well 2.

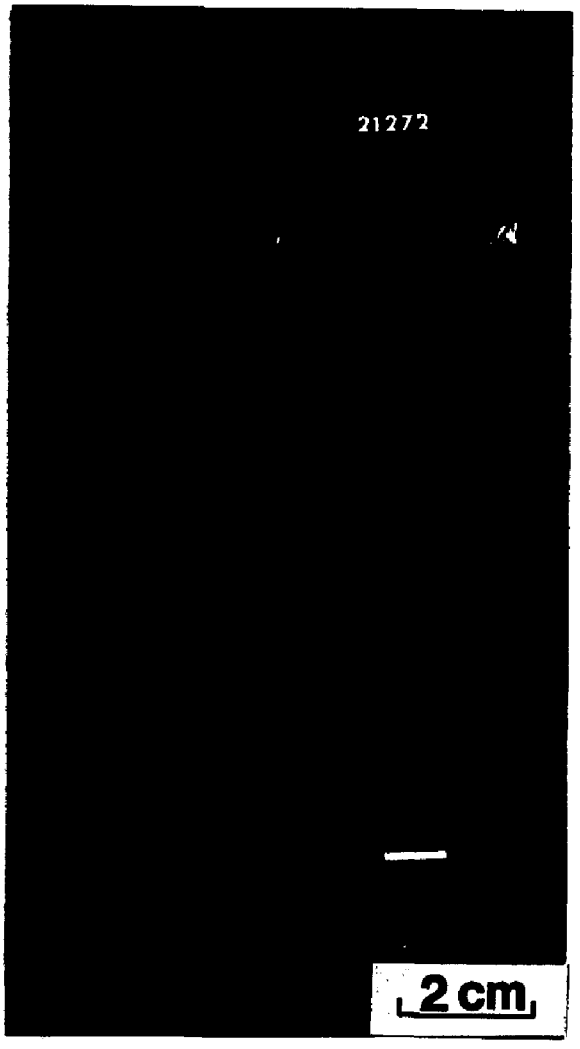

Figure 11. - - Core photograph of mottled dolomudstone/wackestone lithofacies. Burrowed parts (light) have considerable intercrystalline porosity (up to 10%). Sample from 21,272 ft (6,484 m), well 2.

Interpretation. -- Both the dolomudstone/wackestone lithofacies and the mottled dolomudstone/wackestone lithofacies are thought to represent a restricted subtidal to shallow intertidal environment (e.g. Roehl, 1967; Enos, 1983). Burrows are the most common structures of restricted subtidal inner shelf environments (Enos, 1983, p. 288). They range from lacking to thorough. Structureless dolomudstones can be a result of a) complete bioturbation that wipes out all structures, or b) absence of deep burrowers. Which one of the two possibilities explains the structureless dolomudstone can not be judged on the basis of the studied cores. Mottled dolomudstones grade into structureless dolomudstones, which could represent completely bioturbated intervals or intervals where burrowers could not exist, because of changing environmental conditions. Flat-pebble conglomerates and thin grainstone layers are intercalated especially with the nonmottled facies and represent common occurrences of higher energy affecting the low-energy setting.

Peloid-ooid-intraclast dolopackstone/grainstone facies (lithofacies 4).

This lithofacies forms 1 to 3 ft (.3 - 1 m) thick units. Due to pervasive dolomitization grainstone depositional textures are rarely visible in slabbed cores. Petrographic examination reveal abundant ghosts of carbonate grains (e.g. ooids, peloids, intraclasts, skeletal grains) (Figure 12), that allow to infer a depositional texture. This lithofacies is characterized by mosaics of coarse to very coarse crystalline planar-s (subhedral) dolomite. In some examples silicified ooids occur, which show good preservation of their original structures. The available porosity in this facies is variable, ranging from 1 to 12%.

Interpretation. -- These thin layers intercalated in dolomudstones and mottled dolomudstones lithofacies represent periods of higher energy in a generally low energy setting. They may represent low-energy shoaling upward units (e.g. muddy sequence of James, 1984), or subtidal offshore shoals (e.g. Lloyd et al., 1987) or bars as described by Clemons (1989) for the Ellenburger equivalent El Paso Group. Usually they are overlain by a subtidal facies, the transition is gradational rather than sharp.

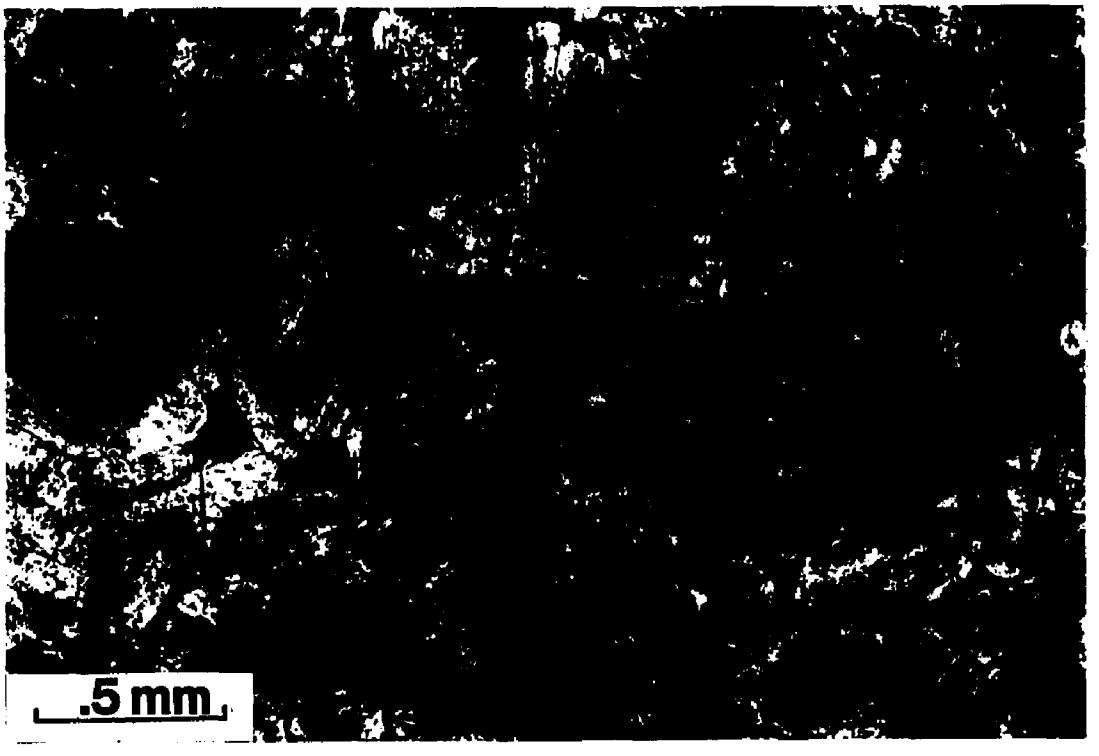

Figure 12. - - Photomicrograph of lithofacies 4 (oolitic grainstone of the peloid-ooid-intraclast dolopackstone/grainstone lithofacies). Ghosts of ooids are preserved in coarse-crystalline planar-s mosaic. Sample from 21,197 ft (6,461 m), well 2.

Sandy dolostones (lithofacies 5).

This facies has been encountered only in the Puckett No. 1 well, Pecos County. It occurs near the transition of Cambrian sandstones to Ellenburger dolostones. Poorly sorted quartz and feldspar grains, subrounded to rounded and up to several mm in size are found within a pyrite-rich matrix of coarse nonplanar dolomite. No bedding has been observed in cored slabs of this facies.

Interpretation. -- This lithofacies has been described in previous studies of the Ellenburger (Barnes et al., 1959; Loucks and Anderson, 1980, 1985) and it is interpreted as the transition from Cambrian sandstones to the carbonate-dominated regime of the Lower Ordovician Ellenburger. Barnes et al. (1959, Plate 2) assigned this facies to the Gorman formation (based on the presence of sand grains), Loucks and Anderson (1980, 1985) to the Lower Ellenburger, for which they inferred an alluvial fan/coastal sabkha setting. The sand content decreases upward as sedimentation became dominated by carbonate deposition.

CLASTIC ROCKS

This lithology comprises poorly sorted arkosic and conglomeratic dolomitic sandstones, and has been encountered at the base of the Ellenburger in the Puckett No. 1 well. Poorly-sorted, rounded to angular quartz and feldspar grains, mm to cm- sized, rock and chert fragments occur in a pyrite-rich dolomite matrix (Figure 13). The rocks show sporadic stratification and usually a grain-supported fabric with sutured grain contacts.

Interpretation. -- Clastic rocks are reported to form a blanket over Precambrian rocks in the study area (e.g. Barnes et al., 1959). Loucks and Anderson (1980, 1985) interpreted this facies to represent an alluvial fan setting. Kerans (1988 a) interpreted a similar facies as a retrogradational marine sequence (equivalent to the Bliss Formation of New Mexico and far West Texas) indicating a westerly onlap during the Late Cambrian.

Clastic units were also described from within the El Paso Group, where they occurred at the base of the Cooks, Jose, McKellington, and Scenic Drive formations (LeMone, 1988, p. 60, Figure 3). It was speculated that these clastic units are synchronous equivalents to the insoluble residue zones recognized in the Ellenburger (e.g. LeMone, 1988; Mazzullo, 1989).

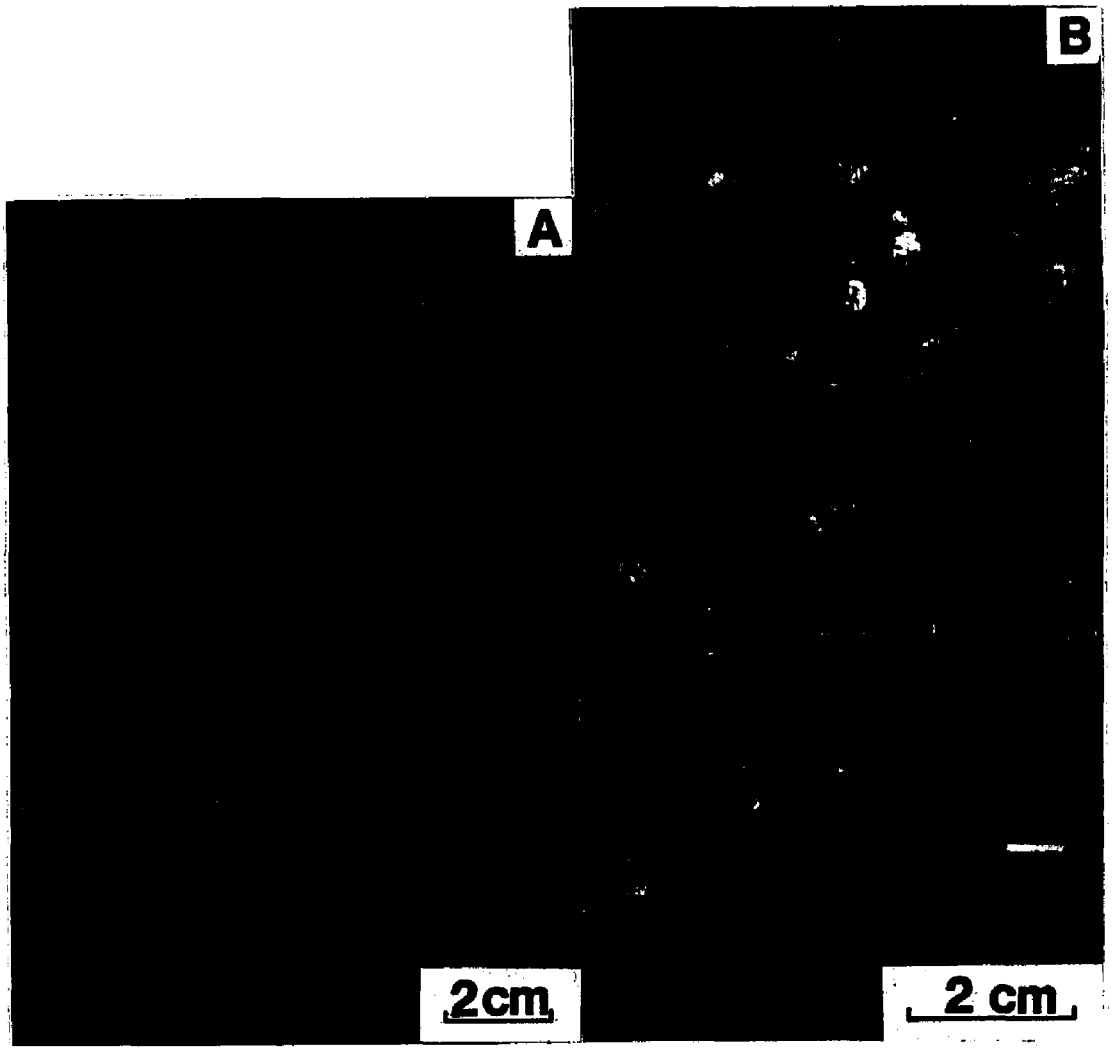

Figure 13. - - Core photographs of clastic rocks. A) Arkose with dolomite and pyrite matrix. Sample from 14,833 ft (4521 m), well 4. B) Arkose conglomerate with poorly sorted, rounded to angular quartz and feldspar grains. Matrix is dolomitic and pyrite-rich. Sample from 14,597 ft (4449 m), well 4.

SUMMARY

To better understand depositional facies and their relationships this study builds on the work of Cloud & Barnes (1948), Barnes et al., (1959), Loucks & Anderson (1980, 1985), and Kerans (1988 a).

The distribution of the major lithofacies seems to reflect the paleogeographic position. Limestones (well 5) increase relative to dolostones (wells 1 to 4) in an eastward direction (Barnes et al., 1959, Fig. 15). This corresponds to a change from more restricted inner shelf conditions in the west to more open marine conditions in the east and southeast near the inferred shelf break. This trend may be of importance for modes of dolomitization. Evaporites , or relicts therefrom, have not been observed in this study. But preserved evaporites have been reported from the Ellenburger of West Texas and southeastern New Mexico (Barnes et al., 1959, Figure 15; p. 693). Loucks and Anderson (1985, p. 27) showed evidence for replaced evaporites in the lower Ellenburger Dolomite in the Puckett Field, but not in the middle and upper Ellenburger in the Puckett Field. Kerans (1988 a, p. 1163) reported on evaporite nodules also from the lower Ellenburger. The presence of former evaporites in the lower Ellenburger dolomite indicates arid to semiarid conditions, at least for the western part of the Tobosa basin during the early Ellenburger (Loucks & Anderson, 1985). Loucks and Anderson (1985, p. 33) discussed a change towards a more humid climate towards the end of the Lower Ordovician, manifested by a well- developed karst surface on top of the Ellenburger.

Depositional environments and facies described from the Ellenburger indicate deposition as epicontinental platform carbonates, ranging from mixed clastic-carbonate deposits during an early marine phase to shallow subtidal to supratidal carbonates during later stages of Ellenburger deposition. Ellenburger carbonate rocks are laterally continuous with carbonates from the El Paso Group, and were deposited on a wide epicontinental shelf. These epeiric seas extended from southeast Arizona, across South New Mexico and West Texas into Central Texas (Cloud and Barnes, 1948; Clemons, 1989), and all across the North American continent as far east as the Appalachian Basin.

Terrigeneous material (dolomitic sandstones, arkosic conglomerates, sandy dolostones) has been found at the base of the Puckett No. 1 well, which penetrates the top of the Precambrian basement. The terrigeneous material overlies Precambrian basement throughout West Texas (Cloud & Barnes, 1948; Barnes et al., 1959; Loucks & Anderson, 1985; Kerans, 1988). During the Cambrian these sands transgressed over the Precambrian surface (Barnes et al. 1959; Kerans, 1988), and were followed by alluvial fan/sabkha conditions during the advance of the early Ordovician sea (Loucks and Anderson, 1980,

Following the transgression of the Ordovician sea, sedimentation of Ellenburger carbonates was dominated by shallow subtidal shelf conditions, with subtidal to supratidal facies occurring repeatedly. Kerans (1988 a, p. 1166) interpreted this phase of Ellenburger deposition as an overall aggradation and progradation, with mottled mudstones, laminated mudstones and gastropod-intraclast-packstone-grainstones as characteristic facies assemblages.

DOLOMITIZATION

STRATIGRAPHIC AND REGIONAL DISTRIBUTION OF DOLOMITE

Petrographic studies and X-ray analyses indicate that 90% of the studied cores are dolostones (Figure 6). In wells 1 to 4 dolomitization was pervasive throughout the cores. Interbedded dolostones/limestones are found in well 5, which is situated close to the inferred shelf edge of the Ordovician Tobosa basin (e.g. figure 5), where more open - marine conditions prevailed during the deposition of the Ellenburger (Barnes et al., 1959; Ross, 1976; Kerans, 1988a). In an eastward (landward) direction more restricted marine conditions existed which corresponds to the completely dolomitized sections of the Ellenburger. The increase of limestones relative to dolostones in an eastward direction has already been noted by Folk (1959, Fig. 15-17, p.127). This westward increase in dolomite proportion was accompanied by an increase in traces of evaporites (Barnes et al., 1959). Based upon the above observation a paleogeographic control on the distribution of dolomite in the Ellenburger Group carbonates is inferred.

Besides different paleogeographic positions the studied wells also belong to different basins and have different present-day burial depths: wells 1 to 3 are from the deep Delaware Basin (12,000 - 22,000 ft, 3,658 - 6,706 m), well 4 (Puckett field) (13,000 and 14,000 ft)(3,962 and 4,267 m) is located at the transition of the Delaware basin to the Val Verde basin, and well 5 (5,100 ft) (1,555 m) is situated in Val Verde basin. Each well had a different tectonic and hydrodynamic history that influenced the dolomitization pattern found in the cores.

DOLOMITE - ROCK TEXTURES

Petrography

Seven dolomite-rock textures have been recognized and are classified according to crystal-size distribution (unimodal or polymodal) and crystal-boundary shape (planar or nonplanar), using the dolomite-rock classification scheme of Sibley and Gregg (1987). In their classification dolomite-rock textures are defined based on crystal-size distribution (unimodal or polymodal) and whether crystal-boundary shape is planar or nonplanar. The classification

scheme employs terms introduced by Friedman (1965), who was the first to recognize the importance of dolomite textures. The classification is descriptive, but carries genetic implications because size distribution is controlled by both nucleation and growth kinetics, and crystal- boundary shape is controlled by growth kinetics (Sibley and Gregg, 1987, p. 967). Crystal growth of planar dolomite crystals occurs at low supersaturations and/or low temperatures. Above some temperature, referred to as critical roughening temperature, nonplanar crystals may form (Sibley and Gregg, 1987). A critical roughening temperature for dolomite has been estimated to lie between 50° - 100° C (Gregg and Sibley, 1984, 1986).

In this study the classification of dolomite-rock textures is based on petrographic and cathodoluminescence studies, aided by analysis of Backscattered Electron Images (BSI). For crystal-size distributions the apparent maximum dimension of the dolomite crystals was measured or estimated, and subdivided using Folk's (1962) size scale.

The following dolomite-rock textures have been defined (Figures 14, 15):

1. Unimodal, very fine- to fine-crystalline planar-s (subhedral) mosaic dolomite.
2. Unimodal, medium- to coarse-crystalline planar-s (subhedral) mosaic dolomite.
3. Coarse- to very coarse-crystalline planar-s (subhedral) dolomite.
4. Medium- to coarse-crystalline planar-e (euhedral) mosaic dolomite.
5. Medium- to coarse-crystalline planar-e (euhedral) dolomite.
6. Coarse- to very coarse-crystalline nonplanar-a (anhedral) dolomite.
7. Coarse- to very coarse-crystalline nonplanar-c (cement) dolomite.

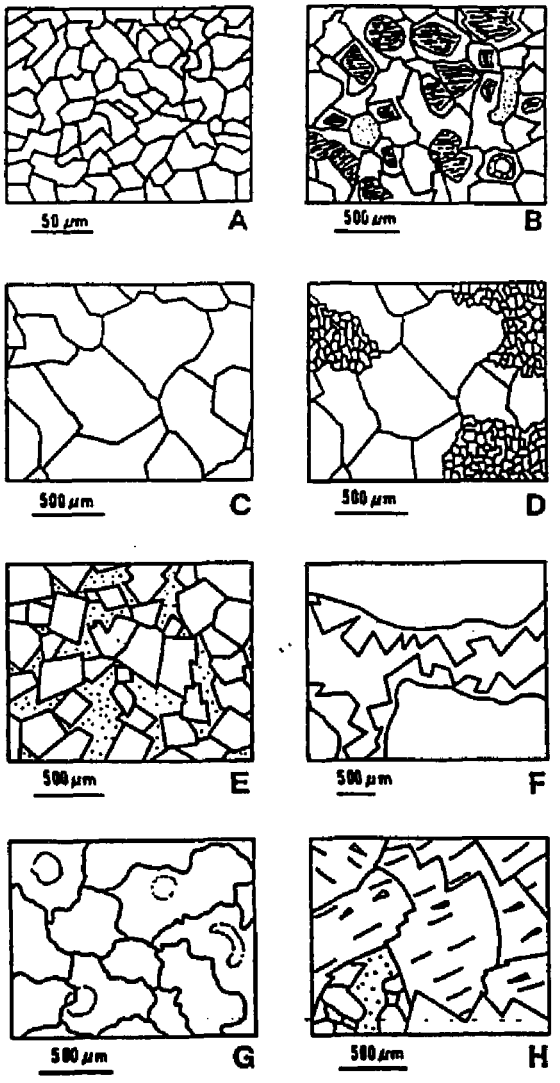

Figure 14. -- Sketch of dolomite-rock textures present in Ellenburger Group carbonates: (A) Unimodal, very fine- to fine- crystalline planar-s (subhedral) mosaic dolomite, (B) Unimodal, medium- to coarse-crystalline planar-s mosaic dolomite, (C) Coarse- to very coarse-crystalline planar-s (subhedral) dolomite (type 3), (D) Polymodal mosaic dolomite composed of dolomite- rock textures A and C, (E) Medium- to coarse-crystalline planar-e (euhedral) mosaic dolomite, (F) Medium- to coarse-crystalline planar-e dolomite, (G) Coarse- to very coarse-crystalline nonplanar-a (anhedral) dolomite, (H) Coarse- to very coarse-crystalline nonplanar-c (cement) dolomite.

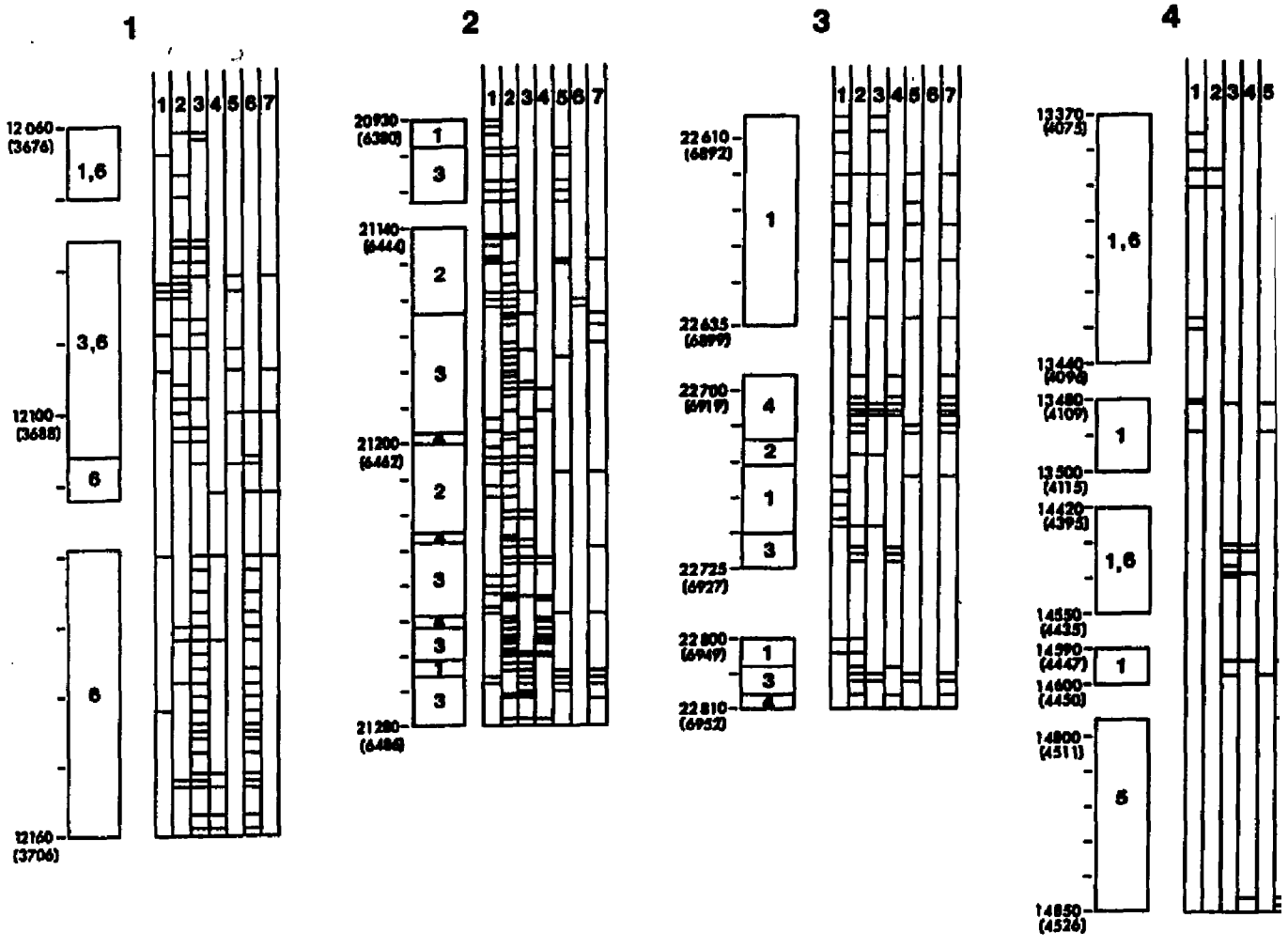

Figure 15. -- Schematic well-logs showing distribution of dolomite-rock textures in the studied Ellenburger cores (well numbers 1 to 5), as defined by thin-section petrography. Presence of different dolomite-rock textures in individual thin-sections is indicated by horizontal bars. Lithofacies are as follows:

1 = Lithofacies 1 (laminated (dolo)mudstones/wackestones).

2 = Lithofacies 2 ((dolo)mudstones/wackestones).

3 = Lithofacies 3 (mottled dolomudstones/wackestones).

4 = Lithofacies 4 (peloid-ooid-intraclast (dolo)packstones/grainstones).

5 = Lithofacies 5 (sandy dolostones).

6 = Lithofacies 6 (karst facies).

Log depth is shown in feet, with meter in parentheses.

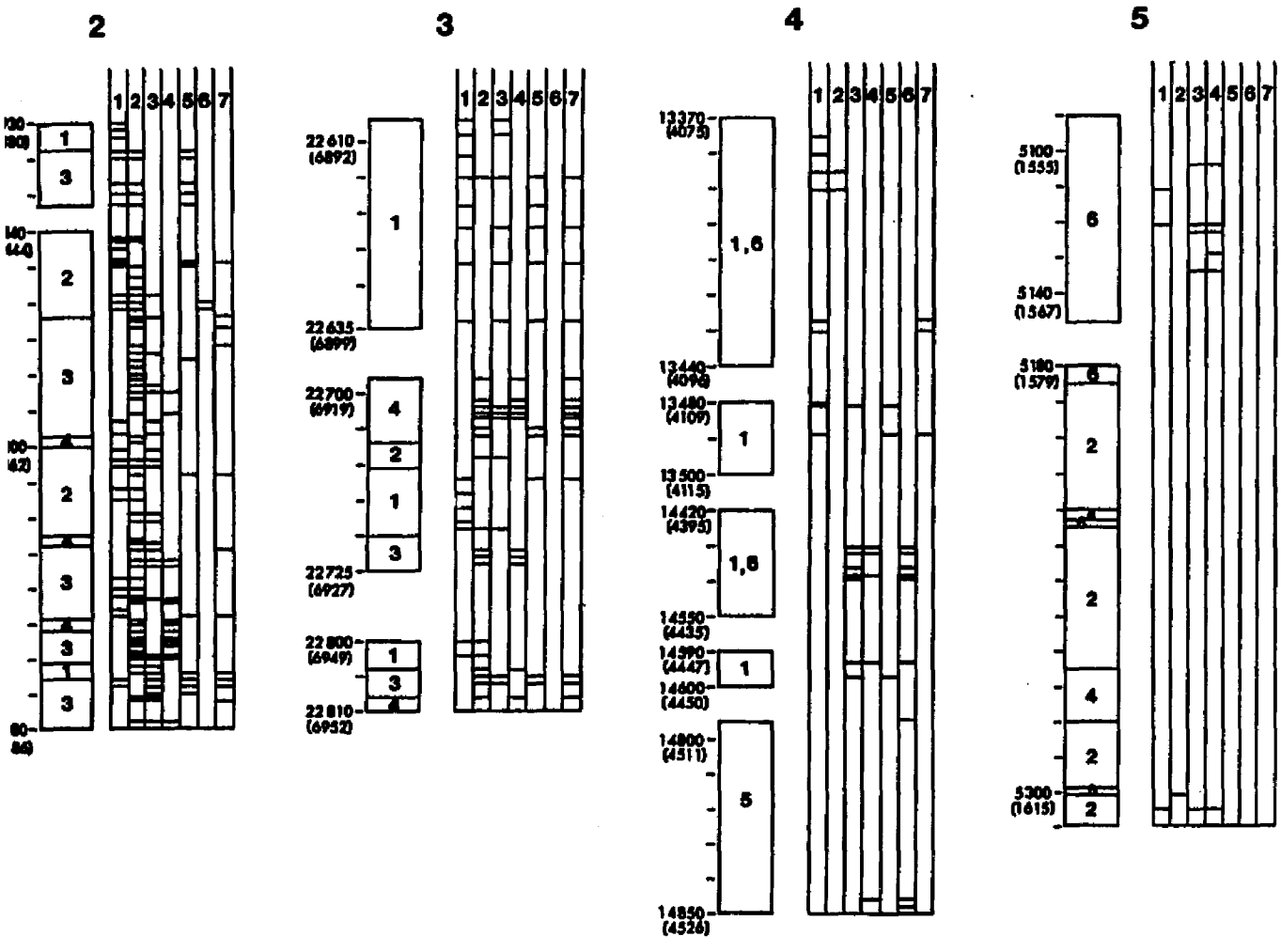

logs showing distribution of dolomite-rock textures in the
umbers 1 to 5), as defined by thin-section petrography.
ock textures in individual thin-sections is indicated by
ollows:

olo)mudstones/wackestones).

ones/wackestones).

mudstones/wackestones).

ntraclast (dolo)packstones/grainstones).

ones).

h meter in parentheses.

Dolomite-rock texture 1: Unimodal, very fine- to fine- crystalline planar-s (subhedral) dolomite.

This type forms dense, dark mosaics of interlocking sub- to anhedral planar-s crystals (< 62 microns) (Figures 14A, 16). It is most common in lithofacies 1 (laminated dolomudstone/wackestone facies) and lithofacies 2 (dolomudstone/wackestone facies). The dense mosaics preferentially replaced fine-crystalline lime-muds, thereby preserving sedimentary structures (laminae), and they are commonly associated with streaks of pyrite. Intraclasts of flat-pebble conglomerates and /or karst breccias are in part also composed of this type. An alternation of very fine-crystalline (dark) with fine-crystalline (clear) dolomite is very common in the laminated dolomudstone/wackestone facies. In places patches of calcite occur within the fine crystalline mosaic.

The luminescence pattern is rather homogeneous dull to dirty- orange mottled. Locally a thin outer orange luminescent zone is present. Clear, fine-crystalline dolomite intercalated with very fine- crystalline dark dolomite shows an orange luminescence color, indicating more than phase of alteration.

Dolomite-rock texture 2: Unimodal, medium- to coarse crystalline planar-s (subhedral) mosaic dolomite.

This type forms dense mosaics of subhedral to anhedral planar-s (subhedral) crystals (100 - 500 microns), that are milky white to clear ,or which show a cloudy core, clear rim texture or vice versa (Figures 14B, 17). Most characteristic for this type is nonmimic replacement of allochems (ooids, peloids, intraclasts, fossils and fossil-fragments). These allochems can be recognized as ghost textures. It is this dolomite type that allows the best recognition of original depositional grain textures.

Under the luminoscope dolomite type 2 shows rather homogeneous dull to dirty orange mottled centers, followed by variable dull and dirty orange zones. Dolomites with cloudy cores and clear rims show dirty orange cores and dull rims, in dolomites with clear cores and dull rims the core is dull and the rim dirty orange. Where crystals line pore space, a thin orange luminescent outer zone is present. Crystal boundaries are discernible, commonly outlined by black intercrystalline material. The ghost textures of allochems appear either as darker spots or are not visible at all.

Type 1 and 2 dolomite also occur as polymodal mosaics.

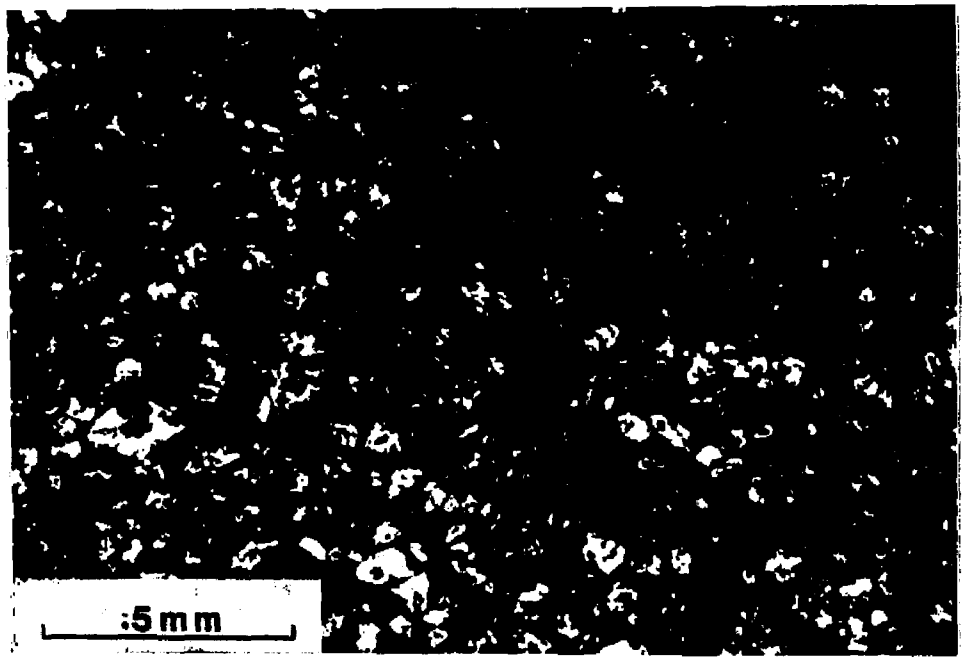

Figure 16. -- Dolomite rock-texture 1: Unimodal, very fine- to fine-crystalline planar-s (subhedral) mosaic dolomite. This type is most common in lithofacies 1 and 3, where it forms dense, dark mosaics of interlocking subhedral to anhedral crystals. Sample from 21,244 ft (6,475 m), well 2. Plane light photomicrograph.

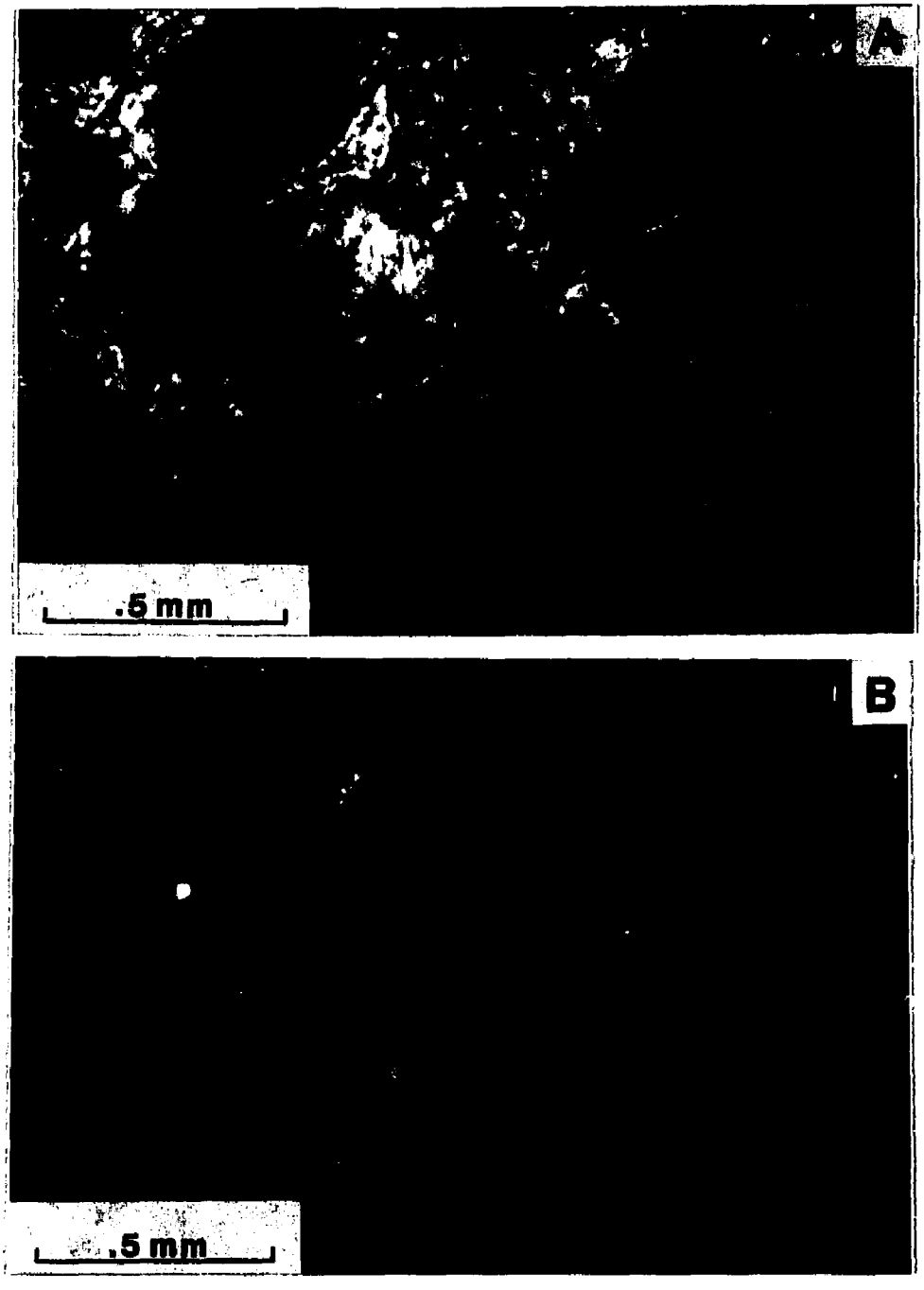

Figure 17. -- Dolomite-rock texture 2: Unimodal, medium- to coarse-crystalline planar-s mosaic dolomite. (A) Plane light photomicrograph, (B) Cathodoluminescence photomicrograph. Most characteristic for this type is a cloudy core, clear rim texture and nonmimic replacement of allochems, which can be recognized as ghosts (A). Under the luminoscope dolomite-rock texture 2 shows homogeneous dull to dirty orange mottled centers, followed by variable dull and dirty zones (B). Sample from 22,705 ft (6,921 m), well 3.

Dolomite-rock texture 3: Coarse- to very coarse-crystalline planar-s (subhedral) dolomite.

This type comprises clear to milky white, coarse- to very coarse-crystalline (up to 1200 microns) planar-s dolomite (Figures 14C, 18) that occurs in patches or irregular zones associated with types 1 and 2, forming polymodal mosaics, or fills fractures cutting across dolomite type 1. It shows no replacement features (e.g. ghosts of allochems).

Two cathodoluminescence patterns are characteristic: 1) Orange to red mottled cores and small zoned outer parts, along crystal boundaries or where the crystals line voids; small zones with bright orange hairlines are most characteristic, and 2) crystals with mottled dull to dirty orange cores, followed by a distinct zonation of orange, dull and nonluminescent zones, with intracrystalline truncation features common between zones in the center and outer zones. This pattern is commonly observed in dolomites filling fractures.

Dolomite-rock texture 4: Medium- to coarse-crystalline planar-e (euhedral) mosaic dolomite.

Mosaics of mostly planar-e, medium- to coarse-crystalline dolomite make up this dolomite type (Figures 14 E, 19). The crystals are clear or have cloudy centered, clear-rim textures. No replacement textures can be observed. This type is encountered in the interior of replaced fossil shells, makes up the mottled parts in the mottled dolomudstone facies, is responsible for sucrosic dolomites in breccias, and occurs near stylolites. Intercrystalline areas are either porous or filled with intercrystalline material.

Planar-e mosaic dolomites have a characteristic luminescence pattern: the cores of crystals are dull to dirty orange. The rim is usually orange luminescent with variable bright orange luminescent bands. In larger crystals alternating dull and orange zones are encountered. The zones of this dolomite type are straight and continuous. In places a thin outer nonluminescent zone has been observed. A zonal pattern, wherein a given zone may be traced continuously around several crystals, is characteristic for planar-e mosaics. Because the crystal-size in individual mosaics is unimodal, one can assume that the nucleation sites were homogeneously distributed (Sibley, 1982; Schofield, 1984). The dolomite crystals have compromise boundaries, so they formed in situ. They grew simultaneously to form planar-e mosaics by growth-coalescence (Schofield, 1984). No intracrystalline truncation features are observed. Evidence for corrosion and partial dissolution of outer zones, however, has been found where crystal-faces line pore spaces. Estimates on individual crystals indicate that up to 20% of the crystals has been removed by dissolution. This results in solution-enlarged porosity.

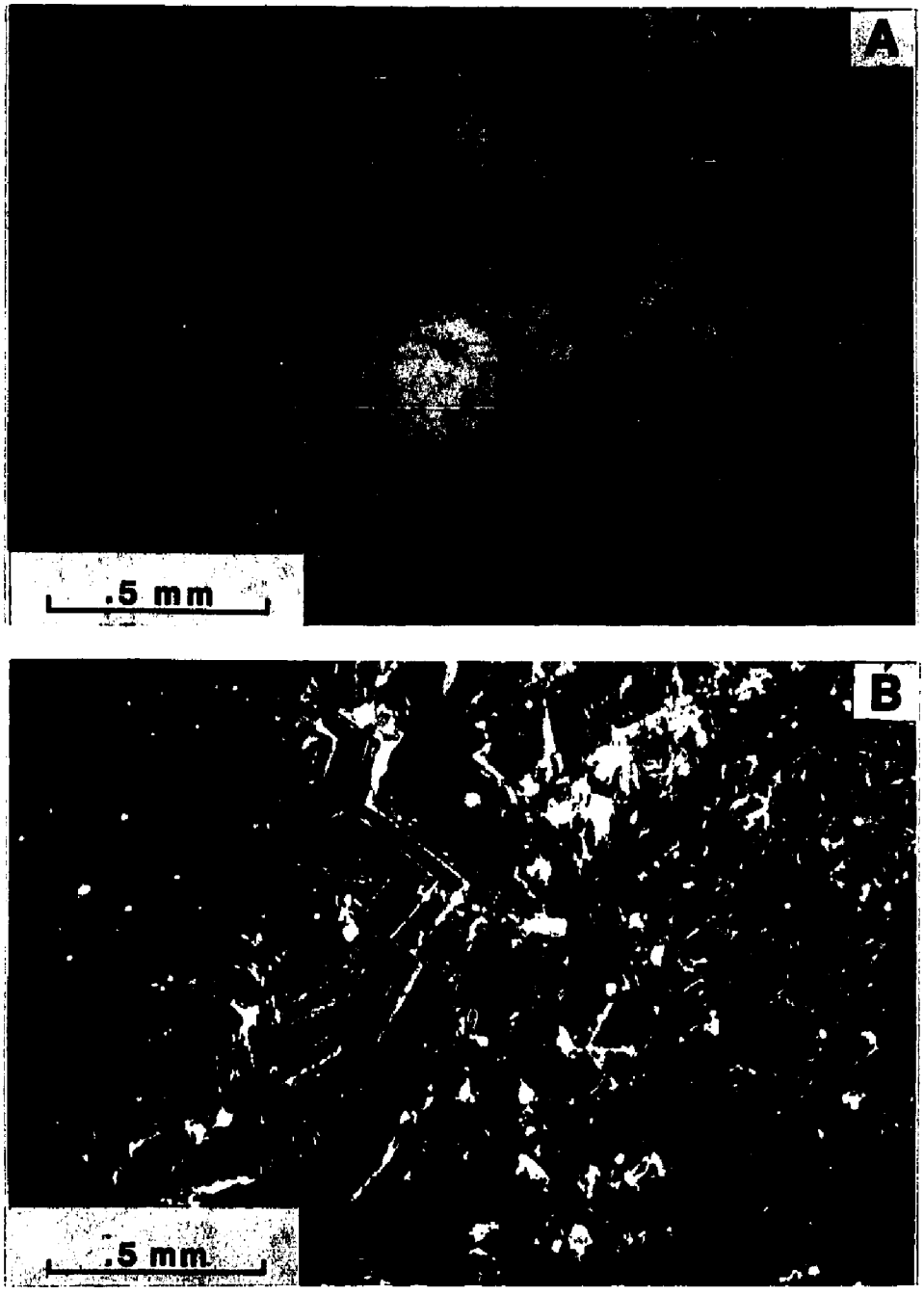

Figure 18. -- Dolomite-rock texture 3: Coarse- to very coarse- crystalline planar-s dolomite. (A) Plane light photomicrograph, (B) Cathodoluminescence photomicrograph. This type forms patches and irregular bands associated with types 1 and 2. It is also observed as fracture fill (A), where it shows complex zonation patterns (B). Sample from 22,719 ft (6,925 m), well 3.

Figure 19. -- Dolomite-rock texture 4: Medium- to coarse crystalline planar-e mosaic dolomite. (A) Plane light photomicrograph of clear, mostly euhedral crystals. No replacement features are observed. (B) Cathodoluminescence picture of (A) reveals multiple zones, which can be continuously traced around several crystals. Note dissolution of crystals (arrows) and intercrystalline porosity (P). Sample from 5,134 ft (1,565 m), well 5.

Dolomite-rock texture 5: Medium- to coarse-crystalline planar-e (euhedral) dolomite.

This type comprises clear, planar-e (euhedral) dolomite crystals lining voids and fractures that are filled with late dolomite or calcite (Figures 14 F, 20). The crystals show unit extinction under crossed nicols, are nonluminescent or show a distinct zonal pattern under the luminoscope, that is locally complex with number and width of the zones variable. The outermost zones commonly are dull to nonluminescent (Fe-rich). Solid hydrocarbon coats in some parts the planar-e dolomites, followed by void filling-calcite and/or nonplanar-c dolomite (saddle dolomite). This common occurrence indicates that this type formed before the onset of hydrocarbon generation. This relationship is used later to constrain the relative timing of late-stage void-filling dolomites.

Dolomite-rock texture 6: Coarse -to very coarse-crystalline nonplanar-a (anhedral) dolomite.

This type comprises dense, tightly packed mosaics of coarse-to very coarse-crystalline nonplanar-a (anhedral) dolomite (Figures 14 G, 21 A). The crystals have irregular, serrated, curved or otherwise indistinct boundaries. They are inclusion-rich and dark, in places showing vague nonmimic replacement, e.g. ghosts of allochems. Preserved crystal faces are rare or absent. Under crossed nicols they show sweeping extinction. Locally intraclasts are observed that are composed of nonplanar-a dolomite, where the nonplanar dolomite grades into crystals with planar boundaries at the rim of the clasts.

Common are also nonplanar-a dolomite crystals that show planar boundaries where crystals border areas filled with calcite, but nonplanar boundaries to neighboring dolomite crystals. The luminescence of this type is fairly homogeneous dark- orange mottled. No zonation has been observed.

Dolomite-rock texture 7: Coarse- to very coarse-crystalline nonplanar-c (cement) dolomite.

Coarse- to very coarse- (up to several mm) crystalline dolomite cement makes up this dolomite type (Figures 14 H, 21 B). Milky-white to clear crystals with sweeping extinction under crossed polars are most characteristic. Under plane light very often triangular surface irregularities (defects) are visible, as well as curved crystal faces (saddle dolomite). Planar-c dolomite lines vugs and fractures and occurs as major void- filling dolomite, thus is responsible

Figure 20. -- Dolomite-rock texture 5: Medium- to coarse- crystalline planar-e dolomite. (A) Plane light photomicrograph of planar-e crystals lining a calcite-filled (Cal) void. Pyrobitumen (black) coating crystals predates precipitation of late calcite. Sample from 21,234 ft (6,472 m), well 2. (B) Cathodoluminescence picture of planar-e crystals that grew discontinuously on dolomite type 1, followed by nonluminescent nonplanar-c dolomite (npl-c). Sample from 12,094 ft (3,686 m), well 1.

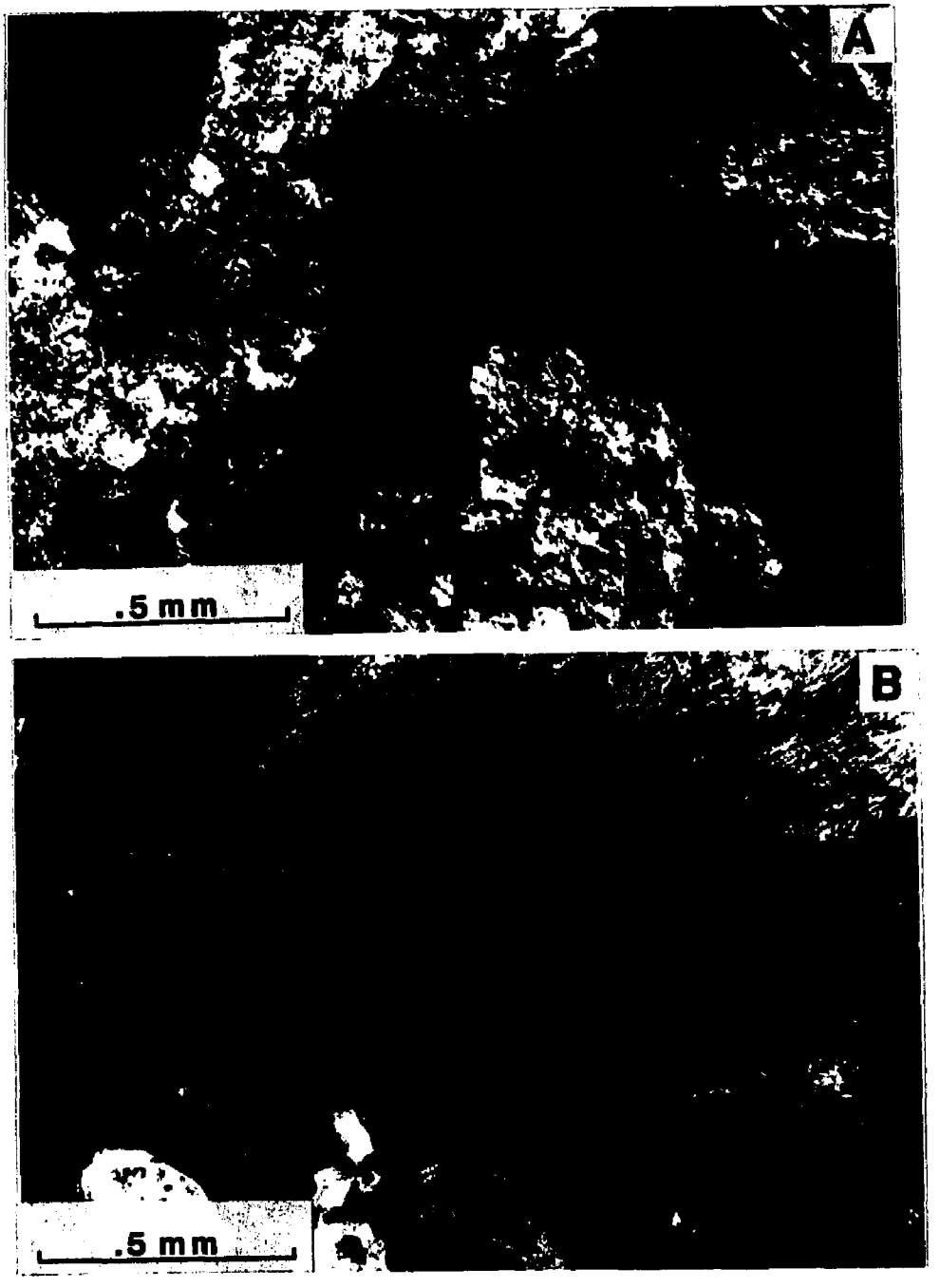

Figure 21. -- Dolomite-rock textures 6 and 7: Nonplanar dolomite. (A) Coarse- to very coarse-crystalline nonplanar-a (anhedral) dolomite, replacing precusor dolostone. Crossed-polarized light. Sample from 12,146 ft (3,702 m), well 1. (B) Coarse-crystalline nonplanar-c (cement) dolomite (saddle dolomite) filling pore space (P). Common is the association with authigenic quartz (qz). Crossed- polarized light. Sample from 21,208 ft (6,464 m), well 2.

for occlusion of pore spaces and fractures phase. Common is the association with authigenic quartz, late stage calcite and /or solid hydrocarbons. Under the luminoscope this type of dolomite is nonluminescent and shows no zonation.

Paragenesis

The paragenetic relationships of Ellenburger dolomite-rock textures are summarized in figure 22. Dolomite types 1, 2, and 6 are of replacement origin, and are volumetrically the most important types. Dolomites types 3, 4, 5, and 7 are void-filling dolomites (Sibley and Gregg, 1987).

Dolomite type 1 (unimodal, very fine to fine-crystalline mosaic dolomite) is interpreted as the earliest phase. Features that suggest an early formation are: 1) It forms unimodal, fine-crystalline dense mosaics in subtidal to supratidal mudstone/wackestone lithofacies, where it predates all dolomite cements. 2) Clasts of flat-pebble conglomerates and karst breccias are composed of this type, indicating early dolomitization (e.g. pre-Middle Ordovician karstification). 3) It is absent in pore-spaces and vugs formed later in the burial environment. 4) It is crosscut by fractures filled with dolomite types 3, 5, or 7.

Dolomite type 2 (unimodal, medium- to coarse-crystalline planar- s mosaic dolomite) represent another replacement phase that forms either unimodal planar-s mosaics or polymodal mosaics with dolomites types 1 and 3. Fossiliferous wackestones and packstones/grainstones are commonly replaced by this type. The good preservation of original depositional textures, the coarse crystal size, and the relative homogeneous luminescence pattern of the replacement phase suggest a major, probably long-lasting dolomitization event during intermediate burial.

Dolomite type 3 (coarse- to very coarse-crystalline dolomite) occurs in polymodal mosaics associated with types 1 and 2. It is observed in fractures cutting across dolomite 1, in patches and irregular clear bands associated with 1 and 2. Contacts between dolomite 3 and earlier types are commonly discontinuous, and intercrystalline truncation features, suggesting periods of dissolution, are observed. Such a dissolution of precursor dolomites seems to prepare the ground for later dolomite cements of dolomite type 3. It is suggested that the dissolution of dolomite and formation of porosity are late secondary burial events that predate the cementing and infilling by even later dolomite/calcite phases.

Dolomite type 4 (medium- to coarse crystalline planar-e mosaic dolomite) does not give many clues as to its pre-dolomite textures. This type is found in the interior of fossil shells, that

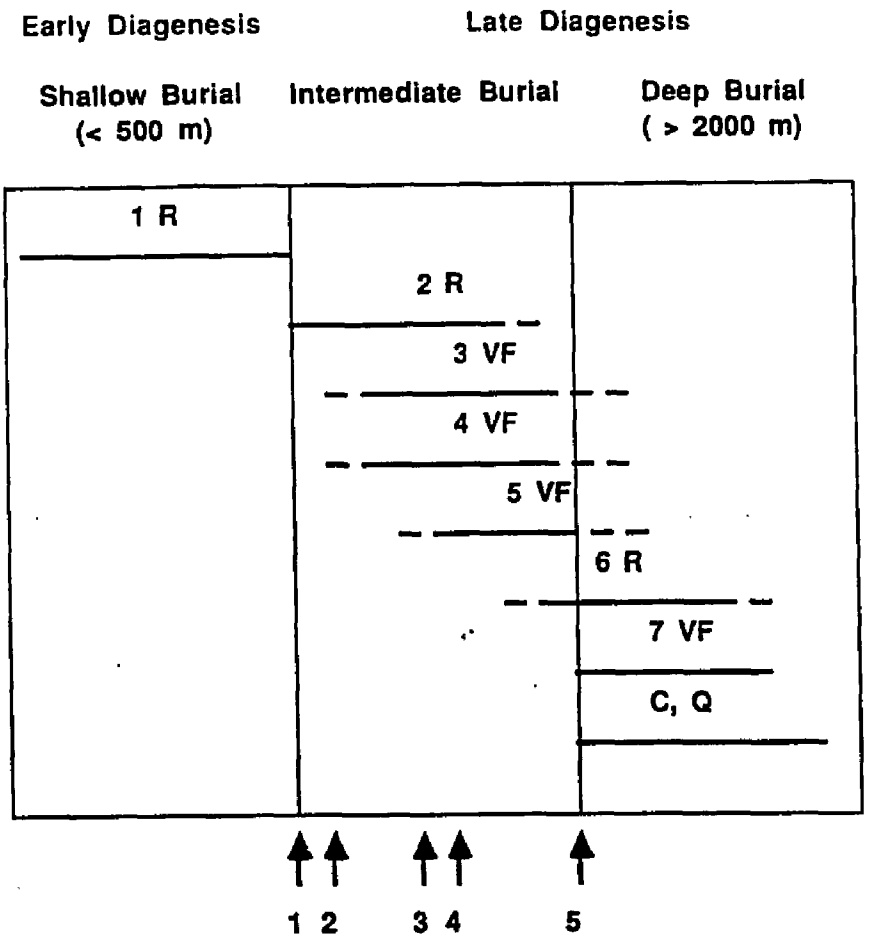

Figure 22. -- Paragenetic sequence of Ellenburger dolomite-rock textures from early to late (burial) dolomitization as indicated by horizontal bars. Dashed lines indicte greater uncertainty in timing. R = replacement dolomites, VF = void-filling dolomites. Numbers refer to dolomite-rock textures:

1 = Unimodal, very fine- to fine-crystalline planar-s mosaic dolomite.

2 = Unimodal, medium- to coarse-crystalline planar-s mosaic dolomite.

3 = Coarse- to very coarse-crystalline planar-s dolomite.

4 = Medium- to coarse- crystalline planar-e mosaic dolomite.

5 = Medium- to coarse-crystalline planar-e dolomite.

6 = Coarse- to very coarse-crystalline nonplanar-a dolomite.

7 = Coarse- to very coarse-crystalline nonplanar-c dolomite.

C = Late calcite, Q = authigenic quartz.

Arrows indicate periods of subaerial exposure and karsting in Palezoic rocks of the passive margin sequence of the Tobosa Basin (from LeMone, 1989): 1 = Pre-Middle Ordovician, 2 = Ordovician - Silurian, 3 = Devonian - Mississippian, 4 = Mississippian - Pennsylvanian, 5 = Pre-Permian.

were replaced by dolomite type 2. It also makes up the mottled parts of the mottled dolomudstone lithofacies, it forms mosaics in karst breccias, and it occurs near stylolites. These occurrences and the paragentic relationships allow an interpreation of dolomite type 4 as of intermediate to late burial origin. It is also important for porosity development, because it is always associated with considerable intercrystalline porosity which also can be solution enlarged.

Dolomite type 5 (medium- to coarse-crystalline planar-e dolomite) is volumetrically minor but it is important for establishing a paragenetic sequence and the timing of certain dolomite types. It is a pore-lining cement that predates hydrocarbons, late calcite and nonplanar-c dolomite, and postdates dolomite types 1 and 2. Dolomite types 3 and 5 are commonly very hard to distinguish and they could therefore be related to a similar mode and time of formation.

The nonplanar dolomites types (6 and 7) are regarded as late- stage dolomites. While nonplanar-c dolomite is clearly the latest phase (it postdates all other dolomite types), the timing of nonplanar-a dolomite is more difficult to assess. It occurs only in certain zones and wiped out all pre-dolomite textures. It is commonly observed within the karst-facies where it replaced a precursor dolostone. In the Puckett well such an occurrence is crosscut by later (?Pennsylvanian) fractures filled with pyrite, pyrobitumen and nonplanar cements. This cross-cutting relationship suggests a pre- Pennsylvanian age of the nonplanar -a dolomite.

With an increasing depth of burial (increasing geothermal gradient), the dolomite textures show no systematic transition from one kind of dolomite to another, such as from planar-e to nonplanar (e.g. Figure 15). Such a gradation should be recorded with increasing geothermal gradient (Gregg and Sibley, 1984; Shukla, 1986; Sibley and Gregg, 1986). The lack of such a transition might indicate a lack of pervasive neomorphism of early formed dolomite during burial diagenesis (Gregg and Sibley, 1986). Stepanek (1988, p. 114) noticed a similar lack of pervasive reequilibration (of stable isotopes) of early formed dolomite during burial despite extensive recrystallization of associated limestones.

Relative Timing

The dolomite paragenetic sequence can be constraind by a major period of karstification, which predates the deposition of Middle Ordovician Simpson Group deposits (pre-Middle Ordovician unconformity and karstification), and by the onset of hydrocarbon generation in Ellenburger carbonates.

Early-diagenetic, ?penecontemperaneous dolomite, characterized by dolomite type 1, pre-dates karstification and all other dolomite types. This type is therefore considered to have

formed prior to Middle Ordovician karstification during Lower Ordovician Ellenburger deposition. Kupecz (1989) used a similar argument to constrain early-diagenetic dolomites (= pre-Middle Ordovician), which compare to dolomite type 1 of this study.

Dolomite type 5 predates the onset of hydrcarbon formation, but post-dates replacement dolomite 1 and 2. In samples from the deep Delaware basin pyrobitumen has been found to coat crystals of dolomite type 5, followed by late calcite and/or nonplanar-c dolomite cements. These late phases can not have formed prior to the emplacement of mature hydrocarbons. Using the Lopatin method for thermal maturity of organic matter (Waples, 1980), the timing of hydrocarbon generation can be estimated and the formation of late-stage dolomites and calcites can be bracketed. By using stratigraphic values for the Delaware basin obtained from Stewart (1983, column 19) and geothermal gradients of 21° C and 28° C (Hills, 1984, p. 265) the onset of hydrocarbon generation within the Ellenburger and the overlying Simpson Group is estimated to be Late Pennsylvanian to Middle Permian (Figure 23).

Using these estimates it can be concluded that late-stage calcite and nonplanar-c dolomite cements can not be older than Late Pennsylvanian /Early Permian. This would indicate a deep burial setting for these latest phases (Figure 23).

A similar Late Pennsylvanian to Early Permian age and a deep burial setting of these late dolomite and calcite cements have been suggested in previously published studies on Ordovician dolomites from West Texas.

High fluid-inclusion homogenization temperatures and light oxygen-isotope compositions of these late dolomites were used by Lee and Friedman (1987) to infer a deep burial setting for those late dolomites. Ijirigho (1981, 1988) presented evidence that the development of excellent secondary porosity occurred during Late Pennsylvanian to Early Permian. At the same time permeability barriers were developed by the precipitation of late stage cements in the secondary pore spaces (Ijirigho, 1981). Stepanek (1988) concluded in his study of dolomitization of collapse breccias in the Ellenburger equivalent El Paso Group, Franklin Mountains, West Texas, that emplacement of saddle (nonplanar-c) dolomites must have occurred later than Devonian time. Taken together, the timing of the late stage cements coincides with the closing stages of the Ouachita orogeny in Late Pennsylvanian to Early Permian time . In the Permian basin this period was a time of high heat flow, rapid basin subsidence and filling (Horak, 1986), creating a favourable setting for the migration of basinal fluids from which the late stage cements precipitated.

These relationships indicate that most of the dolomitization of Ellenburger carbonates must have occurred between deposition of the Ellenburger carbonates and before the end of the Mississippian. During that time period the Tobosa basin was characterized by gradual

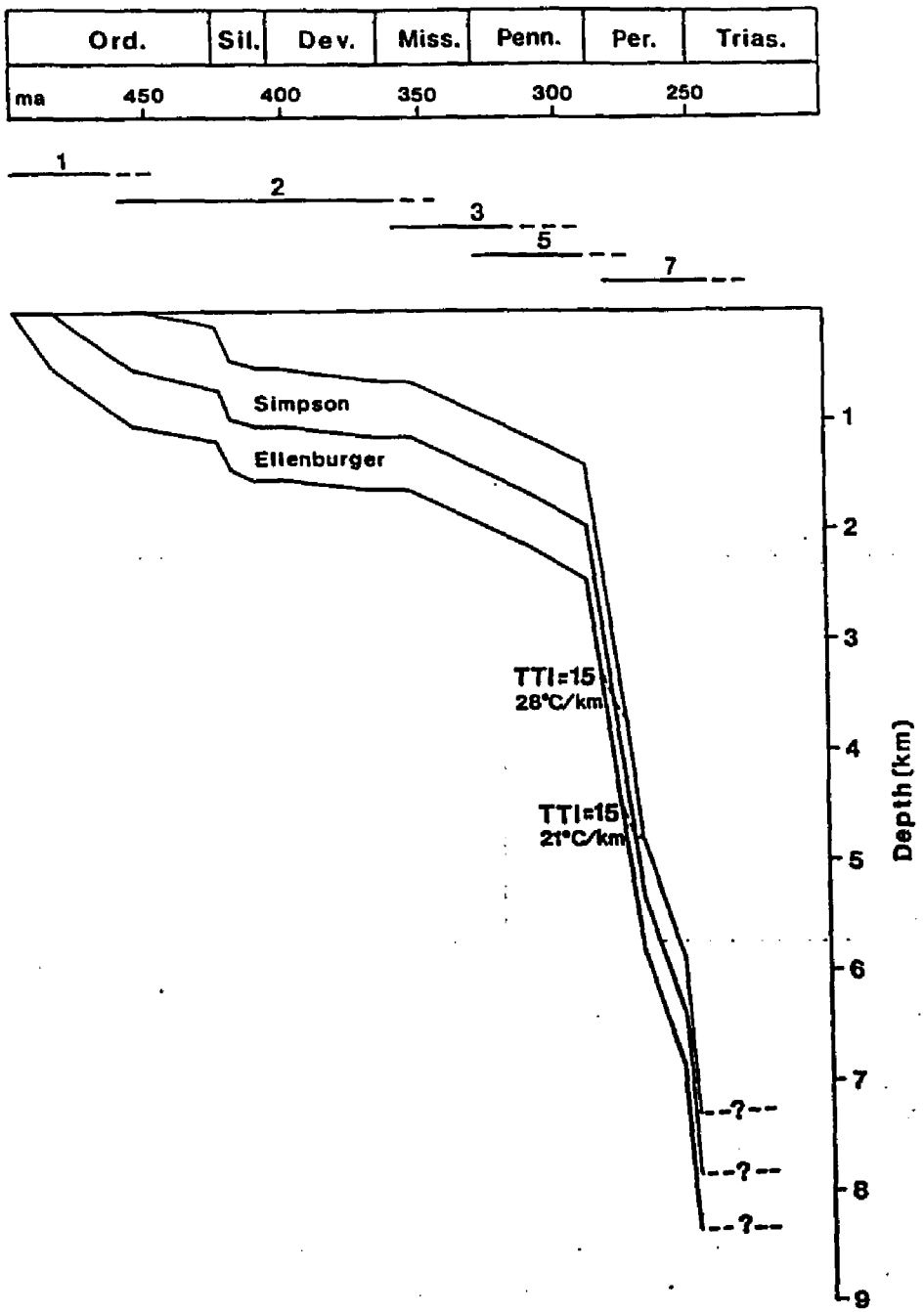

Figure 23. -- Burial-history plot for Ellenburger and Simpson Group rocks in Delaware Basin during the Paleozoic, using compacted stratigraphic thickness data from Stewart (1983). Time- temperature index values (TTI) of 15 are indicated for geothermal gradients of 21° C and 28° C, and a surface temperature of 20° C. Paragentic sequence for part of the dolomite-rock textures is indicated with solid horizontal bars. Dashed lines indicate greater uncertainty concerning timing (see Timing section for details). Numbers refer to dolomite-rock textures (*cf.* figure 22).

subsidence. Major changes occurred at the end of the Pennsylvanian/Early Permian, when the formerly, primarily stable West Texas Craton experienced major disturbances, probably in response to increasing tectonism along the Quachita front (Wuellner et. al., 1987). The Delaware basin subsided rapidly (Figure 23), Ellenburger and Simpson Group strata entered the oil- generation window and passed through it very rapidly. This drastic change is reflected in the dolomite textures with dissolution, porosity creation, hydrocarbon migration and late stage cementation occurring in a relatively small time interval.

Geochemistry of dolomite-rock textures

The separation of Ellenburger dolostones into seven dolomite- rock textures is based on differences in crystal-boundary shape and crystal-size distribution. These dolomite types show also notable differences in their major and minor element distributions. An electron microprobe was used to analyze (n=597) and compare the chemical composition of the different dolomite textures. There exist notable differences among the seven dolomite-rock textures, as well as among dolomites interpreted to represent cements and dolomite textures thought to be of replacement origin.

General characteristics. -- The dolomites vary widely in composition, ranging from near stoichiometric dolomite ($Ca_{50}\ Mg_{50}\ (CO_3)_2$) to calcian dolomites ($Ca_{55.3}\ Mg_{44.7}\ (CO_3)_2$), and dolomites enriched in Fe and/or Mn. Iron substitution is more common. The highest iron concentration, 21.3 mole % $FeCO_3$ (ankeritic composition), was observed in rims of planar-e mosaics with the formula $Ca_{52.6}\ (Mg_{21.3}\ Fe_{21.1})$. The highest Mn content of 1 mole % was recorded in the above sample. Dolomite cements commonly show a positive correlation between Fe and Mn, whereas in replacement dolomites this correlation is weak or not present. $CaCO_3$ varies between 44.3 mole % and 55.8 mole %. $MgCO_3$ ranges from 25.4 mole % to 51.3 mole %, mostly as a result of substitution of Fe for Mg into the dolomite lattice. $SrCO_3$ is present only in small amounts (maximum concentration is 2 mole %), is consistently low for all dolomite types, and commonly below the detection limit of the microprobe.

Geochemistry of dolomite types. -- Petrographic and geochemical characteristics of the different dolomite types are listed in table 2. Table 3 shows r^2-correlations of major and minor elements for the different dolomite types.

Dolomite type 1 (unimodal, very fine- to fine-crystalline planar-s mosaic dolomite). -- Forty-nine analyses from four wells have been performed on this replacement dolomite. Analyses are from lithofacies 1 (laminated dolomudstones) and lithofacies 3 (mottled dolomudstones/wackestones), and from lithoclasts of karst breccias.

This type is characterized by low average and absolute values of Fe, Mn, and Sr. It is calcium rich ($CaCO_3$: m = 52.2; s = 1.6). If the values of the karst breccias and of lithofacies 1

Table 2: Petrographic and Geochemical Characteristics of Dolomite Types.

Dolomite Type	Characteristics	Mean Values (Std. Dev.)					
		CaCO3	MgCO3	Fe	Mn	Sr	Mg
		(mole %)		(ppm)			
1 Replacive Dolomite	v.f.-f.-xx mosaics; CL: homgen. dull; low in Fe, Mn, Sr, Ca-rich.	52.2 (1.6)	47.4 (1.7)	858 (1057) (n = 49)	185 (233)	85 (118)	123266 (5412)
2 Replacive Dolomite and Cement	m.-c.-xx mosaics, CL: mottled cores, Thin zoned rims; low in Fe, Mn, Sr;	50.9 (.7)	48.2 (1.0)	1101 (1843) (n = 48)	227 (174)	13 (39)	126634 (3382)
3 Void-Filling Dolomite	c.-v.c.-xx planar-s; CL: mottled cores, zoned rims; Cement: Fe, Mn (+) Replacive: Fe, Mn (-)	51,0 (1.1)	48.5 (1.2)	1153 (1976) (n = 189)	216 (213)	58 (84)	127332 (3677)
4 Void-Filling Dolomite	m.-c.-xx mosaics, planar-e; CL: zoned; high Fe, Mn;	52.3 (1.8)	45.7 (4.4)	8719 (21550) (n = 132)	596 (993)	88 (140)	118249 (13238)
5 Void-Filling Dolomite	m.-c-xx, planar-e; CL: zoned; high Fe, interm. Mn, low Sr;	50.9 (.8)	48.3 (1.3)	2387 (3239) (n = 137)	308 (429)	33 (69)	126517 (12651)
6 Replacive Dolomite	c.-v.c.-xx mosaics, npl; CL: homog. mottled; low Fe, Mn, Sr;	49.5 (.7)	50.4 (.6)	241 (365) (n = 13)	119 (112)	67 (55)	132051 (1566)
7 Void-Filling Dolomite	c.-v.c.-xx mosaics, npl; CL: nonlu., Ca-rich, high Fe, interm. Mn, low Sr;	52.6 (.9)	45.7 (1.1)	6635 (2272) (n = 29)	261 (192)	10 (29)	118348 (2744)
Dolomite Cements (Total)	CL: zoned; high Fe, Mn; low Sr;	51.4 (1.6)	47.3 (3.0)	4843 (13087) (n = 392)	396 (660)	50 (102)	123378 (9146)
Replacive Dolomite (Total)	CL: homog. mottled; low Fe, Mn, Sr;	51.3 (1.5)	48.2 (1.6)	448 (669) (n = 205)	173 (177)	66 (91)	126197 (5061)

v.f. = very fine; m.-c.-xx = medium- to coarse crystalline; c.-v.c-xx = coarse- to very coarse-crystalline; CL = Cathodoluminescence; (+) = enriched; (-) = depleted; npl = nonplanar;

Table 3: Correlation Coefficients (r2) of Major and Minor Elements for the Different Dolomite-Rock Textures.

Dolomite-Type		Fe - Mn	Fe - Mg	Mn - Mg	$SrCO_3$ - $CaCO_3$
	Total (n=49)	r2: .68 p: .0000	r2: -.63 p: .0000	r2: -.55 p: .0001	r2: .74 p: .000
1	Karst Facies	r2: .59 p: .0048	r2: -.37 p: .0927	r2: -.28 p: .2252	r2: .63 p: .0025
	Facies 1 + 3	r2: -.15 p: .4441	r2: -.05 p: .7845	r2: -.29 p: .1277	r2: -.35 p: .0612
	Total (n=48)	r2: -.04 p: .7588	r2: -.52 p: .0002	r2: .37 p: .0103	---------- ----------
2	Cement	r2: -.17 p: .4730	r2: -.52 p: .0052	r2: .32 p: 1633	---------- ----------
	Replac.	r2: .41 p: .0268	r2: -.13 p: .5100	r2: .34 p: .0767	r2: .47 p: .0107
	Total (n=189)	r2: .51 p: .0000	r2: -.30 p: .0000	r2: .02 p: .7682	---------- ----------
3	Cement	r2: .53 p: .0000	r2: -.34 p: .0002	r2: -.03 p: .7483	---------- ----------
	Replac.	r2: .22 p: .0610	r2: .09 p: .4933	r2: -.59 p: .0181	r2: .23 p: .0546
	Total (n=123)	r2: .61 p: .0000	r2: -.90 p: .0000	r2: -59 p: .0000	---------- ----------
4	Wells 1 - 4	r2: .59 p: .0000	r2: -.58 p: .0000	r2: -.21 p: .0835	r2: .23 p: .0534
	Well 5	r2: .58 p: .0000	r2: -.96 p: .0000	r2: -.61 p: .0000	---------- ----------
5	Cement (n=137)	r2: .69 p: .0000	r2: -.71 p: .0000	r2: -.40 p: .0000	---------- ----------
6	Replac. (n=13)	r2: .50 p: .0823	r2: -.04 p: .8721	r2: -.58 p: .0379	---------- ----------
7	Cement (n=29)	r2: -.19 p: .3296	r2: -.71 p: .0000	r2: -.12 p: .5463	r2: -.46 p: .0010
Cements, all wells	(n=392)	r2: .60 p: .0000	r2: -.87 p: .0000	r2: -.57 p: .0000	---------- ----------
Replac., all wells	(n=205)	r2: .49 p: .0000	r2: -.36 p: .0000	r2: -.09 p: .1887	r2: .48 p: .0000

(laminated dolomudstones/wackestone) and lithofacies 3 (mottled dolomudstones/ wackestones) are considered separately, important differences are apparent. The values of minor elements of lithofacies 1 and 3 are very low (Table 2). Higher Fe values result from lithoclasts of the karst breccias, which show evidence of overprint by Fe-rich fluids (e.g. fractures filled with ferroan dolomite). Notable geochemical differences have been observed between interlaminated dark, very fine crystalline, planar-s dolomite and fine crystalline clear planar-s dolomite in laminated dolomudstone facies. The center of clear crystals compare geochemically to the dark, very fine crystalline dolomites, while the rims of the clear and larger crystals are enriched in iron.

Correlation coefficients (r^2) reveal differences between the samples from the karst facies and lithofacies 1 and 3 (Table 3). r^2 values for samples of lithofacies 1 and 3 are statistically not significant. Note the positive correlation between $SrCO_3$ and $CaCO_3$ in the karst facies.

Dolomite type 2 (unimodal, medium- to coarse-crystalline planar- s mosaic dolomite). -- This type comprises replacement dolomite and cements, and is characterized by nonmimic replacement of allochems and a good preservation of original depositional textures.

Geochemically it is close to a stoichiometric composition (Table 2), and it has higher mean and absolute values of Fe and Mn than type 1. Sr is present in similar low amounts. Replacement dolomites and cements are geochemically distinct. Cements have higher Fe (m = 1796 ppm, s = 2560) and lower Mn values (m = 180 ppm, s = 142) than replacement phases (Fe: m = 623 ppm, s = 769; Mn: m = 261, s = 186). $CaCO_3$ and $MgCO_3$ mole percentages are nearly the same for both replacement dolomites and cements. Cements and replacements are distinct in their r^2-values for Fe- Mg (Table 3).

Dolomite type 3 (coarse- to very coarse-crystalline planar-s dolomite). -- The geochemistry of this type compares for most parts to dolomite type 2, except that type 3 shows higher Fe concentrations (m = 1153, s = 1976). This is due to Fe-rich zones in cements of crystals lining and/or filling pore spaces and fractures. As with dolomite type 2 there are geochemical differences between cementing and replacing phases. Cements have higher Fe values (m = 1681 ppm, s = 2309) and Mn (m = 244 ppm, s = 238) values than replacement dolomites (Fe: m = 244 ppm, s = 377; Mn: m = 168, s = 148).

r^2-values for cements and replacement dolomite are distinct. Replacive dolomites show no correlations. Cements exhibit a weak positive correlation for Fe-Mn, and Fe-Mg are weakly negatively correlated.

Dolomite type 4 (medium- to coarse-crystalline planar-e mosaic dolomite). -- Analyses of this dolomite cement yielded the highest Fe and Mn values in the studied cores. The highest values are from outer ferroan to ankeritic zones of planar-e crystals in well 5. $FeCO_3$ values range from 0 to 21.3 mole % (0 - 118000 ppm), and $MnCO_3$ from 0 to 1.0 mole % (0 - 5784 ppm). Sr also reaches its highest values in this type (2.0 mole %, 770 ppm). Fe shows a strong negative correlation with Mg (r^2 = -.90, p = .0000) which is also reflected in the wide range of the magnesium-ion concentration, ranging from 25.5 mole % to 50.8 mole %. Even if the data from the outer ferroan zones are considered separately the values for Fe and Mn are still higher than in dolomite types 1 to 3. Sr, however is comparatively low. It is also apparent that the wide range of $MgCO_3$ is due to the substitution of Fe for Mg into the dolomite lattice (r^2 = -.90).

Dolomite type 5 (medium- to coarse-crystalline planar-e dolomite). -- This type comprises dolomite cements that come close to a stoichiometric composition, with a mean of 50.9 mole % $CaCO_3$ (s = .9). Fe values as high as 3.1 mole % $FeCO_3$ (17801 ppm) and Mn values up to 0.5 mole % $MnCO_3$ (2650 ppm) have been analyzed. Sr values show similar low amounts as previous types. Fe and Mn show a positive correlation (r^2 = .69, p = .0000), whereas Fe and Mg show a negative correlation (r^2 = -.71, p = .0000).

Dolomite type 6 (coarse- to very coarse-crystalline nonplanar-a dolomite). -- This replacement dolomite comes close to stoichiometric values of Ca and Mg and shows a slight Ca depletion. It is low in minor elements and high in Mg. Geochemical analyses performed on Fe-rich nonplanar-a dolomites could not be used for computation, because they were consistently too low in total weight percentage (< 90%). The nature of the dolomite crystals (e.g. high surface irregularities, holes) did not allow a satisfactory chemical analysis. The Fe values of these nonplanar-a dolomites, however, were much higher in this type (mean = 4483; s = 745). This type exhibits no correlations.

Dolomite type 7 (coarse- to very coarse-crystalline nonplanar-c dolomite). -- This dolomite cement is a calcium-rich dolomite with a mean of 52.6 mole % $CaCO_3$. It has high Fe values (m = 6635 ppm, s = 2272), Mn and Sr are low and compare to all other types. Fe and Mg show a negative correlation (r^2 = -.71, p = .0000).

Dolomite cements. -- Dolomites interpreted as cements have the highest trace element concentrations found in this study (Table 3). Fe and Mn are enriched, while Sr is depleted if compared to the replacement dolomites. The statistically significant correlation coefficients are negative except for Fe-Mn, which shows a positive correlation ($r^2 = .60$, $p = .0000$).

Replacement dolomite. -- Replacement dolomites are characterized by low Fe and Mn values, the average Sr-content is slitly higher than in dolomite cements, but still very low if compared to values in more recent dolomite counterparts. Mg values are also higher than in dolomite cements. In general, replacement dolomites are mostly earlier phases (except for dolomite 6), which are followed by later dolomite cements.

r^2-values for replacement dolomites are distinct from cements. Trace element correlations of Fe, Mn and Mg are weak or not present. A weak correlation exists between $SrCO_3$ and $CaCO_3$.

Compositional Zonation. -- Staining of thin sections did not yield many results with respect to zonation. This lack of staining led to the conclusion that the iron content of most Eilenburger dolomites is below the detectable limit (< 1 % FeO) of the staining technique (Lee and Friedman, 1987, p. 546). This assumption, however, is not supported by the geochemical data and luminescent characteristics of the dolomite types, which show in parts a complex zonation (e.g. figures 24, 26).

Compositional zonation, as observed under cathodoluminescence and by using the microprobe, is a result of incorporation of trace elements into a crystal growing from solution. In dolomites trace elements may partition into either the calcium or magnesium site. The incorporation of a trace element into dolomite is governed by the distribution coefficient (D). When $D > 1$, trace elements will be preferentially incorporated into the crystalline phase, when $D < 1$, trace elements will be preferentially concentratedin the aqueous phase. Estimates of distribution coefficients of dolomite listed in Veizer (1983 a) show D's for iron and manganese to be greater than 1, strontium has D's smaller than 1.

Ideally, trace element concentrations in dolomite provide means to estimate the composition of the fluid from which the dolomite precipitated (Veizer, 1983 a), and to indicate the direction of fluid flow during diagenesis (e.g. Veizer, 1983 a; Gregg and Shelton, 1989; Machel 1989). However, such calculations, as well as the interpretation of this study, are based on the assumption that the concentration of trace elements in the crystal is governed by equilibrium reactions, and that the Mn- and Fe-contents of dolomite precipitated in

equilibrium with the pore-water are determined by the Mn/Ca and Fe/Ca ratios of the pore-water and the corresponding distribution coefficients.

Petrographic observations, however, indicate the presence of compositional sector zoning (e.g. Reeder and Prosky, 1986) in Ellenburger dolomites (e.g. Figures 28, 24). The presence of such phenomena indicates that both major and minor element distributions of these dolomites are influenced by factors relating to the mechanisms and perhaps rates of growth on different crystal-faces, and do not represent equilibrium (Reeder and Prosky, 1986; Reeder and Paquette, 1989). Bulk-solution disequilibrium, such as discussed by Pingitore (1982) and Veizer (1983 a), may be far more common than previously recognized. Such disequilibrium would seriously compromise geochemical models currently used in carbonate diagenesis, as well as the concept of cement stratigraphy. Extreme care must therefore be exercised in the interpretation of geochemical data, especially if only bulk geochemical data are available.

Zonation is best developed in void-filling dolomites (e.g. dolomite types 3, 4, 5); replacement dolomites (e.g. dolomite types 1, 2, 6) shows no zonation, except where followed by thin rims of dolomite cements. In general, zonation of crystals is not identical in different samples, therefore crystal growth was not necessarily synchronous in the studied wells.

A commonly observed cathodoluminescence (CL) pattern consists of mottled, dull to dirty orange-red cores, followed by zoned rims with dull-brown, bright and nonluminescent zones in various combinations. A transition from mottled orange-red, through dull- brown to nonluminescent is consistent with an increasing Fe content, reflecting the quenching effect of Fe on luminescence. Bright luminescent hairlines have higher Mn than Fe concentrations, indicating Mn might activate luminescence (Richter and Zinkernagel, 1981; Pierson, 1981; Fairchild, 1983; Machel, 1985; Gawthorpe, 1987).

Characteristic CL-patterns and quantitative variations in chemistry of various dolomite types are shown in Figures 24 through 34.

The geochemical traverses corroborate the cathodoluminescence patterns and the backscattered electron images, which reveal zonation in void-filling dolomites. A marked chemical zonation exists commonly within individual crystals. This zonation could indicate abrupt changes in pore-fluid chemistry. This is particular evident in crystals of dolomite 4, where the Fe-concentration changes abruptly from 0 to 5-15 mole % $FeCO_3$ from the core to the rim (Figure 34). Fe zonation has also been observed in dolomite types 3 and 5 (Figures 24-26, 28, 32). Zone boundaries between Fe-rich and Fe-poor zones in cements are usually straight and continuous, in contrast to contacts between cores and overgrowths, which are

commonly irregular and anastomosing (Figure 24). Such irregular contacts may occur between individual crystals of different dolomite generations (e.g. dolomite 5 followed by dolomite 7) (Figure 24), or separate replacement dolomite from cements within individual crystals (e.g. in dolomite type 3) (Figures 24, 29, 30).

In general, there is an increasing Fe and Mn substitution during progressive dolomitization. Cores and inner zones of dolomite crystals have lower Fe and Mn concentrations than later dolomite cements, although inner parts that are enriched in Fe compared to rims are observed in places in cements of dolomite type 3. Common to all planar void-filling dolomites, however, are marked changes in Fe and Mn substitution, which are interpreted as aresult of abrupt changes in pore-fluid chemistry during dolomitization. Alternative mechanism that can explain iron-zonation, such as self-patterning processes (e.g. Gregg, 1988; Merino, 1984) might produce similar zoning patterns. Such diseqilibrium conditions need future research.

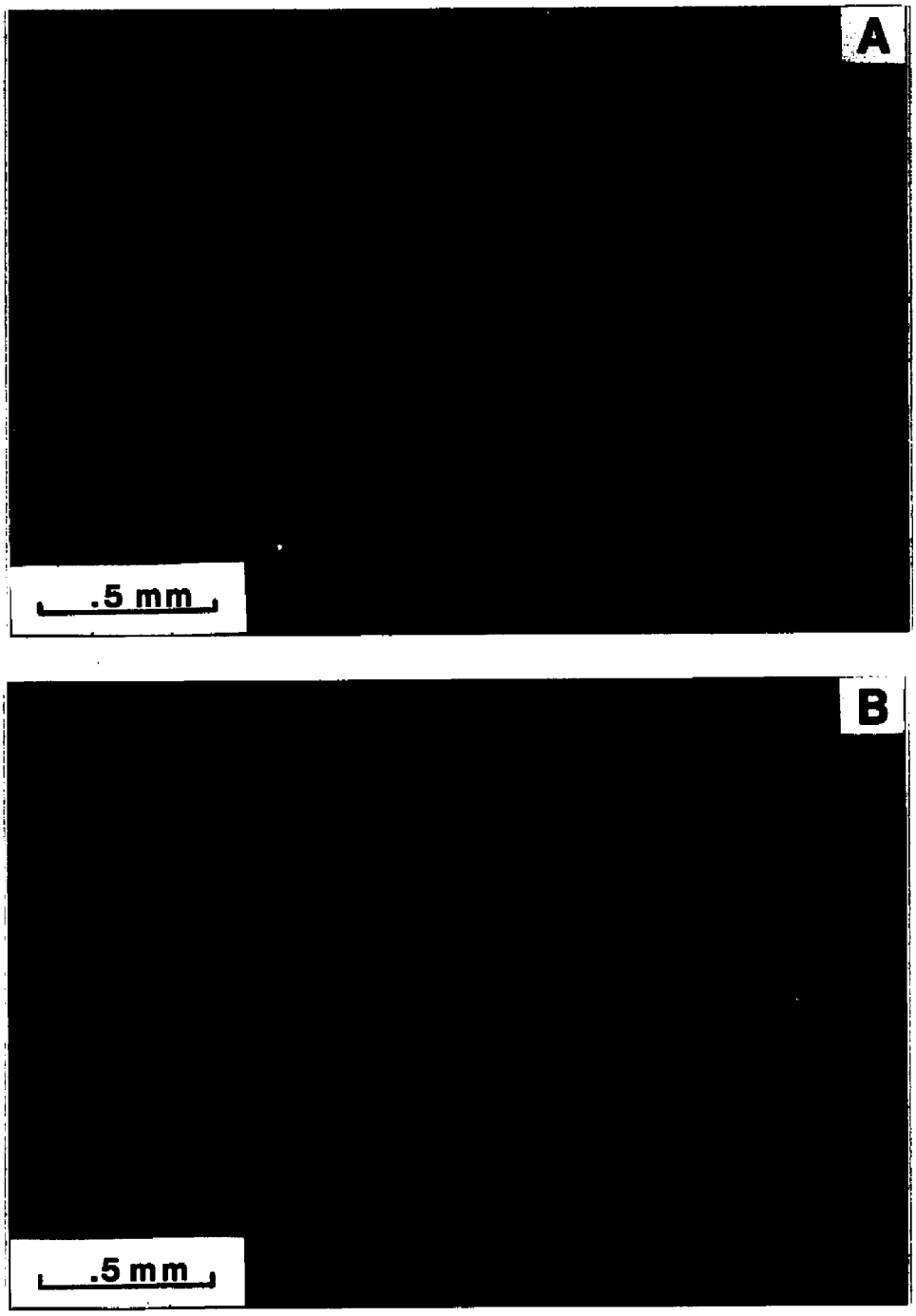

Figure 24. -- Photomicrograph pair of coarse-crystalline void-filling dolomite. A) Coarse-crystalline, clear dolomite filling void in medium-crystalline dolomite (cloudy). Plane polarized light. B) Same view under the luminoscope reveals different dolomite generations, that cannot be recognized under plane polarized light: Early replacive dolomite (a) was discontinuously overgrown by zoned dolomite cement (b), which in turn was followed by nonplanar-c dolomite (c), occluding porosity. Sample from 22,635 ft (6,899 m), well 3.

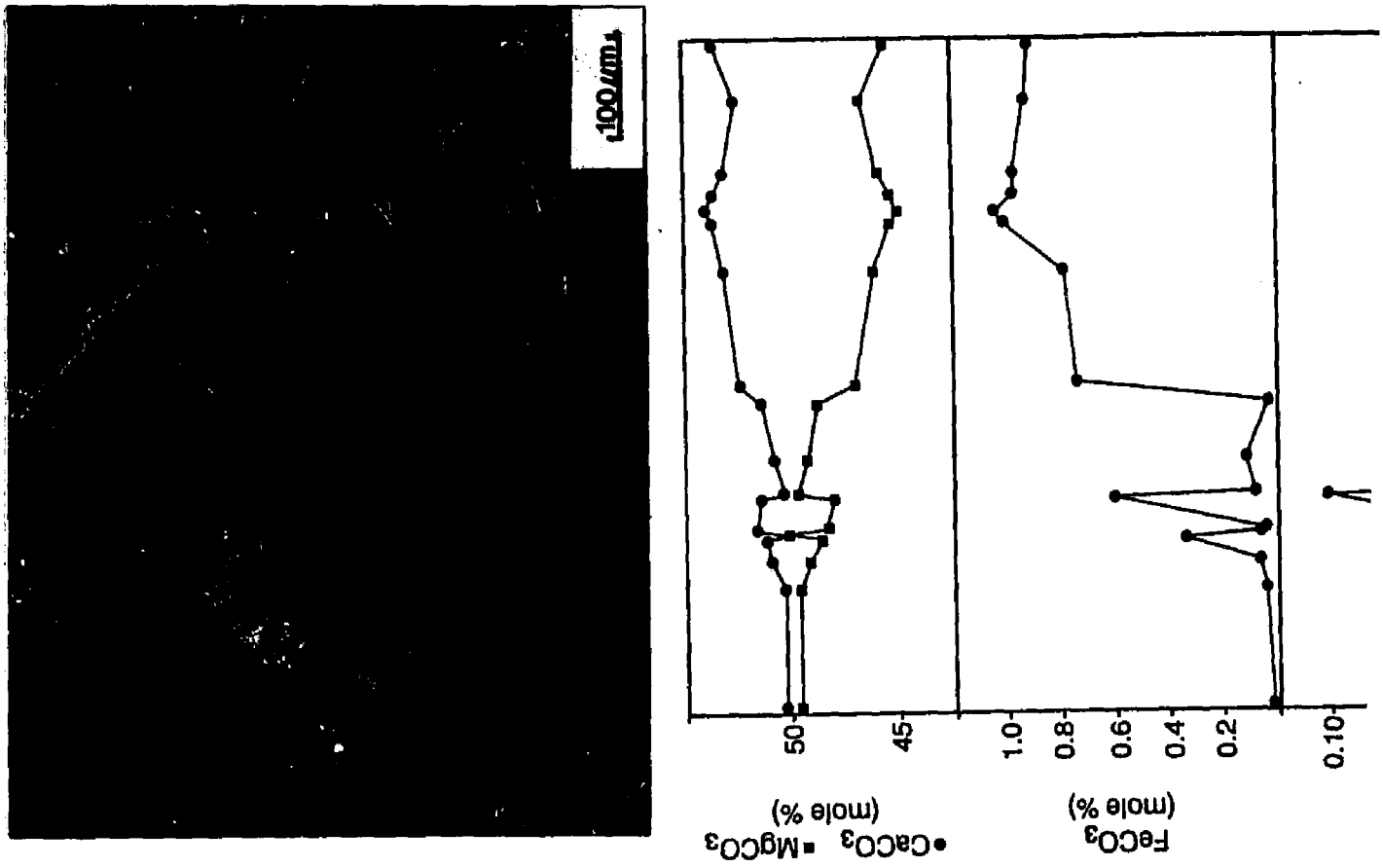

Figure 25. -- Back-scattered electron image (BSI) of planar-s dolomite shown in figure 24 under (b), with corresponding geochemical traverse. Note increasing Fe-content outward in the rim, resulting in a dull to nonluminescent cathodoluminescence pattern and a very light BSI-zone. Nonplanar-c dolomite has lower Fe-concentrations, hence a slight darker BSI-color. Change in stoichiometry is due to substitution of Fe for Mg in outer rims of planar dolomites and in nonplanar dolomite cements, which commonly are also Ca-rich. Sample from 22,635 ft (6,899 m), well 3.

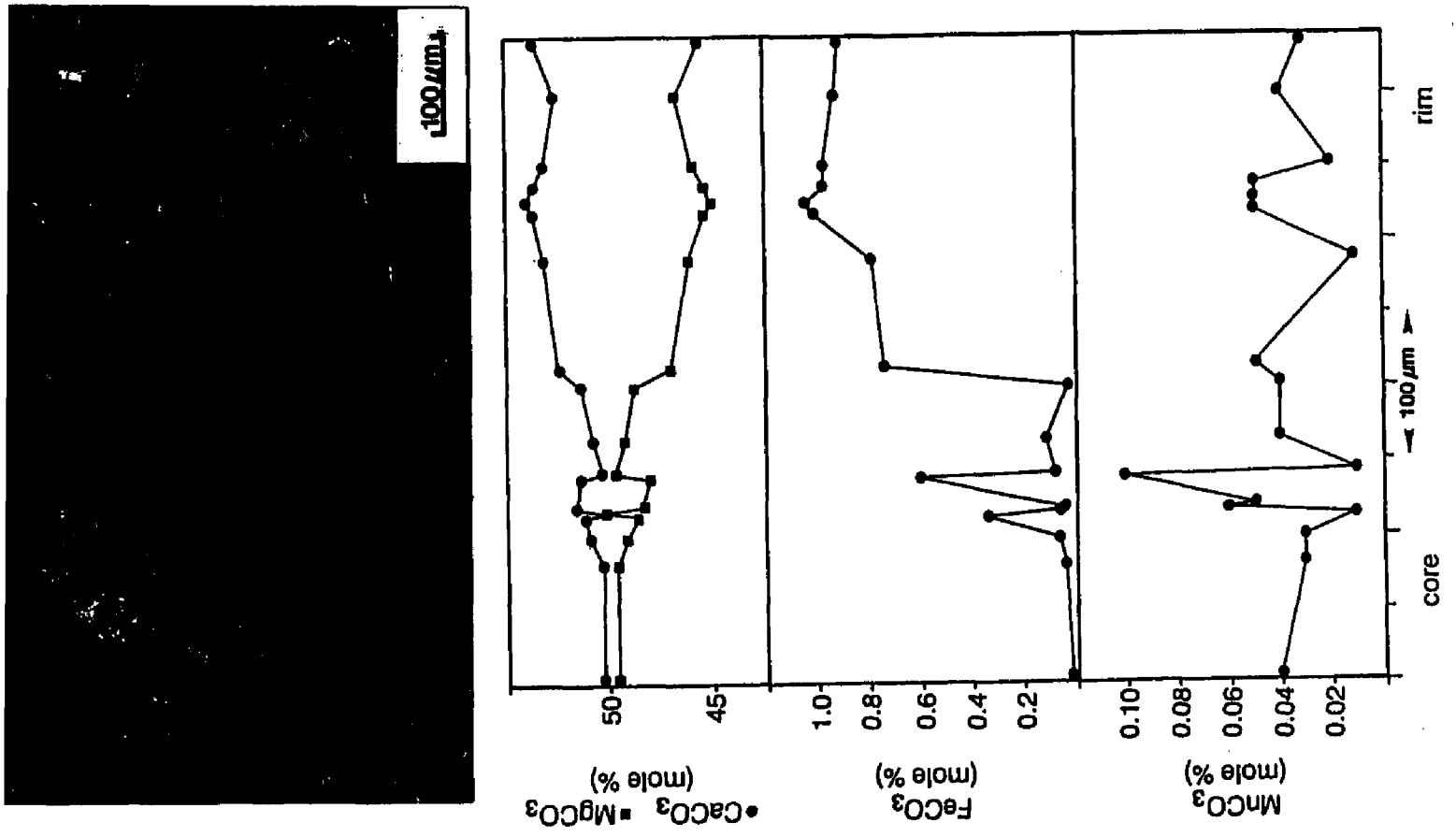

5. -- Back-scattered electron image (BSI) of planar-s dolomite shown in figure 24
ith corresponding geochemical traverse. Note increasing Fe-content outward in
ilting in a dull to nonluminescent cathodoluminescence pattern and a very light
onplanar-c dolomite has lower Fe-concentrations, hence a slight darker BSI-color.
tolchiometry is due to substitution of Fe for Mg in outer rims of planar dolomites
anar dolomite cements, which commonly are also Ca-rich. Sample from 22,635 ft
/ell 3.

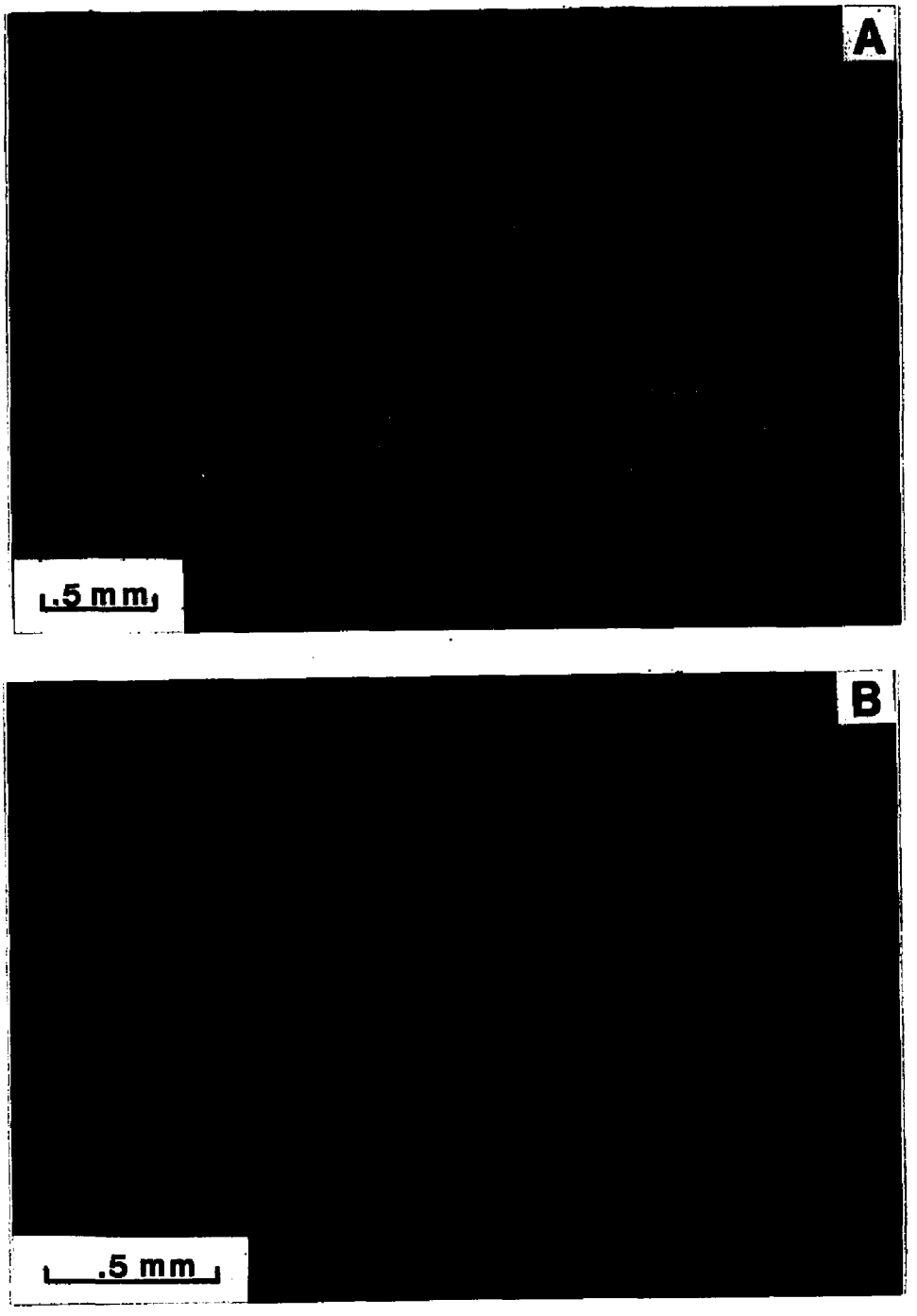

Figure 26. -- Photomicrograph pair of dolomite-rock texture 3 (coarse- to very coarse-crystalline planar-s dolomite). A) Planar-s dolomite filling void in earlier dolomite (type 2), and displaying a cloudy core, clear rim texture. Plane polarized light. B) Close-up of A under cathodoluminescence shows pronounced zonation, where individual zones can be traced continuously around several crystals. Arrows indicate same spot in both figures. Sample from 21,278 ft (6,486 m), well 2.

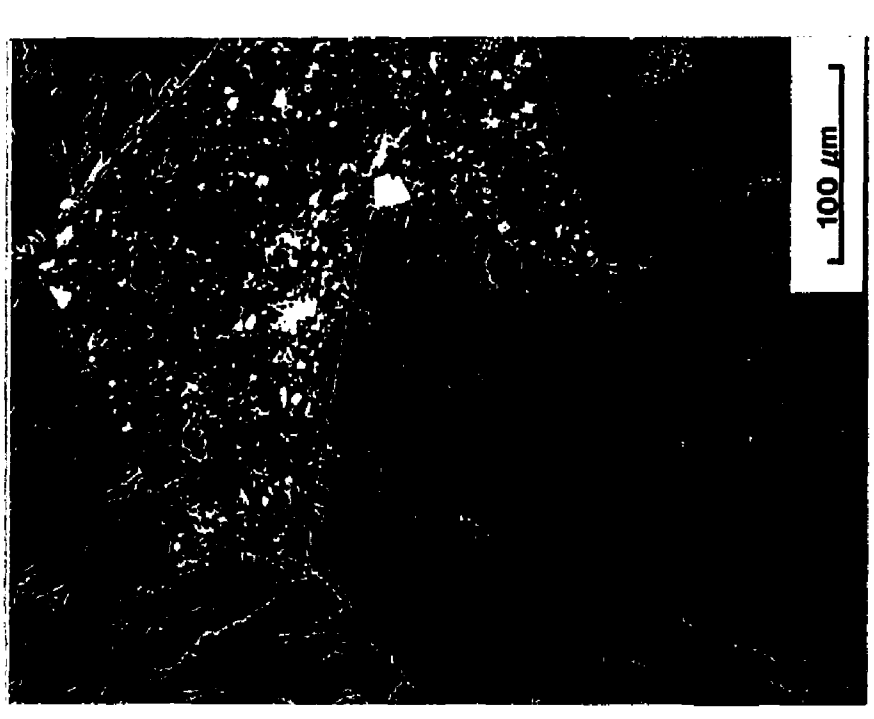

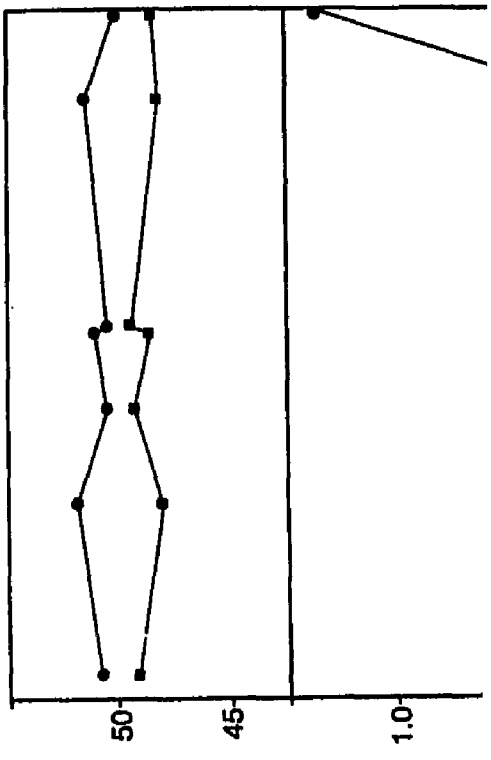

Figure 27. -- Back-scattered electron image of dolomite-rock texture 3 (coarse- to very coarse-crystalline planar-s dolomite) as shown in Figure 26, with corresponding geochemical traverse. Note Fe-rich rim (light). Bright luminescent hairline zone in Figure 26B corresponds to zone where Mn > Fe. Sample from 21,278 ft (6,468 m), well 2.

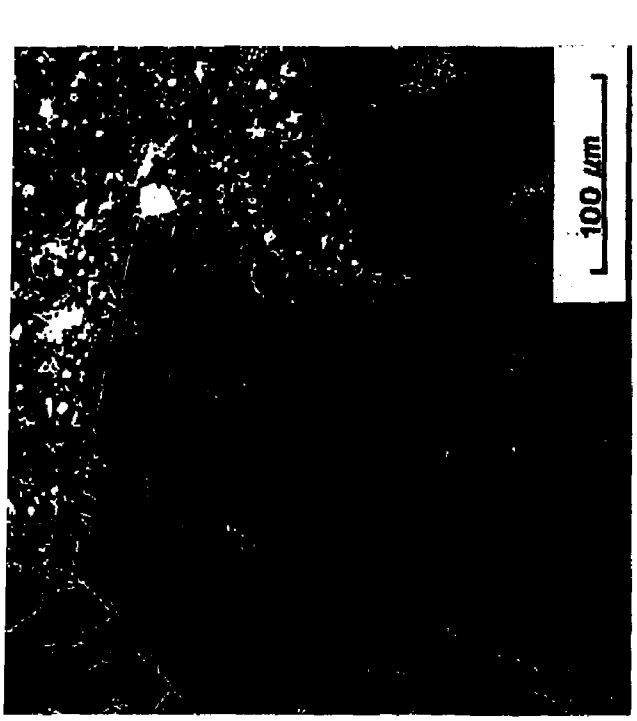

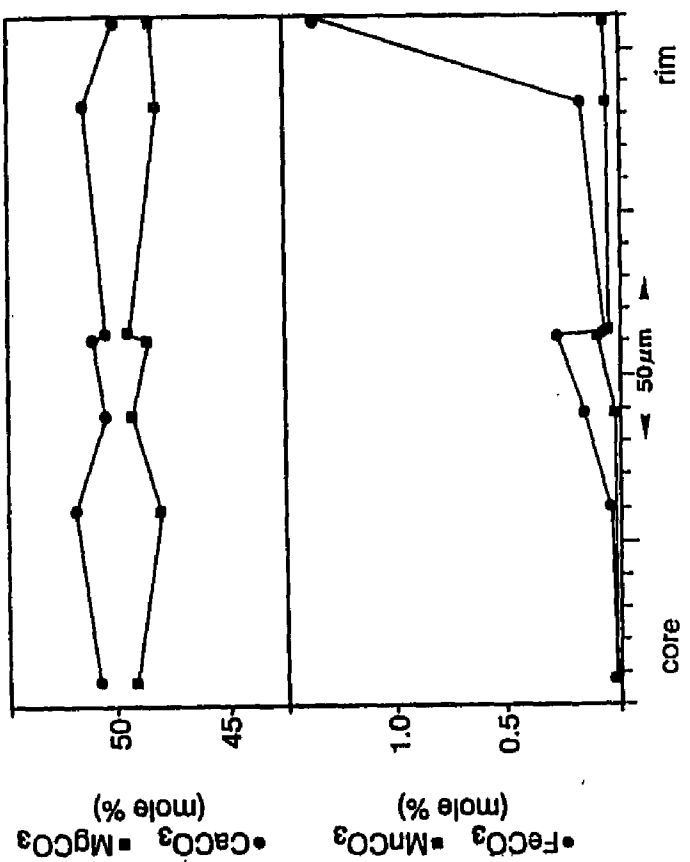

- Back-scattered electron image of dolomite-rock texture 3 (coarse- to very
e planar-s dolomite) as shown in Figure 26, with corresponding geochemical
e-rich rim (light). Bright luminescent hairline zone in Figure 26B corresponds
In > Fe. Sample from 21,278 ft (6,468 m), well 2.

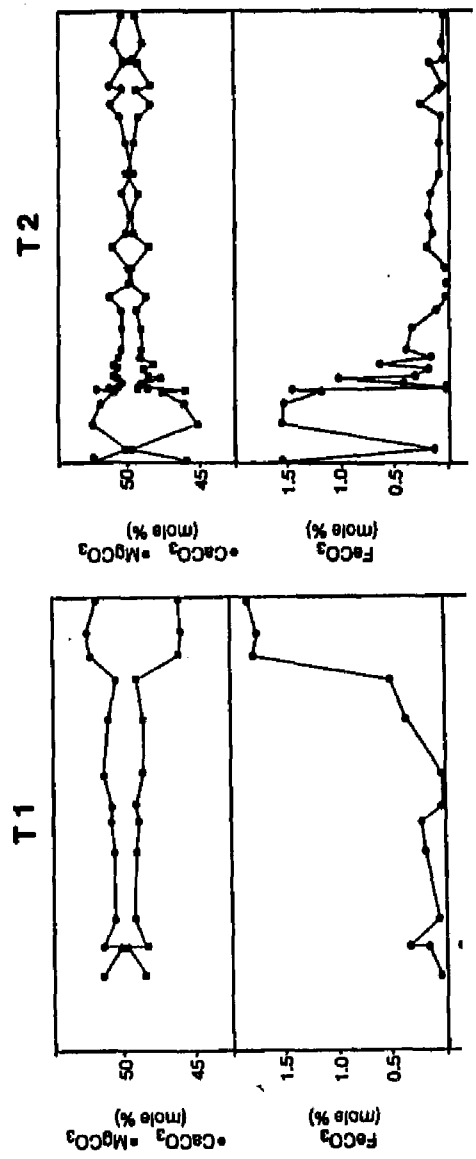

Figure 28. -- Back scattered electron image (BSI) of dolomite-rock texture 3 (coarse- to very coarse-crystalline planar-s dolomite), and corresponding traverses (T1 and T2). Note irregular boundaries between replacive dolomites of the cores and zones of dolomite cements. Fe-rich outer zones (light) are followed by nonplanar-c void-filling dolomite (c) with a sharp and straight contact. Sample from 22,268 ft (6,787 m), well 3.

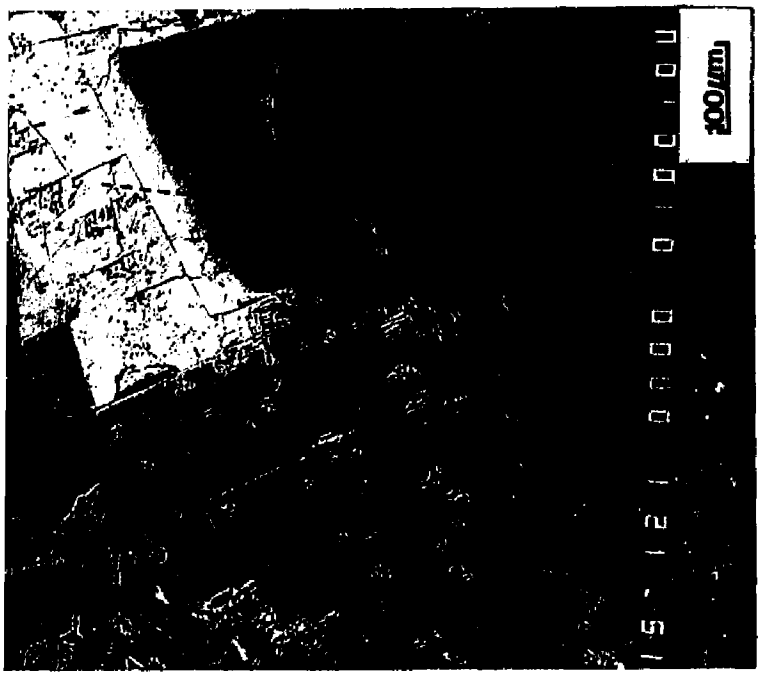

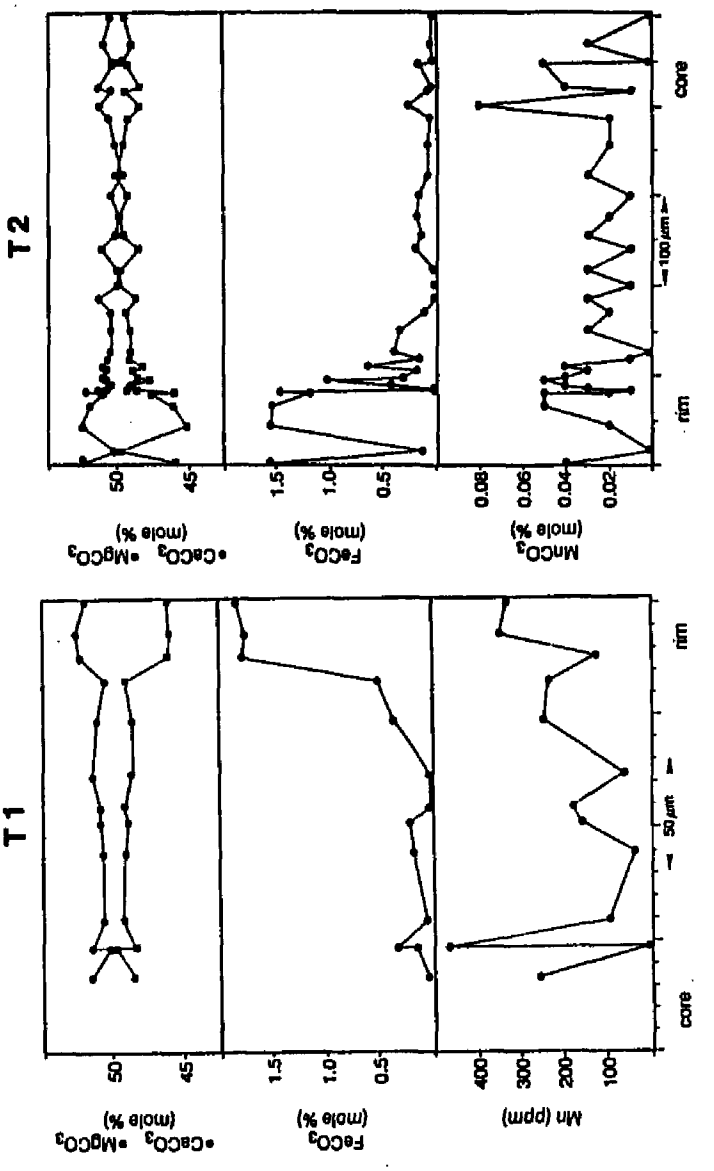

ure 28. -- Back scattered electron image (BSI) of dolomite-rock texture 3 (coarse- to arse-crystalline planar-s dolomite), and corresponding traverses (T1 and T2). Note ir boundaries between replacive dolomites of the cores and zones of dolomite s. Fe-rich outer zones (light) are followed by nonplanar-c void-filling dolomite (c) with a nd straight contact. Sample from 22,268 ft (6,787 m), well 3.

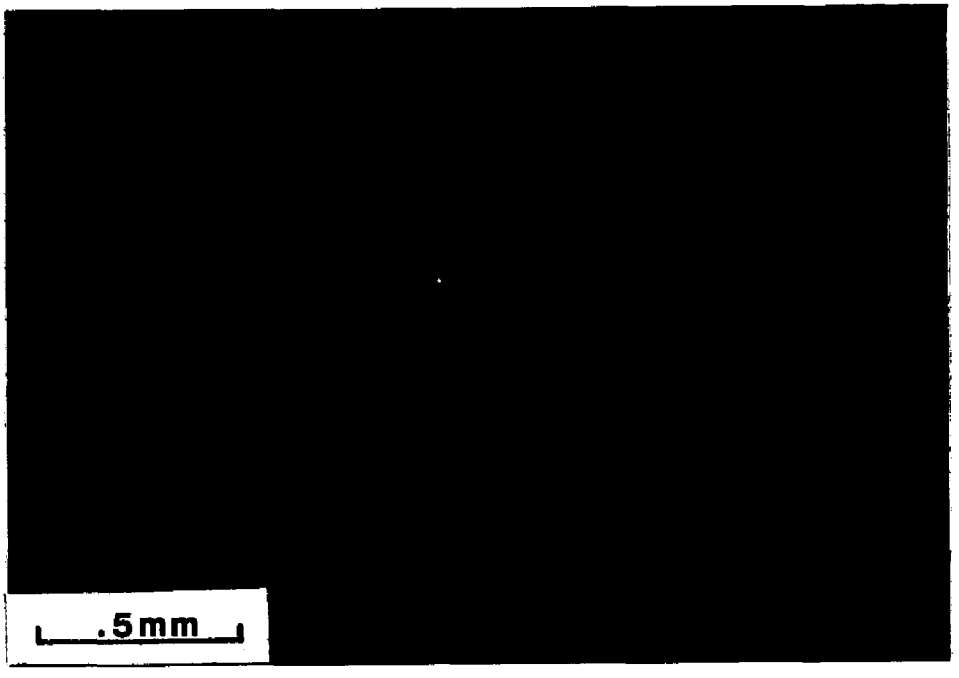

Figure 29. -- Cathodoluminescence photomicrograph of very coarse planar-e dolomite with concentric zonation very commonly observed in dolomite cements. Brighter luminescent zones usually have Mn > Fe. Sample from 21,280 ft (6,468 m), well 2.

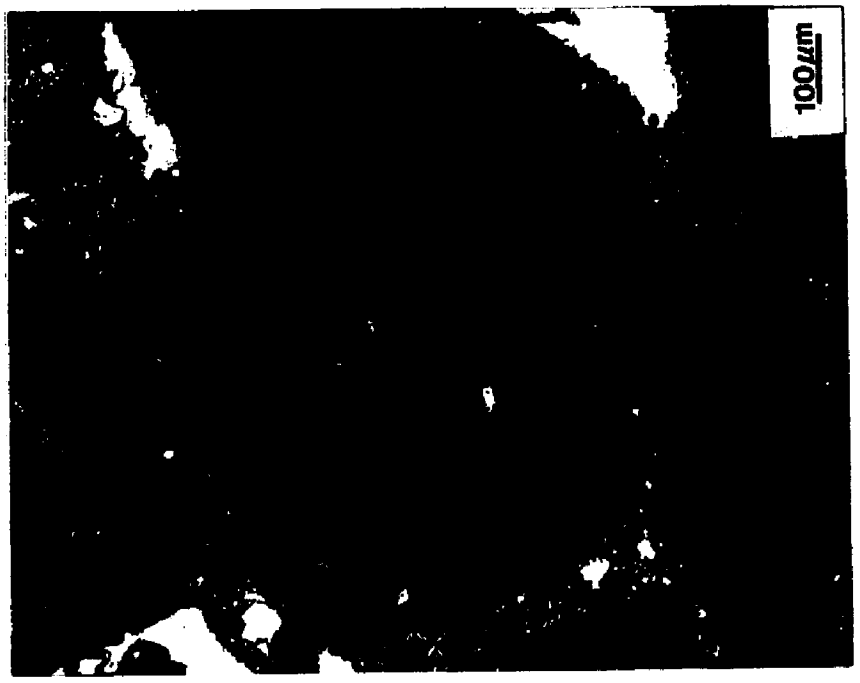

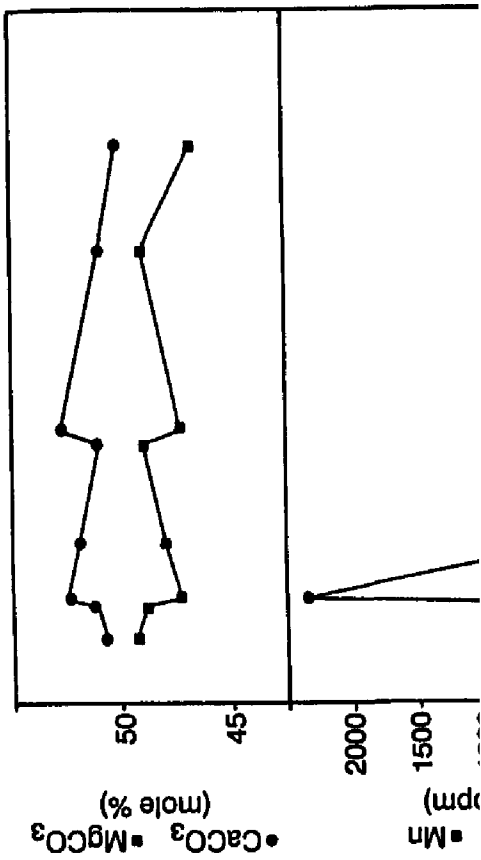

Figure 30. -- Back-scattered electron image of very coarse dolomite crystals shown in figure 29, with corresponding geochemical traverse. Inclusion-rich core could represent earlier replacive dolomite, followed with irregular contact by dolomite cements (relative inclusion-free). Sample from 21,280 ft (6,468 m), well 2.

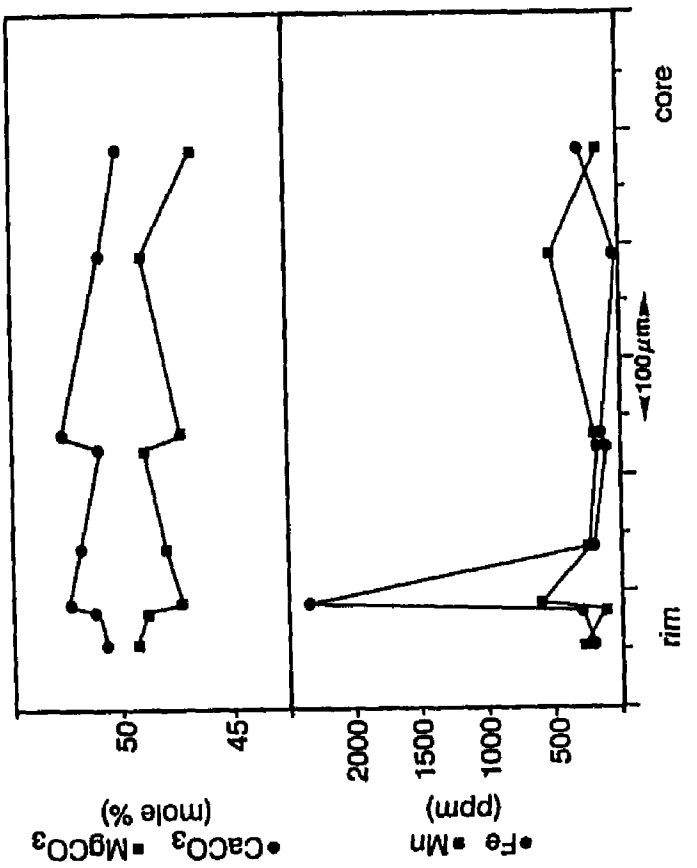

igure 30. -- Back-scattered electron image of very coarse dolomite crystals shown in
› 29, with corresponding geochemical traverse. Inclusion-rich core could represent
›r replacive dolomite, followed with irregular contact by dolomite cements (relative
sion-free). Sample from 21,280 ft (6,468 m), well 2.

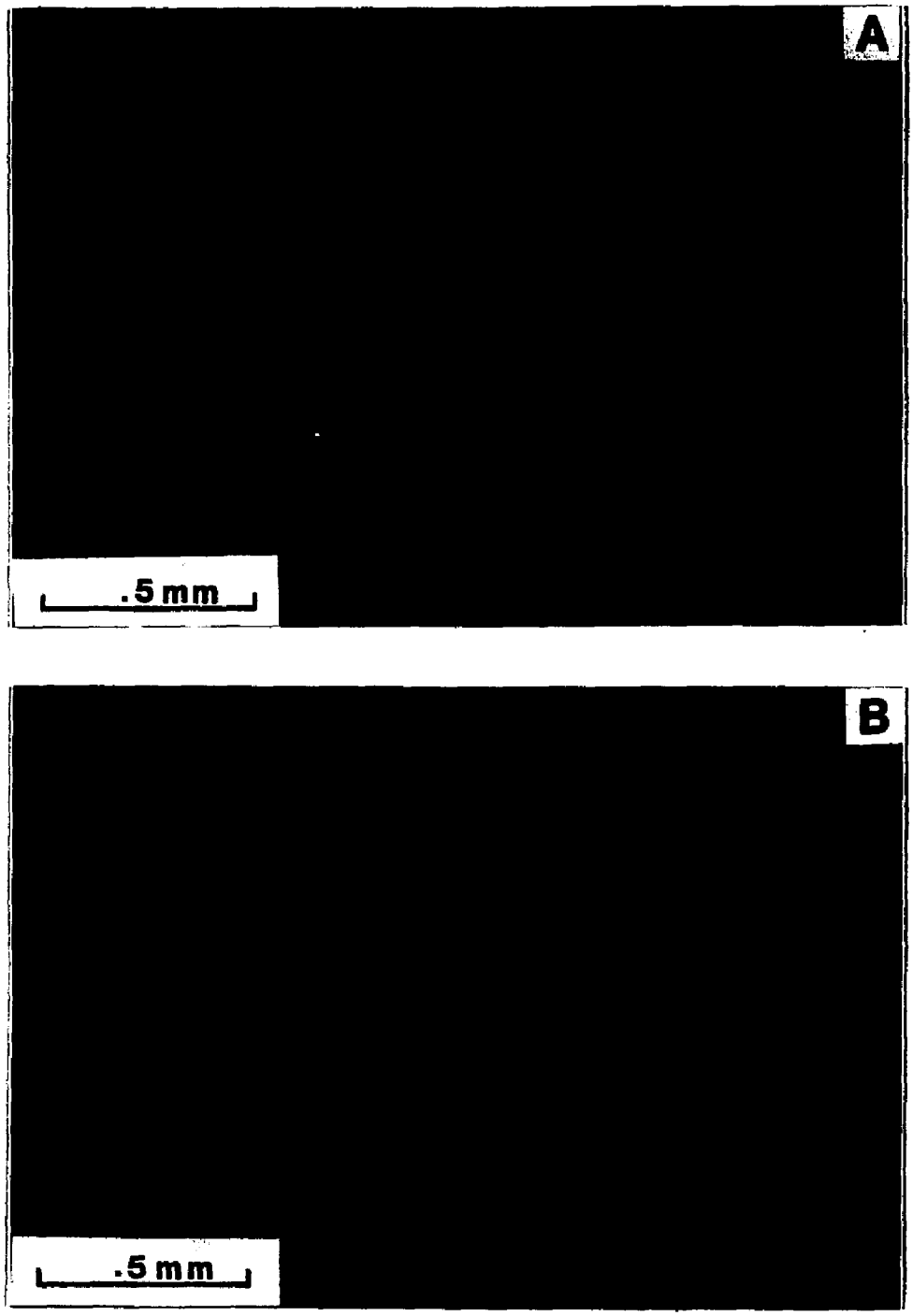

Figure 31. -- Photomicrograph pair of dolomite-rock texture 4 (medium- to coarse-crystalline planar-e mosaic dolomite). A) Clear to cloudy crystals of dolomite type 4 in karst-related facies. Plane polarized light. B) Cathodoluminescence picture of A shows distinct zonation of cores and rims. Rims are dull, with a thin nonluminescent outermost zone. Sample from 14,593 ft (4,448 m), well 4.

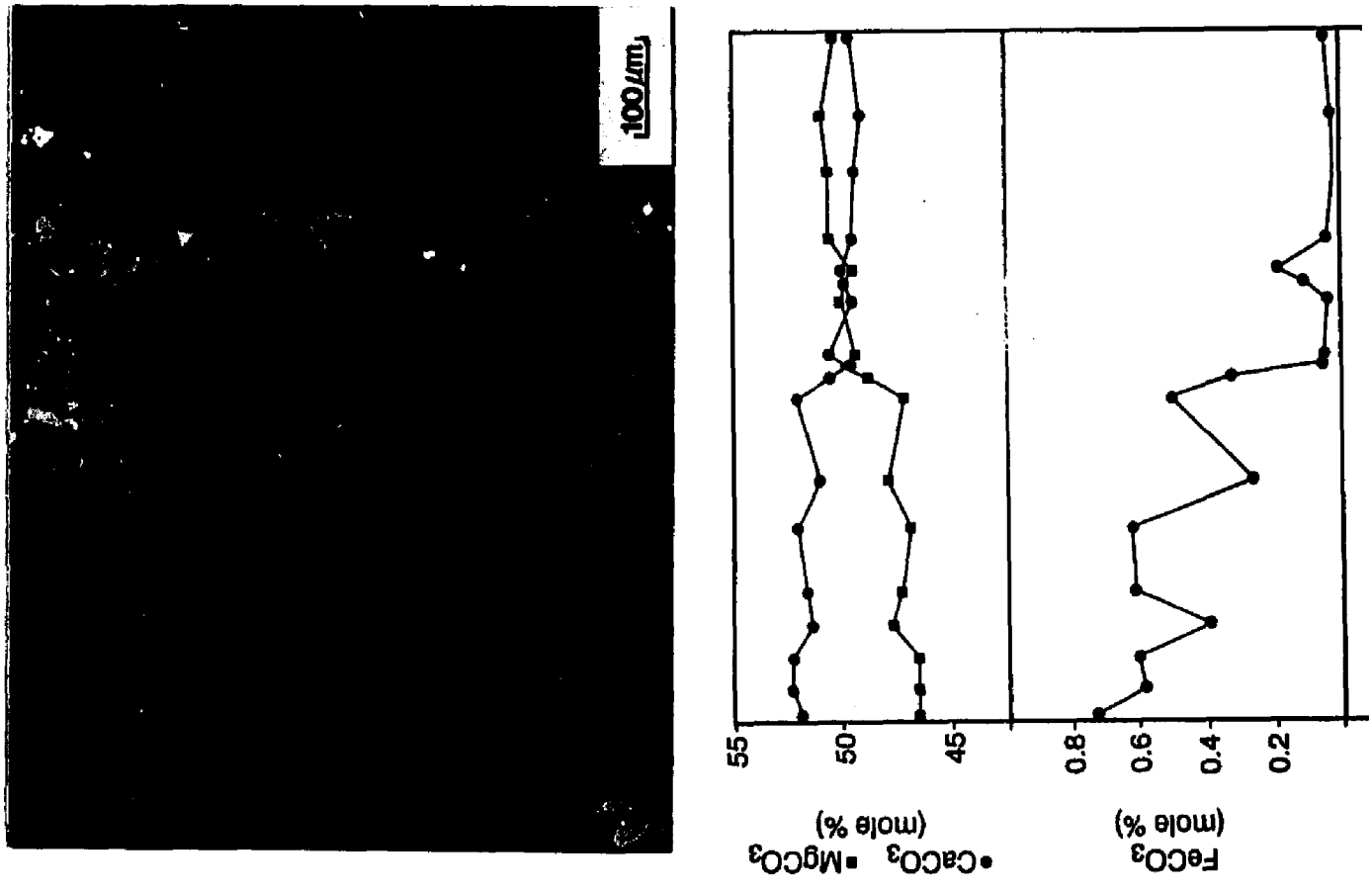

Figure 32. -- Back-scattered electron image of planar-e crystals shown in center of Figure 31, with corresponding geochemical traverse. Light (Fe-rich) rim corresponds to dull rim of cathodoluminescence picture. Note the sharp and straight boundary between rim (light) and core (dark). Compare this zonation and the geochemistry with figure 34. Sample from 14,593 ft (4,448 m), well 4.

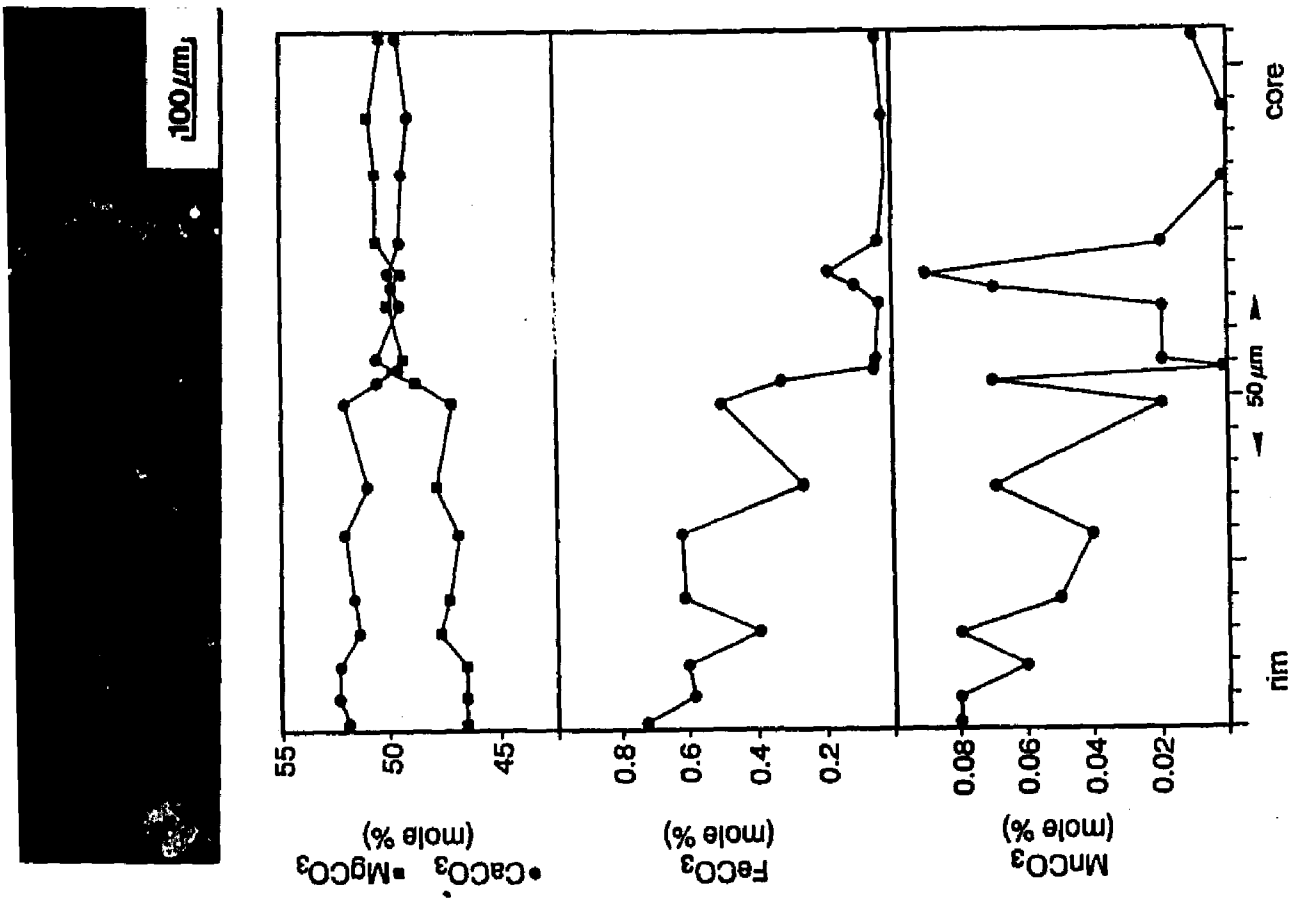

on image of planar-e crystals shown in center of Figure
raverse. Light (Fe-rich) rim corresponds to dull rim of
ıe sharp and straight boundary between rim (light) and
d the geochemistry with figure 34. Sample from 14,593

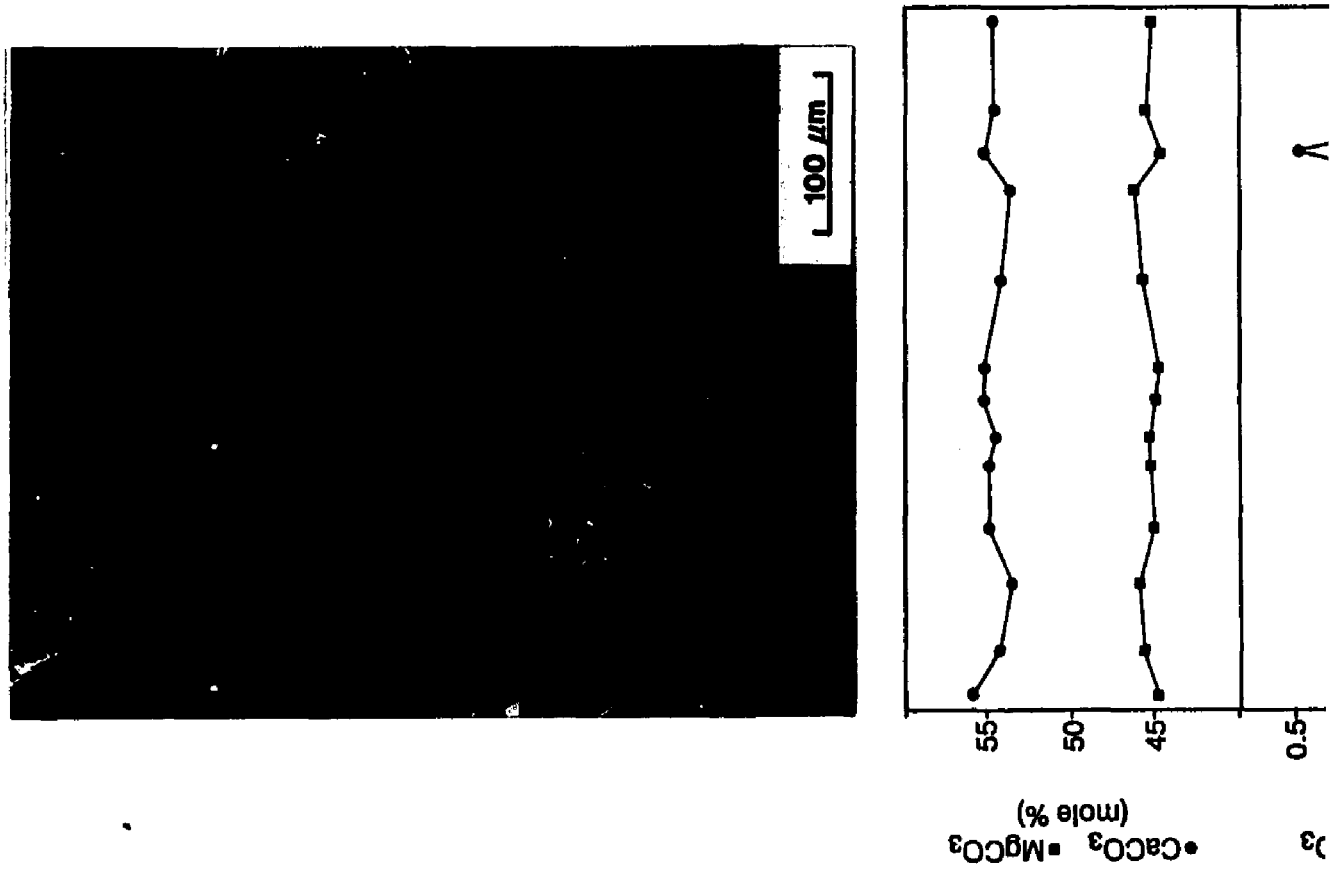

Figure 33. -- Back-scattered electron image (of planar-e dolomite, with corresponding geochemical traverse. Note relative inclusion free core with light hairline zones (Fe-rich). Sample from 5,129 ft (1,563 m), well 5.

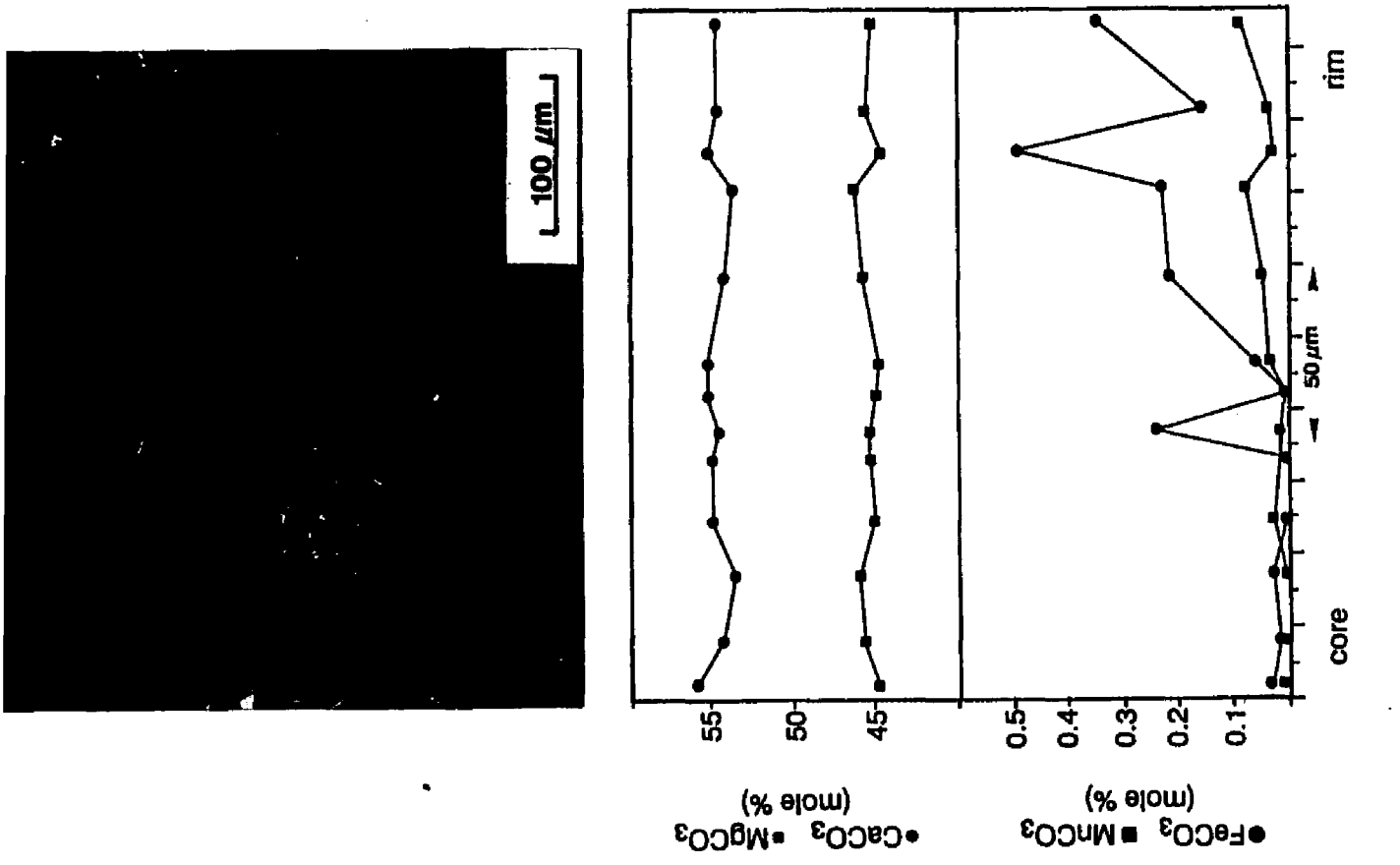

ck-scattered electron image (of planar-e dolomite, with corresponding
e. Note relative inclusion free core with light hairline zones (Fe-rich).
(1,563 m), well 5.

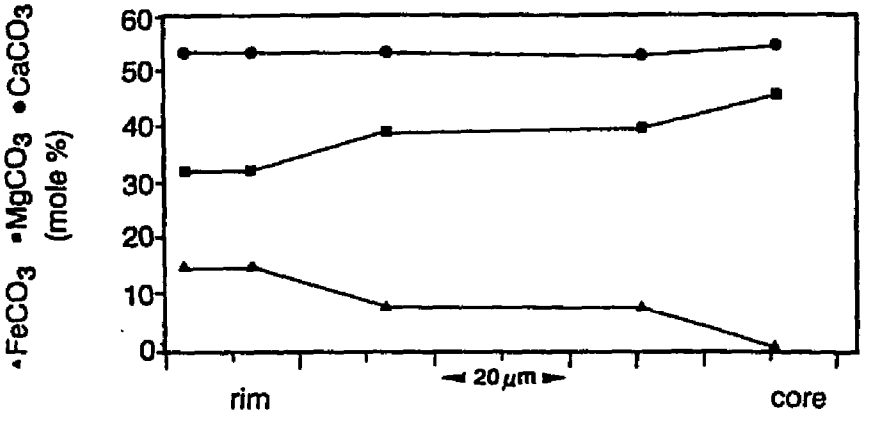

Figure 34. -- Back-scattered electron image of dolomite-rock texture 4 (medium- to coarse-crystalline planar-e mosaic dolomite), with corresponding geochemical traverse. Dark centers correspond to planar-e dolomite shown in figure 33. Light rim (Fe-rich) indicates abrupt chance in pore-fluid chemistry. The zonation is identical to dolomites in figure 32. Note, however, that geochemistry is distinct: $FeCO_3$ contents are much higher in the above examples. Sample from 5,134 ft (1,565 m), well 5.

ORIGIN OF ELLENBURGER DOLOMITES

Ellenburger carbonate rocks have experienced a complex and complicated dolomitization history. Any interpretation of Ellenburger dolomites must address the large-scale early-diagenetic replacement of subtidal to peritidal limestones, as well as the origin of those dolomites that formed in the subsurface during intermediate to deep-burial. Various types of dolomites formed in different diagenetic environments at different times, producing distinctive petrographic characteristics. The origin of dolomite-rock textures, complemented by geochemical analyses, provides important clues in the study of pervasively dolomitized platform carbonates such as the Ellenburger.

The formation of dolomite is governed by thermodynamic and kinetic constraints, which interact and partly counteract each other (e.g. Morrow, 1982 a; b; Land, 1983, 1985; Machel and Mountjoy, 1986; Hardie, 1987). On the basis of these constraints Machel and Mountjoy (1986) consider the following conditions and environments chemically conducive to dolomitization: 1) Environments of any salinity above thermodynamic and kinetic saturation with respect to dolomite (i.e. freshwater/seawater mixing zones, normal saline to hypersaline subtidal environments, hypersaline supratidal environments, schizohaline environments). 2) Alkaline environments (i.e. those under the influence of bacterial reduction and/or fermentation processes, or with high input of alkaline continental groundwater enriched in CO_3^{2-} (and HCO_3^{2-}). 3) Many environments with temperatures greater than 50° C (subsurface and hydrothermal environments).

Under these conditions, the essential components to form massive dolostones are: a) The amount of Mg^{2+} and CO_3^{2-} supplied for dolomitization must be sufficient to form a given mass of dolomite. b) A mechanism (e.g. fluid flow, diffusion) is required to deliver the Mg to the site of dolomitization, and also carry away Ca-ions. c) There must exist chemical conditions favorable for the precipitation of dolomite at the "dolomite-construction site".

In the light of these considerations, and on the basis of lithofacies analysis, stratigraphy, petrographic and geochemical data, Ellenburger dolomites are interpreted to have formed in two distinct environments: a) in normal saline subtidal to hypersaline peritidal environments, under the influence of processes common in alkaline environments (e.g. biogenic sulfate reduction), and b) in subsurface environments with temperatures > 50° C.

Various types of dolomites formed in these environments, and in the following their origin, timing, and the fluids from which these dolomites precipitated, are discussed.

Subtidal Dolomitization

Syndepositional, subtidal dolomitization (e.g. Sass and Katz, 1982; Bein and Land, 1983; Machel and Mountjoy, 1986; Ruppel and Chander, 1988) by Ordovician seawater is proposed for the formation of dolomite type 1.

The following petrographic features suggest that this type formed during early sedimentation of Ellenburger carbonates: 1) it forms dense mosaics of unimodal, very fine- to fine- crystalline planar-s dolomite in subtidal to supratidal mud- supported lithofacies. This texture is typical for dolomites formed under near surface, low-temperature conditions (Gregg and Sibley, 1984; Sibley and Gregg, 1987). Crystal size is controlled by the relation of two rate processes, the rate of nucleation and the rate of growth (Spry, 1969, p. 192). Dolomite commonly replaces selectively fine-crystalline calcium carbonate (e.g. Murray and Lucia, 1967; Sibley et al., 1987). Fine particles have a very large surface area in comparison to their volume, and therefore a rapid nucleation rate. If the nucleation rate is high compared to the growth rate, the resultant crystal size will be small (Sibley and Gregg, 1987, Figure 11). Experimental data (Sibley et al., 1987) indicate that the induction stage of dolomite formation increased with increasing crystal size. This may explain, among others, the selective dolomitization of finer crystalline calcium carbonate and the early dolomitization of subtidal to supratidal lime muds. 2) Clasts of flat-pebble conglomerates and karst-breccias are composed of this type, indicating early dolomitization. 3) It is absent in pore spaces and vugs formed later in the subsurface. 4) It is crosscut by fractures filled with dolomite type 3, 5, or 7.

The timing of this dolomitization event is not precisely constraint. It can only be said that it took place between deposition of Ellenburger carbonates and the post-Ellenburger unconformity, giving a pre-Middle Ordovician age for this dolomite (cf. Kupecz, 1989).

The fluids available and capable to dolomitize extensively mud-supported lithofacies at an early-stage were either normal Ordovician seawater or evaporated marine waters. Facies analysis and stratigraphy do not support an evaporitic setting for the mud-supported facies. Evidence that would suggest coprecipitation of evaporite minerals with the carbonates, such as pseudomorphs, are lacking. The low (< 100 ppm) Sr- concentrations also do not support evaporitic conditions during the formation of dolomite type 1 (e.g. Lumsden and Chimahusky, 1980; Veizer, 1983 a,b; Machel and Anderson, 1989), leaving Ordovician seawater as the most likely source. Bulk stable isotope data obtained by Lee and Friedman (1987) for dolomite type 1 are consistent with this interpretation, indicating an approach towards equilibrium with estimates for Ordovician seawater, possibly modified by sulfate reduction.

Petrographic data indicate that dolomitization of subtidal to peritidal carbonates proceeded via replacement of precursor carbonates. If we accept the reaction (Lippmann, 1973),

(1) $CaCO_3 + Mg^{2+} + CO_3^{2-} \longrightarrow CaMg(CO_3)_2$

as the most likely path of dolomitization, we no longer have to be concerned about the supply and removal of one ionic species at the site of dolomitization. The only concern is the supply of Mg^{2+} and CO_3^{2-} (alkalinity) (Lippmann, 1973; Morrow, 1982). Most of the Ca needed for dolomite formation is supplied by the dissolution of precursor carbonates. The necessary Mg is supplied by seawater, which is considered as the primary agent of massive dolomitization (e.g. Land, 1980, 1985; Morrow, 1982; Given and Wilkinson, 1987).

Possible sources for the CO_3^{2-} required include alkaline waters, which owe their origin to the alteration of silicates (Lippmann, 1973). An alternative source of alkalinity is biogenic sulfate reduction, following the reaction

(2) $2CH_2O + SO_4^{2-} \longrightarrow 2H^+ + S^{2-} + 2HCO_3^-$.

Sulfate reduction promotes dolomitization by simultaneously removing sulfate as a potential inhibitor to dolomite formation (Baker and Kastner, 1981; Morrow and Ricketts, 1988), and by greatly increasing alkalinity. The large increase in alkalinity results in interstitial water supersaturated with respect to dolomite (Gieskes et al., 1982; Compton, 1988, a, b). Experiments by Morrow and Ricketts (1988) also indicate that sulfate in solution inhibits dolomitization by retarding the rate of calcite dissolution, and that the rate of dolomitization of calcite is much more rapid in solutions with higher carbonate and bicarbonate activities.

Early precipitation of pyrite is commonly associated with sulfate reduction. The H_2S produced during biogenic sulfate reduction reacts with reduced iron to form Fe-monosulfides, which later transform to stable pyrite (Berner, 1970, 1984). Disseminated pyrite is found throughout the rocks characterized by dolomite type 1.

Sulfate-reduction dolomites are mainly described from deep-sea settings, such as DSDP-sites (e.g. Baker and Burns, 1985), and the Miocene Monterey Formation of California (Garrison et al., 1984; Burns and Baker, 1987; Burns et al., 1988; Compton and Siever, 1986; Compton, 1988 a, b). Although these occurrences are deep-marine dolomites, several conclusions regarding the origin of these organic dolomites are applicable to early dolomite

formation in Ellenburger shallow-water carbonates:

1) Diffusion from overlying seawater supplies most of the Mg for dolomite formation (Baker and Burns, 1985; Compton and Siever, 1986). 2) Dolomite formation must occur near the sediment-water interface (Baker and Burns, 1985). 3) Sediment-accumulation rate and rate of dolomite formation are important controls on the diffusion flux and the extent of early dolomitization (Compton and Siever, 1986). Accumulation rates of Ellenburger carbonates are in the order of 15-20m/my (cf. Sarg, 1988) and much lower than rates in the Monterey Formation (50-600m/my), thus increasing the residence time for dolomite formation in the uppermost sediment where Mg-flux is a maximum. 4) Geochemical signatures of dolomites from the Monterey Formation (e.g. Burns and Baker, 1987; Compton, 1988) and dolomite type 1 are similar: they are Ca-rich, and have relatively low trace-element concentrations of Fe, Mn, and Sr. Sections in the Monterey Formation that contain these dolomites are characterized by low sedimentation rates, lower detrital mineral content, higher original biogenic carbonate content, and more dolomite (Burns and Baker, 1987). Such conditions were clearly fulfilled during Ellenburger deposition. Given in addition the much warmer temperatures of shallow Ordovician epeiric seas, this could have resulted in extensive early dolomitization.

The proposed subtidal dolomitization by Ordovician sea-water of normal or elevated salinity can explain, 1) the regional extent and early timing of dolomitization, 2) replacement of lime muds and supply of Mg^{2+} to the site of dolomitization, 3) the Ca-rich nonstiochiometric composition, 4) the presence of disseminated pyrite, and 5) some of the stable isotope data.

The model can not explain, 1) oxygen isotope values depleted with respect to estimated Ordovician seawater values, 2) lithoclasts of karst breccias that are affected by Fe-rich fluids (e.g. fractures filled with ferroan dolomite), resulting in high Fe-concentrations of dolomite type 1 in these clasts, and 3) the geochemical differences that exist between the dark, very fine- crystalline planar-s dolomites and the clear, fine-crystalline planar-s dolomites of the laminated dolomudstone/wackestone lithofacies. The very fine-crystalline dolomite compares geochemically to the centers of the clear, fine-crystalline dolomites, while the rims of the clear, coarser crystals are enriched in Fe. These data indicate a distinct nonmarine component that modified the early-stage dolomites later in the diagenetic history. The coarser crystal size may be a result of this later diagenetic overgrowth (e.g. Zenger and Dunham, 1988, Table 2). The positive correlation between $SrCO_3$ and $CaCO_3$ in samples from the karst facies is most likely related to this later diagenetic overprint.

Late-stage dolomites are present in the karst facies, and there is evidence for basinal fluid migration in rocks of the karst facies (e.g. Kupecz, 1989, Amthor and Friedman, 1989 a).

Fluids responsible for the precipitation of these late dolomites could have modified earlier dolomite types. Kupecz (1989) reached a similar conclusion in her study, which shows that early-stage dolomites (which are equivalent to dolomite type 1) were modified by fluids which precipitated late-stage dolomite cements, thereby loosing most of its original signatures. In contrast, early dolomites of this study still retain some of their original characteristics, and allow therefore an interpretation of their origin.

In summary, petrography and geochemistry indicate formation of dolomite type 1 during early diagenesis in a subtidal to peritidal setting under near surface, low-temperature conditions. The Mg necessary for dolomitization of precursor lime muds was supplied by diffusion from overlying seawater. Dolomitization occurred most likely under the influence of sulfate-reduction processes, which promote dolomitization by simultaneously removing sulfate as a potential inhibitor to dolomitization and by greatly increasing alkalinity. There is evidence that dolomite type 1 has undergone further alteration. Such alteration occurred later in the diagenetic history under elevated temperatures, or/and in the presence of fluids other than seawater (e.g. basinal fluids precipitating late-stage dolomites).

Subsurface Dolomitization

Dolomite-rock textures 2 through 7 are interpreted to have formed in a subsurface setting during intermediate to deep burial. These dolomite types comprise replacement dolomites (e.g. types 2 and 6) and void-filling dolomites (e.g. types 3, 4, 5, and 7).

Replacement Dolomites

The replacement dolomites are volumetrically the most important types. They are characterized by distinct different textures: Dolomite type 2 forms dense mosaics of medium- to coarse- crystalline planar-s crystals, which commonly show preservation of minute textural details. Dolomite type 6 forms dense mosaics of coarse-crystalline nonplanar crystals, that are fabric destructive. The distribution of both planar and nonplanar replacement textures requires extensive subsurface-fluid flow.

Dolomite type 2 is mostly confined to rocks of the mottled dolomudstone lithofacies and the dolopackstone/grainstone lithofacies, which probably had higher depositional porosity than rocks of the over- and underlying subtidal to peritidal lithofacies. Such higher porosity zones could have served as permeable horizons for fluids capable of dolomitization. The unimodal coarse-crystalline planar-s texture with allochem ghosts indicates relatively slow replacement of a precursor limestone below the critical roughening temperature, where the

saturation state with respect to dolomite is relatively low, but the residence time of the rock in the dolomitizing fluid is quite long, leading to a low porosity dolostone (Sibley and Gregg, 1987, p. 974). The preservation of primary grain fabric, such as ooids, requires that the volumetric rate of dolomite formation must be equal to the volumetric rate of calcite dissolution (Dockal, 1988). That means that host-phase dissolution and precipitation must occur simultaneously along a thin solution film (e.g. Kinsman, 1969; Veizer, 1978, 1983b; Pingitore, 1982; Maliva and Siever, 1988; Dockal, 1988). It is possible that the planar-s texture is a result of grain-growth from an initial state, where fine-crystalline dolomite rhombs were scattered throughout the limestones (e.g. Morrow, 1982 b). Because the crystal-size of the carbonate grains is large, the dolomite nuclei were likely rather far apart. These crystals grew very slowly, preserving textural details, and eventually joined along compromise boundaries to form dense planar-s mosaics.

Geochemical data indicate an increase in trace element concentrations (e.g. Fe, Mn) during crystal growth. Inner zones have lower trace element concentration than outer, younger zones. This enrichment suggest progressive evolution of pore waters during dolomitization. The fluids were most likely basinal fluids that were expelled during subsidence and burial of the carbonate platform. Mg for dolomitization could have been derived from large-scale dissolution of limestones and dolostones during karst, and/or from basinal areas to the south (e.g. Kupecz, 1989; Kupecz and Land, 1989). In both cases large-scale fluid flow along porosity and permeability pathways is necessary to explain the extent of dolomitization of limestones.

The inferred slow crystal growth requires low supersaturation, a long residence time for the rocks in the dolomitizing solution, and stable hydrological conditions. In the Ellenburger such conditions were best fulfilled during gradual subsidence of the Tobosa Basin during Middle Ordovician to Devonian. Normal rates of subsidence and compaction result in fluid-flow rates far too low to transport 100° C temperatures into shallow (< 1 km), near-surface environment (Bethke, 1983; Cathles and Smith, 1983; Sverjenski, 1986). Calculation by Bethke et al. (1988) showed, that sediment compaction drove groundwaters at velocities less than a few centimeter per year in the Illinois and Arkoma basins because of slow burial. Most burial-compaction flow occurs in the relatively early stages of basin development at depths up to 1000 m (Hanor, 1979; Garven and Freeze, 1984; Machel and Mountjoy, 1986). The associated low flow rates, and the early timing of burial-compaction flow can explain most of the characteristics of the coarse-crystalline planar replacement dolomites.

Coarse-crystalline nonplanar dolomites replaced precursor dolomites in the sandy dolostone lithofacies and the karst facies. The coarse-crystalline nonplanar dolomite texture

is fabric destructive. It is characteristic of epigenetic dolomites formed at elevated temperatures above the critical roughening temperature (Gregg and Sibley, 1984; Sibley and Gregg, 1987). The distribution of the nonplanar textures suggests, that the dolomites formed when warm, reactive fluids moved along paths of increased porosity and permeability generated, for example, by karst-related processes. It is not present in zones of low porosity and permeability, characterized by dolomite type 1 and/or 2. Because this type replaced a precursor dolostone, no large-scale import of Mg is required for dolomitization. These nonplanar dolomites are very close to stoichiometry.

Evidence that basinal fluids affected Ellenburger rocks is present in dolomite cements of paleokarst-deposits (e.g. Amthor and Friedman, 1989 a). This indicates that warm basinal fluids involved in the precipitation of late-stage cements were also capable of replacement dolomitization. This period of dolomitization might be related to the widespread mineralization event that occurred in response to the deformation and uplift of the Ouachita Mountains during Late Paleozoic (cf. Kupecz, 1989; Kupecz and Land, 1989; Amthor and Friedman, 1989). Recently proposed hydrologic models provide mechanisms to funnel large quantities of warm water from deep sedimentary basins onto shallow platforms, and an explanation for anomalous temperatures in shallow burial depths (e.g. Garven and Freeze, 1984; Oliver, 1986; Leach and Rowan, 1986; Bethke et al., 1988).

In summary, two stage of late-diagenetic replacement dolomites have been recognized. Coarse-crystalline planar dolomites are the result of slow replacement of precursor limestones (grainstones) in the presence of evolving burial-compaction fluids during intermediate burial of Ellenburger strata. Fabric destructive nonplanar dolomite formed at elevated temperatures, when warm reactive fluids replaced a precursor dolomite. Both textural types require fluid flow along porous and permeable conduits, such as karst zones, basal sandstones, and grainstones. Because both types are restricted to such zones their origin depends on such porous horizons as fluid pathways. The different textures are a result of differences in precursor lithology, mechanisms of fluid flow, temperatures of dolomitizing fluids, and the rate of replacement.

Void-filling dolomites

Dolomite types 3, 4, 5, and 7 are interpreted as void-filling dolomites, and include planar (e.g. 3, 4, 5) and nonplanar (e.g. 7) textures. Only planar dolomites show compositional zonation, which is in part very complex and not identical in different samples. The chemical composition of the void-filling dolomites documents the progressive evolution of the dolomitizing fluids during diagenesis. Ideally, the concentration of trace elements in dolomite

provide means for estimating the composition of the fluid from which the dolomite precipitated. Both iron and manganese have fractionation factors (D) > 1, and will therefore be preferentially incorporated into the growing dolomite crystal. Cores and inner zones of planar dolomites have characteristically lower trace-element concentration of iron and manganese than outer (= younger) zones. The increasing iron concentration in void-filling dolomites towards the rims and the in part complex zonation is related to the diagenesis in the reducing subsurface environment, with fluctuations in the supply of iron. The latest phases in the paragenetic sequence, nonplanar dolomite cements and calcites, are typically iron-rich. The only fluids that can provide the necessary amount of iron to form, f.e. ferroan dolomites with 21 mole % $FeCO_3$, are basinal brines (Table 4). Most of the Mg necessary comes from dissolution of precursor dolomites. Inter- and intracrystalline dissolution surfaces are commonly observed. Major truncation surfaces occur between earlier replacement dolomites and void-filling dolomites, and between planar and nonplanar void-filling dolomites. Such dissolution events serve two purposes: they create the necessary porosity for the precipitation of void-filling dolomites, and they provide Mg for the precipitation of these cements.

Dissolution events can be related to major periods of karst- development during basin evolution, and the concomitant invasion of freshwater resulting in undersaturated fluids with respect to dolomite. LeMone (1989, Figure 1) shows as many as nine periods of subaerial exposure and karsting in Paleozoic rocks of the Franklin Mountains, Texas. Calculations performed by Bethke et al. (1988) showed that extensive , deep-reaching freshwater incursions occurred in the past as events that accompanied past drops in sea-level. Such a scenario could explain the dissolution between early host dolomites and later void-filling dolomites, as well as intracrystalline truncation features in void-filling dolomites.

Land (1983), and Land and Prezbindowski (1985) argued that fluids in equilibrium with dolomite in their source basin should be dolomite undersaturated upon expulsion from that basin as a result of cooling. Anderson (1983) suggested dissolution as a result of acids produced by the precipitation of sulfides during mineralization. Both arguments may be combined to explain intracrystalline solution features in void-filling dolomites, and the dissolution between planar and nonplanar dolomites. The source of the basinal fluids involved in dolomite precipitation within the Ellenburger foreland basins to the south that formed response to Ouachita tectonism. Fluids were expelled from these areas northward onto the shelf (Kupecz, 1989; Kupecz and Land, 1989; Amthor and Friedman, 1989 a). Mineralization (Barnes, 1956) and precipitation of late stage dolomites (e.g. Amthor and Friedman, 1989 a) occurred in areas close to the tectonic front. Further away from the front to

the north the same fluids might have been responsible for dissolution. The Ca and Mg liberated reprecipitated later under elevated temperatures as nonplanar saddle dolomite, and, after depletion of the Mg, the system changed to calcite precipitation as the latest phase.

If we combine the petrographic and geochemical results of this study a characteristic paragenetic patterns emerges (Figure 35). Early-stage replacement dolomite are discontinuously overgrown by void-filling dolomites. The discontinuous contact indicates dissolution of early formed dolomites prior to overgrowth by later void-filling dolomites. This dissolution is most likely related to a major period of karst development during the pre- Middle Ordovician unconformity. During continuous burial of Ellenburger carbonates compositionally zoned void-filling dolomites precipitated, reflecting fluctuations in the supply of trace elements such as iron and manganese. Intracrystalline truncation features in some of these dolomites are interpreted as incursion of meteoric water as a result of frequent periods of karst in rocks of the passive margin shelf sequence (LeMone, 1988, Figure 1). Void-filling planar dolomites in turn were discontinuously overgrown by nonplanar dolomite cements and/or calcite and authigenic quartz. The nonplanar dolomites (saddle dolomite) are typically enriched in calcium (mean = 52.6 mole% $CaCO_3$) and iron (mean = 6635 ppm), characteristic for phases that precipitated from basinal fluids, which are Ca- and Fe-rich. Homogenization temperatures from fluid inclusions of Ellenburger saddle dolomites (Lee and Friedman, 1987) gave average temperatures as high as 220°C. Freezing temperatures indicated that the fluid inclusions were brines with salinity values ranging from three to five tomes that of seawater (Lee and Friedman, 1987, p. 551). Burial history plot and paragenetic relationships indicate formation under reducing conditions in a deep-burial environment. Fluid inclusion and stable isotopes studies (Lee and Friedman, 1987), as well as geochemical data of late calcite cements also indicate formation under reducing conditions from fluids that probably were basinal brines.

A source of basinal fluids involved in the formation of the planar and nonplanar void-filling dolomites are the foreland basins to the south and southeast (e.g. Kerr, Val Verde basins) that formed during Ouachita tectonism. Fe-rich, warm basinal fluids were expelled northward onto the North American craton during Ouachita orogeny, channeled along paleokarst-related porosity and permeability pathways (Figure 36). Such an interpretation is consistent with recently proposed hydrologic models that provide mechanisms to move large volumes of water from deep sedimentary basins onto shallow platforms.

Table 4: Shown Are the Composition of Two Subsurface Brines from the Gulf and the Composition of Average Seawater.
All Parameters, Except ph, Are in mg/L. (from Hanor, 1987; see reference therein).

	Brine 1 Central Mississippi	**Brine 2** South Louisiana	**Seawater**
TDS	230,000	235,700	35,200
Na	54,200	78,000	10,760
Li	----------	16	.170
K	485	1,065	399
Rb	----------	3.4	.12
Cs	----------	11.8	.0003
Mg	1,770	1,140	1294
Ca	27,600	10,250	412
Ba	24	185	.01
Fe	181	84	.002
Cl	143,600	143,000	19,350
F	----------	.8	1.3
Br	1,090	419	67
I	----------	18	.064
B	----------	44	4.5
NH_3	----------	100	2.0
H_2S	----------	.4	----------
HCO_3	----------	450	45
SO_4	248	.4	2,712
SiO_2	42	48	6.2
Pb	28	----------	.00003
Zn	143	----------	.002
pH	----------	6.2	8.2

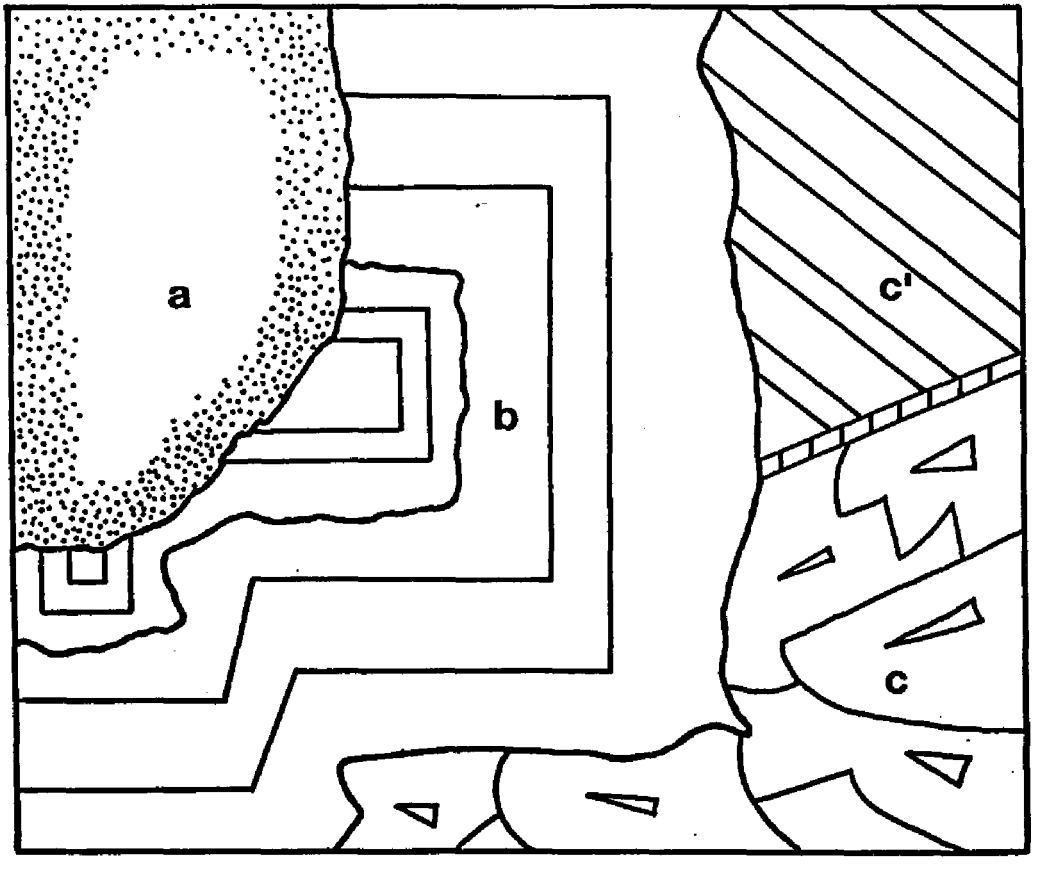

Figure 35: Sketch illustrating observed paragenetic relationships between early replacement dolomites (a), planar void-filling dolomites (b), nonplanar dolomite cements (c), and late-stage calcite cements (c'). Replacements dolomites are discontinuously overgrown by zoned void-filling dolomites, which show in part intracrystalline truncation surfaces. Nonplanar dolomites cements (c), and late-stage calcite cements are commonly the latest phases, occluding pore-spaces.

In their evaluation of the role of basinal fluids in the formation of ore deposits Sharp (1978), and Cathles and Smith (1983) invoked pulses of fluids out of sedimentary basins. Such pulses of basinal fluids have been invoked in the formation of Fe-zonation in late-diagenetic dolomite cements of MVT-deposits (e.g. Farr, 1989). In contrast, Garven and Freeze (1984), Bethke (1985, 1986), and Bethke et al. (1988) have invoked gravity-driven flow induced by tectonic uplift along one basin margin ass a mechanism for driving hot, salty, and possibly metal-rich fluids out of sedimentary basins. In order for warm fluids to reach shallow settings warm, they must have traveled through aquifers rapidly enough to avoid cooling. Bethke et al. (1988) calculated fluid-flow rates of topographic-driven flow in the Arkoma basin in the order of tens of meter per year. Topography-driven fluid flow seems to be the only mechanism that can transport warm basinal fluids onto shallow platform areas fast enough to avoid cooling below temperatures conducive for mineralization and late-stage dolomitization.

Late-stage dolomitization related to such fluid expulsion might be related to the widespread mineralization event that occurred in response to the deformation and uplift of the Ouachita Mountains during Late Paleozoic (e.g. Leach and Rowan, 1986; Oliver, 1986).

A Late Paleozoic age of fluid migration is consistent with reported Pennsylvanian ages of mineralization, diagenesis, and associated fluid migration in Texas. Barnes (1956) describes Pb- mineralization from Central Texas. Smith (1981) cites a Pennsylvanian age for mineralization in Upper Cambrian sediments of Central Texas, where dolomitization accompanied the updip movement of metalliferous brines. Morton (1985) concluded that clay diagenesis must have occurred simultaneously throughout a large area of West Texas during the Pennsylvanian. A Rb-Sr age of 302 +/- 4 m.y. of Devonian clays indicate that the formation of diagenetic illite over a large area was episodic, not gradual, and that diagenetic illite appears to record the initial contact with hydrothermal fluids migrating out of the Ouachita tectonic zone (Morton, 1985). Kupecz (1989), and Kupecz and Land (1989) showed, that the timing and direction of fluid migration associated with the Ouachita orogeny are consistent with the timing and distribution of late-stage dolomites within the Ellenburger Group of West Texas. They propose that reactive fluids were Pennsylvanian pore-fluids which were expelled from basinal siliciclastics during Ouachita Orogeny.

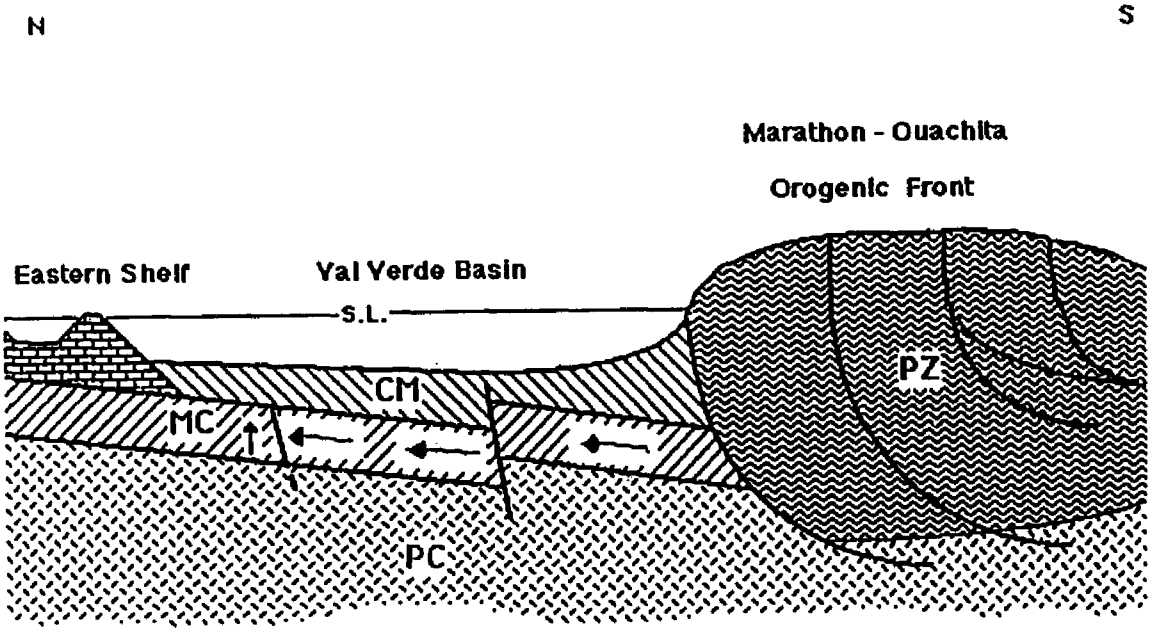

Figure 36: Schematic N-S cross-section illustrating the development of Val Verde foreland-basin topography and the Marathon-Ouachita orogenic front in Late Paleozoic time. (modified from Wuellner et al., 1986). PC = Precambrian basement; MC = Cambrian to Mississippian formations of passive-margin shelf facies of Tobosa basin; PZ = Thrust-faulted Paleozoic rocks of Marathon-Ouachita fold-belt; CM = Rocks of the Val Verde peripheral basin facies (Pennsylvanian-Permian).

Arrows indicate proposed fluid-flow along porous pathways in basal Cambro-Ordovician strata. Gravity-driven fluid flow could be channeled at the discharge-end along paleokarst-related porosity pathways. Under such conditions fluid temperatures could be elevated to levels conducive to mineralization and dolomitization.

The described paragenetic scheme appears to be a common aspect of sedimentary basin evolution. Available information concerning burial diagenesis and basin evolution suggests that trends and timing of dolomitization, porosity formation and destruction, cementation by late calcite and dolomite, are not specific to Ellenburger carbonate rocks. Similar diagenetic relationships as those observed in this study, as well as by Kupecz (1989), have been described from other deeply-buried carbonate rocks elsewhere (e.g. Mazzullo, 1986; Mazzullo and Harris, 1986; Montanez and Read, 1989), and from MVT-districts (e.g. Farr, 1989; Gregg and Shelton, 1989; Voss et al., 1989; Mussman et al., 1988). Such occurrences indicate that diagenetic aspects of carbonate rocks are intimately related to the evolution of sedimentary basins. The distribution of dolomite-rock textures could be related to the mechanism(s) of fluid migration in sedimentary basins. Coarse-crystalline planar replacement dolomites formed from burial-compaction fluids, which are most important in early stages of basin evolution and which are characterized by slow flow rates (< a few centimeter per year). Nonplanar replacement dolomites and cements could be related to basin-wide gravity-driven fluid migration which dominates in mature sedimentary basins with regional topographic gradients resulting from tectonic uplift. In such settings warm basinal fluids can migrate along deep aquifers at velocities of tens of meter per year (Bethke et al., 1988). Such velocities would be fast enough that warm fluids can reach shallow areas with temperatures conducive for mineralization and dolomitization. The timing and pathways of such fluid migration can be predicted from the distribution of porous and permeable aquifers, the distribution of dolomite-rock textures, and from periods of deformation and uplift.

Dolomitization patterns of ancient carbonate rocks such as the Ellenburger have to be interpreted in the context of the tectonic and hydrodynamic history of the entire basin. No single model of dolomite formation can therefore explain all the the dolomites present. Similar diagenetic styles and sequences related to a similar tectonic and hydrodynamic history are most likely present in different basins. The origin of massive dolostones, such as the Ellenburger, is best explained in the context of basin evolution, rather than in the search for one unifying model of dolomite formation.

GEOCHEMISTRY OF LATE CALCITE CEMENTS

Petrography

Coarse-crystalline clear calcite has been observed as a fracture-fill in dolomudstones, and occluding void-spaces that are lined by late-stage dolomites. Calcite has also been found in association with nonplanar-c dolomite, authigenic quartz, pyrobitumen and pyrite. Under the luminoscope this calcite is dull luminescent. Chemical zonation, suggestive of a change in fluid chemistry with time, has not been observed.

Geochemistry

Microprobe analysis data of these calcites are listed in Table 4. In Table 5 they are compared to previously published data.

Iron is present in all samples analyzed. Fe seems to substitute for Ca (r^2: $CaCO_3$-$FeCO_3$: -.67; p = .0992) into the lattice, indicating the environment of calcite precipitation must have been reducing. Calcite associated with pyrite has the lowest Fe-concentrations of the studied samples, suggesting removal of Fe during pyrite formation with the consequent precipitation of Fe- poor calcite.

Manganese is present in rather low amounts compared to published data (Table 5). The incorporation of Mn into the calcite lattice requires reducing conditions. A broad positive correlation exists between Fe and Mn (r^2 = .85; p = 0.162).

The mean values and ranges for magnesium are high compared to other published data (Table 5). Mg is incorporated into the calcite lattice independently of redox potential of the environment of precipitation. No distinctive correlation exists between Mg-Fe and Mg-Mn (Table 4).

Sr concentration are comparatively low (Table 4) and mostly below the detection limit of the microprobe.

Interpretation

Based on paragenesis, petrographic and geochemical characteristics the calcite cements are inferred to be of late, deep-burial origin. Similar late, void-filling dull cements have been described and interpreted to have formed from deep-burial pore fluids (e.g. Grover & Read, 1983, Dorobek, 1987).

Paragenetic relationships indicate the association of the calcite cements with late dolomite cements and authigenic quartz. The calcites are only observed in voids and fractures

Table 5: Geochemical Data on Late Calcite Cements.

	N	Min.	Max.	Mean	Std.Dev.
Fe (ppm)	7	666	2,598	1,402	776
Mn (ppm)	7	0	245	82	92
Sr (ppm)	7	0	252	44	86
Mg (ppm)	7	2,495	5,412	4,447	993
$CaCO_3$ (mole %)	7	97.0	98.0	97.7	.6
$MgCO_3$ (mole %)	7	.1	2.4	1.7	.8
$FeCO_3$ (mole %)	7	.1	.5	.3	.1
$MnCO_3$ (mole%)	7	0	.1	.02	.01
$SrCO_3$ (mole %)	7	0	.03	.01	.01

r^2: Fe - Mn: .85; p = .0162

Fe - Mg: .42; p = .3522

$CaCO_3$ - $FeCO_3$: -.67; p = .0992

Table 6: Published Geochemical Data (in ppm) of Inferred Late Calcite Cements in Comparison with Present Study.

	Fe	Mn	Mg	Sr
Emery (1987): non-ferroan, NFC, and ferroan, FC, calcites.	**NFC:** m = 920 r = 140-1,680 **FC:** m = 3,580 r = 2,030-4,830	m = 120 r = 80-230 m = 230 r = 160-390	m = 1,780 r = 600-2,770 m = 1,400 r = 540-2,840	m = 330 r = 90-840 m = 320 r = 80-560
Dorobek (1987): dull cements.	m = 1,261 r = 0-42,500	m = 293 r = 0-2,475	m = 1,801 r = 0-10,699	---------- ----------
Grover & Read (1983): dull cements	m = 970 r = 0-3,143	m = 440 r = 0-2,475	m = 1,900 r = 430-3,910	m = 30 r = 0-1,000
Moore (1985): post-compaction cements	m = 356 +/-328	m = 293 +/-28	m = 2,268 +/-241	m = < 100
This Study: dull cements	m = 1,402 r = 666-2,548	m = 82 r = 0-245	m = 4,447 r = 2,495-5,412	m = 44 r = 0-252

m = mean; r = range

generated in the subsurface, where they commonly postdate the emplacement of mature hydrocarbons.

Fluid inclusion homogenization temperatures and stable isotope analysis for these calcites were obtained by Lee & Friedman from samples of the same wells as used in this study. A wide range of homogenized temperatures occured at all depth-intervals (Lee & Friedman, 1987, table 1) , ranging from 59 - 317 °C. Carbon and oxygen isotopes values ranged from -1.2 to -16.8 °/oo, and -4.7 to -12.0 °/oo, respectively (Lee & Friedman, 1987, table 2). Based on these analyses, Lee & Friedman (1987) inferred elevated temperatures at the time of precipitation.

The Fe and Mn trace element of the calcites indicate formation under reducing conditions form fluids that probably were basinal brines.

KARSTIFICATION AND BRECCIATION

INTRODUCTION

The Ellenburger Dolomite is commonly referred to as "fractured dolomite" (Galloway et al., 1983). Fracture-related porosity is most abundant in the upper Ellenburger (e.g. Loucks and Anderson, 1985; Kerans, 1988 a, b), with breccia porosity the most common type. Fracturing is also thought to improve permeability by connecting isolated pores and porous zones.

The origin of these fractures is a subject of controversy. Various genetic types of breccias have been reported from the Ellenburger. The most commonly proposed origins of the majority of fractures and related breccias observed in the Ellenburger are tectonic fracturing and karst-related brecciation (collapse breccias).

In a recent study Ijirigho and Schreiber (1986, 1988) proposed a composite classification of fractured and brecciated Ellenburger rocks. They recognized the presence of numerous genetic breccia types, but interpreted 90% of the fractures and breccias that contribute to production as tectonic in origin, with as many as four tectonic epochs recognizable in some wells. Tectonic activity related to foreland deformation along the Ouachita fold belt (e.g. Hills, 1984; Wuellner et al., 1987) between the late Mississippian and the end of the Permian was invoked for the repeated fracturing of Ellenburger rocks.

A karst-related origin for these features was favored by other workers (e.g. Lucia, 1968, 1971, 1988; Loucks and Anderson, 1980, 1985; Tobin, 1985; Kerans, 1988 a), with tectonic fracturing of only local importance. Lucia was the first to recognize the karst nature of Ellenburger - age equivalent El Paso Group carbonates as early as 1968, and he described in detail the geometry, distribution and textural characteristics of karst-related collapse breccias and associated deposits in the Franklin Mountains of west Texas (Lucia, 1968, 1971, 1988). He ascribed the formation of these breccias to the collapse of extensive caverns developed by groundwater dissolution during the El Paso- Montoya unconformity. The major collapse of these caverns occurred during and after Silurian time, fracturing the overlying Upper Ordovician and Silurian rocks.

Other Lower Ordovician karst-related deposits have subsequently been described for Knox (e.g. Mussmann and Read, 1986; Mussmann et al., 1988), Beekmantown (e.g. Friedman and Lee, 1985) and Ellenburger carbonates (e.g. Barnes et al., 1959; Tobin, 1985; Loucks and Anderson, 1980, 1985; Kerans, 1988 a). These exposure surfaces were related to a Middle Ordovician sea level lowstand that was most likely global in extent (e.g. Sloss, 1969; Mussmann and Read, 1986), resulting in prolonged periods of subaerial exposure and

the development of karst-related deposits.

Recently, Kerans (1988 a) introduced a paleokarst model for the upper part of the Ellenburger dolomite. In his model he divided Ellenburger breccias into 1) fracture and mosaic breccias, which represented in-situ brecciation, and 2) matrix-supported and clast-supported chaotic breccias, which represented mixtures of autochthonus and allochthonous materials resedimented by gravitationally driven process (Kerans, 1988 a, p. 1167). Two common associations are characteristic for these breccias and associated deposits: a laterally persistent and a laterally restricted association. The laterally persistent association is traceable on a regional basis and comprises three laterally persistent karst zones: a cave-roof facies, a cave-fill and a lower collapse zone. The cave-roof facies is divided into an upper and lower cave-roof zone. The upper zone comprises an interval of unbrecciated dolostones; the lower zone shows variable development of fracture breccias and associated porosity. Laterally restricted breccias occur in zones that extend for several hundred feet below the Ellenburger-Simpson unconformity (Kerans, 1988 a). Examples of this type are exposed in the Ellenburger equivalent El Paso Group of the Franklin Mountains of West Texas and described by Lucia (1968, 1971, 1988). Within the Ellenburger they are best developed in the southeastern areas of Texas (Pecos and Val Verde counties) (Kerans, 1988 a, p. 1177).

Evidence gathered in this study suggests a karst-related origin for most of the fracturing and brecciation in the studied Ellenburger intervals. Tectonic-induced fracturing is observed locally, modifying in part earlier karst-related brecciation.

Before discussing the evidence for karstification, a discussion of what is meant by karst seems appropriate.

Esteban and Klappa (1983, p. 11) define **karst** as " a diagenetic facies, an overprint in subaerially exposed carbonate bodies, produced and controlled by dissolution and migration of calcium carbonate in meteoric waters, occurring in a wide variety of climatic and tectonic settings, and generating a recognizable landscape."

Paleokarst is used to describe karst features formed by solution associated with a landscape of the past (e.g. Walkden, 1974; Wright, 1982).

James and Choquette (1984) and Choquette and James (1988, p. 3) list and discuss intrinsic and extrinsic factors that influence the development of the wide variety of karst features. The most important intrinsic factors are general lithology, stratal permeability and the availability of fractures and other potential conduits for groundwater. Important extrinsic factors were climate, vegetation, the relationship between initial subaerial relief and diagenetic base level and the time of duration of the exposure (Choquette and James, 1988).

A variety of surface and subsurface karst features are the end result of interacting

processes governed by by the above mentioned factors. The most commonly recognized aspects of subsurface paleokarst are (Choquette and James, 1988): extensive dissolution in the form of caves and cavities, characteristic precipitates that occlude these voids, cave sediments, and karst collapse breccias.

Features commonly associated with paleokarst (Choquette and James, 1988, Table 2, p. 15) that are present in the Ellenburger are:

- Unconformity on top of the Ellenburger
- non-selective dissolution voids
- Dissolution enlarged fractures
- Karst breccias (collapse breccias)
- banded and laminar infill sediments

Karst breccias and associated deposits are most characteristic, and in the following discussion heir distribution, characteristics and importance for modes and timing of dolomitization are examined in more detail.

DISTRIBUTION OF BRECCIAS

Evidence for fracturing and brecciation has been found in all but one of the studied wells. In the Terrill State #1 well (well 2) from the deep Delaware basin no evidence for fracturing and /or brecciation has been found. All other wells show variable extent of fracturing and brecciation.

The most abundant and extensive fracturing and brecciation occurs in the upper Ellenburger indicating a stratabound nature of the breccias. This can be seen in the Continental State #1 well, Lea County, NM, and the J.E. Phillips #1 well, Edwards County, TX, where extensive fracturing, brecciation and solution- related porosity occurs in the upper 200 ft (60 m) below the top of the Ellenburger. In the Puckett No. 1 well, Pecos County, TX, fracturing is observed throughout the core, but fracture porosity is most abundant in the upper 200 feet (60 m) of the Ellenburger (Loucks and Anderson, 1980, 1985).

The most intensive fracturing and brecciation has been observed in well one (Continental State #1, Lea County, NM) and well five J.E. Phillips #1, Edwards County, Tx). Most of the data on karst come from these two cores. They are therefore described in more detail below.

Well 1: Continental State #1, Lea County, New Mexico.

A detailed core log is shown in Figure 37. The 92 ft (28m) of core are characterized by (1) 100% dolomite, (2) absence or marginal preservation of original depositional textures, (3) lack

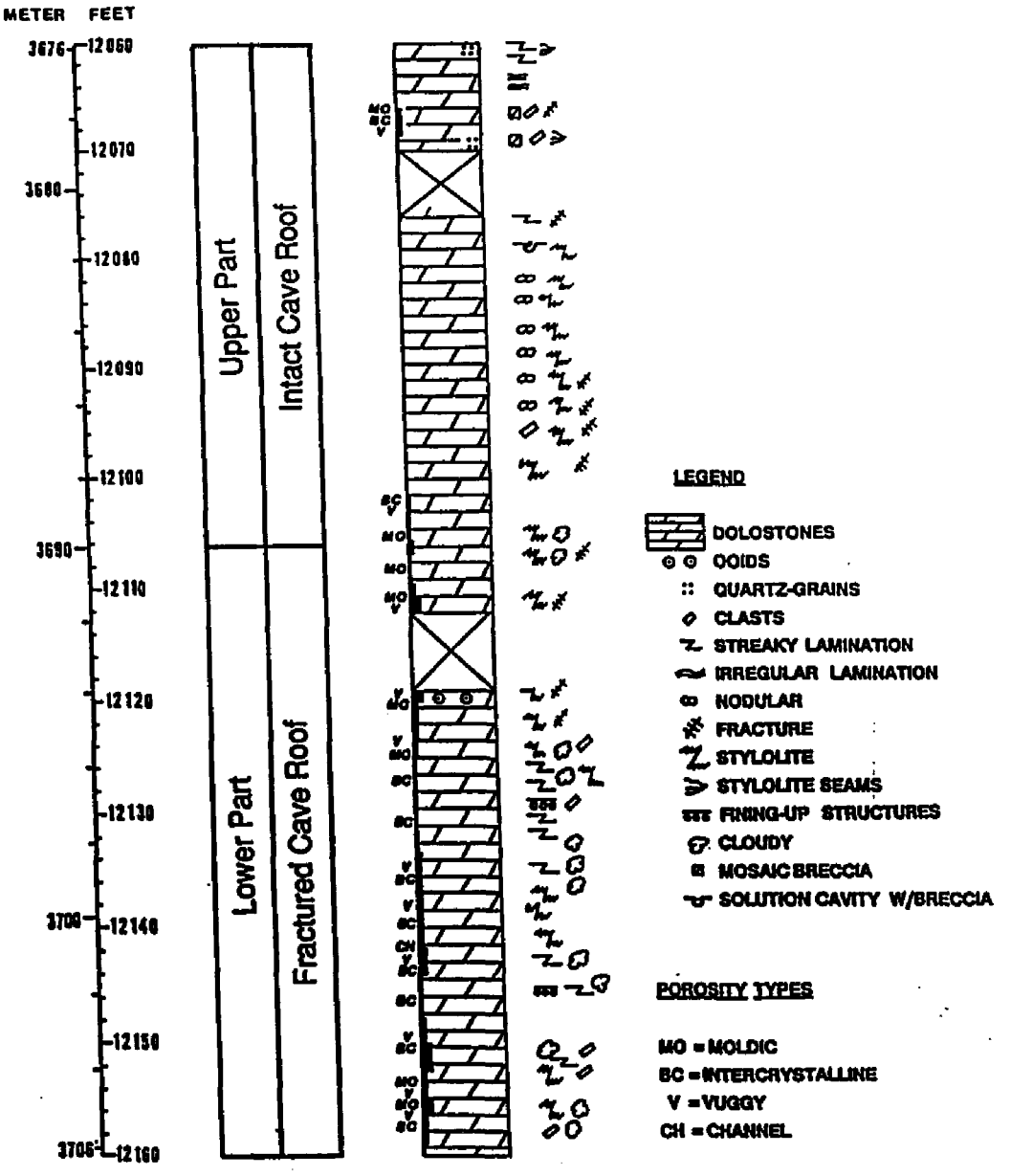

Figure 37. - - Lithologic column of Ellenburger dolomite in Continental State #1 well, Lea County, NM. The core can be subdivided into an upper part of dense, low porosity dolostones and a lower part of dolostones where solution-enlarged moldic, vuggy and solution-enlarged channel porosity are prominent. Upper and lower part can be correlated with the intact cave roof and the fractured cave roof of the paleokarst model of Kerans (1988 a).

of fossils, and (4) abundant stylolites, fractures, and related porosity. Based on correlations of well logs of the cored interval with logs from wells within the Stateline field and on calculations of the Ellenburger top using values from the structure-contour map, the top of the Ellenburger can be placed about 15 feet above the top of the studied core at 12,047 feet (Figure 38). It is therefore considered to be part of the upper Ellenburger, which is most strongly influenced by karst-related processes (Kerans, 1988 a).

The cored interval can be divided into two parts (Figure 37): (1) A lower part (12,107-12,159 ft; 3,690-3,706 m) of dolostones in which solution-enlarged moldic, vuggy, and solution-channel porosity are prominent. In this lower zone cementation by late- stage dolomite and infilling of internal sediment are responsible to a large degree for occlusion of this porosity, resulting in a rather chaotic appearance. (2) An upper 46 ft (14m), composed of dense, low porosity dolostones with an increasing density of fractures and low amplitude stylolites towards the lower part.

Lower Part (12,107-12,160 ft; 3,690-3,706 m). -- The lower part of the core is characterized by a chaotic appearance of solution- enlarged fractures, cm-sized vugs and solution channels (Figures 39 B, C). In many examples these vugs and channels are filled with very coarse dolomite and/or internal sediment. This results in a mosaic of light, irregular bands of coarse dolomite enclosing greenish gray patches of finer crystalline dolomite (Figures 39 C, D), representing most likely the host rock.

Two kinds of internal sediment can be found: (1) a greenish, clayey to marly material that partly occludes vugs and pores which shows in places geopetal infill structures (Figure 39 E, arrow), and (2) fine crystalline, white to brownish dolomite, exhibiting small-scale (mm-cm) fining-upward structures which commonly resemble banded vug sediment fills (Figure 39 E) as described by Esteban and Klappa (1983).

No original depositional textures are left to infer the environment of the precursor limestones. At 12,120 ft (3,694 m) pockets and patches as well as individual silicified ooids occur. Based on petrographic relationships they appear to be reworked particles and do not represent a particular environment for the zone in which they occur.

Under the petrographic microscope the dolostones show a polymodal texture, with fine- to coarse-crystalline planar-s and planar-e mosaics. Late-stage nonplanar (nonluminescent) dolomite cement occludes much of the porosity.

Besides cm-sized vugs and solution channels, intercrystalline and solution-enlarged intercrystalline porosity (Figure 40 D) contribute to the higher amounts of porosity in this zone. Estimates from thin sections and core slabs give porosity values of up to 15%; porosity values calculated from bulk-density logs reach 9%, mercury porosimetry gives values of 6%.

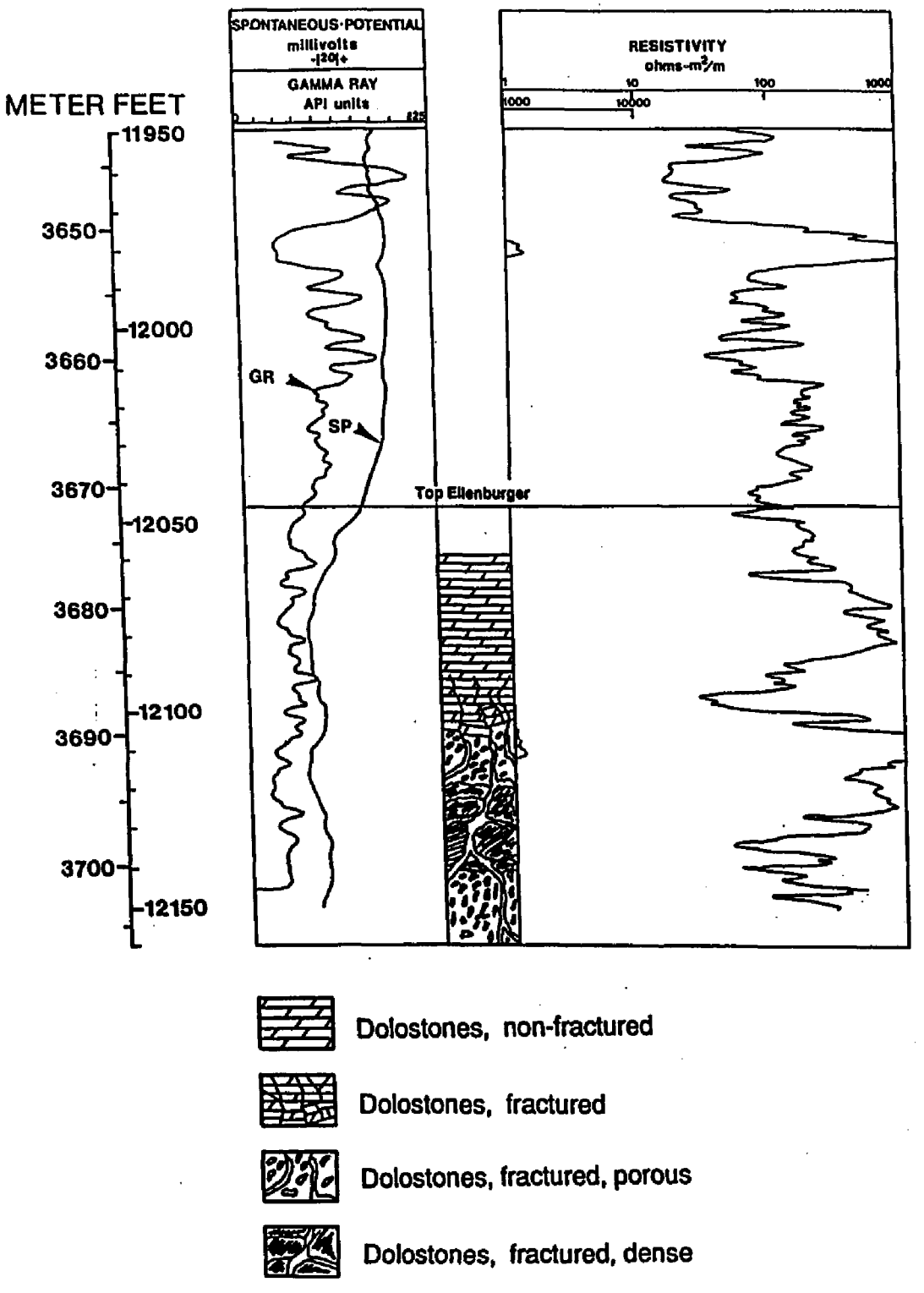

Figure 38. - - Log response of Continental State #1 well in comparison to core fabric.

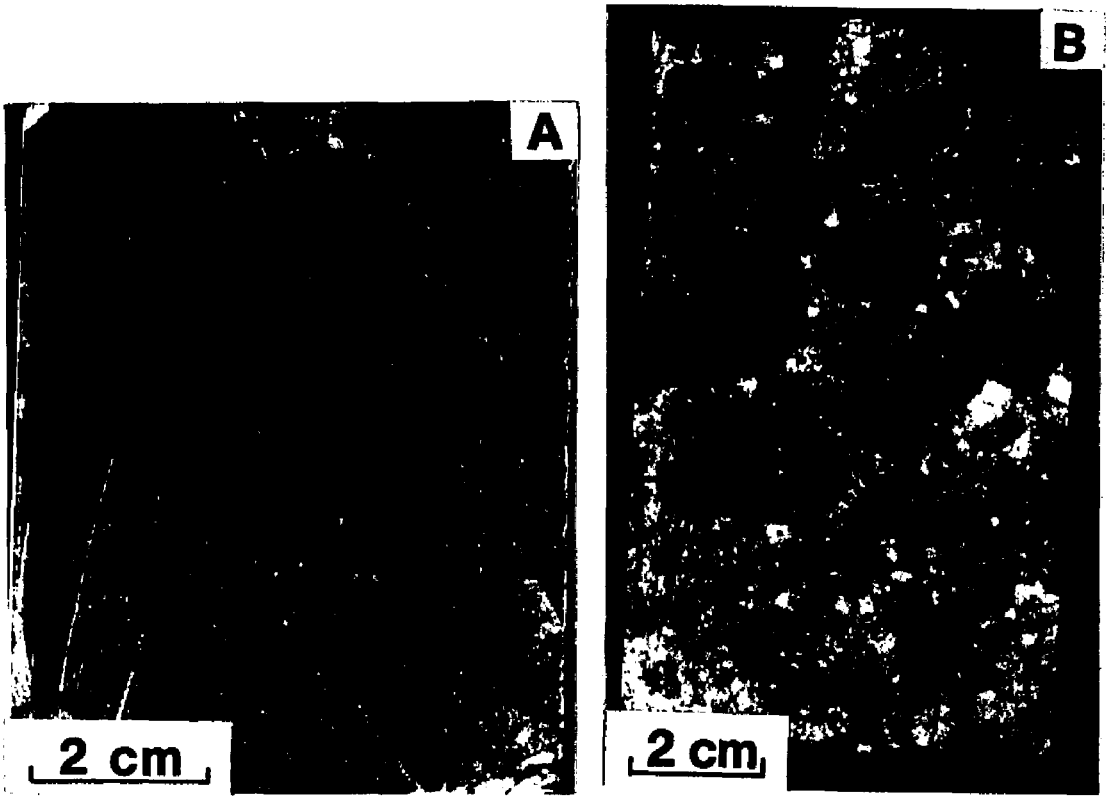

Figure 39. - - Core photographs of Ellenburger karst facies in Continental State #1 well. A) Sample from 12,091 ft (3,685 m) showing nodular texture. B) Vuggy porosity in sample from 12,119 ft (3,694 m).

(over)

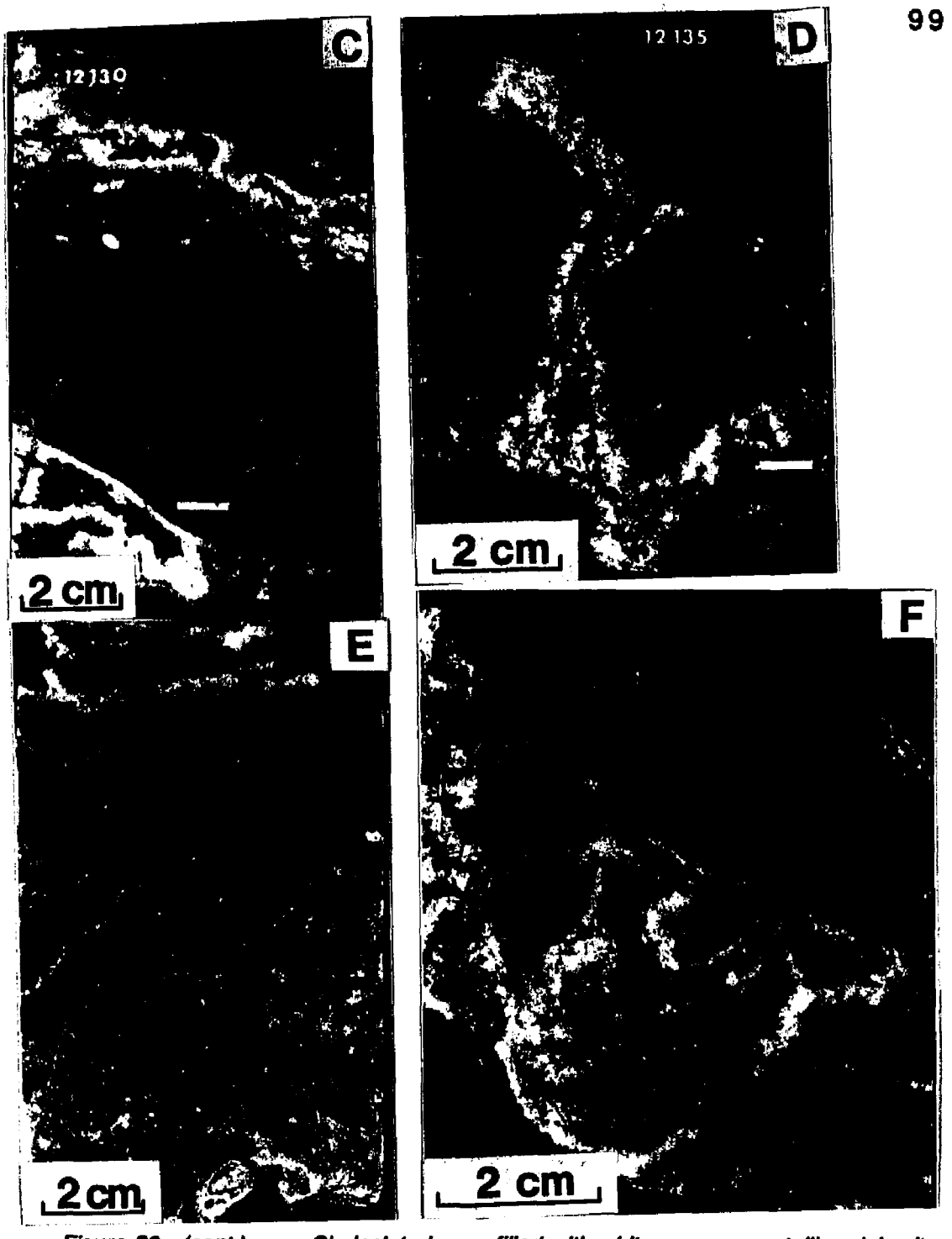

Figure 39. (cont.) - - C) Isolated vugs filled with white, coarse-crystalline dolomite; sample from 12,130 ft (3,697 m). D) Solution-enlarged fracture filled with white coarse-crystalline dolomite (center); sample from 12,135 ft (3,699 m). E) Banded sediment fill and geopetal infill structure (arrow) in sample from 12,128 ft (3,697 m). F) Cm-sized vugs (or breccia porosity?) partly filled with coarse-crystalline dolomite; sample from 12, 140 ft (3,700 m).

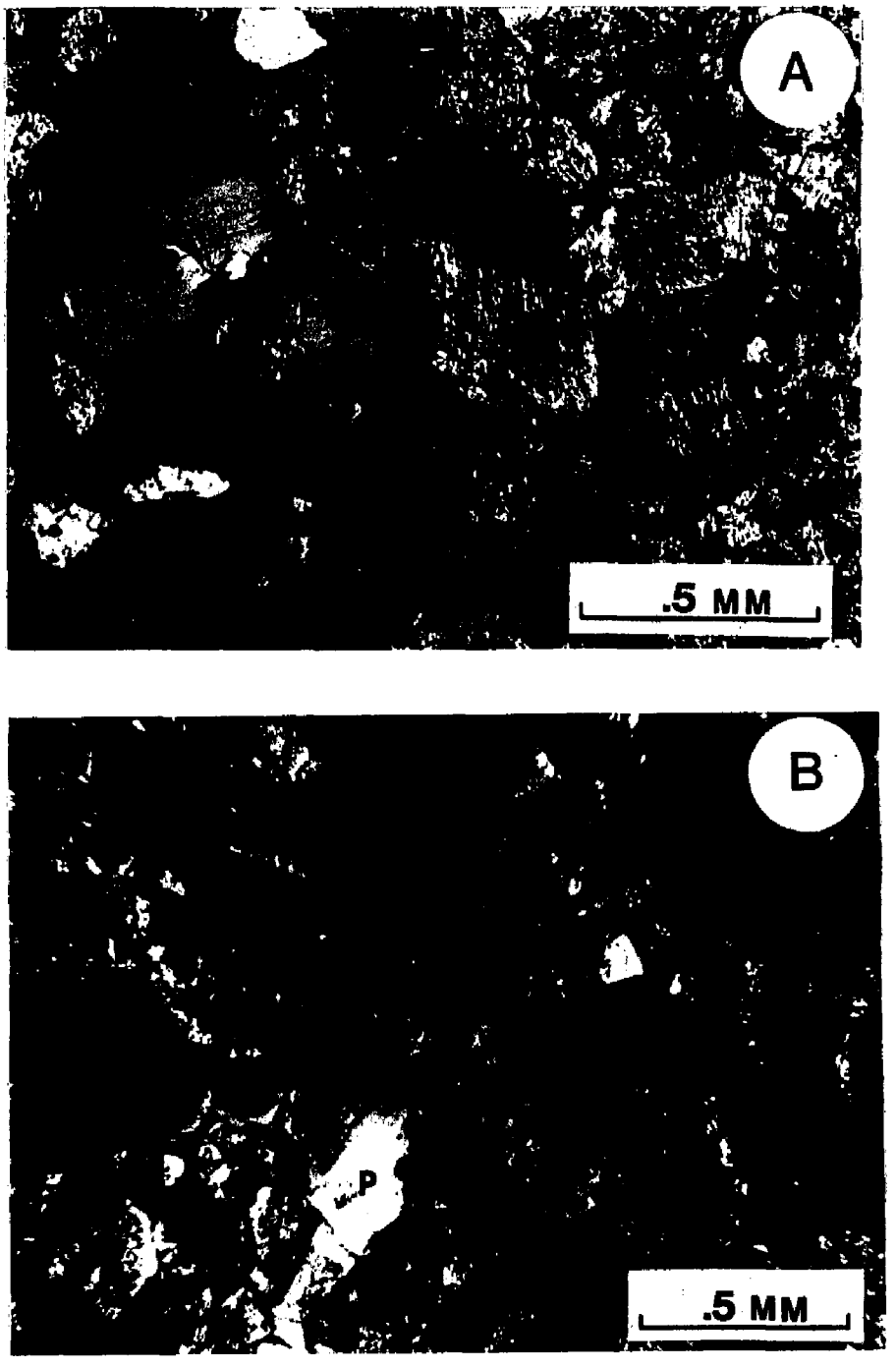

Figure 40. - - Thin-section photomicrographs of dolostones from Ellenburger karst facies in Continental State #1 well, illustrating porosity types. Most of the microporosity is related to intercrystalline pores (A to C), and to solution-enlarged intercrystalline porosity (D). A) Sample from 12,067 ft (3,678 m). B) Sample from 12,087 ft (3,684 m). (over)

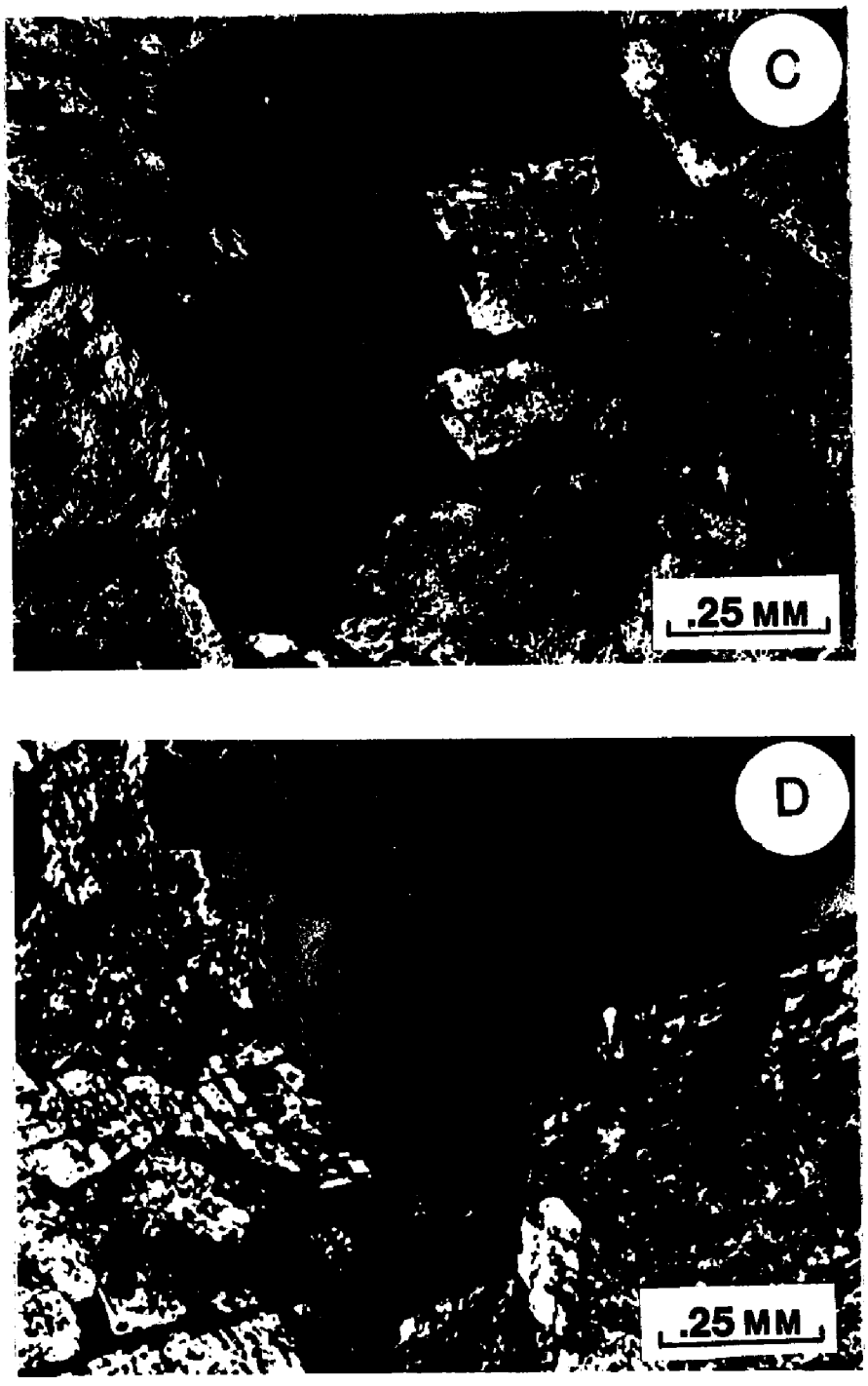

Figure 40 . (cont.) -- C) Sample from 12,111 ft (3,691 m). D) Sample from 12,148 ft (3,703 m).

Upper Part (12,060-12,106 ft; 3,675-3,690 m). -- The upper part consists of 46 ft (14m) of light to medium gray, dense dolostones. Almost no original depositional textures can be recognized. Only in the few uppermost feet a faint parallel lamination in the dolostones, associated with thin (<.5 cm) laminae of fine-grained, rounded to subrounded quartz grains can be recognized. The majority of the upper part consists of dolostones with a nodular texture enhanced by stylolites (fitted fabric)(Figure 39 A). Thick seams (> 2 cm) of black residual material, which form natural breaks in the core, are encountered in this interval (e.g. at 12,082 ft), and can be correlated with peaks on the gamma-ray log (Figure 38). This zone has a characteristic low porosity. In thin sections this is manifested in dense mosaics of mostly planar-s crystals, showing unimodal or polymodal textures. Small amounts of porosity are related to fractures, intercrystalline pores (Figures 38 A, B) and moldic or solution- enlarged porosity along stylolites.

Interpretation. -- The described Ellenburger interval is interpreted to represent the cave-roof facies of the laterally persistent facies association, using the terminology of the paleokarst model of Kerans (1988 a). This interpretation is based on the following characteristics found in the studied core:

(1) The core is situated about 15 feet below the post- Ellenburger unconformity, and is therefore part of the upper Ellenburger, which is most strongly influenced by karst-related processes.

(2) Absence or marginal preservation of original sedimentary textures throughout the core.

(3) Chaotic appearance and fracturing of the dolostones over considerable length in the lower part of the core.

(4) Extensive vuggy and solution-enlarged porosity.

(5) Dissolution-enlarged fractures.

(6) Infilling of vugs and fractures by internal sediment exhibiting geopetal and banded or laminar structures.

The upper part of the core (12,060-12,106 ft; 3,675-3,690 m) corresponds to the relatively intact cave-roof of dense, low porosity dolostones. The thickness of 46 ft (13 m) correlates well with values of other Ellenburger karst facies (e.g. Kerans, 1988 a, p. 1170). The lower part (12,107-12,160 ft; 3,690-3,706 m), characterized by fractures, solution-enlarged fractures and different kinds of porosity represents the lower zone of the cave-roof facies. This zone, about 50 ft (15 m) thick, shows the highest porosity in the core.

Well 5: Phillips #1, Edwards County, Texas.

This core can be subdivided into an upper brecciated part and a lower part composed of unbrecciated limestones and dolostones with intercalated breccias (Figure 41).

The top of the Ellenburger at 5,091 ft (1,552 m) is placed the base of a five feet interval of grayish-red shale that contains olive-gray to yellowish chert beds (e.g. Barnes et al., 1959, plate 1). This contact also corresponds to pronounced log signatures (Figure 41).

Lower part (5,185-5,310 ft, 1,580-1,619 m). -- The lower part composes bedded and nonbrecciated limestones and dolostones with a major intercalated breccia zone (5,219 - 5,227 ft, 1,591 - 1,593 m). The limestones are peritidal, open-marine deposits and are represented by the lithofacies 2 (mudstone/wackestone facies) and lithofacies 4 (peloid-ooid-intraclast packstone/grainstone facies) (see section on depositional environment and facies for details). The lowermost part of the core is made up of dolomudstones. The breccia zone within the limestones comprises clast-supported chert breccias. This breccia horizon can also be identified on the SP and resistivity curves.

Upper part (5,091-5,185 ft, 1,552-1,580 m). -- This zone, directly underlying the red shale horizon consists of a thick (100 ft, 30 m) sequence of matrix-supported breccias that grade at the bottom into a thin zone of clast-supported breccias. XRD - analyses indicate that matrix-supported breccias are composed mostly of dolomite and quartz, while the clast-supported breccias are limestone. This brecciated part is clearly delineated by both the SP and the resistivity logs (Figure 41).

Interpretation. -- The J.E. Phillips #1 core is interpreted to represent part of the laterally restricted facies association of the paleokarst model by Kerans (1988 a). This interpretation is based on the following criteria:

(1) The core is part of the upper Ellenburger, with the post- Ellenburger unconformity represented by a red shale horizon which can be interpreted as a paleosoil.

(2) The breccia of the upper part extends continuously downhole for about 100 ft (30 m) from the unconformity, and is under- and overlain by nonbrecciated rocks.

(3) Evidence for solution-collapse exists in the form of matrix-supported and clast-supported breccias, which show also evidence for vertical displacement.

(4) Breccias, stratified sediments and nonbrecciated host-rock are closely associated within one interval.

(5) The core is situated in an area where laterally restricted breccias are best developed.

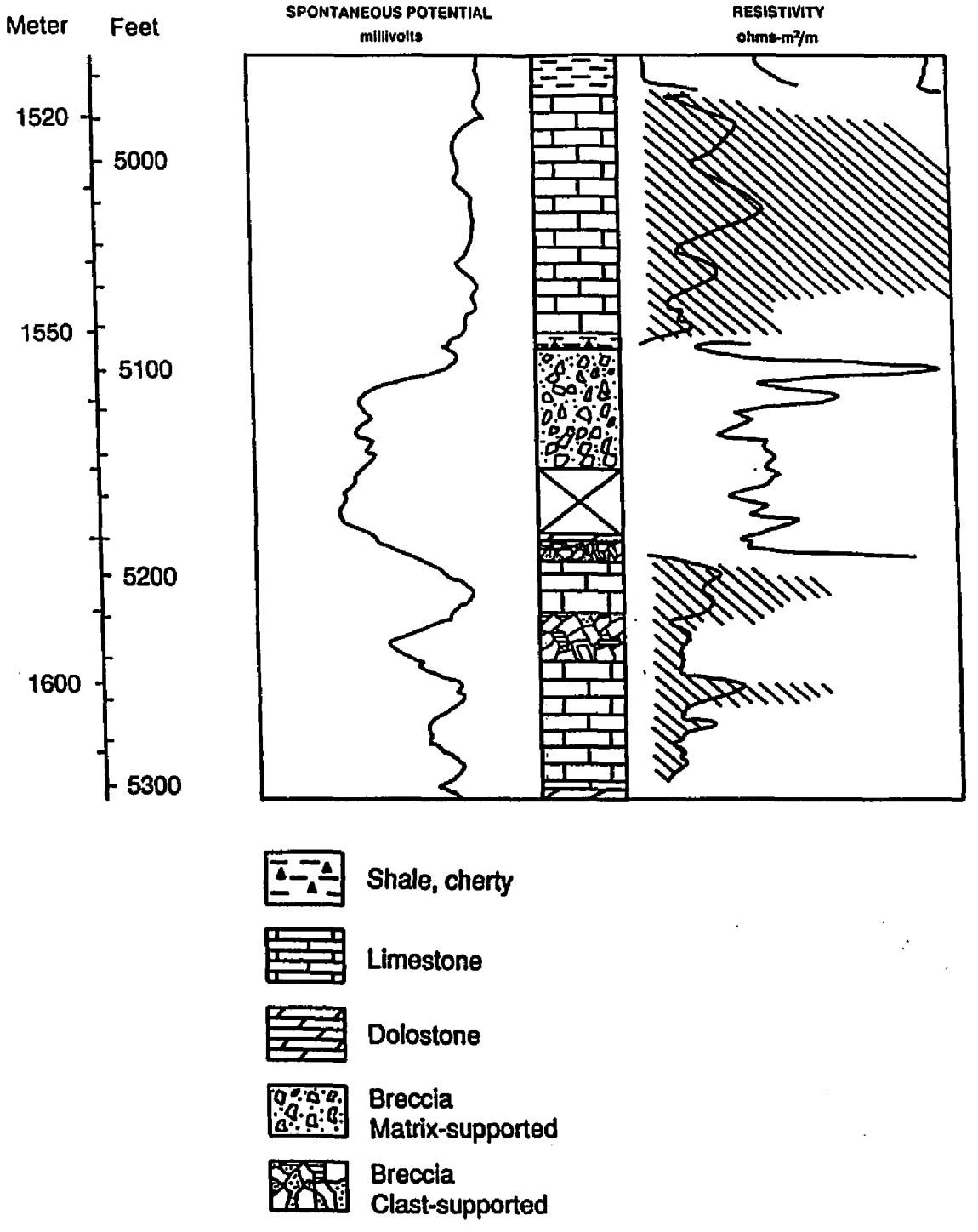

Figure 41. -- Comparison of log response to core fabric in Phillips #1 well, Edwards County, TX. The subdivision in lower part composed of unbrecciated limestones and dolostones with intercalated breccias, and an brecciated upper part is clearly delineated by both the SP and resistivity logs.

Karst Breccias

Various breccia types are recognized in the studied Ellenburger intervals:

a) Matrix - supported chaotic breccias.

b) Clast - supported chaotic breccias.

c) Crackle or fracture breccias.

Matrix-supported chaotic breccias. -- Angular to subrounded lithoclasts, less than 1 mm to several cm in size "float" in a brownish-yellowish sandy dolomite matrix (Figure 42). The clasts are of variable composition. Dolomite clasts, composed of light to medium gray, fine crystalline structureless dolomite are the most common type (80%). Also encountered are subrounded sandstone clasts and shale fragments and varying amounts of chert fragments. The matrix is composed of fine - crystalline dolomite and silt - sized sandy material.

Thin sections show that the majority of the clasts are composed of very fine- to fine - crystalline planar-s dolomite (dolomite type 1)(Figure 43). The planar-s dolomite commonly forms dense mosaics; however, clasts exhibiting a considerable microporosity are also encountered. If clasts are in contact they form sutured contacts, with quartz-grains squeezed between the clasts, and the development of low-amplitude stylolites. The matrix between these clasts is composed of medium- to coarse - crystalline planar-e and planar-s mosaics. These mosaics share a common cathodoluminescence microstratigraphy with dull to brownish zones in planar-s crystals and alternating dull and bright zones in planar-e crystals. A nonluminescent outer rim is frequently observed in planar-e crystals. No detrital dolomite, as described for example by Conglio and James (1988) has been found in the matrix.

In the interstices of the mosaics intercrystalline porosity is developed or silt-sized sandy and dolomitic material fills the pore spaces.

This breccia type has been encountered in the J.E. Phillips #1 well, Edwards County, TX, Val Verde basin, where it is best developed in the upper 100 ft (26 m) of the Ellenburger, that is below the post-Ellenburger unconformity.

Clast-supported chaotic breccias. -- This type can be subdivided according to the major lithoclasts present into limestone breccias and chert breccias (Figure 44).

Subrounded to rounded, mm to 5 cm-sized light-gray limestone clasts and bluish-white chert clasts in greenish-gray clayey matrix are characteristic for the limestone breccia. The breccia exhibits clast-supported fabric, with the interstices filled by the greenish clayey matrix. XRD analyses indicate 100% limestone. The limestone clasts show internal textures that are

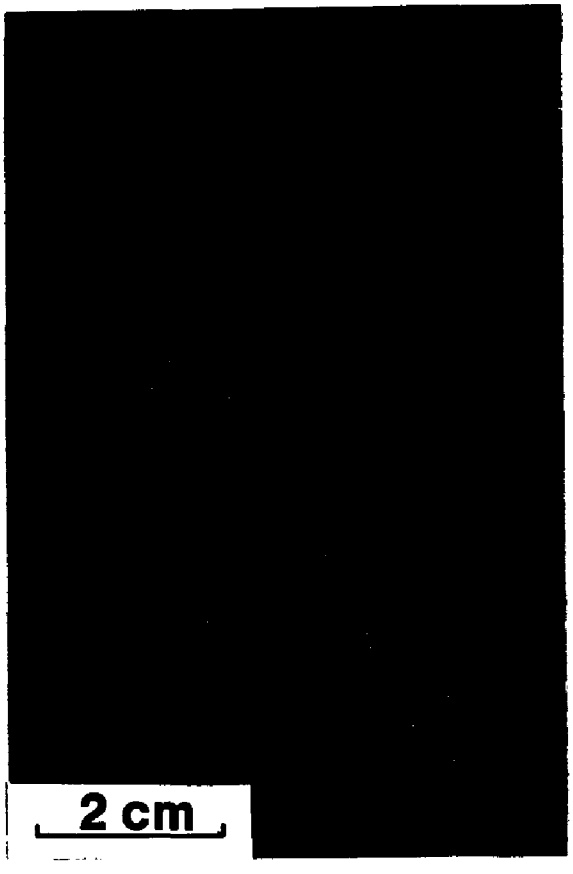

Figure 42. - - Core photograph of matrix-supported karst breccia. Angular to subrounded dolomite lithoclasts (dark) "float" in brownish-yellowish sandy dolomite matrix (light). Sample from 5,134 ft (1,565 m), well 5.

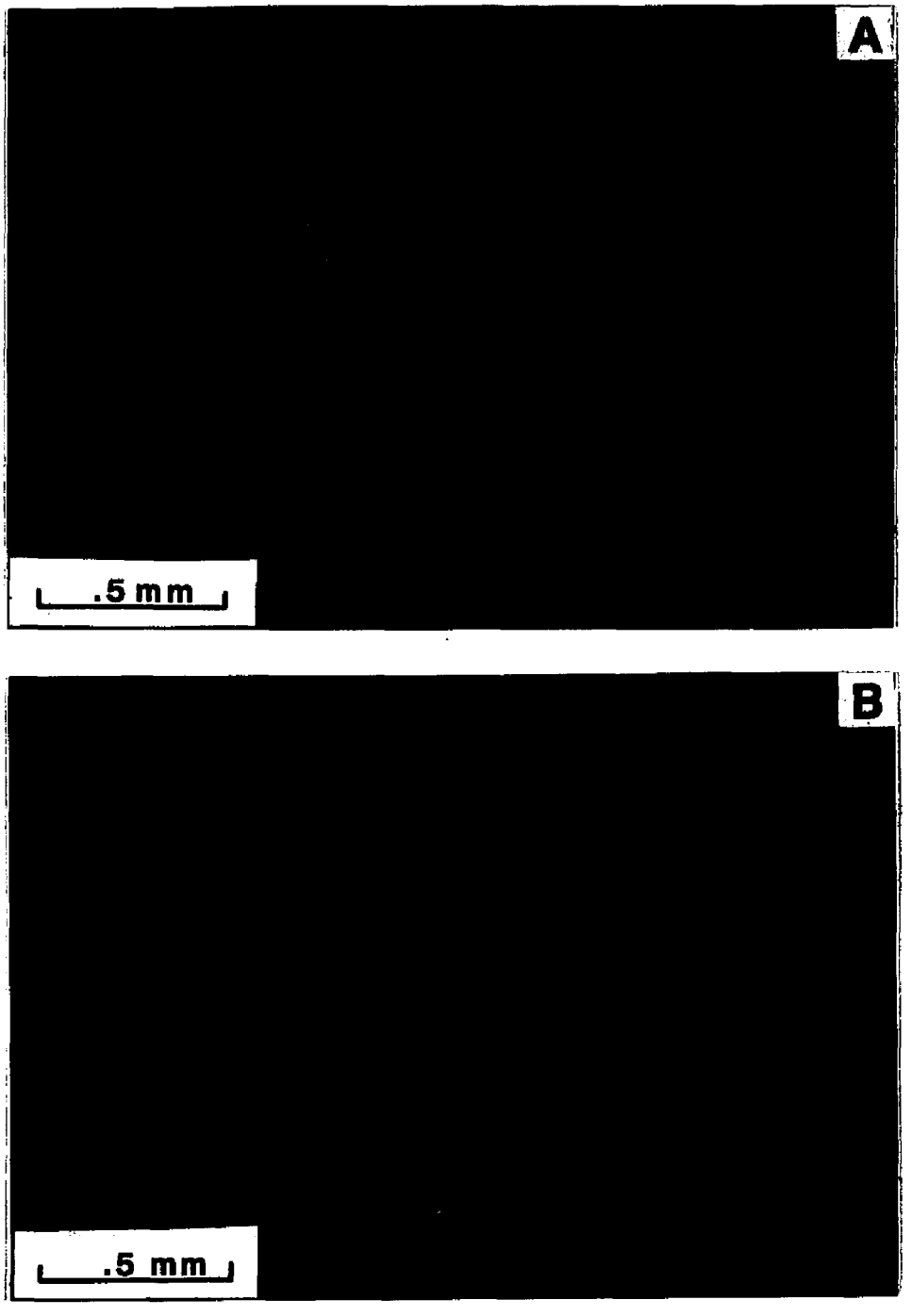

Figure 43. - - Thin-section photomicrographs of matrix-supported breccias. A) Dolomite lithoclasts (LC) composed of dolomite type 1 are cemented by planar-e and planar-s dolomite. Note the clear overgrowth (Z) and planar-e crystal. B) CL-picture of A showing zoned dolomite cement between dolomite lithoclasts (LC). Note nonluminescent zone (Z) of planar-e crystal. These zones attain up to 21 mole % $FeCO_3$. Sample from 5,121 ft (1,561 m), well 5.

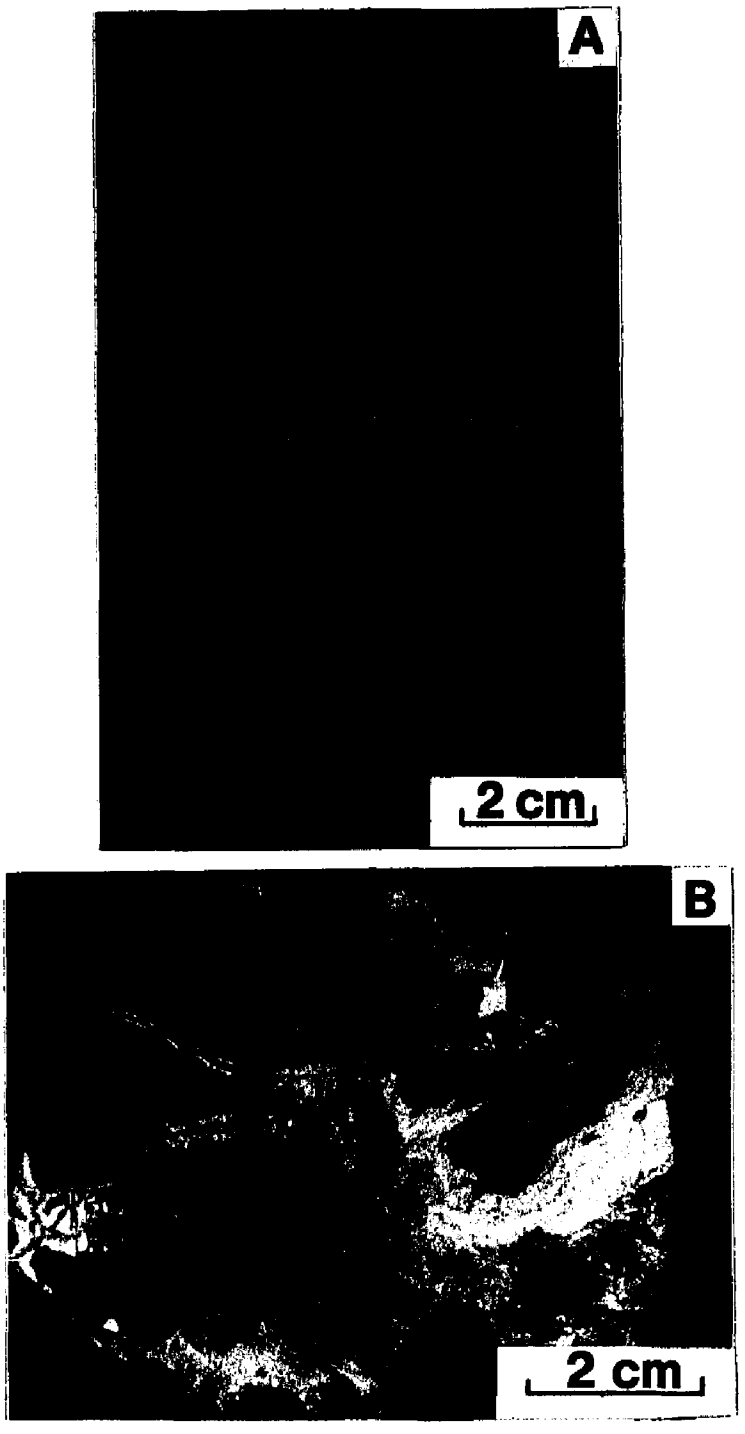

Figure 44. - - Core photographs of clast - supported breccia. A) Clast - supported breccia composed of limestones and chert-clasts. Limestone clasts show internal stratification indicating rotation and displacement. Stratified internal sediment overlies breccia. Sample from 5,184 ft (1,580 m), well 5. B) Clast-supported chert breccia. Note bleached borders of dark chert fragments and very coarse calcite cements. Sample from 5,225 ft (1,593 m), well 5.

identical to the surrounding limestone hostrock: peloid-rich laminae alternating with structureless micrite layers. This lamination indicates the random orientation of the limestones clasts; many clasts are subvertical and tilted. In part this breccia is overlain by a finely laminated greenish-gray argillaceous limestone alternating with thin laminae of pebble-rich units (identical to clasts below). Characteristic are nodular and rounded to disc-shaped clasts and draping of the limestone laminae around the clasts. The internal textures of clasts argue for transported clasts embedded in thin layers in laminated limestone (?cave-fill, infilling of pore space). Conspicuous are disc-shaped clasts which also would argue for erosion and transportation.

Another type of breccia comprises angular chert clasts (up to 10 cm in size) and small (.5 to 2 cm) rounded to subrounded limestone clasts cemented by very coarse, milky white calcite. The dark-gray chert clasts characteristically have milky-white bleached rims, which are cut by fractures along which a pale- yellowish material (?sphalerite) can be found. The very coarse calcite matrix is in part chalkified, producing a highly friable breccia. This breccia type is encountered stratigraphically below the matrix-supported breccia.

Both breccia types have been found in the J.E. Phillips #1 well, Edwards County, Tx.

Crackle breccias. -- This type comprises highly fractured dolostones, with fragments only slightly separated and displaced. No rotation or collapse is observed. It is characterized by narrow to wide gaps (up to 10 mm), which are either partly filled with authigenic quartz and/or milky white dolomite or completely filled with black material (?pyrobitumen) and pyrite.

Crackle breccias are encountered in the upper Ellenburger in the Continental State #1 well, Lea County, NM, where they occur above an interval showing extensive solution-enlarged fractures and porosity (Amthor and Friedman, 1989). In the Puckett No. 1 well, Pecos County, TX, crackle breccias are observed in all studied intervals. The fractures cut across original sedimentary structures resulting in small offsets and small scale brecciation. They are also observed to cut across earlier breccias (Figure 46 A), which were cemented by white coarse crystalline dolomite. Dolomite cemented clasts are incorporated in the fractures which are filled with black material and the clasts of the host breccia. In part these fractures are open or partly cemented by water clear authigenic quartz and/or a late dolomite (e.g. Figure 43 A). These partly open fractures attribute to fracture related porosity and permeability.

Interpretation and discussion

The characteristics of the breccias and their associated deposits suggest a karst-related origin with tectonic fracturing of local importance. This interpretation is based on the following

characteristics found in the studied cores:

(1) Absence or marginal preservation of original sedimentary textures throughout karst-related intervals.

(2) Chaotic appearance and fracturing of the dolostones over considerable length of the cores.

(3) Occurrence of extensive vuggy and solution-enlarged porosity.

(4) Presence of dissolution-enlarged fractures.

(5) Infilling of vugs and fractures by internal sediment exhibiting geopetal and banded or laminar structures.

(6) The breccias are of stratabound nature, e.g. they occur mostly in the upper Ellenburger where they are closely associated with a post-Ellenburger unconformity.

(7) The matrix-supported chaotic and the clast-supported chaotic breccias show evidence of solution collapse, such as gravitational displacement and rotation of clasts, sharp-edged fragments and rubble.

It is suggested that matrix-supported and the clast-supported breccias represent solution structures directly related to the post-Ellenburger erosional periods. Clast-supported chaotic breccias associated with thin stratified deposits form the lower part of the collapse zone, followed by matrix-supported breccias which most likely represent a cave-fill deposit.

(8) The association of different breccia types in one interval together with non-brecciated zones is difficult to explain by tectonic fracturing.

Crackle and fracture breccias represent in situ brecciation and are commonly associated with intact but fractured cave-roofs (Kerans, 1988 a; Amthor and Friedman, 1989 c).

A striking similarity exists between matrix-supported, clast - supported chaotic breccias and karst breccias that are suggested as hosts for Mississippi Valley type ore deposits in Tennessee (e.g. Ohle, 1959, 1980, 1985; Hill et al., 1971; Kyle, 1976, 1983), and Canada (e.g. Collins and Smith, 1975; Anderson and Macqueen, 1982; Rhodes et al., 1984). Matrix-supported chaotic and clast-supported chaotic breccias are similar in many respects to the early fine rock-matrix breccias and late coarse rock- matrix breccias described by Hill et al. (1971) and Kyle (1976, 1983) from age equivalent dolostones of the Knox Group, Tennessee. Cross-sections through collapse breccias (e.g. Kyle, 1983; Ohle, 1985; Sangster, 1988) reveal spatial relationships of these breccias bodies that can not be determined with the restricted core material available for this study but which are helpful in explaining the association of different breccia types. The geometry of such collapse breccias (e.g. Kyle, 1983, p. 86, Fig. 17; Ohle, 1985, p. 1745, Fig. 5) consists of a core of rubble breccia surrounded by mosaic and crackle breccia passing into undisturbed wall rock, thus

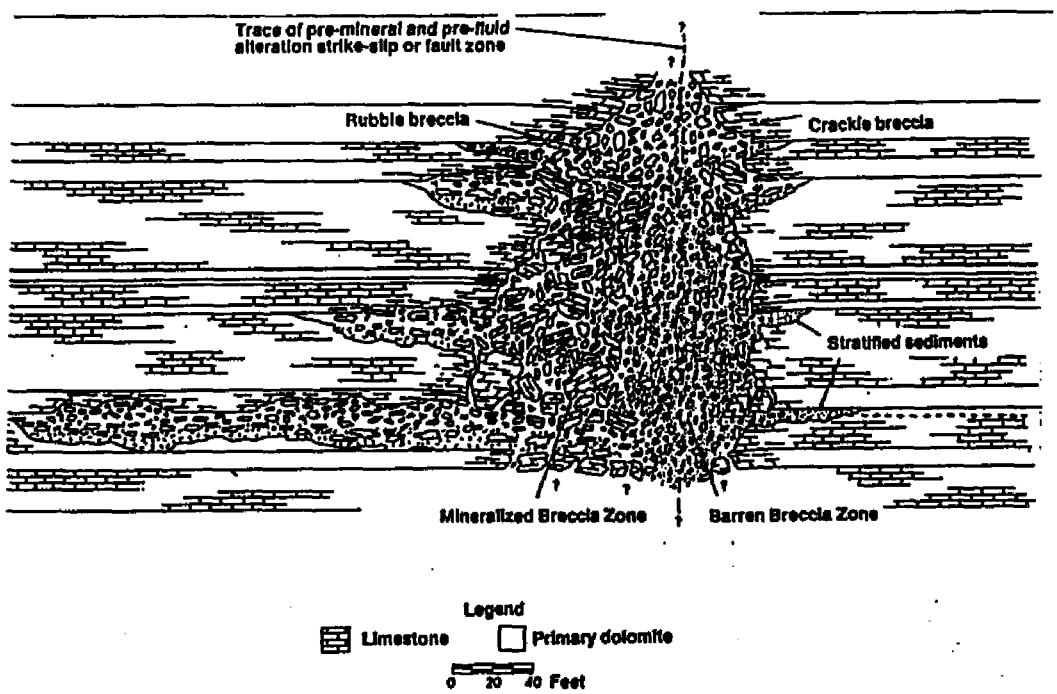

Figure 45. -- Schematic representation of a columnar, ore-bearing, breccia body in East Tennessee (from Ohle, 1985). Such a geometry can explain, a) the association of different breccia types, b) the presence of internal, stratified sediment, and c) intercalated breccias as offshoots in nonbrecciated host rock.

Such a breccia geometry can serve as an analog to explain the association and distribution of breccias and related deposits found in well 5.

explaining the association of different breccia types, the presence of stratified sediments and of non-brecciated host-rock in on interval (Figure 45).

Fracturing and brecciation related to tectonic processes is also observed in the Ellenburger. The products of this process are, however, distinct in many ways from the karst-related features. Evidence for tectonic fracturing has mostly been found in the Puckett No. 1 well and the interpretation is based on these occurrences. Ijirigho and Schreiber (1986, 1988) studied in detail fracture system in the Ellenburger and assigned 90% of the fractures to a tectonic origin. Tectonic fracturing may thus be of greater importance than the data from the here studied cores might imply.

Evidence for tectonic fracturing include:

(1) Tectonic fracturing and brecciation is not stratabound. In the Puckett well it has been observed within all intervals of the Ellenburger.

(2) Tectonic fractures cross-cut earlier breccias that are interpreted to be karst-related. These earlier breccias are cemented by white, late stage dolomite. Fragments of dolomite cemented breccias are incorporated into the fracture gaps that are filled with black material (?pyrobitumen) and pyrite (Figures 46 A, C).

(3) Tectonic breccias comprise only crackle or microdile (Ijirigho and Schreiber, 1988) breccias, representing in situ brecciation with only minor offsets and no rotation and gravitational displacement (Figures 46 B, D).

Thus tectonic brecciation can not explain the association of matrix supported and clast-supported breccias observed. Their origin is related to zones of solution and requires collapse into open space.

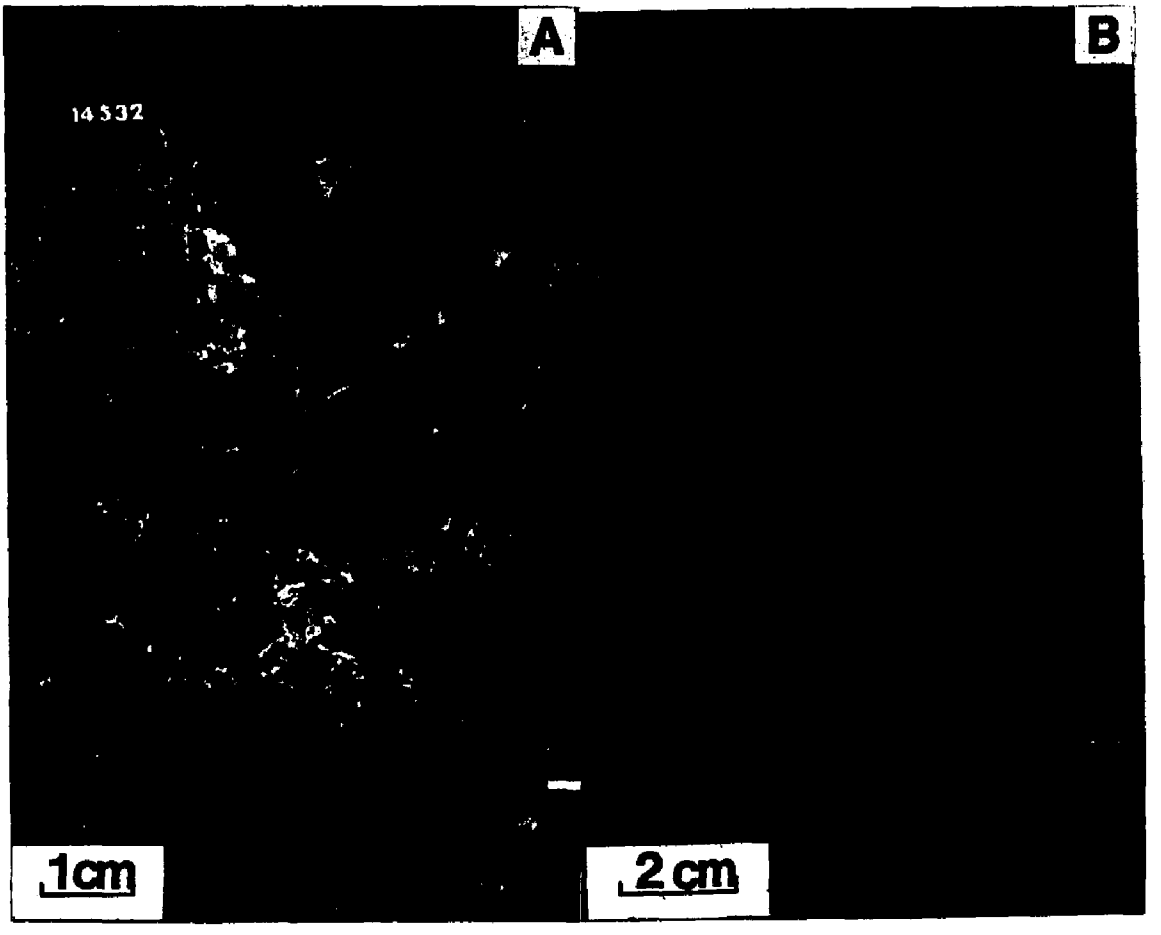

Figure 46.-- Core photographs of tectonic breccias. A) Earlier breccia (?karst-breccia), cemented by coarse crystalline dolomite is crosscut by later fractures filled with pyrobitumen and pyrite. Fragments of dolomite-cemented breccia are incorporated into these fractures. Sample from 14,532 ft (4,429 m), well 4. B) Laminated dolomudstone crosscut and brecciated by fractures filled with pyrobitumen and pyrite. Fractures are in part solution enlarged. Sample from 14,488 ft (4,416 m), well 4.

(over)

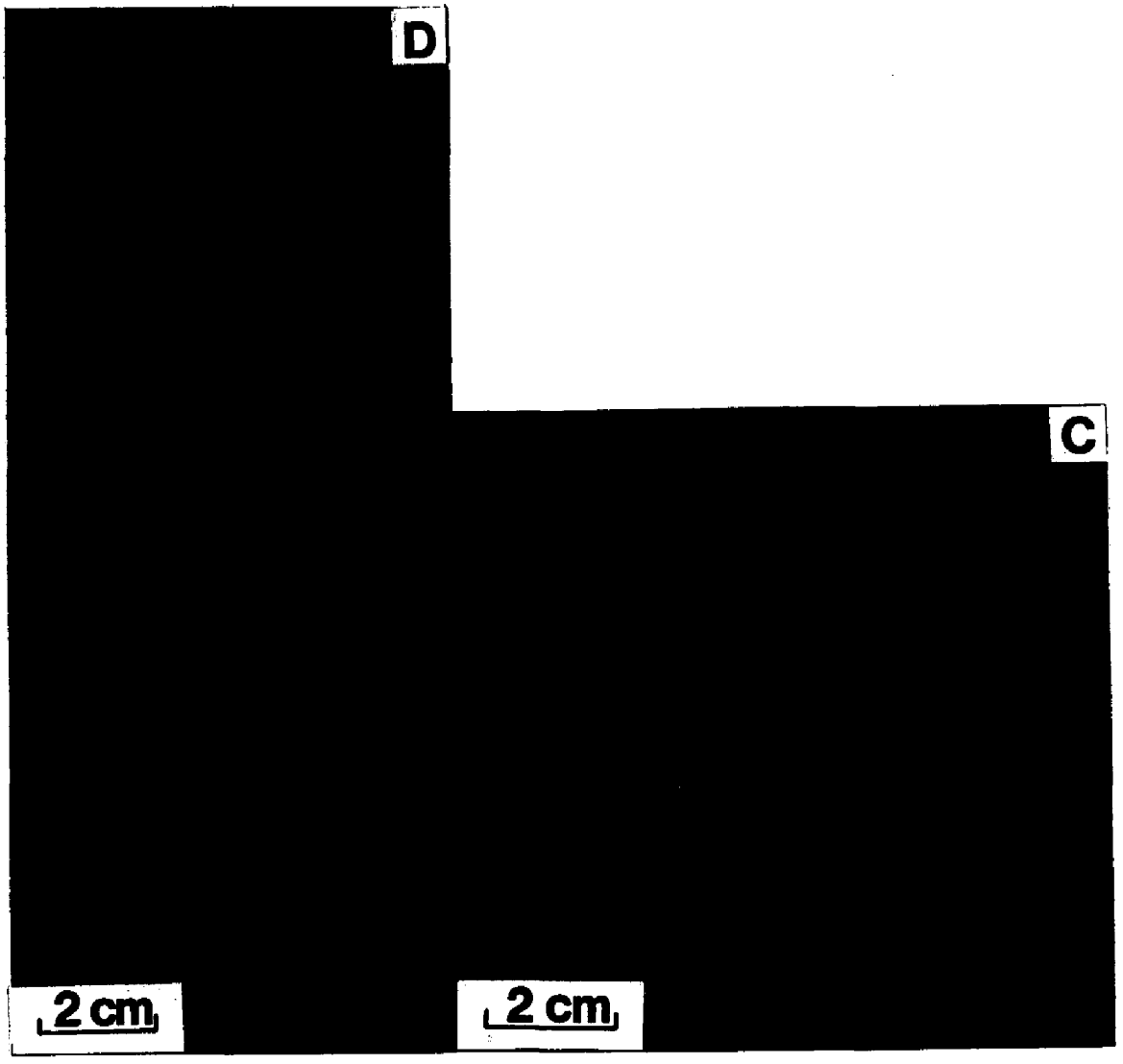

Figure 46. (cont.) - - C) Overprint of earlier breccias by tectonic fractures results in fracture-related porosity that is only partly occluded by precipitation of authigenic quartz. Sample from 14,532 ft (4,429 m), well 4. D) Two generations of tectonic fractures filled with coarse crystalline dolomite. Sample from 22,620 ft (6,895 m), well 3.

KARSTIFICATION AND DOLOMITIZATION

INTRODUCTION

Dolomitization is a common phenomenon associated with paleokarst deposits. This association has been described mainly from MTV-districts (e.g. Ohle, 1959, 1980; Kyle, 1977, 1983; Rhodes et al., 1984) with most studies concentrating on the relationship between dolomitization and the ore-forming process. Fewer studies exist, however, on the dolomitization of paleokarst deposits from such important oil and gas reservoirs as the Ellenburger of the Permian Basin (e.g. Kupecz, 1989) or the age equivalent Arbuckle Group of the Anadarko and Arkoma Basins.

Paleokarst-collapse breccias in the Ordovician El Paso and Montoya Groups of West Texas provide an ideal opportunity to examine the interaction between dolomitizing fluids and karst-related deposits. Excellent exposures of the breccias occur in the Franklin Mountains outside of El Paso, Texas. On the basis of field relationships and petrography, Lucia (1971, 1988) recognized several episodes of dolomitization in these Ordovician units. These include: 1) stratigraphic dolomitization of tidal flat units, 2) selective dolomitization of karst collapse breccias, and 3) precipitation of late fracture-filling baroque or saddle dolomite which may represent the latest phases formed during the second period of dolomitization. Stepanek (1988) documented three major states of dolomitization based on petrography and carbon-oxygen isotope analysis: 1) early "stratigraphic" dolomites, $\Delta\ ^{18}O$ PDB > -6 ‰, 2) replacement dolomites and dolomitic cements in breccias, with compositions trending from Δ^{18} 0 values > -6 ‰ to -8.5 ‰, and 3) late zoned ferroan saddle dolomite cements in karst fractures and vugs.

In this chapter the following points will be addressed: a) The relationship between dolomitization and karstification in Ellenburger rocks on the basis of petrography and geochemistry, and b) Comparison of the results to the studies by Lucia and Stepanek.

The results and interpretation are based on data obtained from wells one and five, which are most strongly influenced by karst-related processes.

Petrographic characteristics

The presence and distribution of different dolomite-rock textures in the karst facies of wells 1 and 5 is distinct and characteristic (Figure 47). Dolomite type 1 (unimodal, very fine to fine-crystalline planar-s mosaic dolomite) has been found in both wells. In well 1 it makes up

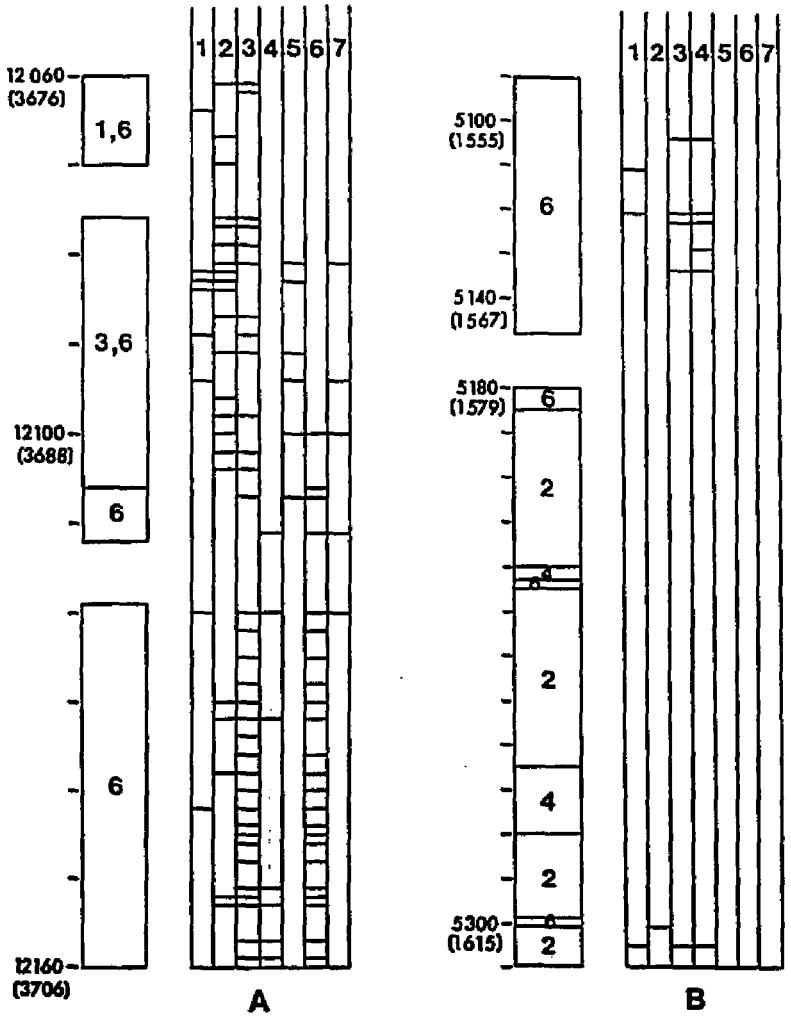

Figure 47. - - Schematic logs illustrating the distribution of dolomite-rock textures (numbers 1 to 7) in well 1 (A) and well 5 (B). Log depth is in feet with meter in parentheses. Logs of well 1 and 2 show the different lithofacies present: 1 = laminated dolomudstones/wackestone lithofacies, 2 = mudstones/wackestones lithofacies, 3 = mottled dolomudstone/wackestone lithofacies, 4 = peloid-ooid-intraclast packstone/grainstone lithofacies, 6 = karst facies. Horizontal bars indicate the presence of dolomite-rock textures in thin-sections: 1 = unimodal, very fine- to fine-crystalline planar-s mosaic dolomite, 2 = unimodal, medium- to coarse-crystalline planar-s mosaic dolomite, 3 = coarse- to very coarse-crystalline planar-s dolomite, 4 = medium- to coarse-crystalline planar-e mosaic dolomite, 5 = medium- to coarse-crystalline planar-e dolomite, 6 = coarse- to very coarse-crystalline nonplanar-a dolomite, 7 = coarse- to very coarse-crystalline nonplanar-c dolomite.

the bulk of the upper part of the core, in well 5 dolomudstones at the bottom of the well as well as lithoclasts of the matrix-supported breccias are composed of this type, which is interpreted to be an early diagenetic replacement dolomite. Very characteristic for the lower part of well 1 is the presence of nonplanar-a replacement dolomite. This very characteristic type has been found in the studied wells only in certain horizons associated with initially high porosity and permeability values, such as the karst facies and the sandy dolostone facies. Gregg (1988) and Sibley and Gregg (1987) relate the origin of this dolomite type to high-temperature fluids. The presence of this type indicates a large-scale replacement of limestone by dolomite at elevated temperatures. Characteristically, no nonplanar-dolomite has been found in the laterally restricted karst-facies of well 5, where late-stage dolomitization seems to be restricted to the collapse breccias.

These collapse breccias are characterized by late-stage dolomite cements. Planar-s and planar-e mosaics enclose dolomite clasts composed of dolomite type 1 (Figure 43). The euhedral crystals share a common cathodoluminescence - microstratigraphy, indicating simultaneous growth (growth-coalescence). Outer ferroan to ankeritic rims are commonly observed in these planar-e crystals. No crystals with detrital cores have been observed. Very fine detrital dolomite might have served as nuclei, but, if present, it is too small to be resolved. The planar-e dolomite is discordant with the dolomite lithoclasts, which are enclosed within the planar-e mosaics. Associated non-brecciated limestones show no signs of dolomitization.

In well 1, nonplanar-c dolomite has been found to be the latest phase filling pores and fractures.

Thus, petrographically at least 3 different stages of dolomitization can be recognized in the karst-facies:

1) Early diagenetic, ?penecontemporaneous dolomite, characterized by dolomite type 1 (pre-collapse), 2) intermediate to late replacement dolomitization of limestones and precipitation of dolomite cements in breccias (during/after collapse), and 3) a latest phase of dolomite cements, which fills fractures and occludes pore spaces (after collapse).

Geochemical characteristics

Geochemically, karst-facies and non-karst related facies are distinct (Table 7). Samples from the karst-facies yield higher mean and absolute values for Fe, Mn and Sr. Mg shows a wide range, mainly as a result of substitution of Fe for Mg into the lattice during dolomitization (Fe-Mg: $r^2 = -.85$; $p = .0$). The high amounts of minor elements in the karst-facies are due to late dolomite cements, which often show a pronounced Fe-zonation. Rims of planar-e cyrstals in karst-breccias of well 5 show Fe concentrations of up to 21 moles % $FeCO_3$. Such

Table 7: Geochemical Data of Karst and Non-Karst Related Lithofacies.

A) Karst Facies (Lithofacies 6)

	N	Min.	Max.	Mean	Std. Dev.
Fe (ppm)	218	0	117974	6189	1792
Mn (ppm)	218	0	5784	514	806
Sr (ppm)	218	0	770	87	131
Mg (ppm)	218	61214	136343	121109	11720
$CaCO_3$ (mole %)	218	48.3	55.8	51.8	1.9
$MgCO_3$ (mole %)	218	25.4	51.3	46.5	3.9
$FeCO_3$ (mole %)	218	0	21.3	1.1	3.1
$MnCO_3$ (mole %)	218	0	1.0	.1	.1
$SrCO_3$ (mole %)	218	0	2.0	.0	.1

r^2: Fe - Mn: .61; p = .0000
Fe - Mg: -.85; p = .0000
Mg - Mn: -.57; p = .0000
$CaCO_3$ - $MgCO_3$: -.53; p = .0000

B) Non-Karst Facies (Lithofacies 1 to 5)

	N	Min.	Max.	Mean	Std. Dev.
Fe (ppm)	378	0	11913	1682	2533
Mn (ppm)	378	0	2646	207	275
Sr (ppm)	378	0	429	37	67
Mg (ppm)	378	109104	133399	126268	3735
$CaCO_3$ (mole %)	379	44.3	54.5	51.1	1.0
$MgCO_3$ (mole %)	379	41.1	50.6	48.3	1.2
$FeCO_3$ (mole %)	379	0	2.0	.3	.4
$MnCO_3$ (mole %)	379	0	.8	.0	.1
$SrCO_3$ (mole %)	379	0	.1	.0	0

r^2: Fe - Mn: .43; p = .0000
Fe - Mg: -.61; p = .0000
Mg - Mn: -.09; p = .0932
$CaCO_3$ - $MgCO_3$: -.62; p = .0000

Table 8: Comparison of DolomiteTypes in Karst Facies of Lower Ordovician Strata (Ellenburger and El Paso Groups) of West Texas.

	Early, penecont. dolomite (pre-collapse)	Intermediate cements and replacive dolomites (during/after collapse)	Late-stage dolomites (after collapse)
Lucia, (1971, 1988)	stratiform dol., $\Delta^{18}O$: - 3.3 to - 4.0	medium-crystalline dol., in breccias; $\Delta^{18}O$: - 3.0 to - 5.0	saddle dol., $\Delta^{18}O$: - 8.0 to - 10.0
Stepanek (1988)	stratigraphic dol., $\Delta^{18}O$: > - 6.0	replcacive dol. and cements in breccias; $\Delta^{18}O$: - 6.0 to - 8.5	baroque dol., $\Delta^{18}O$: - 8.5 to - - 14.5
This Study *	dol. type 1; $\Delta^{18}O$: -- 4.5 to - 7.3	dol. type 6, partly 3; $\Delta^{18}O$: - 4.1 to - 7.7	dol. type 7; $\Delta^{18}O$: - 8.2 to - 11.7

* with isotope data from Lee & Friedman (1987)

ferroan to ankeritic rims indicate abrupt changes in pore-fluid chemistry.

The data also indicate an increasing Fe and Mn substitution during progressive dolomitization. Cores and inner zones of dolomite crystals have lower Fe and Mn concentration than outer zones of later cements. The latest dolomite phases (nonplanar cements) are typically Fe-rich and show high fluid-inclusion temperatures and negative peritidal deposition. This type corresponds to the "stratiform dolomites" of Lucia (1971, 1988) and the "stratigraphic dolomites" of Stepanek (1988) (Table 8). Both interpreted this type as laterally persistent dolomites that had formed during tidal-flat deposition, and before the onset of Ellenburger karstification (e.g. before cavern formations and collapse). Coarse-crystalline replacement dolomites (e.g. dolomite type 6), and void - filling dolomite (e.g. dolomite 3,4) represent later stages of dolomitization closely related to the formation of karst-related deposits in the Ellenburger during the Ellenburger-Simpson unconformity.

The fact that different dolomite-rock textures are characteristic for different karst-facies associations has important implications for the control that the nature of karstification exerts on the dolomitization pattern.

In well 1 (laterally extensive karst facies) coarse-crystalline nonplanar dolomite replaced presumably precursor limestones beneath earlier formed dolomites. This requires a large-scale replacement of limestones, which could have occurred in an incompletely filled cave system, where good porosity and permeability pathways existed for dolomitizing fluids. Subhedral to anhedral planar-cements are found in pores and fractures associated with these replacement dolomites.

In collapse breccias of the laterally restricted karst-facies planar-e dolomite-matrix cements enclose lithoclasts composed of dolomite type 1. No replacement by coarse crystalline dolomite occurred and late-stage dolomitization is apparently restricted to the breccia bodies. Such restricted dolomitization goes along well with the interpretation of the laterally restricted facies association as deep discharge zones focused along faults (Kerans, 1988 a). Meteoric diagenesis related to the post-Ellenburger unconformity created these solution-collapse breccias, which served as fluid conduits for later dolomitizing fluids.

This dolomitization event was probably a long-lasting episode, involving several dissolution and cementation events. Intracrystalline truncation surfaces between replacement dolomites and cements, concomitant with porosity creation and destruction and abrupt changes in pore-fluid chemistry can be taken as evidence for a complex diagenetic history.

Field evidence (Lucia, 1988, p. 87) suggests that fractured and brecciated rocks might have been open for migrating dolomitizing fluids until Silurian and Devonian times, thus allowing a long episode of dolomitization associated with the karst deposits. This

dolomitization phase compares to the internal cements and replacements dolomite in breccias as described by Lucia (1971, 1988) and Stepanek (1988).

The latest dolomite phase observed in the karst-related deposits is a nonplanar-c dolomite (saddle dolomite). It occurs as a void- and fracture-filling phase that cuts across earlier dolomite types. It might be important to note that no Nonplanar-c dolomite has been found in the collapse breccias in well 5. The reasons for this are not clear. One explanation could be the presumably laterally restricted karst facies of well five and the fact that enclosing host rocks are limestones. F.J. Lucia (pers. communication, 1989) pointed out, that in El Paso Group rocks no fractures filled with saddle dolomite have been observed cutting through limestones.

This late dolomite is also described by Lucia (1971, 1988) and Stepanek (1988), who distinguished two zones in the late ("baroque") dolomites. He argued that the emplacement of this latest phase must have occurred later than Devonian time, but prior to the formation of joint-controlled fractures related to Laramide block-faulting and uplift of the Franklin Mountains (Stepanek, 1988, p. 128). For this study dolomite paragenesis, combined with burial-history plots and thermal maturation calculations suggest a late Pennsylvanian to Early Permian age for the nonplanar-c dolomite, thus constraining the influx of higher - temperature, basinal) fluids into Ellenburger carbonates.

Summary

Karstification and dolomitization are closely related in several ways: early dolomitized zones resist dissolution and provide ceiling and roofs for the formation of caveties , which are the result of limestone dissolution beneath such early dolomitized zones. Subsequent collapse after burial and the formation of brecciated horizons formed permeable pathways for the migration of dolomitizing fluids, whereby laterally continuous karst-facies were affected more intensively than laterally restricted karst deposits, where late stage dolomitization was apparently restricted to the breccia bodies. Porosity and permeability pathways created by karst-dissolution seem to be of prime importance for the distribution of different dolomite types. Dolomite-rock textures and their geochemical characteristics indicate multiple episodes of dolomitization, with a considerable amount of dolomite formed during late (burial) stages from fluids with elevated temperatures. Lucia (1988) estimated that about 67% of the dolostones in the El Paso Group formed during that burial episode.

PETROPHYSICS

INTRODUCTION

Ellenburger carbonate rocks have experienced a complex diagenetic history. Although the Ellenburger is a prolific hydrocarbon producer in the Permian Basin not much data have been published on petrophysical properties of these reservoir rocks and on how they might affect performance, that is production of fluids or gas from a reservoir. Virtually no data are available for deeply buried Ellenburger rocks of the Delaware and Val Verde basins. Reservoirs of these deep basins account for 61% of total Ellenburger hydrocarbon production, or 22 Bbbl oil equivalent (Kerans et al., 1989).

The term "petrophysics" pertains to the physics of particular rock types, whereas geophysics pertains to the physics of larger rock systems composing the earth (Archie, 1950). Some of the petrophysical properties of reservoir rock include porosity, permeability, capillary pressure, hydrocarbon saturation, and fluid properties.

Petrophysical characteristics of Ellenburger dolostones have been examined using mercury capillary-pressure analysis (for details on methodology see Appendix A). Preliminary results have been published in Amthor et al. (1988). The following is a more detailed presentation of the results obtained by capillary-pressure analysis of Ellenburger dolostones. It includes the integration and synthesis of petrographic and geochemical data with petrophysical measurements to gain a better understanding of the importance of geologic heterogeneity within these complex reservoir rocks.

In this chapter the following points will be addressed:

a) The distribution of porous and non-porous rocks; and the development of porosity.

b) Characterization of petrophysical properties of the pore-rock system and their variation.

c) The integration of petrophysical parameters with geological and geophysical parameters, illustrated with a case study.

PETROPHYSICAL ANALYSIS

The following parameters have been calculated from petrophysical core-analysis data:

1) Apparent or effective porosity (AP, %):

The apparent or effective porosity is measured with the mercury porosimeter by filling a sample with mercury to a maximum pressure of 15,000 PSIA (Hg-air), and it is calculated as (maximum intrusion volume/bulk volume) x 100. The terms "apparent" and "effective"

porosity are used interchangeably with porosity in this study.

2) Median pore-throat size (MTS, microns):

The median pore-throat size is the 50% (percentile) value obtained from the volume-distribution curve and is measured in microns.

3) Pore-throat size at 20% Hg-saturation (TS 20%, microns):

The pressure at 20% Hg-saturation is read off the capillary-pressure intrusion curve and the corresponding pore-throat size is calculated using equation 2 of Appendix A.

4) Normalized pore-throat size range (NTS):

The normalized throat-size range (Wardlaw et al., 1988) is obtained by subtracting the pressure at 20% Hg-saturation from the pressure at 80% Hg-saturation and normalized by dividing by the pressure at 50% Hg-saturation. This gives a measure of throat-size variability by omitting the initial and final 20% pore-volume portions to avoid boundary effects (Wardlaw et al., 1988). The normalized pore-throat size increases as throat-size variability increases.

5) Minimum recovery efficiency (RE, %):

Recovery Efficiency may be defined as the percentage of trapped hydrocarbons which may be withdrawn from a reservoir rock under a particular set of conditions. With respect to capillary-pressure analysis this definition is slightly modified and reads as follows:

Recovery Efficiency in mercury porosimetry is the percentage or fraction of mercury intruded at maximum pressure that is extruded during pressure reduction to final minimum pressure (usually 14-15 PSIA, or atmospheric pressure).

$$(1) \quad RE\,(\%) = \frac{\text{Max. Intrusion} - \text{Max. Extrusion}}{\text{Max. Intrusion}} \times 100$$

6) Surface area (SA, m^2/g):

Surface area is the area of the pores based on the assumption of cylindrical pore geometry, and summed over the pressure range of mercury intrusion. Surface area is calculated from the summation of the incremental surface area based on the mean diameter (D) and the volume increment (Δ V) between the two points, assuming cylindrical pore geometry for the pores. The data are found using the formula :

$$(2)\quad A = \int_{1}^{max} (4\,\Delta V/D).$$

Surface area is critical to the effectiveness of surfactant and polymer solutions in enhanced-recovery processes (Ebanks, 1987). Because these chemicals have the tendency to adsorb on rock surfaces, the amount lost from circulation depends partly on the surface area of the rock-pore system to which these chemicals are exposed (Ebanks, 1987, p. 11).

Capillary-Pressure Curve Form

The results of mercury porosimetry are displayed as graphs of capillary pressure or throat size versus mercury intrusion (e.g., Appendix B). They are based on petrophysical analysis of 120 core plugs collected from five wells (raw data are listed in Appendix C).

Plotting both cumulative- and incremental intrusion versus throat size on a single graph facilitates capillary-pressure curve interpretation. The form of capillary-pressure curves is controlled by a variety of factors, including the size-distribution of throats, microscopic spatial heterogeneity of the pore system, connectivity, randomness of spatial distribution of throat sizes, and intrusion rate (Wardlaw and Taylor, 1976). Capillary-pressure curves, plotted as percent intrusion over various pressure ranges, and throat-size ranges are classified visually into four endmembers (Tables 9, 10).

1) Steep-convex capillary-pressure curves (Figure 48) correlate with high RE values (max. =60.0 %) and low porosities (Table 10). Much of the intrusion occurs at high pressures (Figure 48) and therefore median throat size is small. RE values are high because throats are well "sorted" and because entry pressures for most throats are much greater than minimum pressures achieved during extrusion. Paradoxically, most samples with steep-convex capillary-pressure curves are usually relatively non-porous because pores are small.

2) Steep-concave capillary-pressure curves (Figure 49) have opposite characteristics. These samples have low RE values (max. = 19.0 %) but higher porosities (Table 10), larger median throat sizes, and commonly large pores. Most intrusion occurs at relatively low pressures because throats are large. This contributes to poor RE (r^2: -.63; p = .0066 for RE versus NTS 20 %; r^2 = -.62, p = .0075 for RE versus MTS). In some cases entry pressures for median throats are not much greater than or even less than minimum extrusion pressure (about 14 PSIA). RE values are also reduced by the well-known phenomenon of shielding of interior throats by throats near the surface of the samples (Wardlaw and Taylor, 1976).

Table 9: Capillary-Pressure Curve Types and Their Petrophysical Characteristics.

	1	2	3	4
	(Steep) Convex	(Steep) Concave	Gently Sloping	Polymodal
AP (%)	low	high	interm.	low
RE (%)	high	low	interm.	low
MTS (μm)	small	large	small	interm.
TS 20% (μm)	small	large	interm.	interm.
NTS	small	large	small	small
SA (m^2/g)	large	interm.	interm.	small

AP = apparent porosity; RE = minimum recovery efficiency; MTS = median pore-throat size; TS 20% = pore-throat size at 20% Hg-saturation; NTS = normalized pore=throat size; SA = surface area.

Table 10: Petrophysical Data of Capillary-Pressure Curve Types.

	1	2	3	4
	(Steep) Convex	(Steep) Concave	Gently Sloping	Polymodal
AP (%)	m: 1.4 s: 1.3	m: 6.5 s: 2.6	m: 2.6 s: 1.6	m: .9 s: .4
RE (%)	m: 23.6 s: 16.4	m: 10.4 s: 4.2	m: 14.8 s: 7.2	m: 12.1 s: 12.8
MTS (µm)	m: .15 s: .64	m: 10.5 s: 4.2	m: .8 s: 1.1	m: 1.3 s: 2.6
TS 20% (µm)	m: 3.9 s: 9.2	m: 25.7 s: 11.1	m: 7.4 s: 6.5	m: 7.6 s: 3.1
NTS	m: 9.8 s: 53.1	m: 34.2 s: 39.5	m: 10.7 s: 14.7	m: 11.4 s: 14.8
SA (m^2/g)	m: .4 s: .6	m: .22 s: .10	m: .21 s: .14	m: .18 s: .12
	n = 55	n = 17	n = 42	n = 6

m = mean, s = standard deviation

AP = apparent porosity; RE = minimum recovery efficiency; MTS = median pore throat-size; TS 20% = pore throat-size at 20% Hg-saturation; NTS = normalized pore-throat size; SA = surface area.

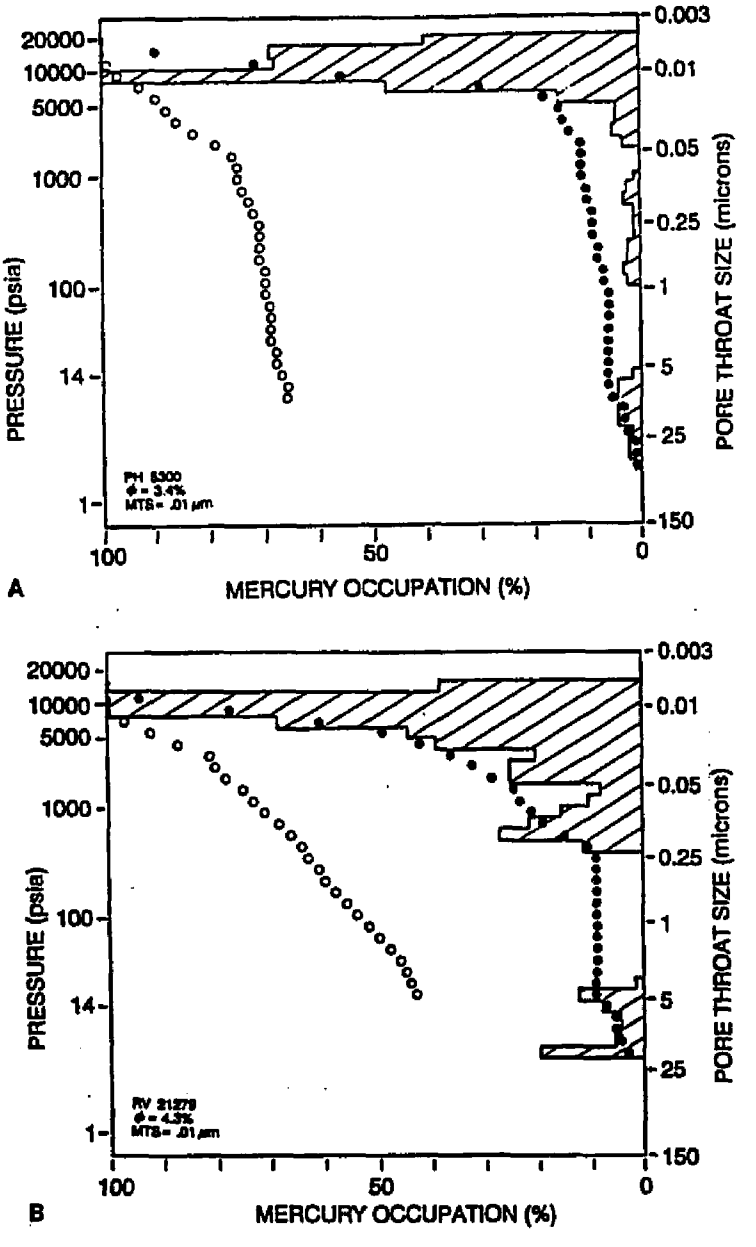

Figure 48. - - Examples of (steep) convex capillary-pressure curves. A) sample from 5,300 ft (1,615 m), well 5. Porosity (Ø) = 3.4%, median pore-throat size (MTS) = .01 microns. B) Sample from 21,279 ft (6,486 m), well 2. Porosity (Ø) = 4.3%, median pore-throat size (MTS) = .01 microns. ● = Cumulative intrusion, ○ = Extrusion, ■ = Both. Hachured histograms = incremental intrusion.

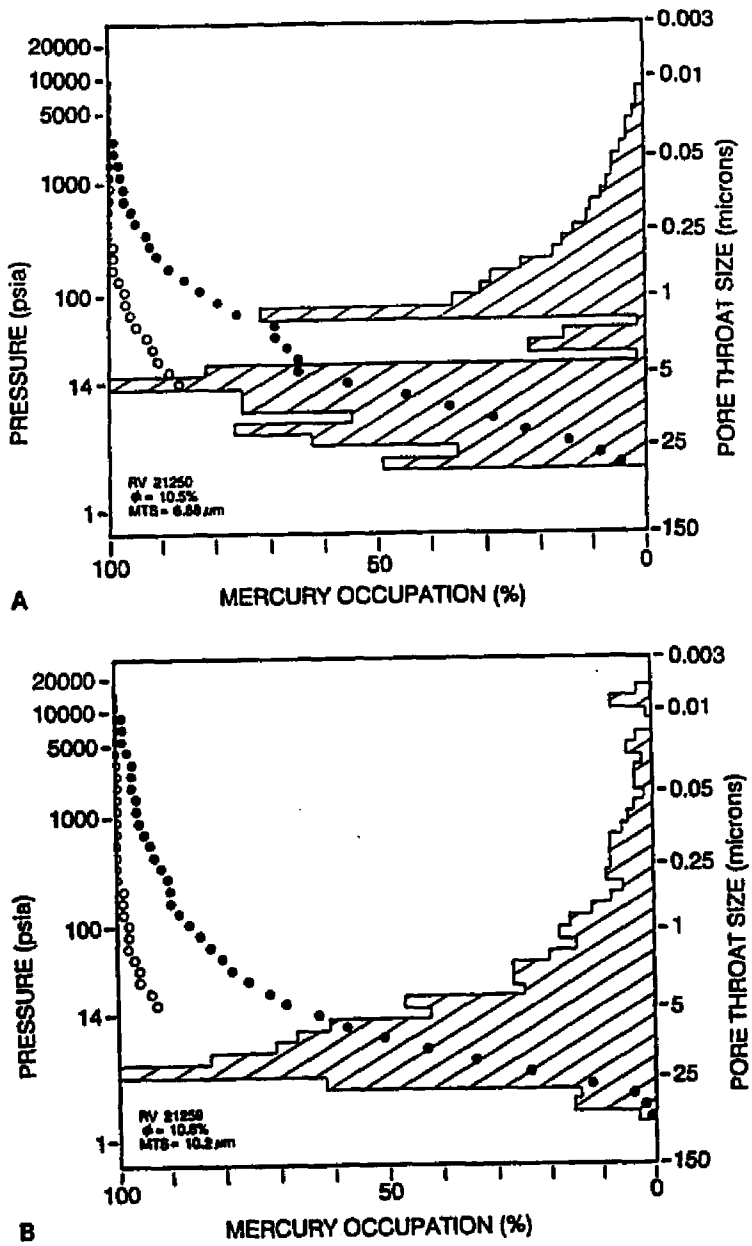

Figure 49. - - Examples of (steep) concave capillary-pressure curves. A) Sample from 21,250 ft (6,477 m), well 2. Porosity (Ø) = 10.5%, median pore-throat size (MTS) = 6.88 microns. B) Sample from 21, 259 ft (6,480 m), well 2. Porosity (Ø) = 10.6%, median pore-throat size (MTS) = 10.2 microns. ● = Cumulative intrusion, ○ = extrusion, ■ = Both. Hachured histograms = incremental intrusion.

During pressure reduction, when low pressures are reached, snap-off has already occurred in many small throats and numerous domains containing non-wetting-phase-filled large throats are isolated from the sample surface and cannot be drained.

3) Gently-sloping capillary-pressure curves (Figure 50) correspond to samples with moderate RE values, intermediate median throat sizes, and variable porosities. This is the only type of sample for which average throat size is an accurate measure of the throat-size distribution because throat sizes in these rocks tend to be approximately normally distributed. RE values can be highly variable (min. = 0, max. = 39.0 %) depending on variation in aspect ratio and median throat size. They are usually not as high as in steep-convex samples (max. = 60 %) and better than in steep-concave samples (max. = 19.0 %) (Table 10).

4) Polymodal capillary-pressure curves (Figure 51) commonly result from "bimodal porosity" which has been much discussed in recent years (e.g., Keith and Pittman, 1983; Pluim and others, 1985). This is because high water saturations due to "bound" water in micropores often misled petroleum geologists in the past into condemning reservoirs which could in fact produce water-free oil with very high water saturations. Petrophysical characteristics for these rocks are extremely variable (Table 10), and depend very sensitively on the positions and relative heights of the two (or more) modes on an incremental throat-size plot. A mode at very low pressure (large median throat size) greatly reduces RE values, but may be correlated with higher porosities, whereas samples with modes at very high pressures (small median throat size) may correlate with intermediate to high RE values but lower porosities.

Porosity

Distribution. -- Porosity values for a total of 120 samples from different lithofacies are listed in table 11. It is apparent that Ellenburger rocks are characterized by generally low porosities (mean = 2.5 %, range = 0 to 11.9 %). All of the porosity in the Ellenburger rocks described here is confined to dolostones. Analyzed limestone samples commonly had no observable porosity.

Original depositional textures seem to have some control on the amount and distribution of porosity. Samples from lithofacies 1 (laminated dolomudstones) and lithofacies 2 (dolomudstones/wackestones) have the lowest porosity values of the studied samples (Table 11). Higher values are found in lithofacies 3 (mottled dolomudstones/wackestones), and in lithofacies 4 (dolopackstones/grainstones). The highest porosity values have been found in samples assigned to the dolopackstone/grainstone lithofacies (mean = 5.5, std. dev. =

Table 11: Apparent Porosity Values of Different Lithofacies.

	N	AP %			
		Min.	Max.	Mean	Std.Dev.
Total	120	.2	11.9	2.5	2.4
Lithofacies 1	16	.3	2.2	.5	.9
Lithofacies 2	18	.2	4.3	1.1	1.2
Lithofacies 3	45	.3	10.6	2.3	2.1
Lithofacies 4	10	.4	11.9	5.5	3.8
Lithofacies 6	31	.8	6.5	2.4	3.4

Lithofacies are as follows: 1 = laminated dolomudstones; 2 = dolomudstones/wackestones; 3 = mottled dolomudstones/wackestones; 4 = peloid-ooid-intraclast packstones/grainstones; 6 = karst facies.

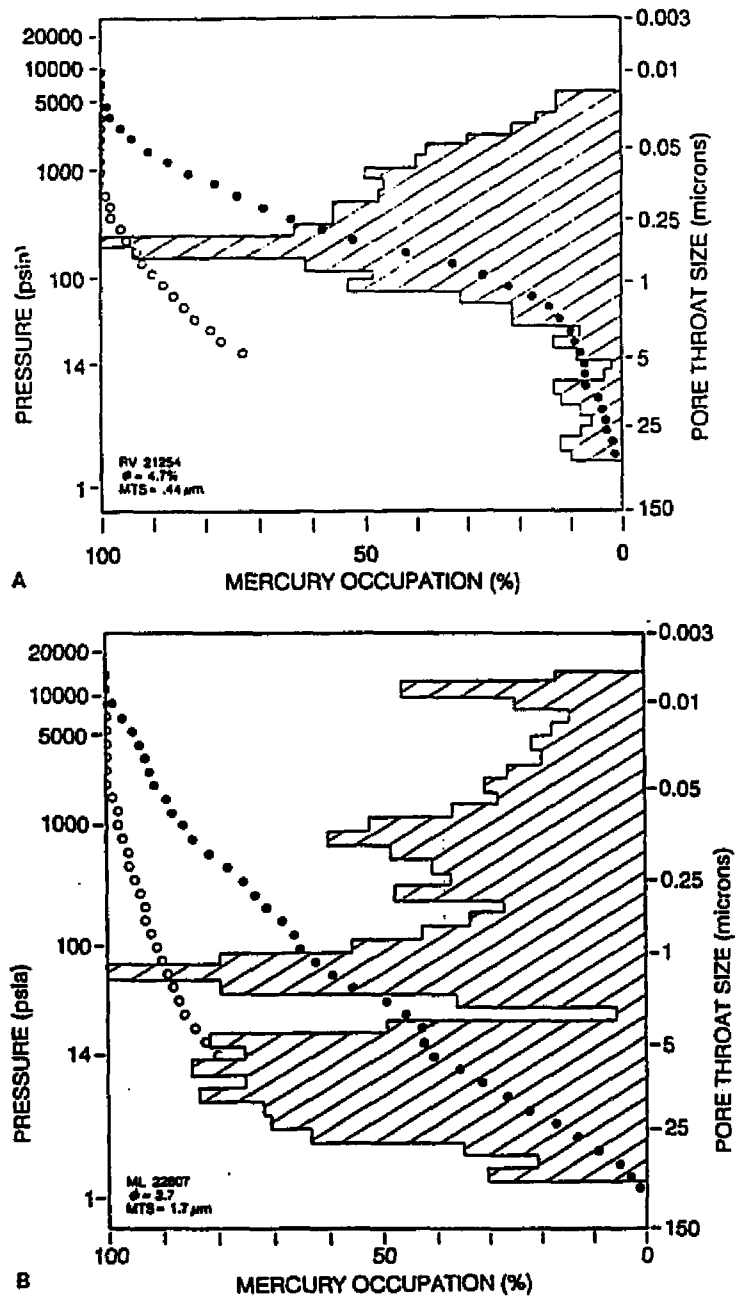

Figure 50. - - Examples of gently sloping capillary-pressure curves. A) Sample from 21,254 ft (6,478 m), well 2. Porosity (Ø) = 4.7%, median pore-throat size (MTS) = .44 microns. B) Sample from 22,807 ft (6,952 m), well 3. Porosity (Ø) = 3.7%, median pore-throat size (MTS) = 1.7 microns. ● = Cumulative intrusion, O = Extrusion, ■ = Both. Hachured histograms = incremental intrusion.

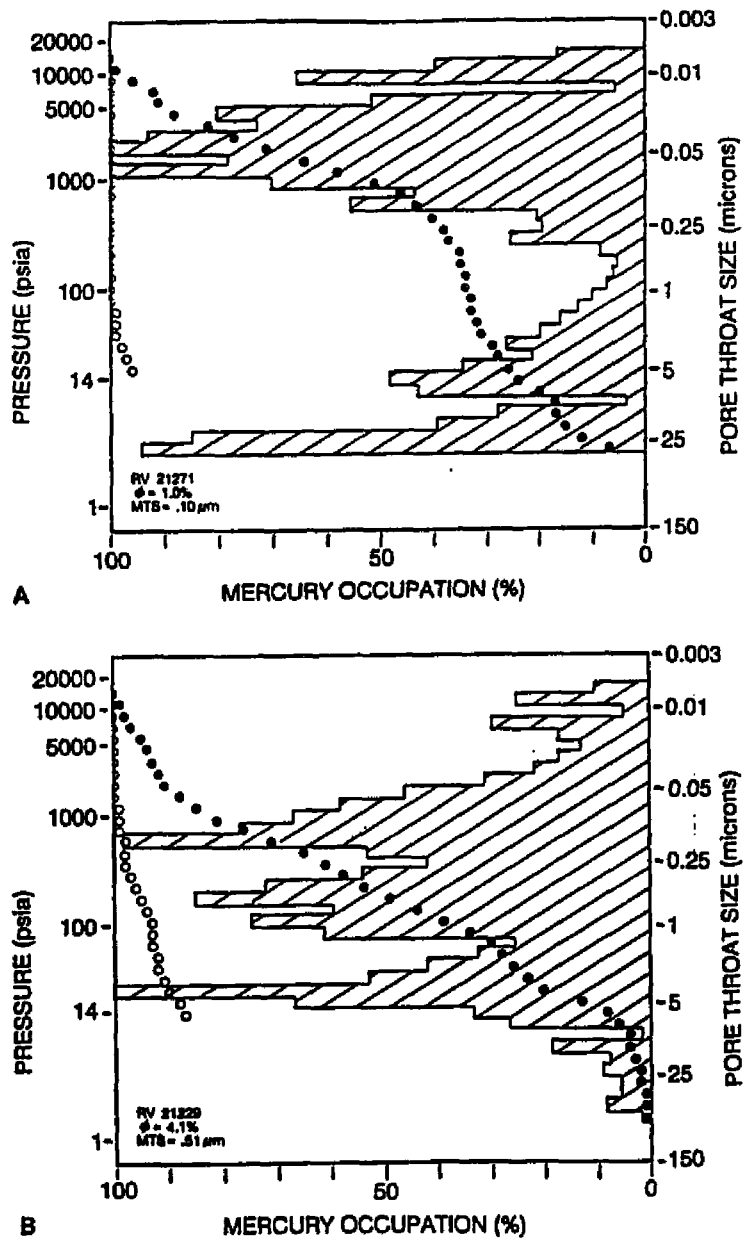

Figure 51. - - Examples of polymodal capillary-pressure curves. A) Sample from 21,271 ft (6,483 m), well 2. Porosity (Ø) = 1.0%, median pore-throat size (MTS) = .1 microns. B) Sample from 21,229 ft (6,471 m), well 2. Porosity (Ø) = 4.1%, median pore-throat size (MTS) = .51 microns. ● = Cumulative intrusion, ○ = Extrusion, ■ = Both. Hachured histograms = incremental intrusion.

3.8). High porosity values are also found in the karst facies (mean = 3.4, std. dev. = 2.4).

Porosity-depth plots for three of the studied wells (Figures 52 - 54) show that thin porous zones are isolated and sealed off vertically by relatively nonporous zones. These dense zones act as intraformational seals, and result in vertical heterogeneity within the studied Ellenburger intervals.

Porosity Types. -- All of the porosity in the studied Ellenburger rocks is confined to dolostones . The most common porosity types are (Choquette and Pray, 1970):

a) non-fabric selective vug, channel and fracture porosity,

b) fabric selective intercrystalline porosity.

Vug porosity is especially common in the karst facies of well 1 (Figure 55 A), and in the dolopack/grainstone facies of well 2, where it occurs mainly as a result of solution enlargement of intercrystalline porosity. This porosity type is associated with the highest porosity values. The sizes of the vugs varies from small to large megapores, and shape is usually highly irregular. This porosity is locally occluded by the precipitation of late-stage minerals (e.g., dolomite, calcite, and quartz).

Channel porosity is very common in the karst facies of well one, where mm- to cm-wide, highly irregular channels are encountered (Figure 55 B). The channels are commonly partly or totally occluded (especially the smaller ones) by the precipitation of late-stage dolomites resulting in an unconnected pore system (Figure 55B). Such an isolated pore system could explain the comparatively low effective porosity values of such zones (mean = 3.4 %), if compared to visual estimates from core slabs (up to 15 %).

Fracture porosity is responsible for most of the porosity found in samples from well four (Figure 55 C). Open tectonic fractures with mm-wide gaps are observed. These open fractures are partly occluded by dolomite, quartz and minor pyrite cements. The porosity values associated with this fracture porosity are commonly low (max. = 2.2 %). The fracture porosity may be more important in improving the connectivity between porous zones, and thus increasing the permeability.

Fabric-selective intercrystalline porosity is very common in all of the studied samples. Commonly it occurs in mosaics of planar-e and planar-s dolomites, and it is especially characteristic of the matrix of matrix-supported karst breccias (Figure 56, and the burrowed parts of the mottled dolomudstone/wackestone lithofacies. Porosity values in the mottled dolomud/wackestone facies reach up to 10% (Table 11. In many cases this intercrystalline porosity is solution enlarged (Figure 57), or it may even be reduced vuggy porosity.

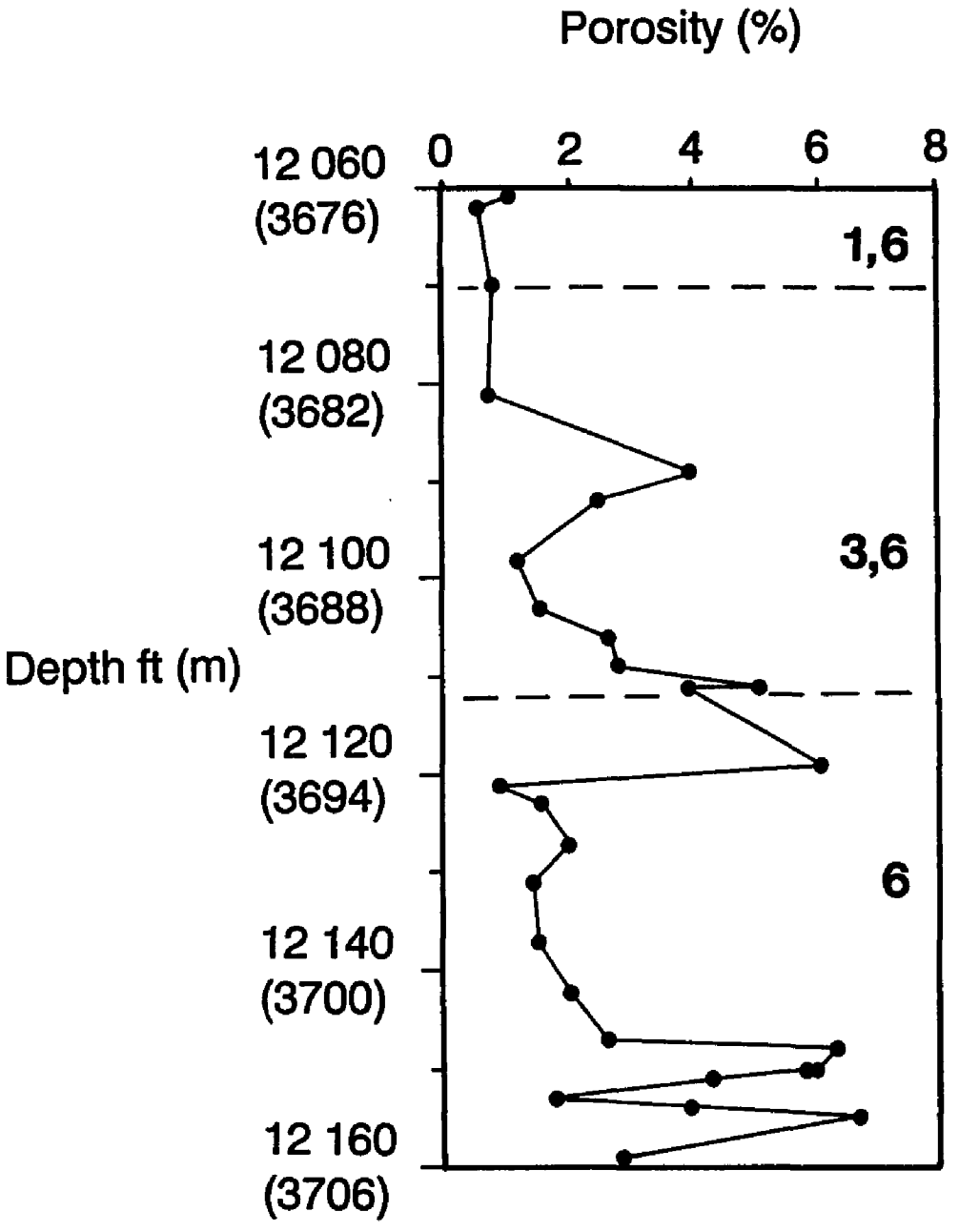

Figure 52. - - Porosity - depth plot for well 1. Numbers refer to lithofacies: 1 = Laminated dolomudstones/wackestones; 3 = Dolomudstones/wackestones; 6 = Karst Facies.

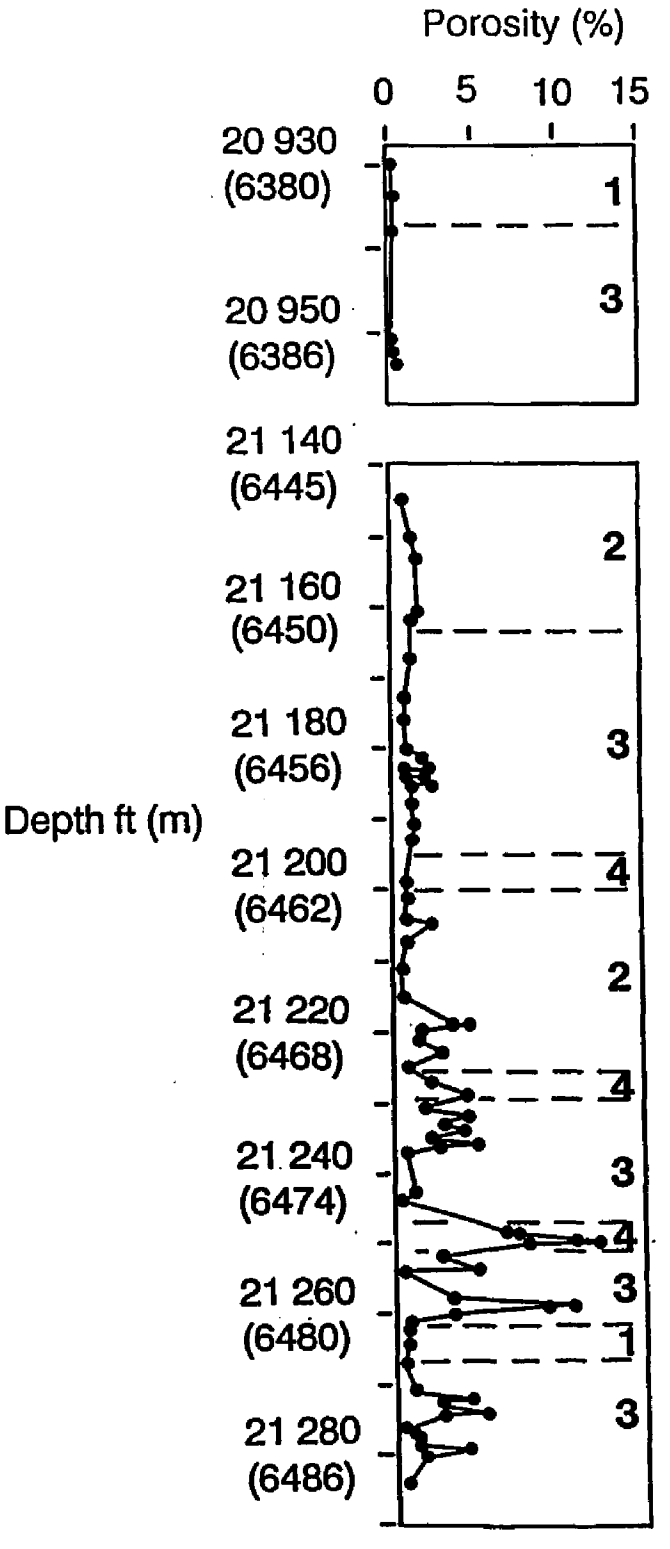

Figure 53. - - Porosity - Depth plot for well 2. Numbers refer to lithofacies: 1 = Laminated dolomudstones/wackestones; 2 = Dolomudstones/wackestones; 3 = Mottled dolomudstones/ wackestones; 4 = Peloid/ooid/intraclast packstones/grainstones.

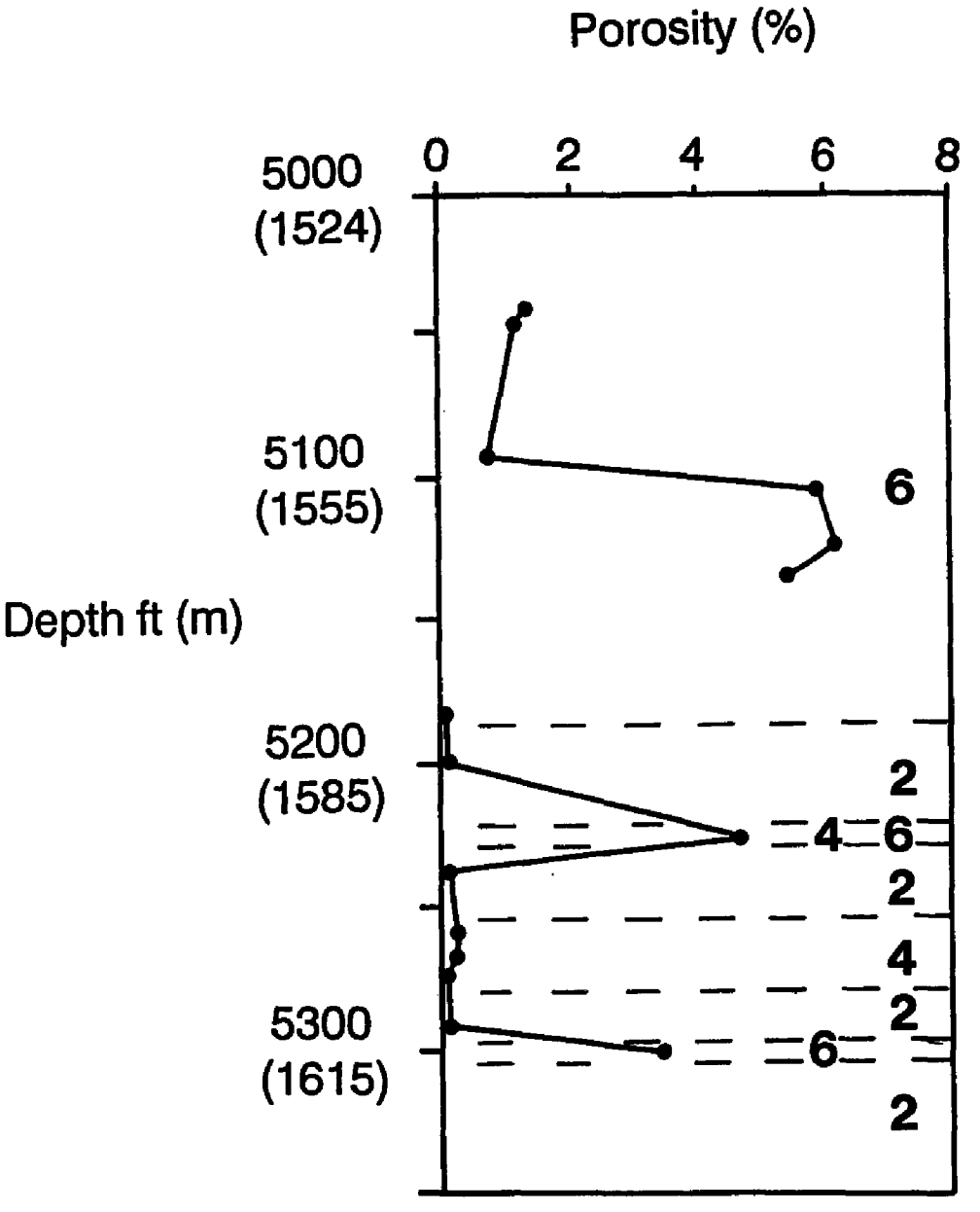

Figure 54. - - Porosity - depth plot for well 5. Numbers refer to lithofacies: 2 = Mudstones/wackestones; 4 = Peloid/ooid/intraclast packstones/grainstones; 6 = Karst facies.

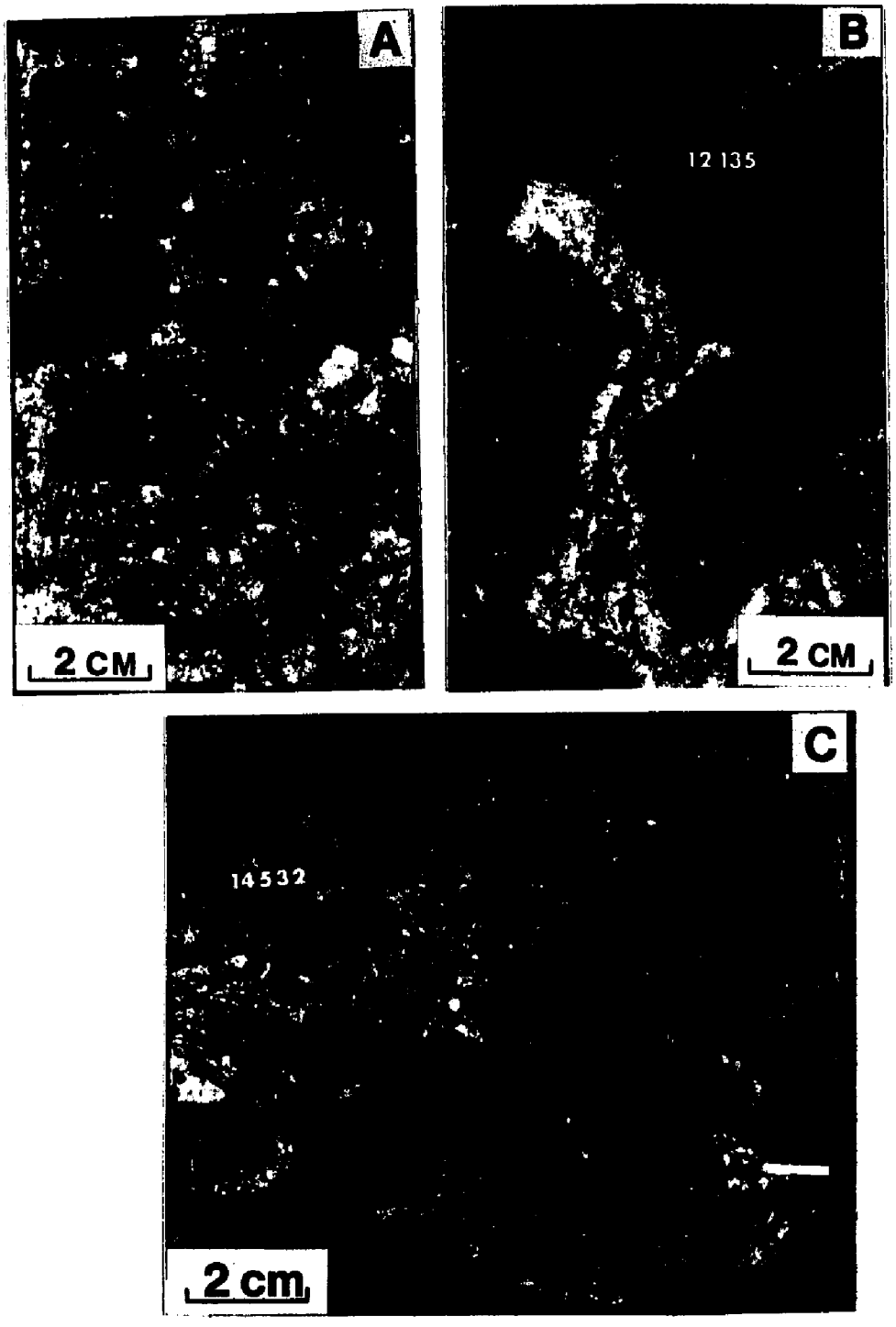

Figure 55. - - Core photographs illustrating porosity types. A) Vug porosity in sample from 12,119 ft (3,685 m), well 1. B) Channel porosity, filled with coarse-crystalline dolomite (white); sample from 12,125 ft (3,699 m), well 1. C) Fracture porosity (P), partly filled by authigenic quartz (Q). Sample from 14,532 ft (4,4429 m), well 4.

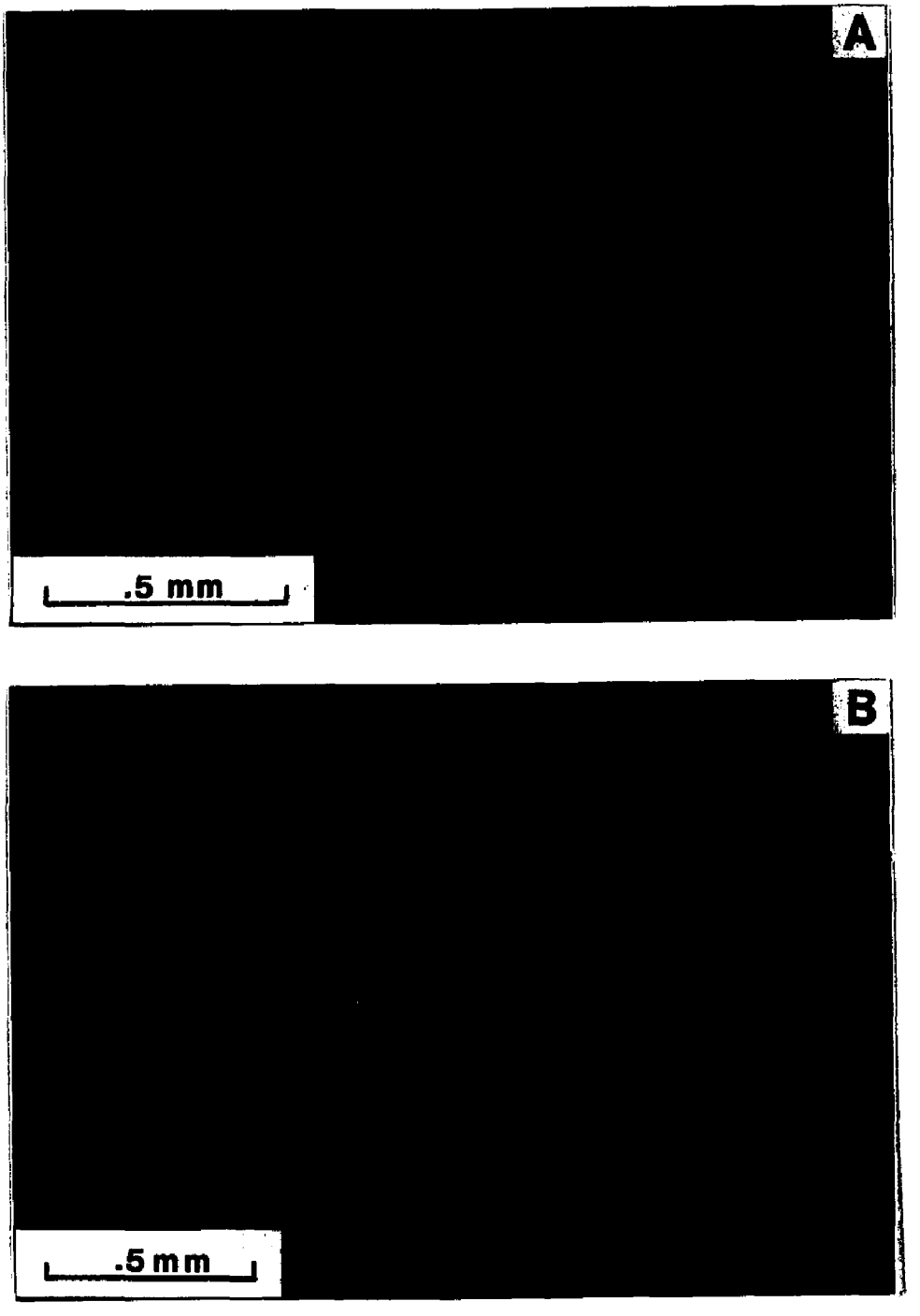

Figure 56. - - Thin-section photomicrographs of intercrystalline porosity. A) Intercrystalline porosity (P) in dolomite type 4. Plane polarized light. B) Same view under Cl. Note dissolution and corrosion of outer zone of individual dolomite crystals (arrows). Sample from 5,134 ft (1,565m), well 5.

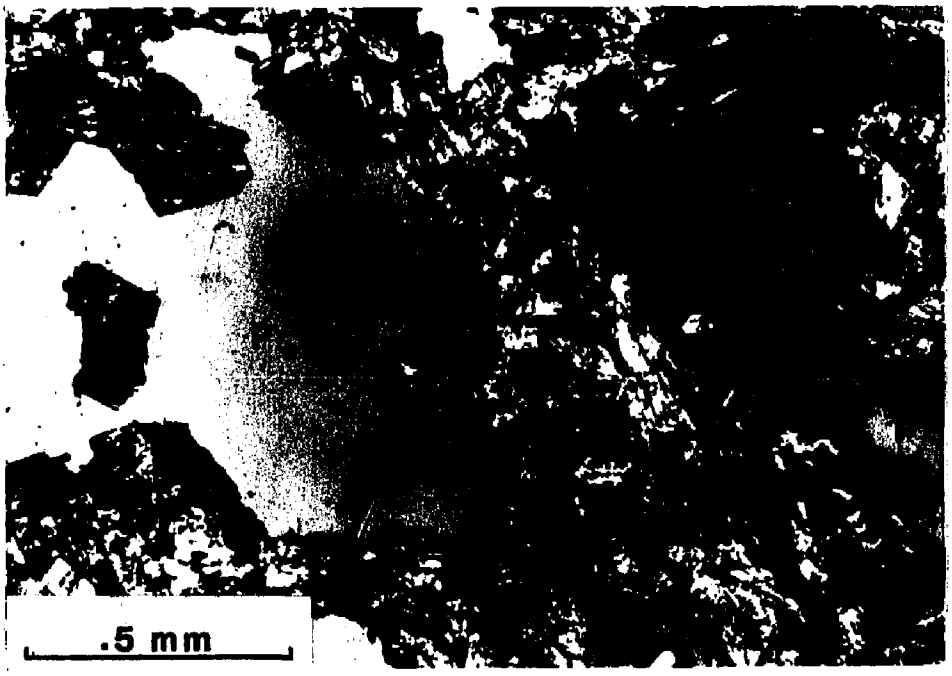

Figure 57. -- Thin-section photomicrograph illustrating solution-enlarged intercrystalline porosity (P) in coarse crystalline planar-s mosaic dolomite. Sample from 21,249 ft (6,477m), well 2, has effective porosity of 7.5%. Plane polarized light.

Porosity Development. -- Karstification (e.g., Lucia, 1968, 1970, 1988; Loucks and Anderson, 1980, 1985; Kerans, 1988) , and tectonically induced fracturing (e.g., Loucks and Anderson, 1980, 1985; Galloway et al., 1983; Ijirigho and Schreiber, 1986, 1988) are commonly cited to be most important for porosity development in the Ellenburger. However, volumetrically significant secondary porosity accompanies dolomitization of Ellenburger rocks in the deeper parts of the Delaware basin. Effective porosity values of up to 12 % have been found in the deep (21,250 ft, 6,477 m) Delaware basin (Table 11).

Dolomitization is considered to be intimately associated with the development of secondary porosity, because dolomitization pre- and postdates dissolution and corrosion and no secondary porosity generation occurred in limestones. The most common porosity types are non-fabric selective vug porosity (Figure 55), and intercrystalline porosity (Figure 56). Vug porosity was created either as a result of limestone dissolution, followed by replacement and cementation by late-stage dolomites (e.g., karst facies), or as a result of leaching within coarse - crystalline mosaics of type 2 dolomite. It varies in shape and size (up to several mm). No evidence remains to indicate what has been leached out (e.g. fossils, calcite). Dissolution and corrosion of zoned dolomite crystals are observed using cathodoluminescence, suggesting that in many examples dolomite has been dissolved (Figure 56).

Intercrystalline porosity is also of importance within Ellenburger dolostones (Figure 56), where it occurs mainly in planar-s mosaics of dolomite type 4. But this intercrystalline porosity is in many cases also solution enlarged, or may even be a reduced vuggy porosity. Both vug and intercrystalline porosity are partly or totally occluded by late-stage calcites or nonplanar dolomite cements.

Even where no significant amounts of porosity have been produced the effects of leaching can be observed in the dolomites. Within individual crystals of dolomite type 3 intracrystalline truncation features are observed between inner and outer zones (Figure 58). Such irregular contacts suggest that dissolution/corrosion occurred prior to overgrowth by later phases.

Dolomitization, leaching, and secondary porosity development are intimately associated in the Ellenburger carbonates. The resulting porous zones are not uniformly distributed, but are isolated and sealed off by nonporous zones composed of dense mosaics of dolomite types 1, partly 2, and 6. These dense zones provide intraformational seals and result in vertical heterogeneity (e.g., Amthor and Friedman, 1989c).

The distribution of porous and nonporous zones, and their respective petrographic characteristics have important implications for Ellenburger reservoir development. The nonporous zones are characterized by dolomites interpreted to be of penecontemporaneous

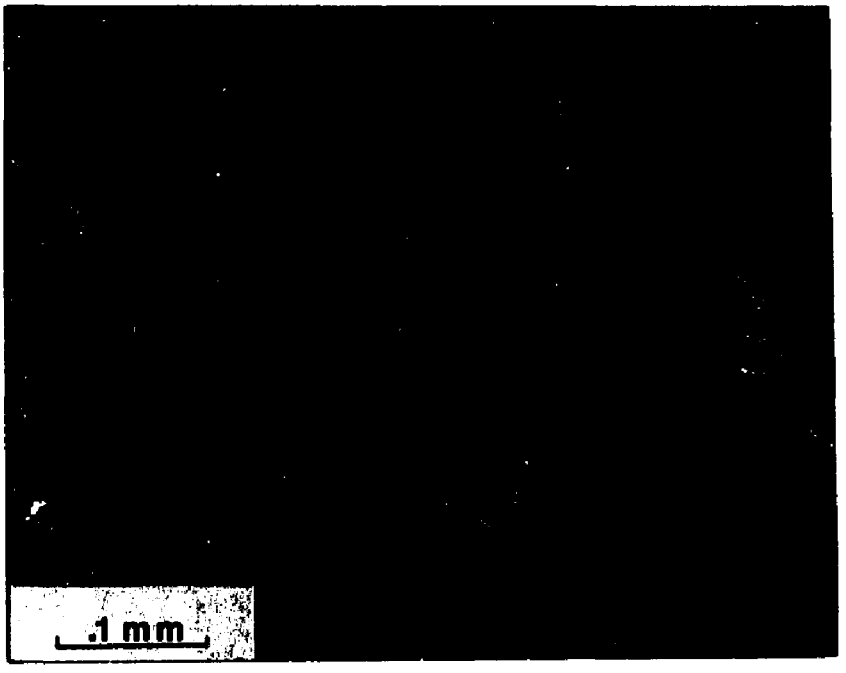

Figure 58. -- Intracrystalline truncation features (arrows) in crystal of coarse-crystalline planar-s dolomite. These irregular contacts suggest partial dissolution/corrosion prior to overgrowth by later phases. Sample from 12,132 ft (3,698 m). Back-scattered electron image photomicrograph.

or early replacement origin (e.g., dolomite type 1). In certain karst-related zones late-stage nonplanar replacement dolomite forms dense, low porosity intervals. The porous zones, however, are characterized by coarse crystalline dolomites interpreted to be of later diagenetic origin (e.g., dolomite types 2, 3, 4, and 5). This distribution of dolomite-rock textures suggests that the porous zones were preserved as limestone until later in the diagenetic history, and were then subjected to late-stage dolomitization. Such porous zones are confined to the mottled dolomudstone lithofacies and dolopackstone/grainstone lithofacies, which most likely had higher depositional porosities than the overlying inter- to supratidal (laminated) mudstone lithofacies. Such higher porosity zones could serve as pathways for later dolomitizing fluids. Leaching and secondary porosity development are closely associated with this dolomitization event (or events), that resulted in isolated porosity zones. Such zones indicate the importance of permeable horizons for the distribution of dolomite-rock textures and thus for the formation of favorable secondary porosity within otherwise dense dolostones and limestones. The development of this secondary porosity occurred most likely in a (deep) burial environment during the Late Paleozoic, when the Permian Basin was characterized by a time of high tectonic mobility (Horak, 1986), and a period of maximum maturation and mobility of fluids (e.g. Ijirigho, 1989). At the same time, however, precipitation of late-stage dolomite - and calcite - cements was responsible for the partial or total occlusion of the secondary pore spaces.

The distribution of secondary porosity within the studied Ellenburger cores shows that porosity and hydrocarbon production is not restricted to paleokarst horizons (e.g. Britt, 1988; Kerans, 1988 a). Production may occur from nonkarstic porous zones within the Ellenburger, and from all the formations within the group (e.g. Mazzullo, 1989). The distribution of such porous horizons is characterized by frequent changes of porous dolostones and nonporous dolostones and limestones. It is apparent that exploration for Ellenburger reservoirs must also consider these nonkarstic porous zones beneath the post - Ellenburger unconformity.

Correlation between Petrophysical Parameters

Porosity and permeability data are the most commonly used petrophysical parameters to characterize reservoir rocks. However, these parameters might not always be the most useful in predicting reservoir performance (e.g. Krause et al., 1987).

In hydrocarbon exploration and production it is not only the amount of void space available to hydrocarbons which is of interest, but the fraction of that void space which may in fact contain hydrocarbons, and the (generally much smaller) fraction from which hydrocarbons

may be readily removed. Thus, the relationships between recovery efficiency (RE) and other petrophysical parameters (e.g., permeability, porosity, throat size, and surface area) are critical to reservoir description and to hydrocarbon production and secondary recovery (Krause et al., 1987; Amthor et al., 1988; Kopaska-Merkel and Friedman, 1989).

It is an axiom of capillary-pressure studies that more fluid enters a sample under increasing pressures over a given range than exits under decreasing pressures over the same range (Wardlaw and Taylor, 1976). This results from hysteresis effects and from snap-off (Wardlaw et al., 1988). The hysteresis effect dictates that extrusion occurs at lower pressures than intrusion: Throats are drained of nonwetting fluid not at the pressure at which they were filled, but at some lower pressure. The cause of this relationship is not known, but it may be related to wettability. Contact angle, contact-angle hysteresis, and surface roughness all may play a part in this phenomenon (Wardlaw et al., 1988). A considerable amount of experimental work has been devoted to studying the mechanisms which control patterns of intrusion and extrusion of nonwetting fluids on a microscopic scale (e.g., Yu and Wardlaw, 1986 a,b; Yu et al., 1986). This does not concern us here, and the interested reader is referred to the relevant literature. Here empirical relationships of petrophysical parameters resulting from macroscopic fluid behavior are considered. RE is weakly positively correlated with small throats (RE - SA: $r^2 = .49$, $p = .0000$), and inversely correlated with intrusion occurring at low pressures (large throats). In other words, the larger the throats, the lower the RE (RE - MTS: $r^2 = -.26$, $p = .0042$; RE - TS20 %: $r^2 = -.33$, $p = .0003$). This is a consequence of three controlling factors: accessibility ratio, hysteresis, and experimental procedure (Kopaska-Merkel and Amthor, 1988; Amthor et al., 1988):

a) The accessibility ratio (Wardlaw and Taylor, 1976) is a measure of the propensity for isolation of throats by snap-off during extrusion, and is inversely proportional to throat size (capillary-pressure). Drainage from small throats is more efficient (they are more accessible) because snap-off during withdrawal of fluid from small throats (at high pressures) has not yet isolated many domains within the rock. At lower pressures, when large throats are drained, snap-off in smaller throats over the entire range of pressures encountered to that point has isolated many domains which include large throats. These are no longer connected to the rest of the pore system, and can never be drained (Wardlaw and Taylor, 1976). Snap-off is enhanced in samples in which pore and throat size are not correlated (Wardlaw et al., 1988), because the smallest throats may have supercritical aspect ratios (pore size to throat size). If the sizes of adjacent pores and throats are independent, then small throats on average are connected to relatively larger pores. In such a case, the aspect ratio increases with decreasing throat size and recovery may be inhibited by snap-off (Wardlaw, 1976),

suppressing extrusion at high pressures and isolating large throats which still contain nonwetting fluid. The accessibility of throats is also controlled by connectivity, and by spatial randomness of throat-size distribution.

In summary, small throats have high aspect ratios which, if above a critical value may cause snap-off. This tends to isolate large throats which therefore have low accessibility ratios and retain their nonwetting fluids at low pressures.

b) The hysteresis effect, which dictates that extrusion occurs at lower pressures than intrusion, also restricts extrusion from large throats. Some of the mercury intruded initially (at very low pressures) cannot be extruded. This effect does not occur for small throats, because their mercury is extruded at higher pressures attained earlier in the extrusion process.

c) A third cause of the negative correlation between throat size and RE relates to the experimental apparatus. Because the range of pressures under which mercury is intruded begins at 1.5 to 2 PSIA, whereas in our experiments extrusion can only be measured down to atmospheric pressure (14-15 PSIA), some mercury intrudes which cannot be extruded in our experimental apparatus simply because of the different pressure ranges covered. This problem is exacerbated in samples with large median throat sizes [which are usually more porous (Wardlaw, 1976)] because in these samples many throats are large enough to have been intruded below atmospheric pressure.

In a few analyses extrusion pressure was brought down to 2 PSIA (Hg-air). In all these examples no considerably greater extrusion occurred, suggesting that mercury which has not been recovered at atmospheric pressure (14,7 PSIA) can not be recovered on mere pressure reduction alone.

In the following, correlations between various petrophysical parameters are examined, and possible implications for the prediction of reservoir performance are discussed.

Porosity - Permeability. -- Twenty out of 120 samples fulfill the criteria for estimation of permeability values from capillary-pressure data (Jennings, 1987, p. 1208). Because of differences in the techniques used, the method of Jennings (1987) has been slightly modified in this study. The second-quartile pressure, P_2, is read off the capillary-pressure curve at a Hg-saturation of 50%. This provides the saturation where 50% of the total pore volume intruded at the maximum pressure reached during the analysis is filled with mercury. To obtain the estimated permeability the corresponding pressure is entered into the equation (Jennings, 1987, p. 1208),

$$K = e^{[(\ln P_2)(-2.5)+11.9]} \qquad (5)$$

where K is the permeability in millidarcys (md), and P_2 is the pressure at 50% Hg saturation.

Estimated permeability values range from 1 md to 11,200 md, with a mean of 943 md (n = 20). All other samples have permeabilities below 1 md, or they have polymodal volume distributions, making permeability estimates less accurate (Jennings, 1987, p. 1208). Thus, the majority of the studied Ellenburger dolostones consists of low-porosity, low-permeability rocks with intercalated thin intervals of higher porosity and permeability (Figures 59, 60).

Correlation coefficients (r^2) reveal some of the relationships between permeability and other petrophysical parameters (Table 12). A positive correlation exists between MTS and K (r^2 = .61, p = .0000) and between TS 20% and K (r^2 = .61, p = .0042) for all 20 samples. NTS and K are positively related (r^2 = .58, p = .0067) for all samples and for samples from facies 6. RE and K are weakly negatively correlated in facies 6 (r^2 = -.48, p = .0314); no correlation exists in lithofacies 3 and 4 (mottled dolomudstones and dolopackstones/grainstones, respectively). Apparent porosity and K show a positive correlation only in facies 3 and 4 (r^2 = .64, p = .0345), no correlation exists for facies 6 and the total number of samples.

The correlation coefficients reveal differences between the karst facies (lithofacies 6), mottled dolomudstone facies (lithofacies 3), and the dolopackstone/grainstone facies (lithofacies 4). These three facies include most high-porosity samples. The positive correlation between porosity and permeability in samples from lithofacies 3 and 4 indicates that the porosity-creating process also enhanced the permeability. In the karst facies such a positive correlation has not been observed, suggesting that diagenetic modifications were stronger for different samples.

Recovery Efficiency - Porosity. -- If the total of 120 analyses are considered no relationship between RE and porosity is observed (r^2 = -.07, p = .4532)(Table 12). Only for samples from well 1 and the karst facies RE and porosity are inversely correlated (Table 12). Samples from well 2 show no correlation, in wells 3 and 4 a weak positive is found, but most correlations are statistically insignificant. No correlation is observed in facies 1 to 4, a weak negative correlation exists in the karst facies.

Recovery Efficiency - Median Throat Size. -- Median throat size (MTS) and RE show a weak negative correlation for the total of 120 samples (r^2 = -.26, p =.0042) (Table 12). The correlation is negative for all wells and all facies, although some correlations are statistically insignificant. The strongest negative correlations are found in the karst facies and in well 1 were most of the samples belong to the karst facies (Table 12).

Table 12: Correlation Coefficients (r^2) Between Petrophysical Parameters.

	1 RE- AP	2 RE-MTS	3 RE-TS20	4 RE-SA	5 AP-MTS	6 AP-TS20	7 AP-SA
Well 1 (n=28)	r2= -.55 p = .0027	r2= -.48 p = .0091	r2= -.58 p = .0012	r2= .52 p = .0049	r2= .65 p = .0002	r2= .78 p = .0000	r2= .09 p = .6688
Well 2 (n=73)	r2= -.04 p = .7566	r2= -.18 p = .1142	r2= -.38 p = .0010	r2= .66 p = .0000	r2= .79 p = .0000	r2= .43 p = .0002	r2= .11 p = .3379
Well 3 (n=6)	r2= .25 p = .6335	r2= -.28 p = .5897	r2= -.31 p = .5487	r2= .05 p = .8831	r2= .03 p = .9146	r2= -.32 p = .5374	r2= .70 p = .1189
Well 4 (n=8)	r2= .13 p = .7484	r2= -.39 p = .3439	r2= .46 p = .2551	r2= .32 p = .4438	r2= -.41 p = .3075	r2= -.42 p = .2974	r2= .41 p = .3116
Well 5 (n=5)	r2= -.53 p = .3567	r2= -.33 p = .5934	r2= -.53 p = .3597	r2= .13 p = .8103	r2= .92 p = .0315	r2= .69 p = .1978	r2= -.88 p = .0483
Lithofacies 1 (n=16)	r2= .03 p = .8820	r2= -.38 p = .1423	r2= -.19 p = .4873	r2= .60 p = .0145	r2= -.31 p = .2446	r2= -.02 p = .8930	r2= .51 p = .0407
Lithofacies 2 (n=18)	r2= .08 p = .7335	r2= -.10 p = .6829	r2= -.20 p = .4404	r2= .55 p = .0178	r2= .62 p = .0057	r2= -.31 p = .2103	r2= .65 p = .0036
Lithofacies 3 (n=45)	r2= -.04 p = .7694	r2= -.23 p = .1175	r2= -.44 p = .0025	r2= .70 p = .0000	r2= .73 p = .0000	r2= .45 p = .0018	r2= .18 p = .2403
Lithofacies 4 (n=10)	r2= .01 p = .9194	r2= -.13 p = .7184	r2= .06 p = .8359	r2= .71 p = .0206	r2= .79 p = .0064	r2= .71 p = .0205	r2= -.15 p = .6739
Lithofacies 6 Total (n=31)	r2= -.13 p = .4803	r2= -.44 p = .0128	r2= -.55 p = .0014	r2= .51 p = .0033	2= .45 p = .0110	r2= .47 p = .0076	2= .14 p = .4444
Lithofacies 6 Well 1 (n=24)	r2= -.41 p = .0470	r2= -.44 p = .0281	r2= -.55 p = .0056	2= .78 p = .0000	r2= .62 p = .0013	r2= .76 p = .0000	r2= .01 p = .9109
Lithofacies 6 Well 5 (n=5)	r2= -.53 p = .3567	r2= -.33 p = .5934	r2= -.53 p = .3597	r2= .13 p = .8103	r2= .92 p = .0315	r2= .69 p = .1978	r2= -.88 p = .0483
Lithofacies 6 Well 1+5 (n=29)	r2= -.20 p = .3031	r2= -.48 p = .0083	r2= -.60 p = .0007	r2= .51 p = .0044	r2= .43 p = .0196	r2= .44 p = .0153	r2= .13 p = .5119
Total (n=120)	r2= -.07 p = .4532	r2= -.26 p = .0042	r2= -.33 p = .0003	r2= .49 p = .0000	r2= .44 p = .0000	r2= .32 p = .0005	r2= .16 p = .0780

AP = apparent porosity; RE = minimum recovery efficiency; MTS = median pore-throat size; TS 20% = pore-throat size at 20% Hg-saturation; NTS = normalized pore-throat size; SA = surface area.
Lithofacies are as follows: 1 = laminated dolomudstones; 2 = dolomudstones/wackestones; 3 = mottled dolomudstones/wackestones; 4 = peloid-ooid-intraclast packstones/ grainstones; 6 = karst facies.

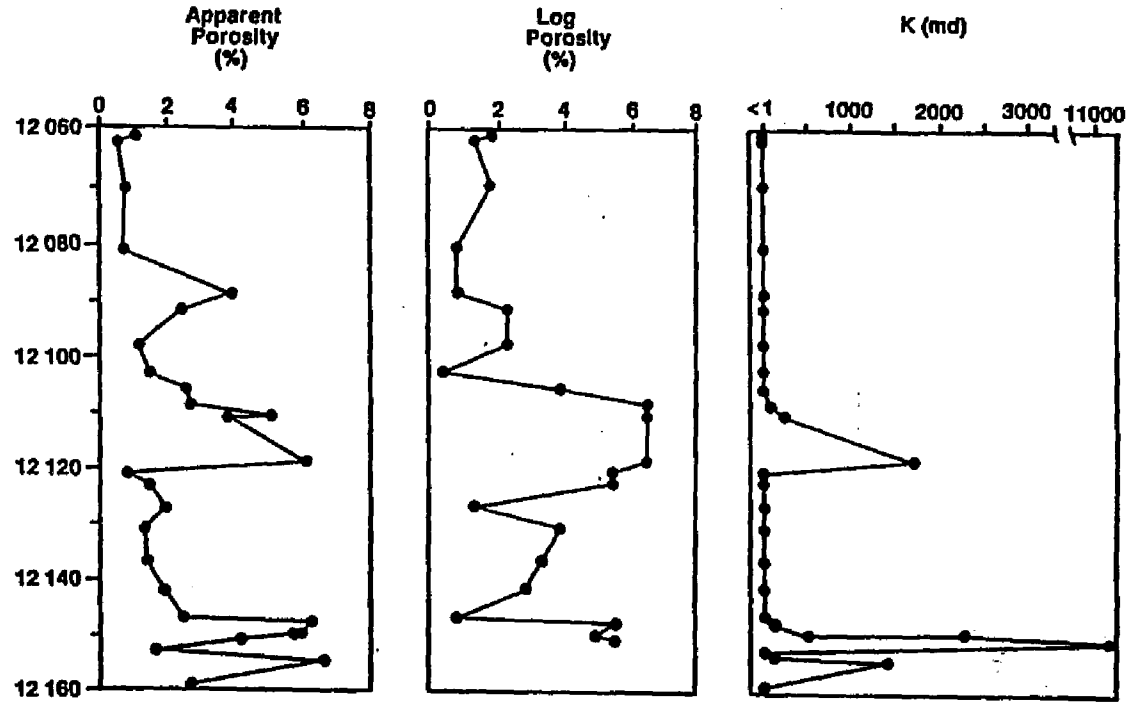

Figure 59. - - Comparison of apparent porosity, log porosity,and permeability values for well 1.

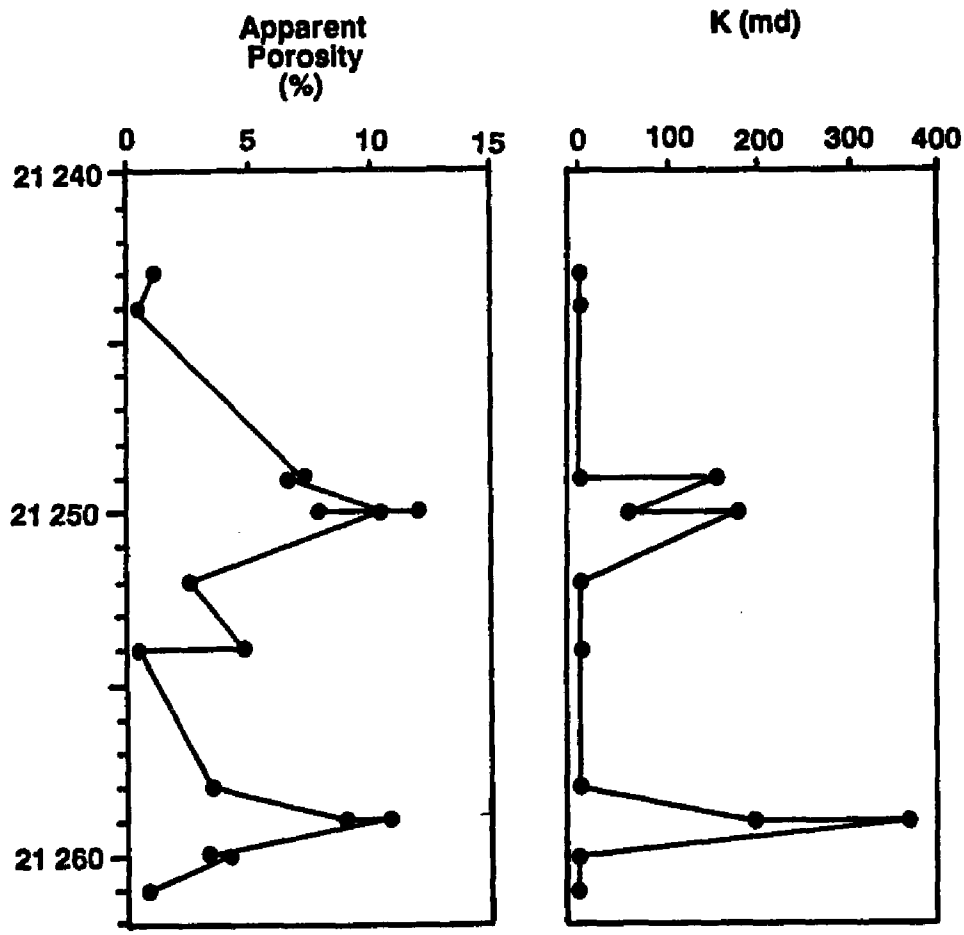

Figure 60. - - Comparison of apparent porosity and permeability values for a 20-feet sequence of well 2.

Recovery Efficiency - Throat size at 20% Hg-Saturation. -- A weak negative correlation exists for this pair if all samples are considered, as well as for all wells and all facies with the exception of well 4 and lithofacies 4 (dolopackstones/ grainstones) (Table 12). The strongest negative correlation are observed in wells 1 and 3, and in the karst facies (Table 12).

Recovery Efficiency - Surface Area. -- A weak positive correlation is observed for the total of 120 samples (r^2 = .49, p = .0000) (Table 12). Statistically significant correlations exist for wells 1 and 2, and for all facies. Because small pores and throats contribute more to the surface area then do larger pore and throats, RE is also correlated with small throats. In other words, the smaller the throats (larger SA), the better RE.

Porosity - Median Throat Size. -- A weak positive correlation exists for these parameters (r^2 = .44, p = .0000) for all samples, and has been observed in all facies, except facies 1. The karst facies and the depositional facies show no notable differences with respect to this correlation coefficient (Table 12).

Porosity - Throat size at 20% Hg-Saturation. -- These parameters also show a weak positive correlation (r^2 = .32, p = .0005). Samples from facies 1 and 2 display a negative correlation, indicating the influence of intercrystalline microporosity in these dense and low-porosity facies. All other facies have positive correlation coefficients (Table 12), showing the importance of larger throats for the amount of porosity in the porous facies 3,4, and 6.

Porosity - Surface Area. -- Because smaller pores and throats contribute more to the surface area, a large surface area translates into smaller pores and throats. A positive correlation means that small pores and throats are responsible for the porosity present, a negative correlation exists if large pores and throats (small SA) contribute to porosity.

In lithofacies 1 and 2 a positive correlation exists, indicating the importance of microporosity in these rocks. The porous lithofacies 3, 4, and 6 show no or a negative correlation (Table 12), suggesting that large pores and throats are responsible for the porosity in these facies.

Discussion

From comparison of the correlation coefficients (Table 12) it is apparent, that no simple relationship exists between the various petrophysical parameters. The results also indicate

that averaging data does not provide the detailed information necessary for reservoir characterization. Results computed for each well, for example, do not show many of the important relationships. A distinction in different facies, however, appears to be more useful for studying the geologic features that have a significant effect on the petrophysical properties and therefore on the performance of reservoir rocks.

There is no simple relationship between recovery and porosity. All correlations that have been found in this study are negative. Wardlaw (1976, 1980) reported positive relationships from two data sets. Krause et al., (1987) (for sandstones) and Kopaska-Merkel and Friedman (1989) described and discussed negative relationships between porosity and recovery efficiency. It is safe to say that no consistent relationship exists.

The observed negative correlation, however, has important implications for the performance of reservoir rocks of the Ellenburger karst facies. The negative relationship between recovery and porosity, MTS, and TS20% in the karst facies and the concomitant positive relationship of porosity and permeability with MTS and TS20% suggests that these rocks may not be the best "performers". High - porosity, high - permeability rocks might not necessarily be the best candidates for enhanced recovery projects, and lower porosity, lower permeability rocks may respond better to secondary recovery methods (Amthor et al., 1988; Kopaska-Merkel and Friedman, 1989).

Recovery efficiency depends largely on the aspect ratio (pore size to throat size). It is suggested that dissolution of limestones and dolomitization (replacement and cementation) resulted in a decrease in the size of small throats, but increased the pores. The resultant large aspect ratio could result in "snap-off" in throats before mercury extrusion can occur from pores. As a result the nonwetting phase becomes disconnected and is trapped in the pores. This is an important mechanism of trapping oil in water-wet reservoir rocks during waterflooding (Li and Wardlaw, 1986).

The diagenetic processes that are active in the karst facies may increase porosity and permeability, but this results not necessarily in increased recovery. Rather the increase in porosity and permeability might lead to critical aspect ratios, above which "snap-off" occurs.

Similar conclusions have been reached by Hutcheon and Oldershaw (1985), who conducted experiments to determine the extent to which mineral reactions affect petrophysical properties. In their study (Hutcheon and Oldershaw, 1985, p.375) they found, that porosity and permeability may increase during hydrothermal treatment, but this result does not necessarily equate to increase in recovery efficiency. They attribute this fact to an unfavorable change in aspect ratio: pores increased in size, and pore throats became smaller (mainly as a result of smectite growth). This requires inhomogeneous cementation patterns,

which have been observed in thin-sections of the karst facies.

It is also apparent that diagenetic modifications of the pore system are stronger for different samples. The porous facies 3 and 4 have not been as strongly modified as samples from the karst facies. In facies 3 and 4 porosity and permeability are proportional, indicating that the porosity-creating process (dolomitization) also enhanced permeability. No negative relationship between recovery and porosity has been observed in these facies.

Thus, the karst facies is different in many respects from the non-karst facies. This is attributed to the influence of karst-related processes that shaped this important Ellenburger facies. Dissolution of limestone and the resulting solution collapse created vug porosity which was then strongly modified by dolomitization. Replacement of limestone by nonplanar dolomite and cementation by late-stage dolomites resulted in zones of dense, low-porosity dolostones and zones with isolated vuggy porosity. In facies 3 and 4 dolomitization favorably increased the porosity and permeability, and the modification of the pore system was less pronounced. Samples from these zones are characterized by petrophysical parameters that indicate a better performance and suggest that such rocks are good candidates for secondary-recovery projects.

Because of the importance of the karst facies for reservoir development within the Ellenburger (e.g., Kerans, 1988), and because it is petrophysically so different from other facies in this study, it seems appropriate to highlight its properties in a case study.

CASE STUDY

Petrophysical Character of Ellenburger Karst Facies

Petrophysical analyses were performed on 27 core plugs of the karst facies of the Continental State #1 well (well 1) (Figure 61) (Amthor and Friedman, 1989 c). The karst facies of the studied Ellenburger interval is interpreted to represent the cave-roof facies of the laterally persistent facies association, using the terminology of the paleokarst model of Kerans (1988 a). Details on stratigraphic and petrographic aspects of the karst facies in the Continental State #1 well have been provided in the chapters on "Karstification and Brecciation" and "Karstification and Dolomitization". The objective of the case study is to provide core-analysis data of petrophysical properties of this Ellenburger karst facies and to demonstrate how petrophysical data obtained from high-pressure mercury porosimetry can help in recognizing the nature and extent of micro-scale reservoir heterogeneity.

Based on the results from capillary-pressure analyses, the cave-roof facies is subdivided into four petrophysical units (Figures 62, 63). Petrophysical parameters that have been utilized in characterizing and defining the four zones are:

(1) median pore-throat size, (2) pore-throat size at 20 % Hg-saturation, (3) normalized pore-throat size range, (4) effective porosity, and (5) minimum recovery efficiency.

Summaries of the data for five petrophysical parameters are listed in tables 13 and 14.

In the following the four petrophysical units are described in detail. It will be shown that the subdivision into four units strongly reflects the karst-generated heterogeneities in the upper Ellenburger.

Unit 1 (U1) (12,060-12,106 ft)(3,676-3,690 m)

This unit is composed of dense, low-porosity dolostones characteristic of the upper part of the core. The available porosity ranges from .6 to 3.9 %. Samples from this zone show steep convex or gently sloping capillary-pressure curves with bimodal or polymodal pore-throat size distributions (Figure 64). Both curve types are characterized by higher fractions of high-pressure intrusion (> 100 PSIA), which corresponds to small pore-throat sizes (mean = .3 microns, std. dev. = .4). Samples of this unit have the highest minimum recovery efficiency (mean = 33.6 %, std. dev. = 16.8) of all four units.

All samples of unit 1 can be adequately characterized using their respective capillary-pressure curve form. Samples with steep convex curve forms (e.g. Figure 64 A) have very low porosities, small median pore-throat sizes and high RE. Samples showing this curve

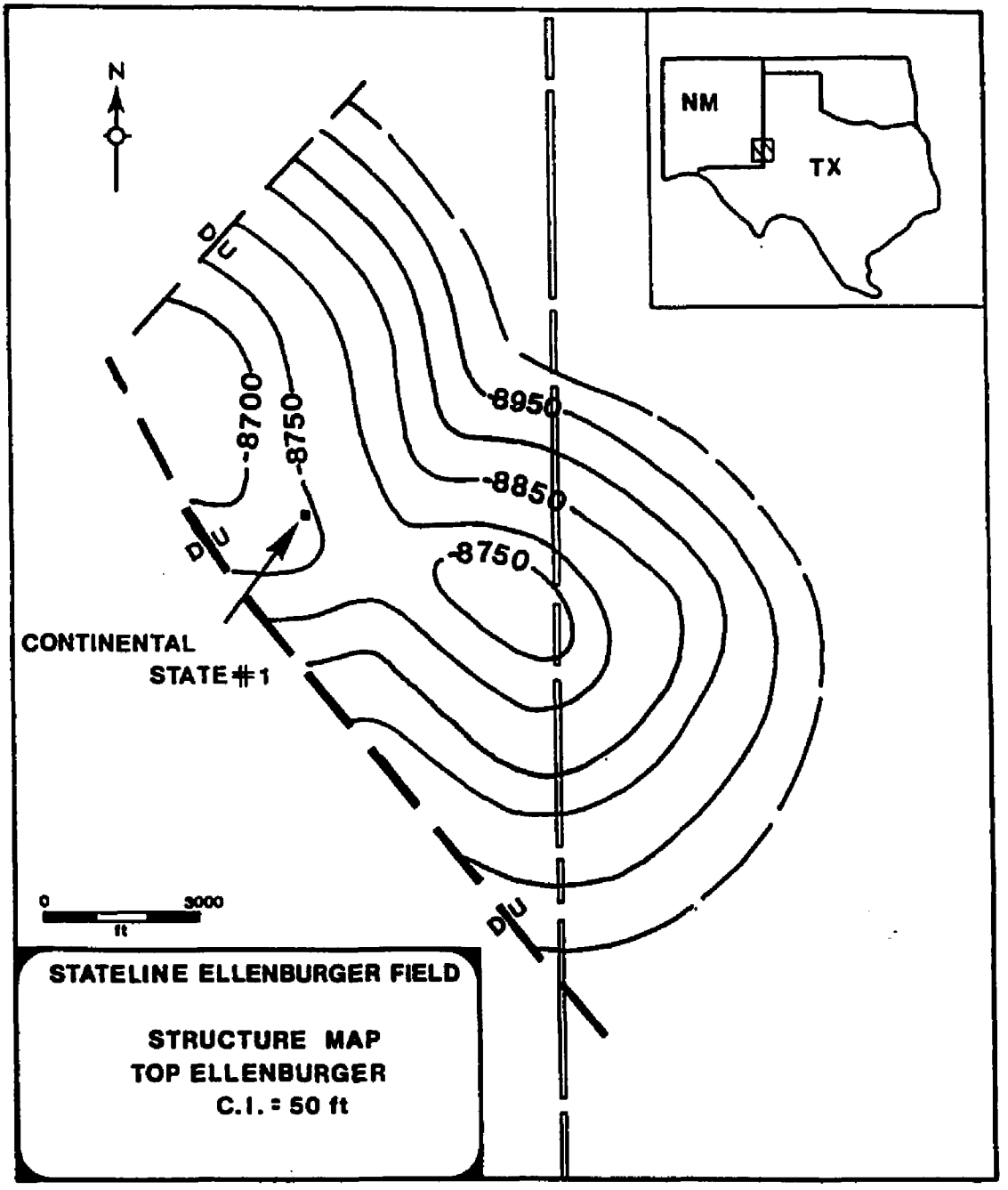

Figure 61. - - Location map of Continental State #1 well, drilled in Section 5, Township 24-S, Range 38-E in the Stateline Ellenburger field, Lea County, NM. Structure map modified from Moore (1982).

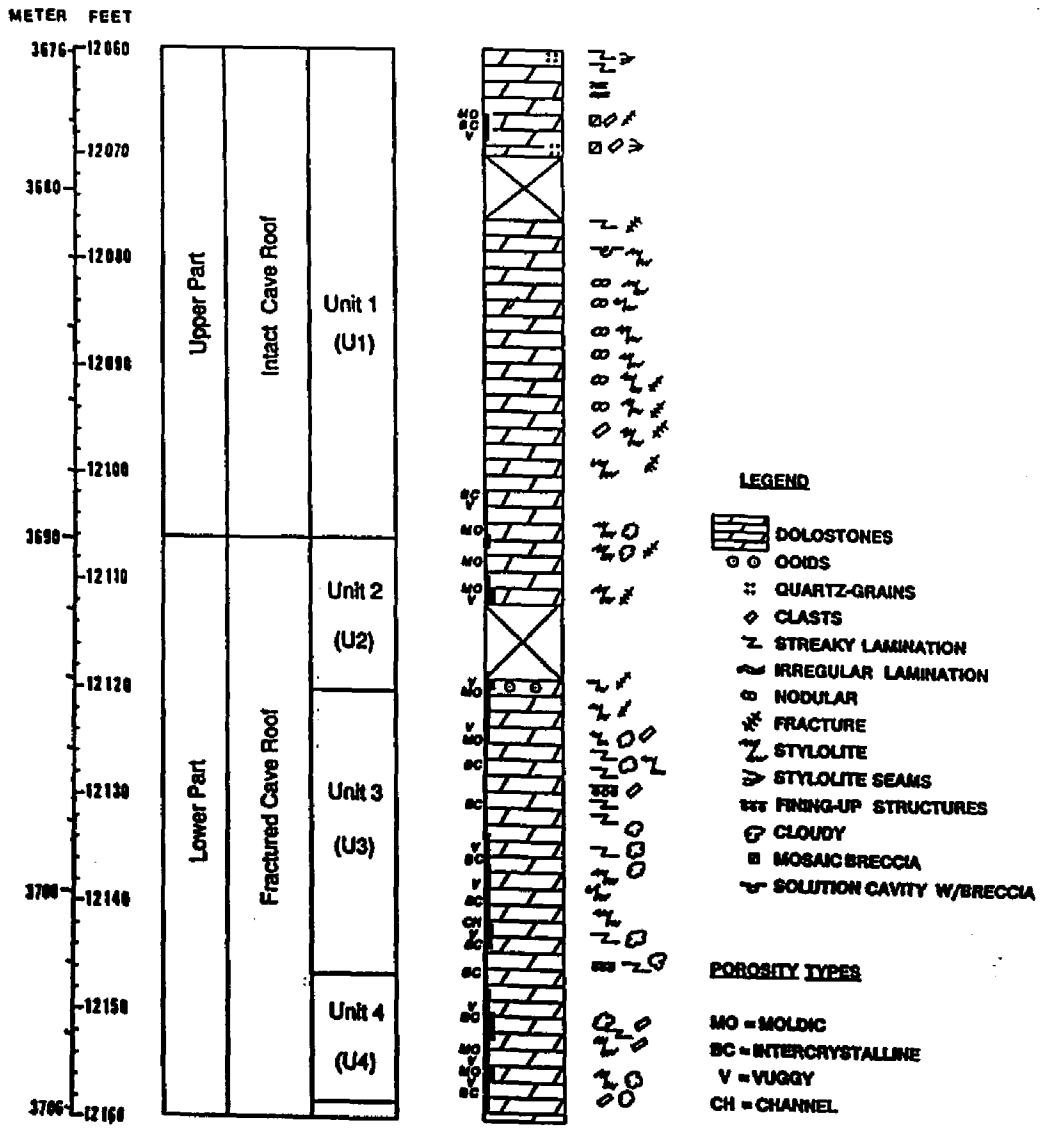

Figure 62. - - Lithologic column of Ellenburger Dolomite, Continental State #1 well, Lea County, NM. The core is subdivided into an upper and lower part and four petrophysical units (U1 to U4), which can be correlated with the intact cave roof (unit 1) and the fractured caver roof (units 2-4) of the the paleokarst model of Kerans (1988 a).

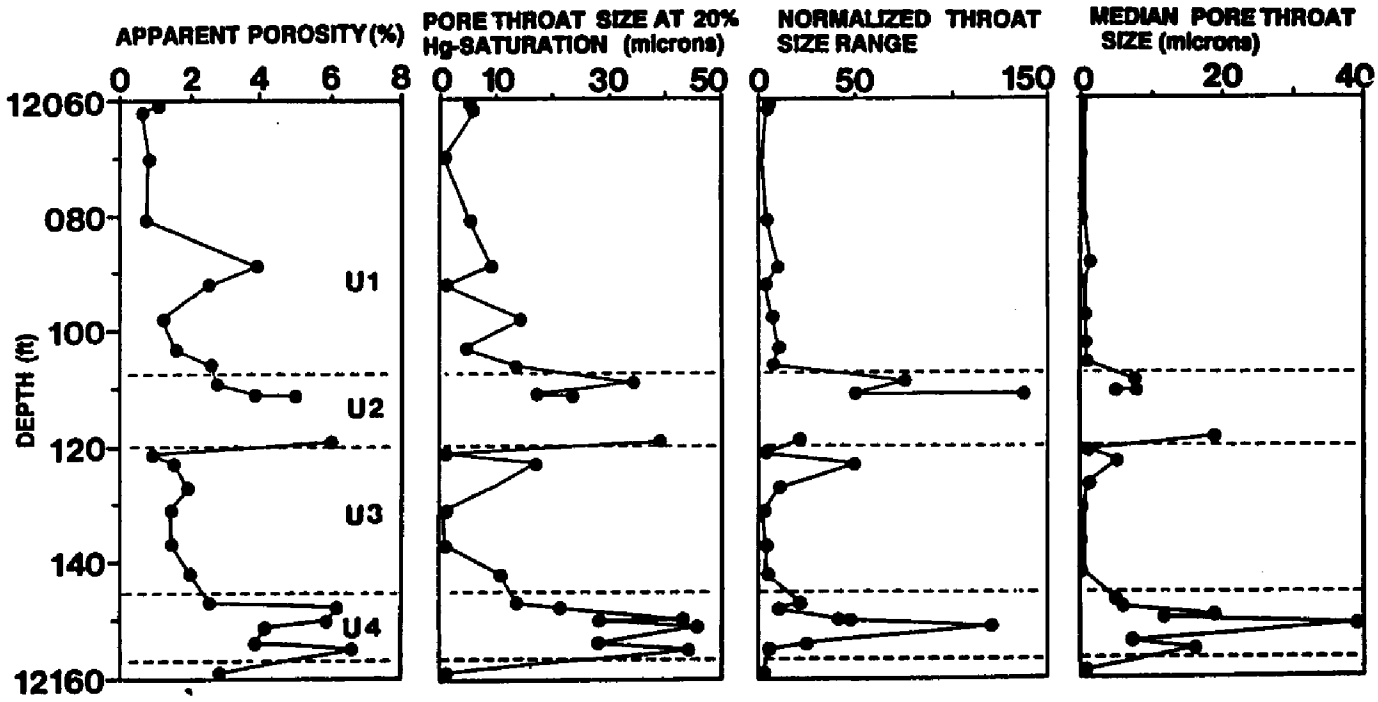

Figure 63. - - Four petrophysical units (U1 - U4), were defined by correlation of petrophysical parameters. Data for parameters and units are listed in Tables 13 and 14.

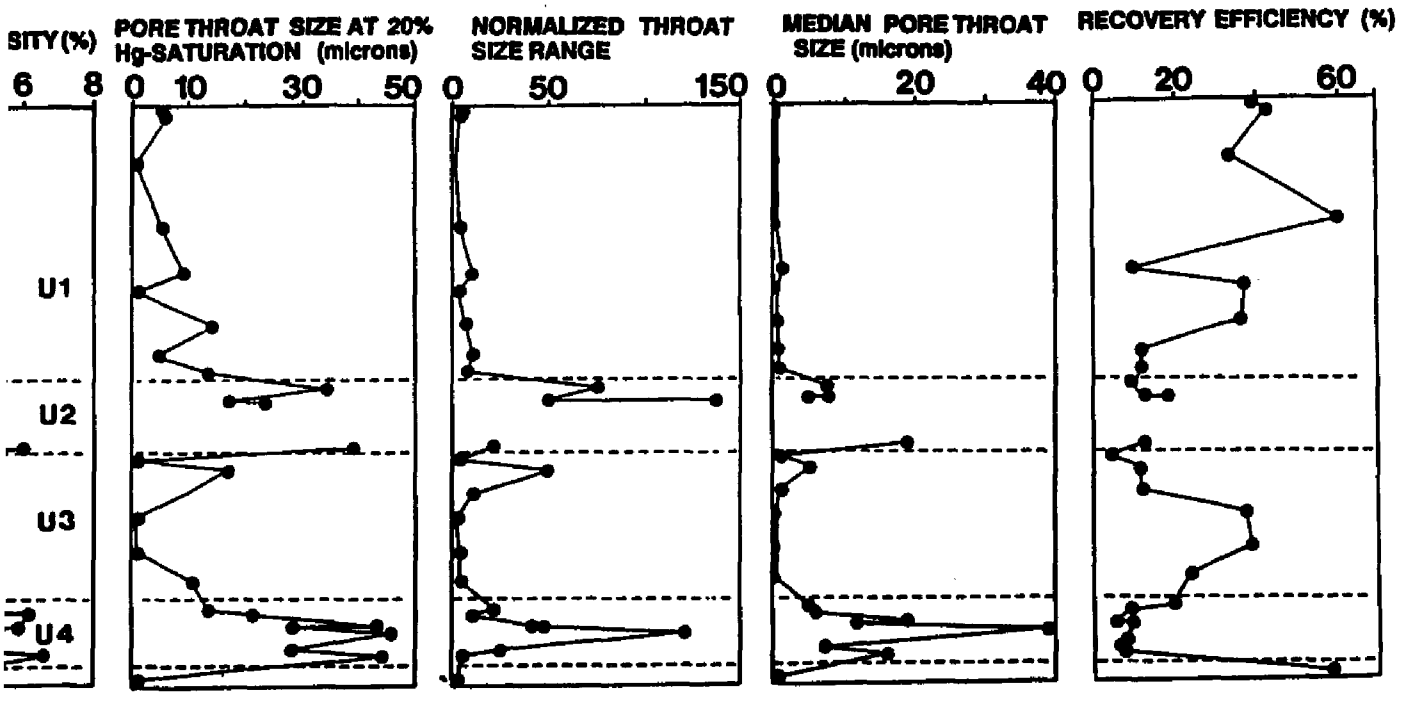

petrophysical units (U1 - U4) were defined by correlation of
Data for parameters and units are listed in Tables 13 and 14.

Table 13: Petrophysical Data for 27 Samples of Karst Facies in Well 1, Obtained From Capillary-Pressure Curves.

SAMPLE DEPTH (ft)	APPARENT POROSITY (%)	MEDIAN PORE-THROATSIZE (microns)	PORE-THROAT SIZE AT 20 % Hg-SATURATION (microns)	NORMALIZED THROAT-SIZE RANGE	RECOVERY EFFICIENCY (%)	CURVE TYPE
12061	1.1	.08	4.8	5.5	38.5	1
12062	.6	.05	6.2	3.3	42.9	1
12070	.8	.04	.1	.8	33.3	1
12081	.7	.03	4.8	3.0	60.0	1
12089	3.9	1.13	9.0	10.8	8.3	2
12092	2.4	.05	.1	1.5	37.5	1
12098	1.1	.10	14.5	5.9	36.6	1
12103	1.5	.7	3.8	10.1	11.3	2
12106	2.6	.6	12.9	5.9	12.0	2
12109	2.7	7.5	34.3	77.4	9.0	3
12111A	5.0	8.1	16.5	47.7	12.3	3
12111B	3.8	4.7	22.5	136.0	19.0	3
12119	6.0	18.3	39.4	18.3	12.0	3
12121	.8	.1	.3	1.0	3.3	1
12123	1.6	5.2	16.4	50.4	11.1	2
12127	1.9	.5	9.0	10.2	11.4	2
12132	1.3	.02	.04	1.0	37.5	1
12142	1.9	.06	10.1	3.0	23.2	1
12147	2.5	4.5	12.9	21.2	19.4	2
12148	6.2	5.8	21.0	9.3	8.8	3
12150A	5.9	18.9	43.1	45.7	4.9	3
12150B	5.7	10.6	27.3	40.6	9.3	3
12151	4.2	39.2	45.0	119.0	3.3	3
12154	3.8	6.4	27.5	24.2	6.3	3
12155	6.5	16.1	43.8	3.7	6.8	3
12159	2.7	.02	.1	1.4	58.2	1

CAPILLARY-PRESSURE CURVE TYPE: 1 = (STEEP) CONVEX
2 = GENTLY SLOPING (POLYMODAL)
3 = (STEEP) CONCAVE

Table 14: Statistical Data on Petrophysical Units.

		UNIT 1	UNIT 2	UNIT 3	UNIT 4
		12,060 - 12,106 (ft)	12,107 - 12,120 (ft)	12,121 - 12,147 (ft)	12,148 - 12,158 (ft)
Available Porosity (%)	m:	1.6	4.4	1.6	5.4
	s:	1.1	1.5	0.5	1.1
Median Pore-Throat Size (microns)	m:	0.3	9.7	1.5	16.2
	s:	0.4	6.0	2.3	12.4
Pore-Throat Size at 20% Saturation (microns)	m:	6.2	28.2	7.1	34.6
	s:	5.1	10.5	6.7	10.5
Normalized Throat Size Range	m:	5.2	69.9	13.0	22.6
	s:	3.5	50.5	17.9	17.4
Minimum Recovery Efficiency (%)	m:	31.2	13.1	20.6	6.6
	s:	17.3	4.2	13.5	2.3
Number of samples		n=9	n=4	n=7	n=6

m = mean s = standard deviation

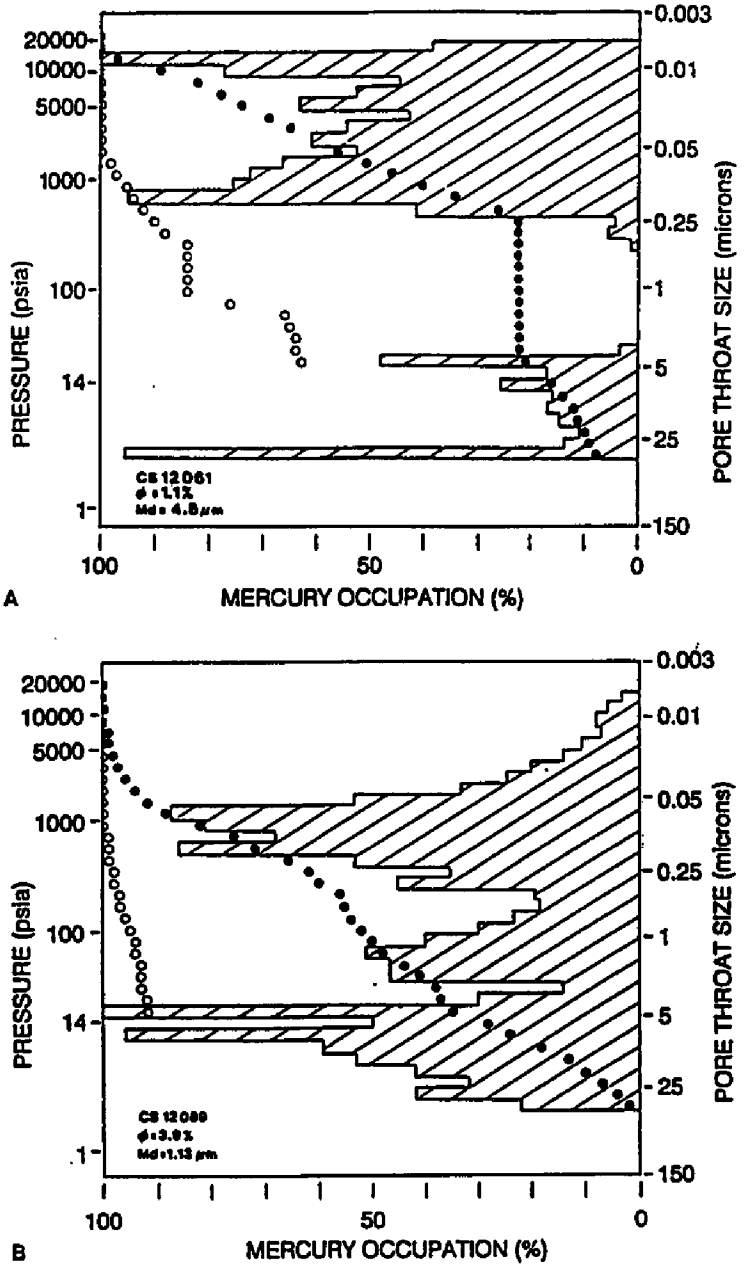

Figure 64. - - Capillary-pressure curves typical for unit U1. A) Sample from 12,061 ft (3,676 m). Porosity (Ø) = 3.9 %, median pore-throat size (Md) = 1.13 microns. B) Sample from 12,089 ft (3,685 m). Porosity (Ø) = 1.1%, median pore-throat size (Md) = 4.8 microns. ● = Cumulative Intrusion, O = Extrusion, ■ = Both. Hachured histograms = incremental intrusion.

form are found in the upper 20 feet of unit 1. Samples with gently sloping capillary-pressure curves make up the lower part of the unit. These samples show a broad range of pore throat sizes, high normalized throat size values (polymodal), and have slightly higher porosities, but lower minimum recovery. A larger amount of low pressure intrusion (< 100 PSIA), indicating larger throat sizes, is related to fracture and/or stylolite- enhanced porosity in the lower part of unit 1.

Unit 2 (U2) (12,107-12,12,120 ft)(3,690-3,694 m)

All samples analyzed in this unit are characterized by (steep) concave capillary-pressure curve forms (Figure 65). This translates into larger median throat sizes (mean = 9.7 microns; std. dev = 6.0), higher porosity values, but also lower minimum recovery efficiencies than in unit 1. The median pore throat size at 20% Hg-saturation (mean = 28.2 microns; std. dev. = 10.5) is much larger than in unit 1, indicating the presence of large pore openings in this unit. This is consistent with the presence of solution-enlarged fractures and vugs in this part of the core. Thin sections of sample 12,111B also reveal low amounts of intercrystalline porosities. In the capillary-pressure curves this is manifested in two modes of smaller throat sizes and an overall polymodal pore throat distribution (Figure 65 A).

Unit 3 (U3) (12,121-12,147 ft)(3,694-3,702.5 m)

This unit compares to unit 1, but is more complex and variable in character. Unit 3 is also characterized by gently sloping (Figure 64) and convex curve forms, but the median throat size (mean = 1.5 microns; std. dev. = 2.3) is slightly larger, and so is the median pore throat size at 20% Hg- saturation (mean = 7.1 microns; std. dev. = 6.7). Samples with convex curves have low porosities, small median throat sizes, small throat sizes at 20 % Hg-saturation and high minimum recovery efficiencies. Samples with gently-sloping, polymodal curves show a wide range of pore sizes (larger normalized throat sizes) with distinct modes at low pressures, which correlates with larger median pore throat sizes and higher porosities. Overall unit 3 is very similar to unit 1, representing a tight, low-porosity zone.

Unit 4 (U4) (12,148-12,158 ft)(3,703-3,706 m)

Samples with (steep) concave capillary-pressure curves (Figure 67) characterize this unit which is very similar to unit 2. The following are characteristics of the concave capillary curves that define unit 4: large median throat sizes, large pore-throat sizes at 20% Hg-saturation, the highest porosity values found in the core and the lowest minimum recovery efficiencies. These characteristics correlate with the centimeter - sized vugs, solution channels and

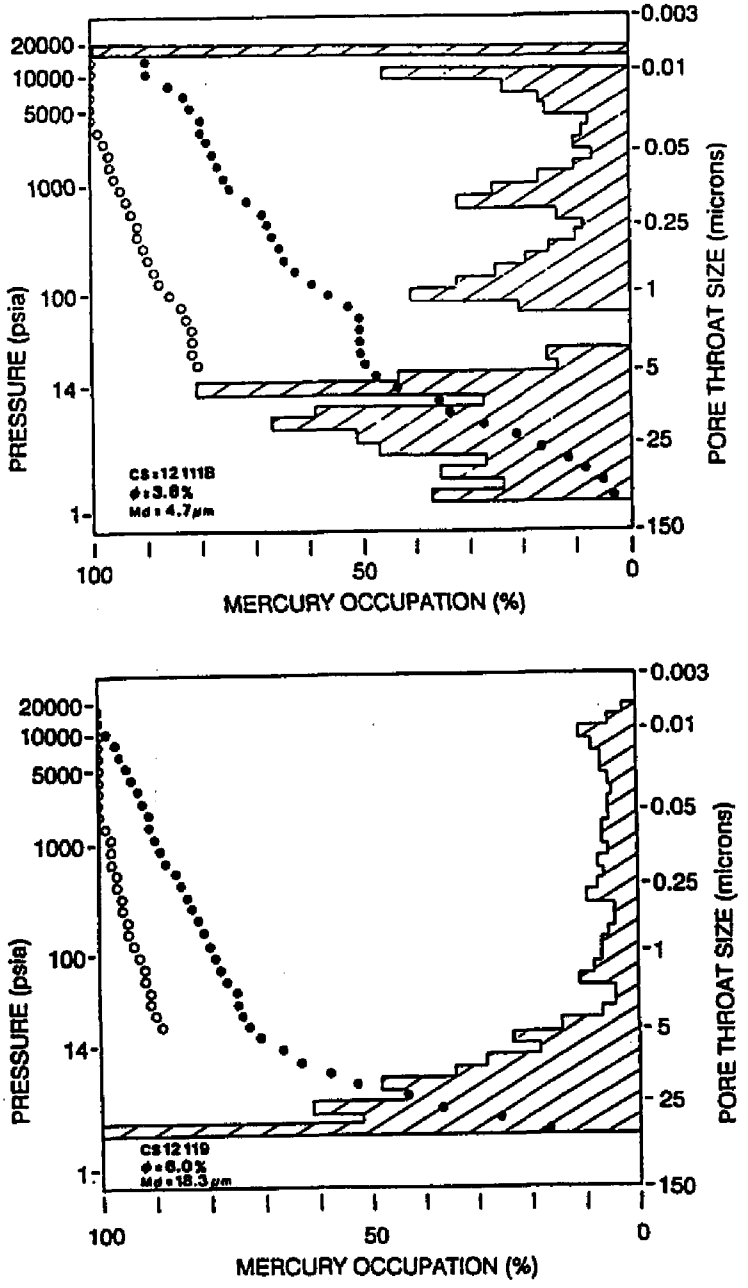

Figure 65. - - Capillary-pressure curves characterizing unit U2. A) Sample from 12,111 ft (3,691 m). Porosity (Ø) = 3.8 %, median pore-throat size (Md) = 4.7 microns. B) Sample from 12,119 ft (3,694 m). Porosity (Ø) = 6.0%, median pore-throat size (Md) = 18.3 microns. ● = Cumulative Intrusion, O = Extrusion, ■ = Both. Hachured histograms = incremental intrusion.

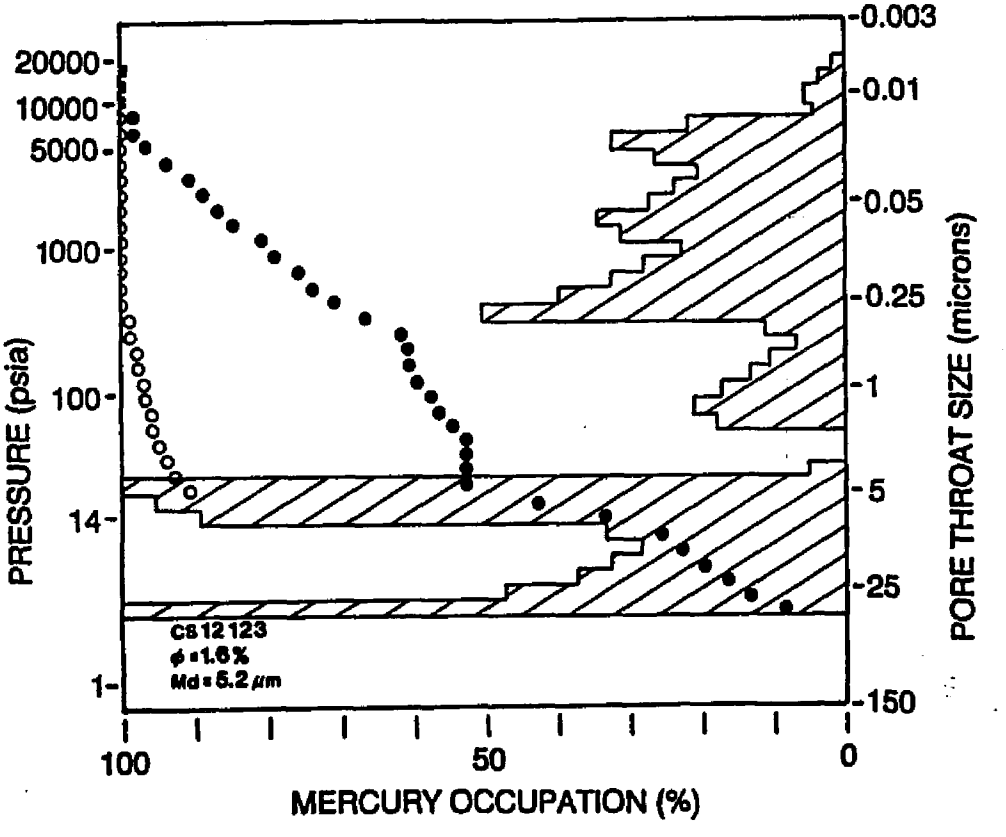

Figure 66. - - Capillary-pressure curve characterizing unit U3. Sample from 12,123 ft (3,695 m). Porosity (Ø) = 1.6%, median pore-throat size (Md) = 5.2 microns. ● = Cumulative Intrusion, O = Extrusion, ■ = Both. Hachured histograms = incremental intrusion.

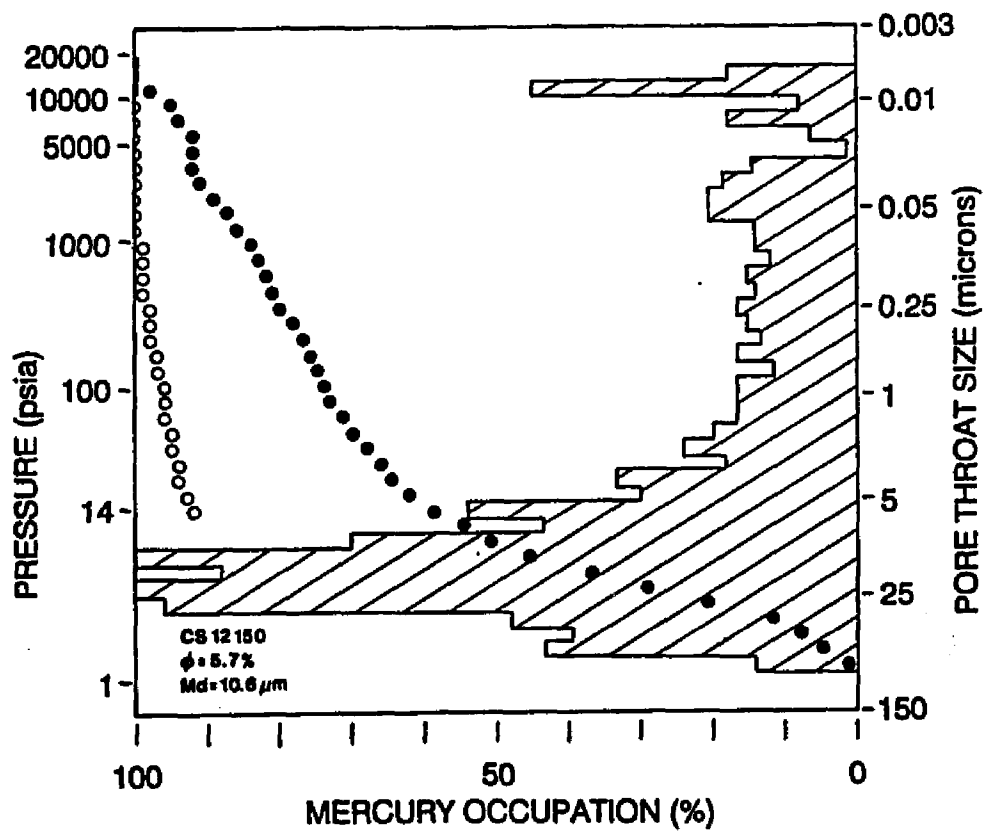

Figure 67. - - Characteristic capillary-pressure curve for unit U4. Sample from 12,150 ft (3,703 m). Porosity (Ø) = 5.7%, median pore-throat size (Md) = 10.6 microns. ● = Cumulative Intrusion, ○ = Extrusion, ■ = Both. Hachured histograms = incremental intrusion.

solution-enlarged intercrystalline porosity that are encountered in this part of the core.

Unit 4 is followed by two feet of dense, greenish-gray, fine crystalline dolostones that constitute the end of the cored interval and which have not been included in this study.

Discussion

By using petrophysical parameters derived from high-pressure mercury capillary data 92 feet of Ellenburger karst facies are subdivided into four petrophysical units (Figure 63)(Tables 13, 14). Characteristics of capillary-pressure curves and petrophysical parameters derived from capillary data were used to define each unit. It can be shown that the subdivision into four units strongly reflects the karst-generated heterogeneities in the upper Ellenburger.

Kerans (1988 a, p. 1174, Fig. 13), lacking core-analysis data, used 30-minute shut-in-pressures to define permeable zones within the upper Ellenburger karst facies. The use of petrophysical parameters derived from capillary-pressure curves permits a more detailed characterization of the cave-roof facies of the upper Ellenburger.

Unit 1 is thought to represent the intact cave roof with dense, tight dolostones. Low effective porosities and small median throat sizes reflect the pervasive early diagenetic dolomitization of presumably fine-grained, low-energy peritidal precursor carbonates of the upper Ellenburger, resulting in dense mosaics of mostly planar-s crystals of dolomite type 1 (Figures 68 A, B). Towards unit 2 the fracture density increases, creating fracture and stylolite enhanced porosity. This is indicated by an increase in median pore throat size, normalized throat size ranges and effective porosity.

Units 2 to 4 are interpreted to represent the fractured cave-roof facies of the Ellenburger karst model (Kerans, 1988b). Two porous and permeable zones, units 2 and 4, are separated by a dense, tight zone, unit 3, resulting in vertical heterogeneity within the cave-roof facies. The petrophysical characteristics of the porous zones are large median pore-throat sizes, large pore-throat sizes at 20% Hg-saturation, high normalized throat-size ranges and low minimum recovery efficiencies. The large and variable median pore-throat sizes are a result of a) the extensive dissolution and solution enlargement that occurred along the fractures in the cave-roof facies creating solution-enlarged porosity (Figure 68 D, 69 D), and b) the large scale replacement of limestone by nonplanar dolomite and cementation by late stage dolomites, occluding and reducing the available porosity. The values of effective porosity as determined by mercury porosimetry are lower than the visual estimates from core slabs and thin sections mainly for two reasons: (1) The experimental method does not account for very large pore-throat sizes. The size of the samples in mercury porosimetry is restricted and usually very

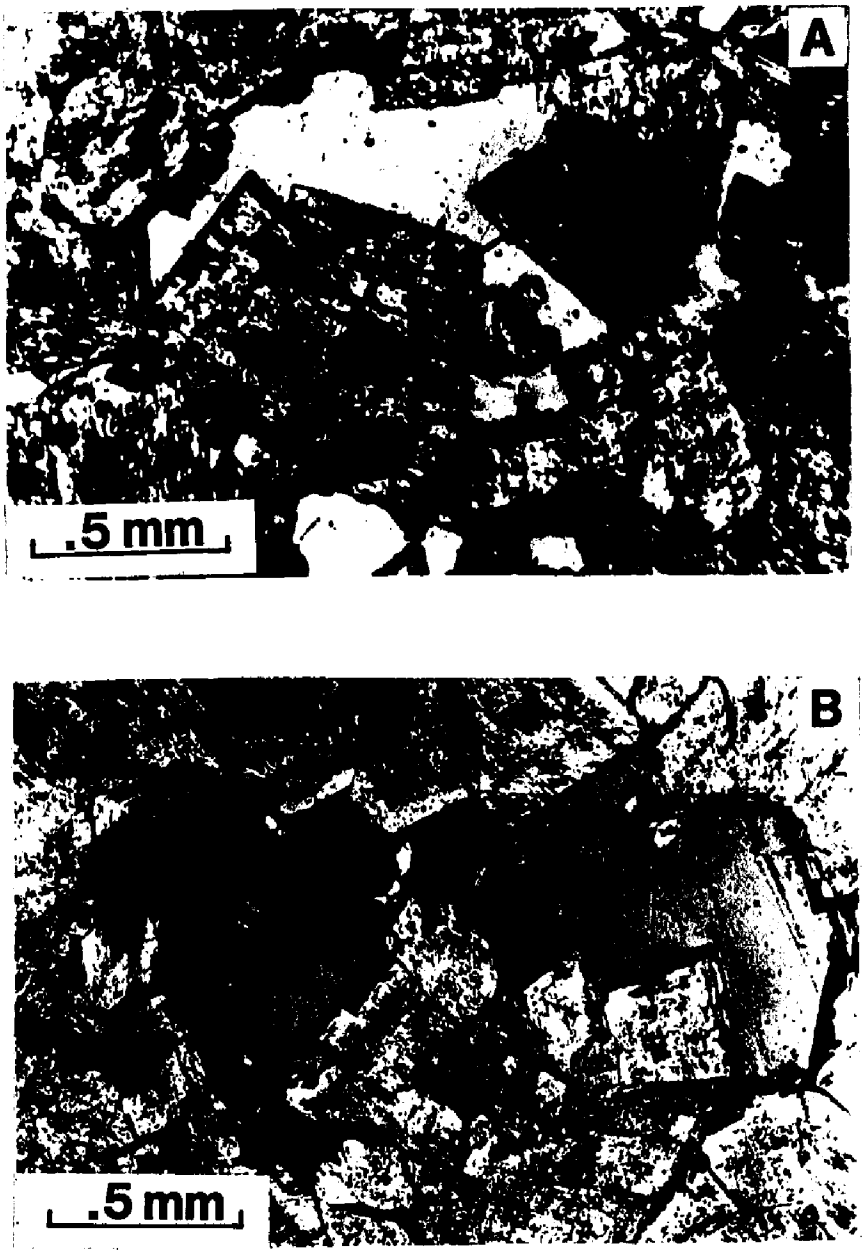

Figure 68. - - Thin-section photomicrographs of Ellenburger karst facies illustrating porosity types. Most of the microporosity is related to intercrystalline pores (A to C) and to solution-enlarged intercrystalline porosity (D). A) Sample from 12,067 ft (3,678 m). B) Sample from 12,087 ft (3,684 m) .

(over)

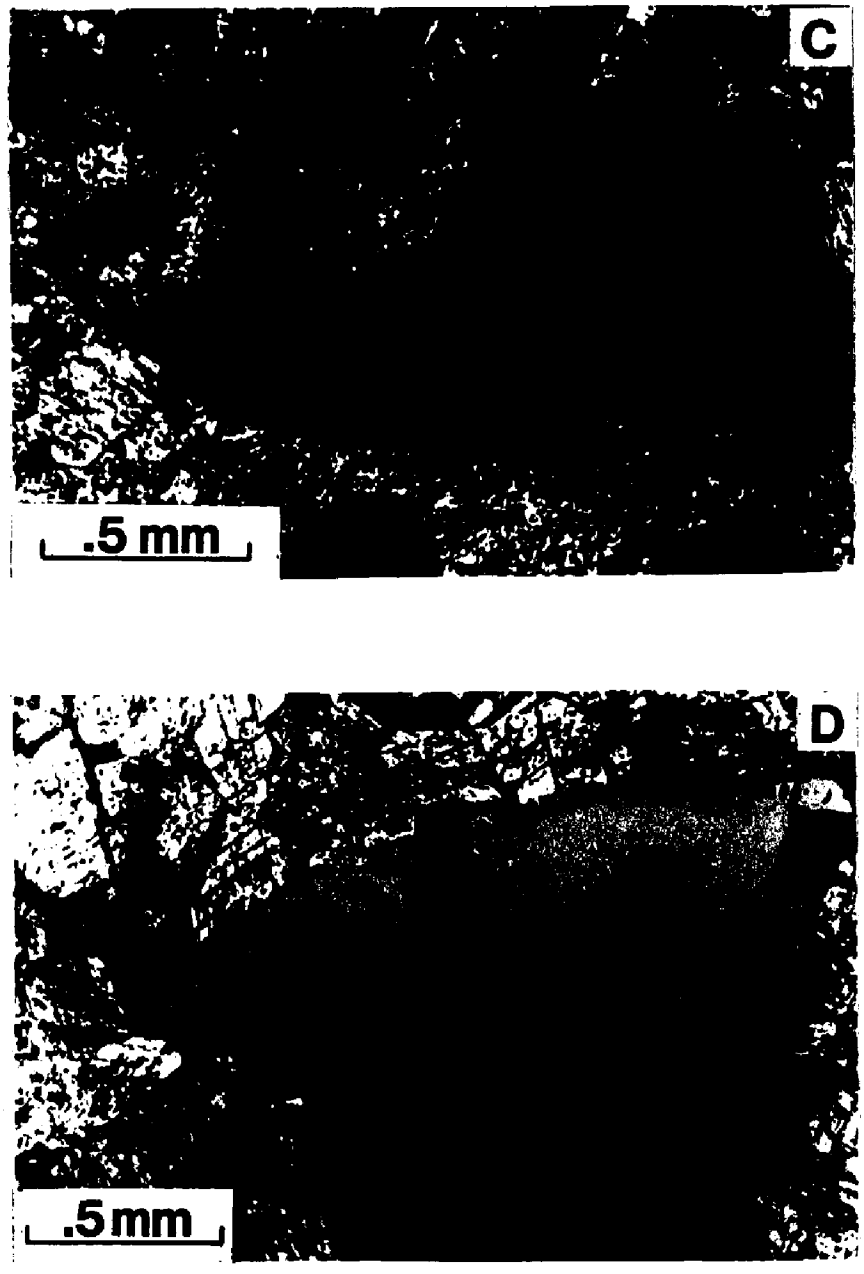

Figure 68. (cont.) - - C) Sample from 12,111 ft (3691 m). D) Sample from 12,148 ft (3,703 m).

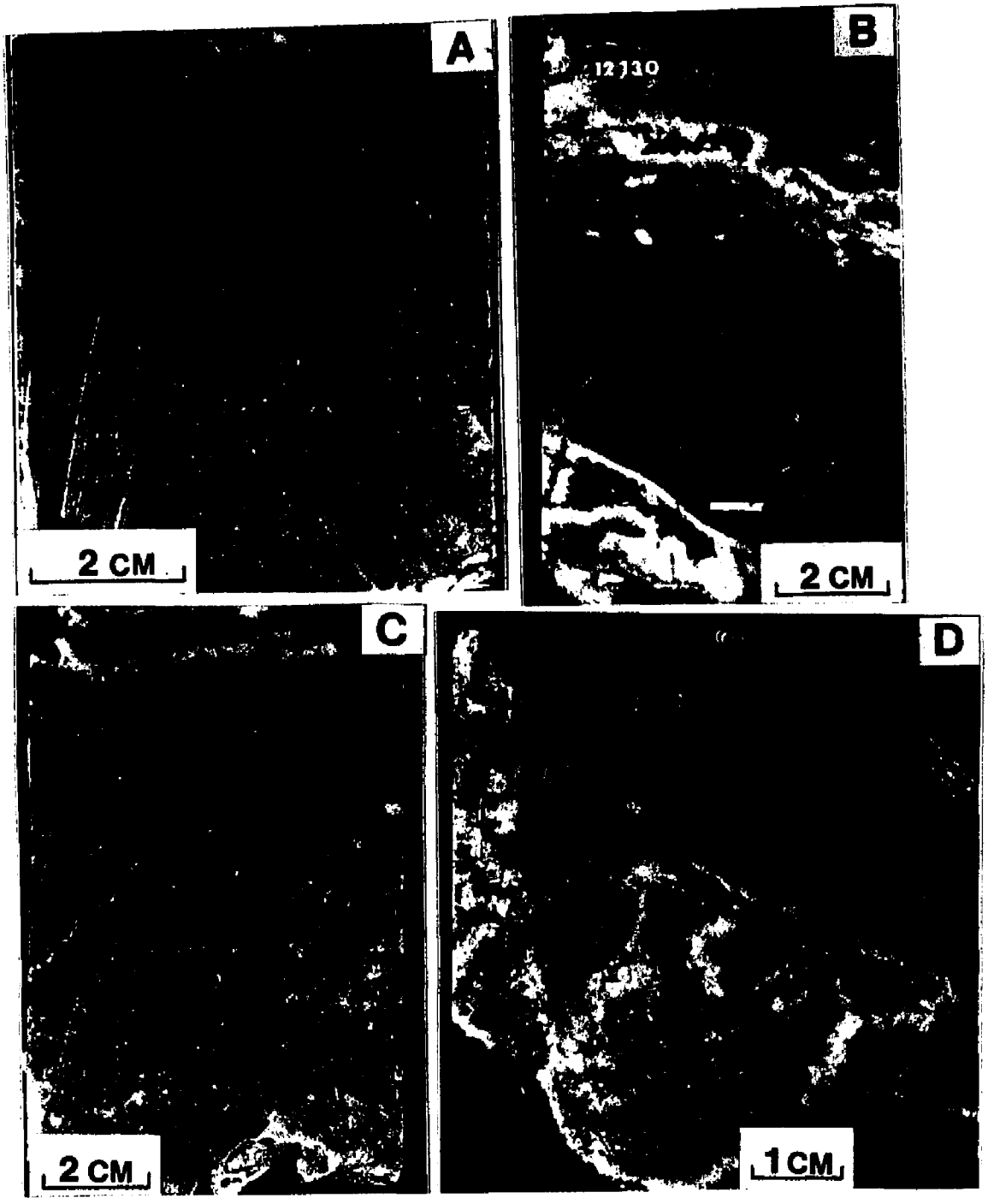

Figure 69. - - Core photographs of Ellenburger karst facies. A) Sample from 12,091 ft (3,685 m), unit 1, showing nodular texture commonly observed within the intact cave roof. B) Isolated vugs, filled with white, coarse-crystalline dolomite, sample from 12,130 ft (3,697 m), unit 3 (fractured cave roof). C) Banded sediment fill and geopetal infill structure (arrow) in sample from 12,128 ft (3,697 m), unit 3 (fractured cave roof). D) Cm-sized vugs partly filled with coarse crystalline dolomite; sample from 12,140 ft (3,700 m), unit 3 (fractured cave roof).

small. Hence large pore throats and pores may go unnoticed. (2) Many vugs and voids observed in hand specimen are isolated. Pore throats and the walls of large pores have very commonly been cemented and/or occluded by a late-stage dolomite and/or infilling of internal sediment (Figure 69 B, D). These pores and throats do not contribute to the available or effective porosity. This void space would not be available for hydrocarbons either. The effective porosity obtained by mercury porosimetry may therefore be the better estimate of the available porosity, although it has to be considered as a minimum value. Effective porosity values derived from mercury porosimetry are also in good agreement with density log derived porosity. In addition, porosity reported by Kerans (1988 a, p. 1179) for the lower part of the cave-roof facies typically range from 2 to 5%.

In summary, the units 1 to 4 are a reflection of the highly variable processes that generated the karst facies and of the later diagenetic modifications, resulting in the heterogeneous nature of the lower part of the core.

Graphs of petrophysical parameters derived from high-pressure mercury porosimetry curves reveal relationships that might help to evaluate the significance of these parameters for predicting reservoir performance. In figures 70 and 71 petrophysical parameters such as median pore-throat size, pore-throat size at 20% Hg-saturation and recovery efficiency are plotted against effective porosity and density-log porosity. In all graphs the values for the porous units 2 and 4 (open circles and squares, respectively) are separated and distinct from zones 1 and 3, thus reflecting the subdivision into four petrophysical units.

Figures 70 A and B show that samples with larger pore-throat sizes tend to have higher apparent porosities (r^2: .65; p = .0002) and density-log porosities (r^2: .52; p = .0095). A similar positive relationship between median pore-throat size and apparent porosity has been found for other Ellenburger dolostones and for Hunton Group carbonates (Amthor et al., 1988; Kopaska-Merkel and Friedman, 1989). Figures 70 C and D indicate a similar trend for the pore-throat size at 20% Hg-saturation (r^2: . 78; p = .0000 and r^2: . 63; p = .0009 for apparent and density-log porosity, respectively).

It is not only the amount of void space available to hydrocarbons that is of interest, but the fraction of that void space which may in fact contain hydrocarbons, and the (generally much smaller) fraction from which hydrocarbons may be readily removed. Thus, the relationship between porosity and recovery efficiency is critical for reservoir description. Figure 69 shows plots of apparent and density-log porosity and median throat size at 20% Hg-saturation versus minimum recovery efficiency. Figures 69 C and D show an inverse relationship between the throat size at 20% Hg-saturation and RE (r^2: -.59; p = .0012) and a weak relationship between median throat size and RE (r^2: -.48; p= .0091). Data presented by Wardlaw et al.,

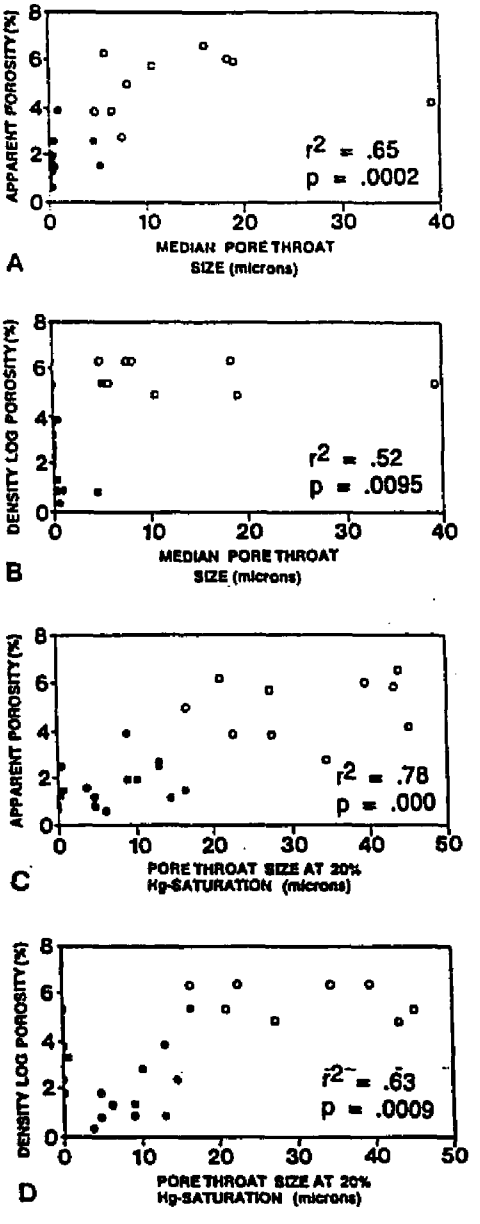

Figure 70. -- Graphs of petrophysical parameters. ● = U1, ○ = U2, ■ = U3, □ = U4. A) Apparent porosity versus median throat size. B) Density-log porosity versus median pore-throat size. C) Apparent porosity versus pore-throat size at 20% Hg-saturation. D) Density-log porosity versus pore-throat size at 20% Hg-saturation.

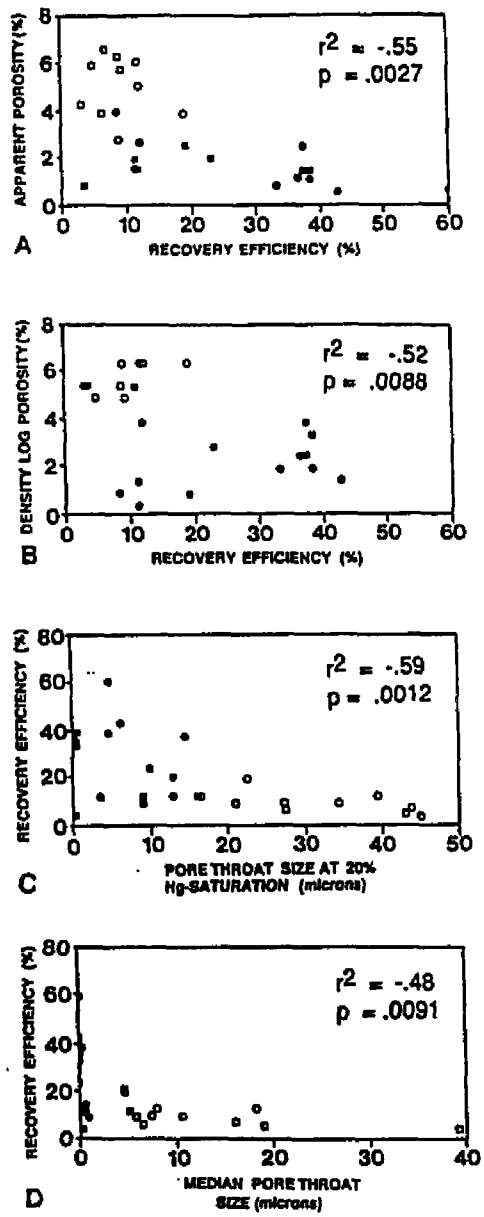

Figure 71. - - Graphs of petrophysical parameters. ● = U1, ○ = U2, ■ = U3, □ = U4. A) Apparent porosity versus recovery efficiency. B) Density-log porosity versus recovery efficiency. C) Recovery efficiency versus pore-throat size at 20% Hg-saturation. D) Recovery efficiency versus median pore-throat-size.

(1988: Table 2) show a similar inverse relationship. Figures 69 A and B indicate that samples with higher porosities tend to have lower recoveries (r^2: -.55; p= .0027, and r^2: -.52; p= .0088 for apparent porosity and density-log porosity, respectively). Reasons for the negative relationship between porosity and RE are extensively discussed in the previous chapter and in Amthor et al. (1988). One reason that needs to be emphasized here is the pore-throat size ratio (aspect ratio). Li and Wardlaw (1986) and Wardlaw et al. (1988) discuss the influence of the critical aspect ratio on recovery efficiency. For a given wettability (contact angle) there is a critical pore to throat radius above which mercury continuity is broken by "snap-off" in throats before mercury extrusion can occur from pores. As a result the nonwetting phase becomes disconnected by snap-off and is trapped in the pores. This is an important mechanism of trapping of oil in water-wet reservoir rocks during waterflooding (Li and Wardlaw, 1986).

These relationships suggest for the porous zones 2 and 4, that the desired positive relationship between porosity and RE may not hold and that recovery from these zones could be low. This behavior may strongly influence any secondary or tertiary recovery methods applied to this karst-influenced zone.

Summary

The studied Ellenburger core is interpreted to represent part of the Ellenburger karst-facies (cave-roof facies). The lower part of the core (12,107-12,158 ft; 3,690-3,706 m), characterized by fractures, solution-enlarged fractures and different types of porosity represents the fractured cave-roof facies, while the upper part of the core (12,060-12,106 ft; 3,676-3,690 m) corresponds to the relatively intact cave-roof facies.

Using petrophysical parameters derived from high-pressure mercury porosimetry such as median pore-throat size, pore-throat size at 20% Hg-saturation, normalized pore-size range, effective porosity, and minimum recovery efficiency, the cave-roof facies is subdivided into four petrophysical units (U1 to U4). Unit 1 corresponds to the intact cave roof, units 2-4 to the fractured cave roof. Units 1 and 3 are dense and tight zones, which separate two porous and permeable zones, units 2 and 4, resulting in vertical heterogeneity within the cave-roof facies.

The petrophysical units 1 to 4 reflect the highly variable processes that generated the karst facies as well as later diagenetic modifications, resulting in a heterogeneous nature of the lower part of the core (fractured cave roof).

Graphs of petrophysical parameters derived from high-pressure mercury porosimetry reveal relationships that might help to evaluate the significance of these parameters for predicting reservoir performance. The relationships indicate that for the porous units 2 and 4,

the desired positive relationship between porosity and minimum recovery efficiency may not hold and that recovery from these zones could be low. This behavior might strongly influence any secondary or tertiary recovery methods applied to this karst-influenced zone.

CONCLUSIONS

1) The distribution of major rock types and lithofacies in Lower Ordovician Ellenburger Group rocks from the subsurface indicates deposition as epicontinental platform carbonates, ranging from mixed clastic-carbonate deposits during an early marine phase to shallow subtidal to supratidal carbonates during late stages of Ellenburger deposition.

2) Petrographic studies and X-ray analyses indicate that 90% of the studied samples were pervasively dolomitized. Based on the regional and stratigraphic distribution of dolomite in the Ellenburger cores, a paleogeographic control on the distribution of dolomite is inferred.

3) Seven dolomite-rock textures have been recognized and were classified according to crystal-size distribution and crystal- boundary shape.

4) Paragenetic relationships of the dolomite-rock textures indicate that Ellenburger carbonate rocks were subjected to a complex diagenetic history involving both early and late-diagenetic dolomitization. Unimodal, very fine to fine- crystalline planar-s dolomites formed penecontemporaneously and/or during early diagenetic dolomitization. Coarse- crystalline replacement dolomites and planar and nonplanar dolomite cements formed after burial of Ellenburger carbonate rocks.

5) With increasing depth of burial the dolomite-rock textures show no systematic transition from one kind of textures to another, such as from planar to nonplanar. The lack of such a transition might indicate a lack of pervasive neomorphism of early formed dolomites during burial diagenesis.

6) Using dolomite paragenesis combined with burial-history plots and estimates of thermal maturation, it is concluded that late late-stage calcite and nonplanar dolomite cements can not be older than late Pennsylvanian-Early Permian, which correlates with a deep-burial (> 2.5 km) setting of these latest phases.

7) The separation of Ellenburger dolostones into seven dolomite-rock textures is based on differences in crystal- boundary shape and crystal-size distribution. These textures also show significant differences in their major and minor element distributions.

8) There is an increasing incorporation of iron and manganese into the lattice during progressive dolomitization. Early diagenetic dolomites are low in iron and manganese, whereas later diagenetic phases are enriched. The geochemistry of the dolomite- rock textures correlates with the petrography: different dolomite-rock textures are also geochemically distinct. Dolomite cements and replacement dolomites can be distinguished using textural criteria and on the basis of their geochemical composition.

9) Ellenburger dolostones were strongly modified by karst- related brecciation, that resulted from an unconformity developed on top of the Ellenburger. Breccia types and associated deposits indicate a karst-related origin for most of the brecciation and fracturing observed in the Ellenburger cores. Tectonic-induced fracturing has been observed locally, modifying in part earlier karst-related brecciation. Tectonic brecciation can not explain the observed association of matrix-supported and clast-supported breccias. Their origin is related to zones of solution and requires collapse into open space.

10) Karstification and dolomitization are closely related. Early dolomitized zones did resist dissolution and provided ceiling and roofs for the formation of caverns, which are the result of limestone dissolution beneath such early dolomitized zones. Subsequent collapse after burial and the formation of brecciated horizons formed permeable pathways for the migration of dolomitizing fluids, whereby laterally continuous karst-facies were affected more intensively than laterally restricted karst deposits, were late-stage dolomitization was apparently restricted to the breccia bodies. Porosity and permeability pathways created by karst-dissolution seem to be of prime importance for the distribution of different dolomite types.

11) The integration of petrographic and geochemical data with petrophysical data obtained by high-pressure mercury porosimetry led to recognition of nature and extent of micro-scale heterogeneity within the complex Ellenburger reservoir rocks.

12) Dolomitization leaching, and secondary porosity development are intimately associated in the Ellenburger carbonates. The resulting porous zones are not uniformly distributed but are isolated and sealed off by nonporous zones composed of dense dolostones. These dense zones provide intraformational seals and resulted in vertical heterogeneity.

13) The porous zones are commonly characterized by late diagenetic dolomites. This distribution of dolomite-rock textures suggests that the porous zones were preserved as limestones until later in the diagenetic history. Such zones indicate the importance of permeable horizons for the distribution of dolomite-rock textures and thus for the formation of favorable secondary porosity within otherwise dense dolostones and limestones.

14) Examination of various petrophysical parameters such as recovery efficiency, permeability, porosity, pore-throat size, and surface area reveal no simple relationships.

15) The diagenetic modifications (e.g. by dolomitization and karstification) of the rock-pore system are stronger for different lithofacies. Rocks of the karst facies were stronger modified than were samples from lithofacies 3 (mottled dolomudstones/wackestones) and lithofacies 4 (peloid-ooid- intraclast dolopackstones/grainstones). Rocks form these lithofacies are characterized by petrophysical parameters that indicate that these rocks are good candidates for enhanced-oil recovery projects.

16) The petrophysical characteristics of Ellenburger karst facies are outlined in a case study. Using petrophysical parameters such as median pore-throat size, pore-throat size at 20% Hg- saturation, normalized pore-throat size, effective porosity, and minimum recovery efficiency, the karst facies in the Continental State # 1 well, Lea County, New Mexico is subdivided into four petrophysical units. These units reflect the highly variable processes and diagenetic modifications that generated the karst facies, resulting in the heterogeneous and complex nature of this important lithofacies.

APPENDIX A

MERCURY POROSIMETRY

Principle

Mercury porosimetry is used extensively for the characterization of porous media and has been subject of a review (Van Brakel et al., 1981). The technique is based on the behavior of mercury as a non-wetting liquid (contact angle > 90°) towards most substances (Purcell, 1949) (but see Wardlaw et al., 1988, for an exception). Mercury does not penetrate into openings and pores of most substances unless pressure is applied. Samples are sealed into a penetrometer, evacuated, filled with mercury and then put under increasing pressure. With each pressure increment, smaller pore throats are invaded by mercury (Wardlaw, 1976). The precise throat size corresponding to a given pressure depends on the model of throat geometry used (Wardlaw and Taylor, 1976; Dullien, 1979) as well as on values for interfacial tension of mercury and air, and mercury contact angle (eq. [1]). The model of Wardlaw (1976; Wardlaw and Taylor, 1976; Wardlaw and McKellar, 1981) for crystalline dolostones is used here, in which throats are assumed to be sheet-like and pores tetrahedral, or in which pores are low-face-number polyhedra that approach the tetrahedral form during progressive dolomitization (Wardlaw, 1976, figure 12). Throat geometry is important, because throat size (usually assumed to be either a "diameter" or a "radius") is calculated from capillary pressure using one or another of a family of related equations in which the choice of formula depends upon the model for throat shape (Wardlaw and McKellar, 1981). In the model used here, throat size is the distance (d) between parallel bounding surfaces of a sheet-like throat and is calculated by the equation :

$$(1) \qquad d = \frac{2\gamma \cos\theta}{p}$$

where γ is the interfacial tension (485 dynes/cm for Hg/vacuum), θ is the contact angle (140° for Hg/vacuum, measured in Hg) and p is the pressure in psia. If d is measured in microns and p in psia, then this equation reduces for the purpose of routine analyses to

$$(2) \qquad d = \frac{108 \text{ microns psia}}{p \text{ psia}}$$

A contact angle of 140° is used, because it is among the most frequently quoted values for

the contact angle of mercury (Van Brakel et al., 1981, p. 2). It should be noted, however, that contact angles as high as 180° are reported (e.g., Wardlaw et al., 1988) and there is no general agreement as to what value to use for the mercury-solid contact angle (Good & Mikhail, 1981).

In principle, every non-wetting fluid could function in the same way as mercury, but few alternatives have been investigated (Van Brakel et al., 1981). Wetting phases, however do not show such capillary-pressure properties. If two immiscible phases are present (such as oil and water), one phase usually is the wetting phase with respect to the rock wall. This phase can spontaneously imbibe into the pore-network. Water is commonly the wetting phase in sandstones, but in carbonates the wetting phase may be oil. For such oil-wet rocks capillary-pressure data must be interpreted differently than has been followed in this study.

Samples were analyzed for capillary-pressure data in a commercially available Micromeritics Pore Sizer 9305 (Kopaska-Merkel et al., 1987; Micromeritics Manual, Pore Sizer 9305, 1983). Samples were evacuated to a pressure of 10 to 20 microns of mercury and then pressurized incrementally, allowing equilibration at each increment.

Ellenburger samples were pressurized to 15,000 PSIA (Hg-air). These pressures are considerably greater than those reached in many published studies of this type. For comparison, Ghosh et al. (1987) and Gosh and Friedman (1989) pressurized their samples to 5,000 PSIA (Hg-air), and Jennings (1987) used 2,000 PSIA (Hg-air) as his maximum pressure value. High-pressure analysis has been used in previously published studies on the Ellenburger and Hunton Group carbonates (Amthor et al., 1988; Kopaska-Merkel and Amthor, 1988) and on Hunton Group carbonates (Kopaska-Merkel, 1988; Kopaska-Merkel and Friedman, 1989). After intrusion measurements were completed, extrusion data were collected while pressure was incrementally reduced to atmospheric pressure (about 14.7 PSIA), and in certain cases below atmospheric pressure (2 PSIA). Following a delay caused by hysteresis, successively larger pore throats (and their connected pores) were vacated by mercury during the extrusion process at successively lower incremental pressures. During both intrusion and extrusion, data points were collected at standard pressure points (e.g., 500, 1,000, 5,000, 10,000 PSIA) with supplemental readings, where appropriate, in porous rocks. In general, data were collected such that the increment in intrusion was not much larger than machine error between successive readings (Kopaska-Merkel, 1988).

Data reduction was accomplished using a BASIC computer program purchased from the Micromeritics Corporation (RUN9305.BAS, v. 1.03), which receives data directly from the porosimeter during the run, and calculates a variety of derived petrophysical parameters (incremental and cumulative throat diameters, average and median throat diameters, pore

surface areas and volumes, and apparent skeletal density). These parameters are presented in tabular and graphic format. Further data analysis was accomplished using STATS+.

For further discussion of mercury porosimetry, its principle and geological applications, see Purcell (1949), Archie (1952), Stout (1964), Smith (1966), Berg (1975), Wardlaw (1976, 1979, 1980), Wardlaw and Taylor (1976), Schowalter (1979), Wardlaw and McKellar (1981), Van Brakel et al., (1981), Jennings (1987), Amthor et al., (1988), Kopaska-Merkel and Amthor (1988), Etris et al., (1988), Kopaska-Merkel (1988), Ghosh and Friedman (1989), Amthor and Friedman (1989a), Kopaska-Merkel and Friedman (1989).

The results of mercury porosimetry are generally displayed as graphs of capillary pressure versus cumulative mercury intrusion (e.g., Wardlaw, 1976) or throat size. Plotting both cumulative and incremental intrusion versus throat size on a single graph facilitates capillary-pressure curve interpretation.

Limitations of Technique

Besides the uncertainties in assigning values to the surface tension and contact angle of mercury, results obtained by mercury porosimetry are limited in a number of ways (e.g., Van Brakel et al., 1981; Jennings, 1987). Three points are particularly important:

(a) The calculations of pore-throat sizes are based on cylindrical pores. This is, of course, far from reality. Pores and pore throats are rarely cylindrical in natural materials, hence equation (1) constitutes a special model. Such a model may not represent pores in actual materials, but is generally accepted as the practical means of treating what, otherwise, would be a most complex problem.

Calculation of pore-throat size is further complicated by a shielding effect, in which small throats near the sample surface prevent intrusion of large throats in the sample interior until sufficient pressure is attained to intrude the smaller surficial throats (Wardlaw, 1976).

(b) The volume of mercury that can enter the pore space of a sample during a mercury porosimetry analysis is limited (among other factors) by the maximum pressure attained during the analysis.

(c) The size of the samples in mercury porosimetry is restricted and is usually very small. As a result, very large pores may go unnoticed. This size limitation is especially critical for vuggy rocks of the karst facies. The result is not necessarily representative of an infinite pore space for this reason, and because large pores which intersect the surface are directly accessible to mercury, not shielded by throats (Van Brakel et al., 1981). This boundary effect is greatest in small samples (Larson and Morrow, 1981).

Why Such High Pressures?

As mentioned above pressure ranges used are considerably greater than those reached in most previously published studies. Consideration of three points led to the conclusion that high-pressure tests are valuable in evaluation of reservoir rocks:

1. The apparatus used, a Micromeritics Pore Sizer 9305, is capable of analyzing a wide range of pressures and corresponding pore sizes. High-pressure runs can be performed up to 206 MPa (30,000 PSIA) and low-pressure runs down to 0.1 MPa (0.015 PSIA). The machine can analyze pore-throat sizes ranging from 180 to 0.0006 microns. This leads to a better evaluation of the full range of pore-throat sizes present, and to a more adequate characterization of the reservoir rocks.

2. The analyses are designed to duplicate pressures which might occur under deep-burial conditions. This seems to be necessary when addressing problems inherent in understanding pore systems in deeply-buried carbonate (dolomite) reservoirs.

Capillary-pressure of 20,000 PSIA (Hg-air) would correspond to a value between 2000 and 4000 PSIA brine-air. This in turn would occur at depths of 9,200 ft. (2.8 km) or less. Thus, the high-pressure analyses correspond to subsurface conditions in the heart of the economic hydrocarbon zone. See Purcell (1949), Smith (1966), Schowalter (1979) and Kopaska-Merkel and Amthor (1988) for discussion of conversion from gas-water and oil-water systems to Hg-air capillary-pressures.

3. A considerable proportion of porosity in many samples was intruded at pressures greater than 2,000 PSIA (Kopaska-Merkel and Amthor, 1988, Figure 2a, p. 56-60). In sample 5,300 from well 5 (Figure 48 A) virtually all of the intrusion occurred at pressures greater than 2,0000 PSIA. This porosity (3.4%) would remain undetected if investigation is limited to lower pressures (e.g., Jennings, 1987; Wardlaw et al., 1988).

Several implications arise from high-pressure intrusion:

a) When runs are carried up to 15,000 PSIA or more, then apparent skeletal density very closely approximates true skeletal density. This is indicated by the convergence of incremental intrusion towards zero with increasing pressure (decreasing throat size) (see Appendix C).

b) The percentage of the pore volume that is not invaded at maximum pressure is often referred to as irreducible water saturation (S_{wi}) (Jennings, 1987). However, as Wardlaw & Taylor (1976) pointed out the term "irreducible saturation" is inappropriate in this context, because it is dependent on the maximum pressure. The higher the pressure attained during an analysis the more closely the pore space unoccupied by mercury at maximum pressure approximates the true value of minimum unsaturated pore volume (U_{min}) (Wardlaw & Taylor,

approximates the true value of minimum unsaturated pore volume (U_{min}) (Wardlaw & Taylor, 1976).

c) Considerable intrusion at pressures greater than 2,000 PSIA indicates that in many samples microporosity is present which would go unrecognized unless high pressures were used. This may result in underestimation of available porosity.

In summary, it appears that capillary-pressure data generated by mercury porosimetry cannot adequately characterize reservoir rock unless pressures of 2,000 PSIA or more are attained, and that data collected at high pressures are definitely relevant to evaluation of the production potential of reservoir rocks at economically-important subsurface depths (e.g., Kopaska-Merkel and Friedman, 1989).

APPENDIX B

Typical Report Format of Capillary-Pressure Analysis

The complete data printout for a mercury porosimetry analysis consists of six to seven pages (e.g. pages 181 - 186). Explanation for the data headings used in the report are as follows (Micromeritics Instruction Manual Pore Sizer 9305, 1983):

Total Intrusion Volume is the maximum volume of mercury intruded into the pores at the maximum pressure attained.

Total Pore Area is the area of the pores based on the assumption of cylindrical pore geometry, and summed up over the pressure range of mercury intrusion into the pores.

Median Pore (Throat) Diameter (or Radius) is the 50 % (percentile) value obtained from both area and volume distribution curves. Frequently, these values will differ because the smaller pores contribute more to the total pore surface area than larger pores for a given increment of mercury intrusion volume. Therefore, the area distributions will have a tendency to shift to the smaller pore sizes when compared to pore volume distributions.

Average Pore (Throat) Diameter (4V/A) is obtained by assuming that all pores are cylinders. Thus, when the pore volume ($V = \pi d l^2 / 4$) is divided by the pore area ($A = \pi d l$), the pore diameter (d) is equal to 4V/A. Therefore, the volume increment of cylindrical capillaries which includes a distribution of pore sizes will yield a pore diameter value that is the average diameter for this group of capillaries.

Bulk Density is calculated from the sample weight (g) and the sample volume (cc) at the initial mercury filling pressure. Penetrometer volume minus the volume of mercury in the penetrometer with the sample gives the sample volume (cc). The volume of mercury (cc) is obtained from the weight of the mercury (g) divided by the density of mercury. The weight of mercury is the difference between the weight of the penetrometer with sample and filled with mercury and sample.

Apparent (Skeletal) Density is the density of the sample as calculated for the bulk density and adjusted for the pore volume measured at the maximum pressure attained during the run. Therefore, if all the pores of the specimen are filled with with mercury at this maximum pressure, and all the other measurements of volumes and weights are performed accurately, and the density value for mercury used in the calculation is close to its actual value at the ambient temperature of the filling step, the apparent density value obtained in this calculation should come within a few percent of the actual density for the material evaluated.

% Capillary allows the operator to judge the choice of the penetrometer used in making the run. It provides the percentage of the available intrusion volume used in the penetrometer. This number should perferably range between 25% and 90% of a given stem volume (.392 cc in this case). Page one (and perhaps page two) list the actual data points obtained and the subsequent calculation results in seven colums. Page two is printed only if there are more than 45 data points in the table used in making the run.

Column 1 lists the measured pressure points (psia) obtained in the run corresponding to the table of pressure points selected for this analysis.

Column 2 lists the corrected pressure points, i.e. the mercury head correction has been made (plus 4.45 psia in the high pressure run).

Column 3 lists the pore (throat) diameters (μm), or radii if requested, corresponding to the pressure values in column 2. The surface tension (γ) and the contact angle (θ), listed in the first table on the summary page are used to calculate these pore sizes by the Washburn equation:

$$d = \frac{4\gamma\cos\theta}{p} \quad \text{or} \quad r = \frac{-2\gamma\cos\theta}{p}$$

Column 4 lists the actual cumulative volume of mercury intruded into the sample at the given pressure points in column 2, and is normalized to unit mass basis (cc/g) by dividing each penetration increment (cc) by the sample weight (g). The summary page gives the total pore volume.

Column 5 lists the actual cumulative pore surface area (m^2/g) for the corresponding pressure points. Surface area is calculated from the summation of the incremental pore

surface area based on the mean diameter (D) and the volume increment (Δ V) between the two points, assuming cylindrical geometry for the pores. The data are found using the formula

$$A = \int_{1}^{max.} (4\Delta V / D)$$

The summary page gives the total pore surface area.

Column 6 lists the mean pore diameters, or radii if requested. Mean diameter is the half-way value between two consecutive points ((D + D) / 2 = D). These values are used in conjunction with the incremental distribution function (DV) in the last column.

Column 7 is the last column and lists the incremental distribution function (DV) related to either the diameter or the radius of the pores as requested. This function gives the pore size distribution which is plotted. Similar calculations performed for surface area (DA) are also plotted (the tabulation of DA values is not shown).

The last four pages (either from three through six or four through seven) are reserved for plots. In order to use the full width of the page for these plots, the ordinate (y-axis) scale is normalized to 100%, which equals the maximum value of the plotted function. This normalization factor is printed on the y-axis of the plot for reference.

First Plot, Page 3 or 4: Cumulative pore volume (cc/g) vs. pore diameter, or radius (μm). Here 100% = total pore volume intruded at the maximum pressure reached during the analysis.

Second Plot, Page 4 or 5: Cumulative pore surface area (m /g) vs. pore diameter, or radius (μm). From the rise of these curves above the baseline, one can estimate into which pore size range the pore volume or pore area fall. Here, 100% = total pore surface area.

Third & Fourth Plots, Pages 5 & 6 or 6 & 7: The incremental pore size distribution curves are plotted for pore volume and pore area, respectively. For the incremental pore volume plot, 100% = the largest increment in the tabulation of incremental pore volume (DV), and, for the incremental pore surface area plot, 100% = the largest increment of the pore surface area (DA).

PR#1
150N
MICROMERITICS PORE-SIZER 9305
V1.00 PAGE 1

RV 21249 10-10-87
JA 10:23
PENETROMETER NUMBER 104

PRESSURE PSIA	CORRECTED PRESSURE PSIA	PORE RADIUS um	CUM. INTR. VOLUME cc/g	CUM. PORE SURFACE AREA m2/g	MEAN RADIUS um	INCR. INTR. VOLUME cc/g
2.1	2.1	51.2954	0.0010	0.0000	66.7505	0.0010
3.1	3.1	34.6421	0.0024	0.0001	42.9688	0.0013
4.1	4.1	26.2154	0.0040	0.0002	30.4288	0.0016
5.1	5.1	21.0862	0.0057	0.0003	23.6508	0.0017
6.2	6.2	17.3825	0.0067	0.0004	19.2344	0.0010
7.3	7.3	14.7632	0.0077	0.0006	16.0729	0.0010
8.4	8.4	12.8300	0.0088	0.0007	13.7966	0.0011
9.4	9.4	11.4651	0.0096	0.0009	12.1475	0.0009
10.4	10.4	10.3627	0.0101	0.0009	10.9139	0.0004
12.4	12.4	8.6913	0.0113	0.0012	9.5270	0.0012
15.8	15.8	6.8210	0.0129	0.0016	7.7561	0.0017
19.6	19.6	5.4986	0.0142	0.0020	6.1598	0.0012
22.8	22.8	4.7268	0.0152	0.0025	5.1127	0.0011
32.0	36.1	2.9835	0.0152	0.0025	3.8551	0.0000
55.0	59.1	1.8238	0.0161	0.0032	2.4036	0.0008
100.1	104.1	1.0349	0.0179	0.0058	1.4293	0.0019
154.0	158.0	0.6821	0.0195	0.0095	0.8585	0.0016
245.0	249.0	0.4329	0.0206	0.0132	0.5575	0.0010
440.0	444.0	0.2428	0.0218	0.0203	0.3378	0.0012
760.0	763.9	0.1411	0.0229	0.0316	0.1919	0.0011
1100.0	1103.9	0.0976	0.0236	0.0440	0.1194	0.0007
2000.0	2003.9	0.0538	0.0244	0.0637	0.0757	0.0007
3000.0	3003.9	0.0359	0.0247	0.0787	0.0448	0.0003
4000.0	4003.9	0.0269	0.0248	0.0858	0.0314	0.0001
6000.0	6003.9	0.0180	0.0250	0.1024	0.0224	0.0002
8000.0	8003.9	0.0135	0.0251	0.1166	0.0157	0.0001
10000.0	10003.9	0.0108	0.0252	0.1351	0.0121	0.0001
15000.0	15003.9	0.0072	0.0255	0.2015	0.0090	0.0003
10000.0	10003.9	0.0108	0.0255	0.2015	0.0090	0.0000
8000.0	8003.9	0.0135	0.0255	0.2015	0.0121	0.0000
6000.0	6003.9	0.0180	0.0255	0.2015	0.0157	0.0000
4000.0	4003.9	0.0269	0.0255	0.2015	0.0224	0.0000
2000.0	2003.9	0.0538	0.0255	0.2015	0.0403	0.0000
500.0	503.9	0.2139	0.0254	0.1993	0.1338	-.0001
170.0	173.9	0.6198	0.0249	0.1971	0.4168	-.0004
60.0	63.9	1.6864	0.0239	0.1953	1.1531	-.0010
15.0	18.9	5.6921	0.0226	0.1946	3.6893	-.0013

MICROMERITICS PORE-SIZER 9305
V1.00 PAGE 2

RV 21249 10-10-87
JA 10:23
PENETROMETER NUMBER 104

SAMPLE WEIGHT =	5.8060 g	PEN CONSTANT =	21.6300 ul/pF
PEN WEIGHT =	68.8520 g	THETA =	140.0000 DEGREES
PEN+SAM WEIGHT =	74.6580 g	GAMMA =	485.0000 dyn/cm
PEN+SAM+Hg WEIGHT =	135.4000 g	FILL PRESSURE =	1.3 PSIA
PEN VOLUME =	6.7190 cc	Hg DENSITY =	13.5438 g/cc
STEM VOLUME =	1.1310 cc	HEAD CORR. FACTOR =	4.4500

INTRUSION (PRESSURIZATION) DATA SUMMARY

TOTAL INTRUSION VOLUME =	0.0255 cc/g
TOTAL PORE AREA =	0.2015 m2/g
MEDIAN PORE RADIUS (VOLUME) =	7.0135 um
MEDIAN PORE RADIUS (AREA) =	0.0189 um
AVERAGE PORE RADIUS (4V/A) =	0.2532 um
BULK DENSITY =	2.5988 g/cc
APPARENT (SKELETAL) DENSITY =	2.7833 g/cc
% CAPILLARY =	13.0957

MICROMERITICS PORE-SIZER 9305
V1.00 PAGE 3
RV 21249 10-10-87
JA 10:23
PENETROMETER NUMBER 104

CUMULATIVE PORE VOLUME PER GRAM % vs. PORE RADIUS (microns)
Maximum Intrusion = 0.0255 cc/g

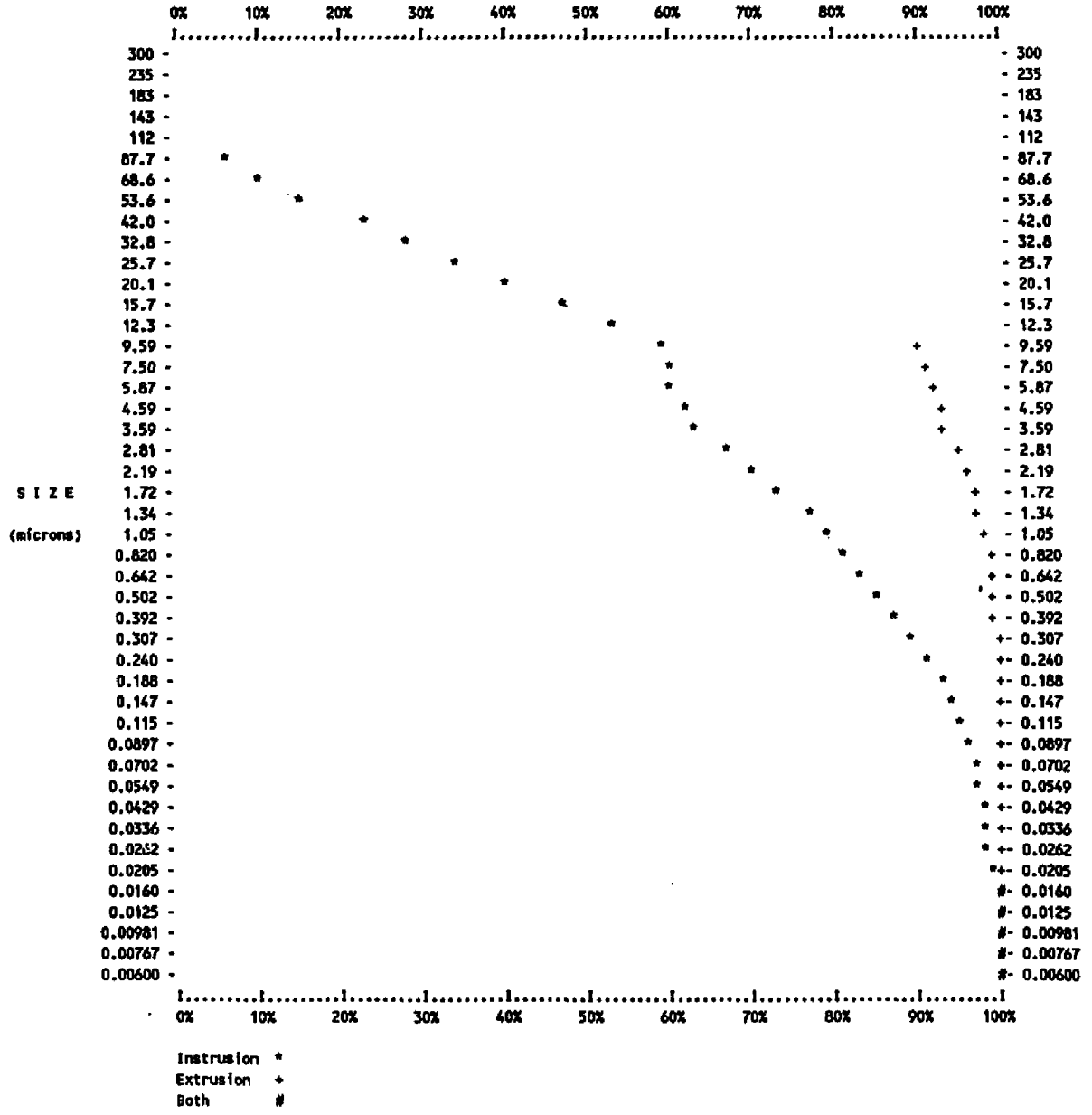

MICROMERITICS PORE-SIZER 9305
V1.00

RV 21249
JA
PENETROMETER NUMBER 104

PAGE 4
10-10-87
10:23

CUMULATIVE SURFACE AREA PER GRAM % vs. PORE RADIUS (microns)
Maximum Pore Surface = 0.2015 m2/g

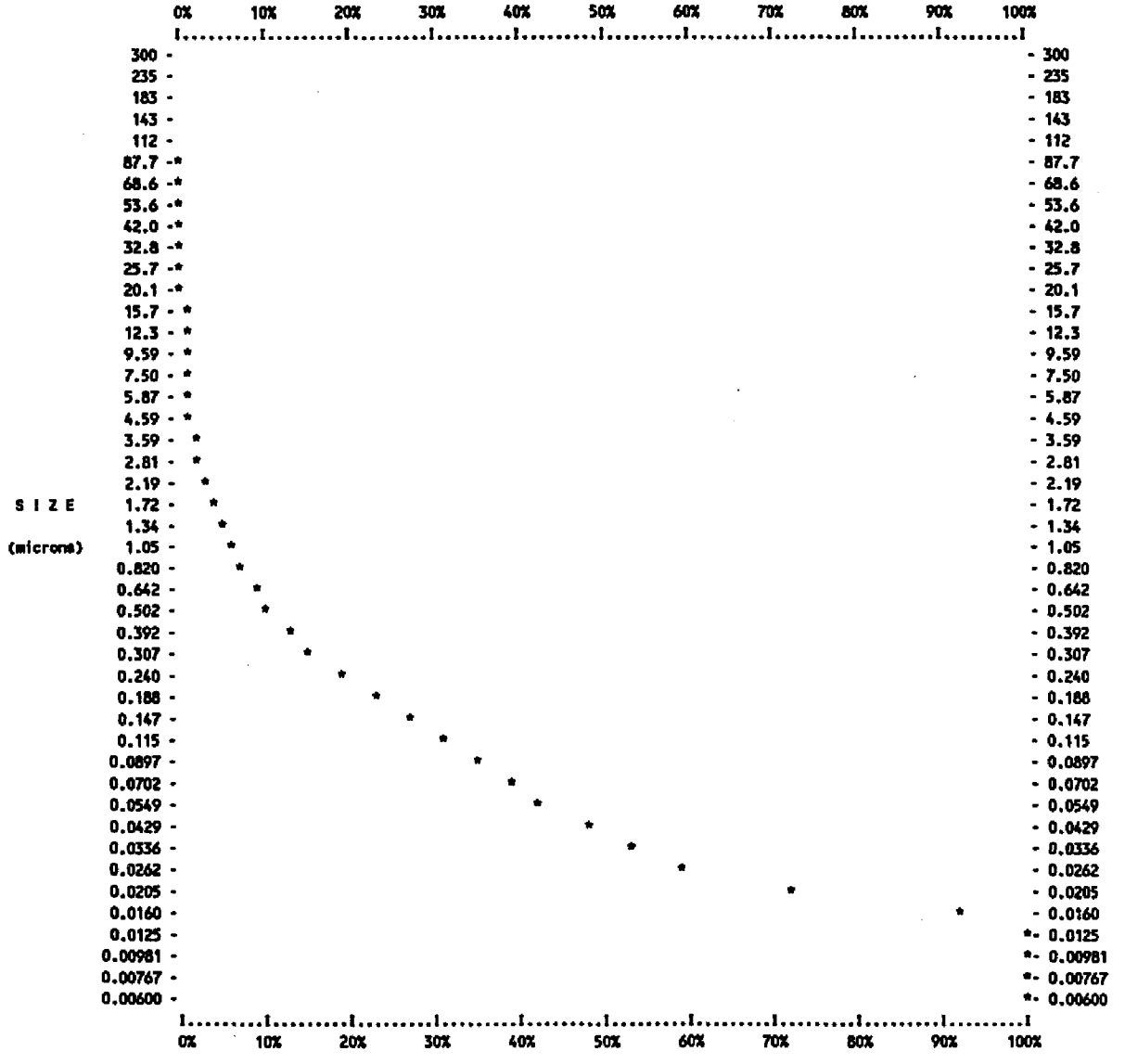

MICROMERITICS PORE-SIZER 9305
V1.00 PAGE 5
RV 21249 10-10-87
JA 10:23
PENETROMETER NUMBER 104

INCREMENTAL VOLUME PER GRAM % vs. PORE RADIUS (microns)
Maximum Incremental Volume = 0.0019 cc/g

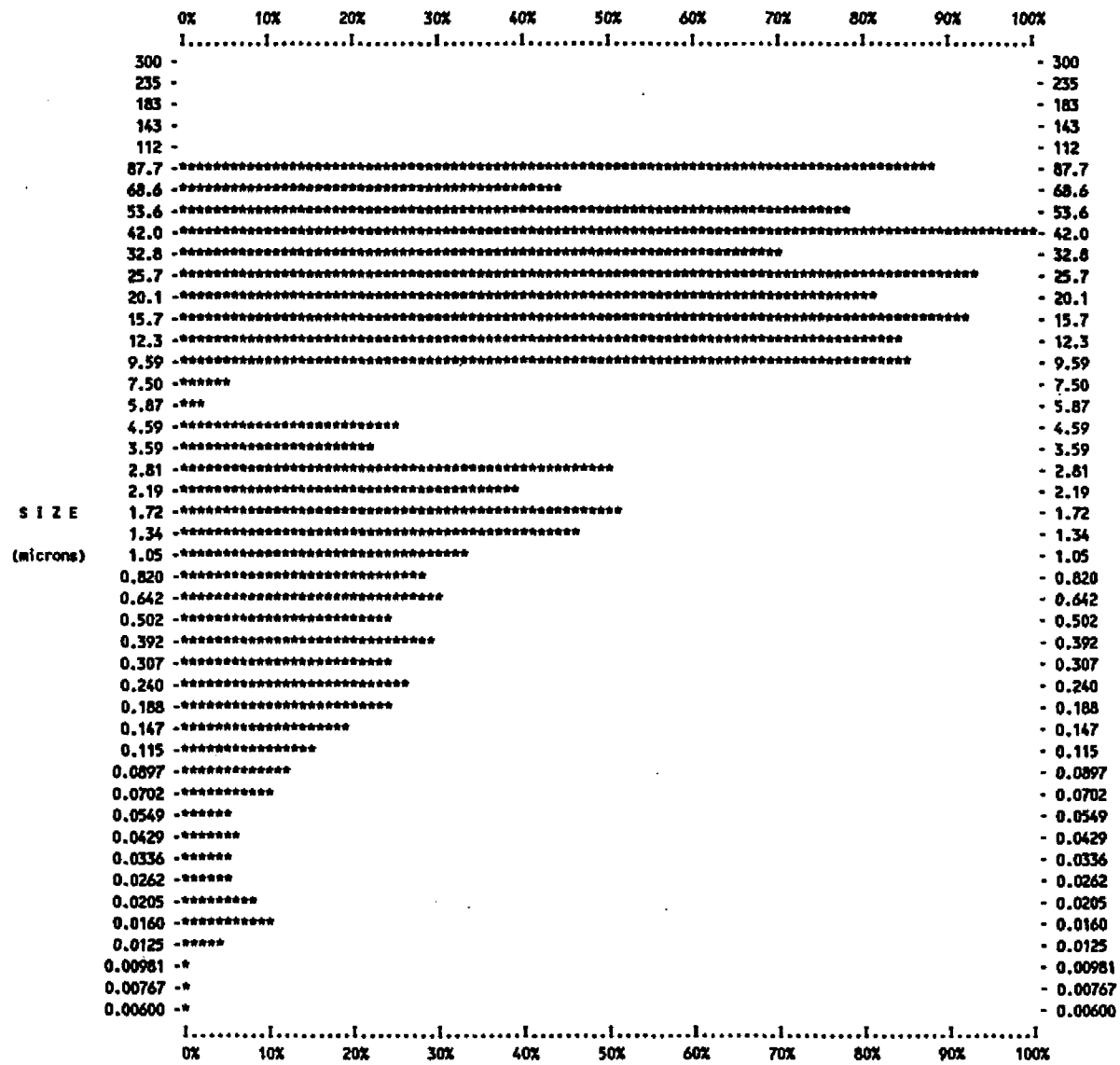

MICROMERITICS PORE-SIZER 9305
V1.00 PAGE 6
RV 21249 10-10-87
JA 10:23
PENETROMETER NUMBER 104

INCREMENTAL SURFACE AREA PER GRAM vs. PORE RADIUS (microns)
Maximum Incremental Surface Area = 0.0414 m2/g

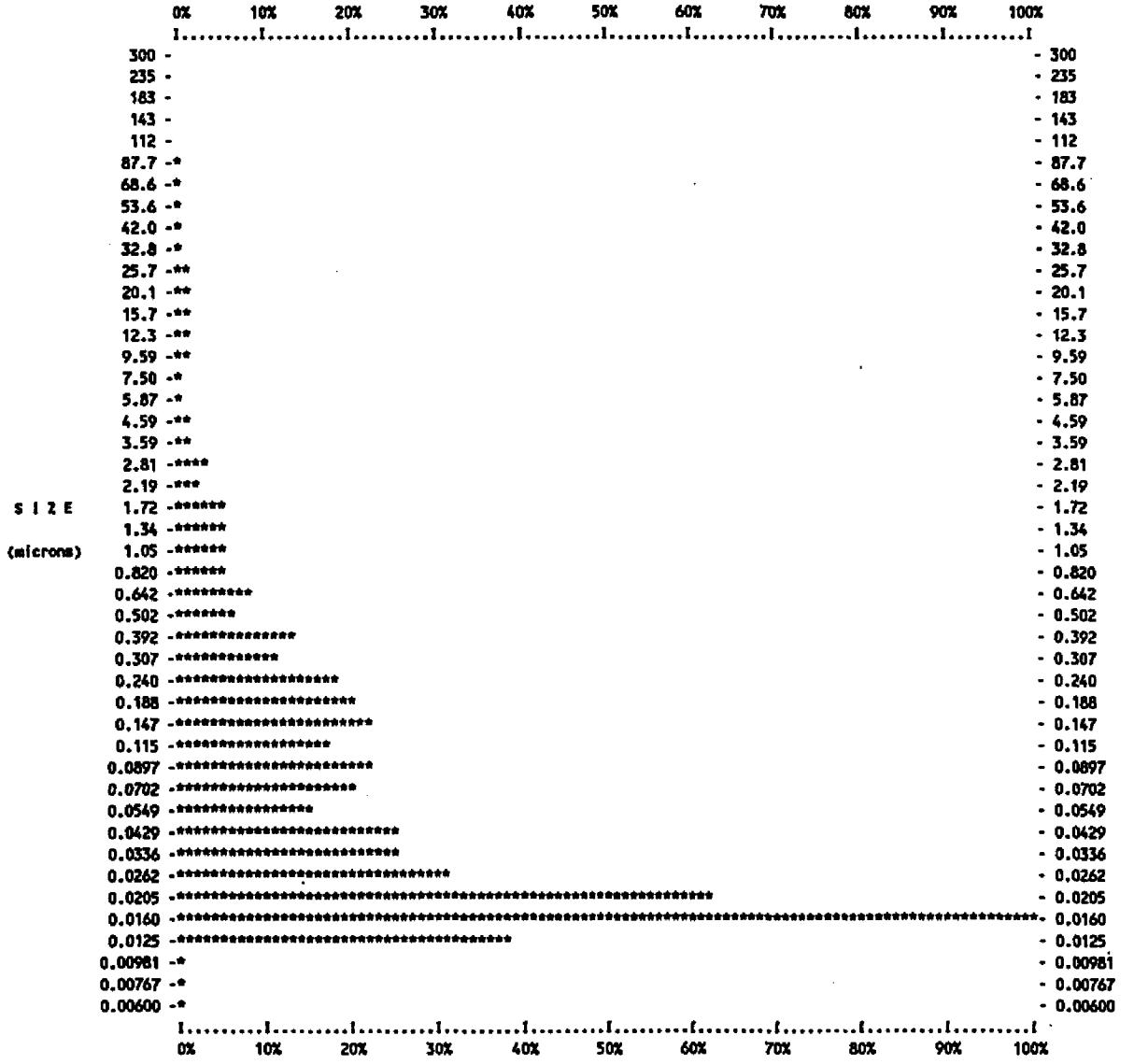

APPENDIX C

Capillary-Pressure Data of Ellenburger Group Dolostones

Well No.	Sample (ft)	AØ (%)	MTS (µm)	TS20% (µm)	NTS	RE (%)	IncSA (m^2/g)	SA (m^2/g)	Curve Type	Litho-Facies	LogØ (%)	K (md)
1	12061	1.1	.08	4.8	5.5	38.5	.24	.07	1	1	1.8	<1
1	12062	.6	.05	6.2	3.3	42.9	.14	.03	1	1	1.3	<1
1	12070	.8	.04	.1	.8	33.3	.16	.03	1	1	1.8	<1
1	12081	.7	.03	4.8	3.0	60.0	.22	.05	1	1	.8	<1
1	12089	3.9	1.1	9.0	10.8	8.3	.18	.02	2	6	.8	<1
1	12092	2.4	.1	.1	1.5	37.5	.50	.06	1	6	2.3	<1
1	12098	1.1	.1	14.5	5.9	36.6	.25	.08	1	6	2.3	<1
1	12103	1.5	.7	3.8	10.1	11.3	.11	.03	2	6	.3	<1
1	12106	2.6	.6	12.9	5.9	12.0	.13	.02	2	6	3.8	<1
1	12109	2.7	7.5	34.3	77.4	9.0	.15	.03	3	6	6.4	<1
1	12111	5.0	8.1	16.5	47.4	12.3	.37	.10	3	6	6.4	250
1	12111	3.8	4.7	22.5	136.0	19.0	.34	.11	3	6	6.4	220
1	12119	6.0	18.3	39.4	18.3	12.0	.27	.07	3	6	6.4	1670
1	12121	.8	.1	.3	1.0	3.3	.09	.02	1	6	5.4	<1
1	12123	1.6	5.2	16.4	50.4	11.1	.07	.01	2	6	5.4	<1
1	12127	1.9	.5	9.0	10.2	11.4	.18	.06	2	6	1.3	<1
1	12132	1.3	.02	.04	1.0	37.5	.60	.19	1	6	3.8	<1
1	12137	1.4	.07	.8	3.3	38.5	.28	.08	1	6	3.3	<1
1	12142	1.9	.06	10.1	3.0	23.2	.36	.06	1	6	2.8	<1
1	12147	2.5	4.5	12.9	21.2	19.4	.28	.10	2	6	.8	<1
1	12148	6.2	5.8	21.0	9.3	8.8	.14	.02	3	6	5.4	107
1	12150	5.9	18.9	43.1	45.7	4.9	.36	.13	3	6	4.9	2277
1	12150	5.7	10.6	27.3	40.6	9.3	.46	.20	3	6	4.9	466
1	12151	4.2	39.2	45.0	119.0	3.3	.14	.03	3	6	5.4	11226
1	12153	1.7	.2	3.4	3.7	8.0	.16	.04	2	6	-	<1
1	12154	3.8	6.4	27.5	24.2	6.3	.16	.04	3	6	-	115
1	12155	6.5	16.1	43.8	3.7	6.8	.20	.05	3	6	-	1367
1	12159	2.7	.02	.1	1.4	58.2	1.21	.40	1	6	-	<1
2	21145	.5	.03	.6	1.8	12.5	.13	.02	1	2	-	<1
2	21150	1.0	.02	.06	1.7	24.3	.32	.11	1	2	-	<1
2	21153	1.1	.03	.05	1.1	34.1	.28	.06	1	2	-	<1
2	21161	1.4	.00	.20	1.8	30.6	.35	.07	1	2	-	<1
2	21162	.9	.09	.20	2.0	12.1	.10	.02	1	2	-	<1
2	21167	.9	.01	.90	2.2	24.2	.43	.18	1	3	-	<1
2	21173	.5	.32	7.9	15.0	10.5	.09	.02	2	3	-	<1
2	21176	.4	.16	16.4	3.7	18.8	.04	.01	2	3	-	<1
2	21180	.7	.09	3.0	4.0	16.7	.11	.02	1	3	-	<1
2	21181	1.3	.13	.5	10.1	26.1	.14	.02	1	3	-	<1
2	21183	2.0	.16	.4	3.9	26.8	.23	.05	1	3	-	<1
2	21183	1.3	.01	1.8	2.6	24.5	.26	.08	2	3	-	<1

Well No.	Sample (ft)	AØ (%)	MTS (µm)	TS20% (µm)	NTS	RE (%)	IncSA (m^2/g)	SA (m^2/g)	Curve Type	Litho-Facies	LogØ (%)	K (md)
2	21183	.7	.05	.15	1.7	.0	.11	.02	1	3	-	<1
2	21184	.7	.06	1.1	1.9	8.3	.11	.02	1	3	-	<1
2	21184	1.6	.0	.33	1.8	24.1	.19	.02	1	3	-	<1
2	21185	2.0	.20	1.2	3.8	23.3	.21	.04	2	3	-	<1
2	21185	.8	.07	2.3	3.7	16.7	.16	.03	2	3	-	<1
2	21191	1.0	.08	4.3	3.6	24.3	.18	.03	1	3	-	<1
2	21193	.8	.01	.02	.75	36.7	.41	.15	1	3	-	<1
2	21199	.4	.04	.3	2.5	6.3	.08	.02	1	4	-	<1
2	21201	.6	.72	18.0	87.6	19.0	.20	.10	2	2	-	<1
2	21204	.4	.01	.01	.38	13.3	.29	.18	1	2	-	<1
2	21205	2.0	.08	.15	1.8	34.2	.35	.08	1	2	-	<1
2	21207	.6	.03	2.3	3.1	27.3	.23	.09	1	2	-	<1
2	21211	.2	.09	12.0	3.6	.0	.03	.01	1	2	-	<1
2	21215	.3	.05	33.0	4.5	.0	.06	.04	2	2	-	<1
2	21219	3.5	.60	3.7	9.8	11.7	.28	.05	2	2	-	<1
2	21219	4.3	.59	3.8	14.8	11.9	.44	.10	2	2	-	<1
2	21220	1.4	.06	.24	2.5	.0	.26	.06	1	2	-	<1
2	21221	1.2	.08	.18	1.5	13.6	.14	.03	1	2	-	<1
2	21223	2.7	.31	1.5	5.6	14.3	.22	.03	2	2	-	<1
2	21225	.6	.04	4.3	4.0	4.8	.16	.04	1	2	-	<1
2	21227	2.0	.12	1.8	4.2	23.3	.32	.07	2	4	-	<1
2	21229	4.1	.51	3.8	4.9	13.2	.28	.57	2	4	-	<1
2	21231	1.6	.09	.34	1.8	8.9	.19	.03	1	3	-	<1
2	21232	4.1	.33	.75	3.1	26.8	.29	.06	2	3	-	<1
2	21233	2.6	1.27	6.5	11.2	9.4	.14	.03	2	3	-	2
2	21234	3.6	.29	3.5	3.8	13.3	.30	.05	2	3	-	<1
2	21235	2.2	.09	.40	1.3	12.7	.21	.04	1	3	-	<1
2	21236	2.4	.30	12.9	8.3	10.1	.22	.06	2	3	-	<1
2	21236	4.7	4.0	16.4	25.5	9.1	.22	.04	2	3	-	36
2	21237	.4	.08	7.9	2.6	13.3	.06	.02	2	3	-	<1
2	21243	1.0	.32	13.0	5.0	16.7	.09	.02	2	3	-	<1
2	21244	.4	.04	.15	1.4	15.4	.07	.01	1	3	-	<1
2	21249	7.2	1.03	4.8	4.8	16.1	.36	.07	2	4	-	1
2	21249	6.6	7.01	23.5	15.3	11.4	.20	.04	3	4	-	156
2	21250	11.9	5.0	14.0	4.0	12.0	.12	.03	3	4	-	61
2	21250	7.8	6.3	17.5	6.6	13.4	.13	.04	3	4	-	107
2	21250	10.5	6.9	18.0	7.1	13.4	.11	.01	3	4	-	177
2	21252	2.6	1.3	6.0	14.0	8.6	.14	.04	2	3	-	2
2	21254	4.7	.44	1.1	3.3	30.5	.21	.02	2	3	-	<1
2	21254	.4	.04	4.25	5.7	.0	.11	.07	1	3	-	<1
2	21258	3.4	.40	1.55	4.2	20.3	.21	.02	2	3	-	<1
2	21259	8.9	1.85	10.0	3.8	18.6	.26	.06	3	3	-	200
2	21259	10.6	10.2	22.0	4.8	8.5	.25	.09	3	3	-	365
2	21260	3.3	.8	8.5	9.3	9.9	.21	.06	2	3	-	<1
2	21260	4.1	.35	1.1	3.2	8.6	.24	.09	2	3	-	<1
2	21261	.8	.1	.7	1.5	14.3	.12	.02	1	1	-	<1
2	21262	.6	.1	8.0	3.7	9.1	.09	.03	4	1	-	<1
2	21264	.6	.06	.25	2.5	5.0	.11	.02	1	1	-	<1

Well No.	Sample (ft)	AØ (%)	MTS (µm)	TS20% (µm)	NTS	RE (%)	IncSA (m^2/g)	SA (m^2/g)	Curve Type	Litho-Facies	LogØ (%)	K (md)
2	21267	.3	.43	7.0	25.0	9.1	.09	.06	2	3	-	<1
2	21271	1.0	.1	8.0	3.4	5.4	.14	.03	4	3	-	<1
2	21272	4.3	4.87	12.0	18.4	8.2	.17	.02	3	3	-	58
2	21272	2.5	.35	9.0	7.5	7.5	.27	.05	2	3	-	<1
2	21273	2.8	.34	6.5	6.7	15.4	.26	.07	2	3	-	<1
2	21274	5.4	1.11	14.5	6.2	6.4	.18	.02	2	3	-	<1
2	21274	2.7	.15	.75	1.7	6.9	.18	.04	1	3	-	<1
2	21276	.4	.04	6.5	2.3	6.7	.09	.02	1	3	-	<1
2	21277	1.0	.02	.04	1.5	41.7	.45	.15	1	3	-	<1
2	21278	1.2	.02	1.75	3.0	34.1	.46	.14	1	3	-	<1
2	21278	.9	.03	.18	1.9	41.2	.36	.17	1	3	-	<1
2	21279	4.3	.01	.03	1.0	60.4	2.56	.76	1	3	-	<1
2	21280	1.9	.01	.23	1.3	52.2	.91	.50	1	3	-	<1
3	22617	1.2	.20	4.8	5.8	38.6	.15	.03	2	1	-	<1
3	22635	1.4	.15	31.5	10.0	10.0	.27	.06	1	1	-	<1
3	22700	.7	.07	.11	2.7	8.3	.13	.05	1	4	-	<1
3	22716	.5	.02	45.0	1.3	21.1	.17	.08	1	2	-	<1
3	22805	.6	4.85	42.5	400.0	10.0	.09	.27	1	1	-	<1
3	22807	3.7	1.71	13.5	11.4	22.8	.26	.08	2	4	-	<1
4	13431	.3	7.12	9.5	3.8	.0	.01	.01	4	1	-	<1
4	13488	1.2	.05	4.4	6.2	4.8	.39	.14	4	6	-	<1
4	14532	1.4	.22	3.4	6.8	14.3	.20	.06	4	6	-	<1
4	14590	2.2	.40	4.8	3.9	11.5	.17	.04	2	1	-	<1
4	14594	.7	.10	1.4	3.7	11.1	.12	.03	2	1	-	<1
4	14595	.4	.09	5.5	3.1	.0	.08	.04	1	1	-	<1
4	14600	.7	.04	12.5	44.4	39.1	.23	.12	4	1	-	<1
4	14598	1.6	.65	3.0	6.5	13.3	.16	.06	2	1	-	<1
5	5123	6.1	.16	.29	2.6	26.4	.75	.16	1	6	-	<1
5	5134	5.4	.08	.41	2.4	24.9	.92	.11	1	6	-	<1
5	5225	4.7	.08	.23	2.4	51.1	.91	.14	1	6	-	<1
5	5300	3.4	.01	.02	.8	34.6	3.40	.92	1	6	-	<1
5	5104	5.9	.10	.95	3.7	23.2	.93	.20	2	6	-	<1

AØ = Effective Porosity

MTS = Median Pore-Throat Size

TS20% = Pore-Throat Size at 20% Mercury Saturation

NTS = Normalized Pore-Throat Size

RE = Minimum Recovery Efficiency

IncSA = Incremental Surface Area

SA = Cumulative Surface Area

LogØ = Log-Porosity

K = Permeability

APPENDIX D

Electron-Microprobe Data of Ellenburger Dolomite-Rock Textures

Minimum, maximum, mean, and standard deviation values of major and minor elements are shown for the seven dolomite-rock textures. Analyses of dolomite-rock texture 1 (unimodal, very fine- to fine-crystalline planar-s mosaic dolomite) are listed for different lithofacies, analyses of dolomite-rock texture 2 (unimodal, coarse- to very coarse-crystalline planar-s mosaic dolomite), and dolomite-rock texture 3 (coarse- to very coarse-crystalline planar-s dolomite) are subdivided into dolomite cements and replacement dolomites.

1) Dolomite-rock texture 1 (unimodal, very fine to fine-crystalline planar-s mosaic dolomite).

1 A) Lithofacies 1, 3 and 6:

	N	Min.	Max.	Mean	Std.Dev.
Fe (ppm)	49	0	4996	858	1057
Mn (ppm)	49	0	1121	186	233
Sr (ppm)	49	0	397	85	118
Mg (ppm)	49	114098	130795	123266	5412
$CaCO_3$ (mole %)	49	50.1	55.3	52.2	1.6
$MgCO_3$ (mole %)	49	44.3	49.7	47.4	1.7
$FeCO_3$ (mole %)	49	0	.8	.1	.2
$MnCO_3$ (mole %)	49	0	.2	.0	.04
$SrCO_3$ (mole %)	49	0	.0	.0	.01

1 B) Lithofacies 6 (karst facies):

	N	Min.	Max.	Mean	Std.Dev.
Fe (ppm)	21	157	4996	1597	1260
Mn (ppm)	21	0	1121	325	291
Sr (ppm)	21	0	397	186	117
Mg (ppm)	21	114098	128416	118110	3631
$CaCO_3$ (mole %)	21	50.4	55.3	53.6	1.2
$MgCO_3$ (mole %)	21	44.3	49.3	45.8	1.3
$FeCO_3$ (mole %)	21	0	.8	.3	.2
$MnCO_3$ (mole %)	21	0	.2	.1	.1
$SrCO_3$ (mole %)	21	0	.0	.0	.01

1 C) Lithofacies 1 and 3:

	N	Min.	Max.	Mean	Std.Dev.
Fe (ppm)	28	0	953	303	215
Mn (ppm)	28	0	249	82	79
Sr (ppm)	28	0	105	10	27
Mg (ppm)	28	120041	130795	127133	2543
$CaCO_3$ (mole %)	28	50.1	55.1	51.1	.9
$MgCO_3$ (mole %)	28	46.7	49.7	48.6	.8
$FeCO_3$ (mole %)	28	0	.2	1	.04
$MnCO_3$ (mole %)	28	0	.0	.0	.01
$SrCO_3$ (mole %)	28	0	.0	.0	.00

2) Dolomite-rock texture 2 (unimodal, medium- to coarse-crystalline planar-s mosaic dolomite).

2 A) Dolomite cement and replacive dolomite:

	N	Min.	Max.	Mean	Std.Dev.
Fe (ppm)	48	14	8362	1101	1843
Mn (ppm)	48	0	671	227	174
Sr (ppm)	48	0	199	13	39
Mg (ppm)	48	116316	134387	126634	3382
$CaCO_3$ (mole %)	48	49.5	52.7	50.9	.7
$MgCO_3$ (mole %)	48	45.1	50.1	48.2	1.0
$FeCO_3$ (mole %)	48	0	1.4	.2	.3
$MnCO_3$ (mole %)	48	0	.1	.0	.03
$SrCO_3$ (mole %)	48	0	.0	.0	.01

2 B) Dolomite cement:

	N	Min.	Max.	Mean	Std.Dev.
Fe (ppm)	20	14	8362	1769	2560
Mn (ppm)	20	30	656	180	142
Sr (ppm)	20	0	24	1	5
Mg (ppm)	20	116316	131225	125287	3806
$CaCO_3$ (mole %)	20	49.7	52.7	51.1	.7
$MgCO_3$ (mole %)	20	45.1	49.7	48.3	1.1
$FeCO_3$ (mole %)	20	0	1.4	.3	.4
$MnCO_3$ (mole %)	20	0	.1	.0	.02
$SrCO_3$ (mole %)	20	0	.0	.0	.00

2 C) Replacive dolomite:

	N	Min.	Max.	Mean	Std.Dev.
Fe (ppm)	28	22	3801	623	769
Mn (ppm)	28	0	671	261	186
Sr (ppm)	28	0	199	21	49
Mg (ppm)	28	122395	134387	127597	2652
$CaCO_3$ (mole %)	28	49.5	52.1	50.7	.7
$MgCO_3$ (mole %)	28	46.1	50.1	48.4	.9
$FeCO_3$ (mole %)	28	0	.6	.1	.1
$MnCO_3$ (mole %)	28	0	.1	.0	.03
$SrCO_3$ (mole %)	28	0	.0	.0	.01

3) Dolomite-rock texture 3 (coarse- to very coarse-crystalline planar-s dolomite).

3 A) Dolomite cement and replacive dolomite:

	N	Min	Max.	Mean	Std.Dev.
Fe (ppm)	188	0	14466	1153	1976
Mn (ppm)	188	0	1275	216	213
Sr (ppm)	188	0	645	58	84
Mg (ppm)	188	109104	136343	127332	3677
$CaCO_3$ (mole %)	189	44.3	54.2	51.0	1.1
$MgCO_3$ (mole %)	189	41.1	50.7	48.5	1.2
$FeCO_3$ (mole %)	189	0	2.4	.2	.3
$MnCO_3$ (mole %)	189	0	.8	.0	.1
$SrCO_3$ (mole %)	189	0	.1	.0	.01

3 B) Dolomite cement:

	N	Min.	Max.	Mean	Std.Dev.
Fe (ppm)	119	0	14466	168	2309
Mn (ppm)	119	0	1275	244	239
Sr (ppm)	119	0	645	54	85
Mg (ppm)	119	109104	136343	126861	3642
$CaCO_3$ (mole %)	120	44.3	54.1	51.1	1.1
$MgCO_3$ (mole %)	120	41.1	50.3	48.3	1.2
$FeCO_3$ (mole %)	120	0	2.4	.3	.4
$MnCO_3$ (mole %)	120	0	.8	.0	.1
$SrCO_3$ (mole %)	120	0	.1	.0	.01

3 C) Replacive dolomite:

	N	Min.	Max.	Mean	Std.Dev.
Fe (ppm)	69	0	1984	246	377
Mn (ppm)	69	0	637	168	148
Sr (ppm)	69	0	346	64	83
Mg (ppm)	69	113705	136262	128143	3596
$CaCO_3$ (mole %)	69	49.2	54.2	51.0	1.0
$MgCO_3$ (mole %)	69	45.6	50.7	48.8	1.1
$FeCO_3$ (mole %)	69	.0	.3	.0	.1
$MnCO_3$ (mole %)	69	.0	.3	.0	.04
$SrCO_3$ (mole %)	69	.0	.0	.0	.01

4) Dolomite-rock texture 4 (medium- to coarse-crystalline planar-e mosaic dolomite).

	N	Min.	Max.	Mean	Std.Dev.
Fe (ppm)	132	0	117974	8719	21550
Mn (ppm)	132	0	5784	596	993
Sr (ppm)	132	0	770	88	140
Mg (ppm)	132	61214	135522	118249	13238
$CaCO_3$ (mole %)	132	48.9	55.8	52.3	1.8
$MgCO_3$ (mole %)	132	25.4	50.8	45.7	4.4
$FeCO_3$ (mole %)	132	0	21.3	1.6	3.9
$MnCO_3$ (mole %)	132	0	1.0	.1	.2
$SrCO_3$ (mole %)	132	0	2.0	.0	.2

5) Dolomite-rock texture 5 (medium- to coarse-crystalline planar-e dolomite).

	N	Min.	Max.	Mean	Std.Dev.
Fe (ppm)	137	0	17801	2387	3239
Mn (ppm)	137	0	2646	308	428
Sr (ppm)	137	0	429	33	69
Mg (ppm)	137	111763	133399	126254	3735
$CaCO_3$ (mole %)	137	48.9	52.9	50.9	.8
$MgCO_3$ (mole %)	137	43.2	50.6	48.3	1.3
$FeCO_3$ (mole %)	137	0	3.1	.4	.5
$MnCO_3$ (mole %)	137	0	.5	.1	.1
$SrCO_3$ (mole %)	137	0	.1	.0	.0

6) Dolomite-rock texture 6 (coarse- to very coarse-crystalline nonplanar-a dolomite).

	N	Min.	Max.	Mean	Std.Dev.
Fe (ppm)	13	0	1217	241	365
Mn (ppm)	13	0	379	119	112
Sr (ppm)	13	0	168	67	55
Mg (ppm)	13	129022	134929	132051	1566
$CaCO_3$ (mole %)	13	48.3	50.6	49.5	.7
$MgCO_3$ (mole %)	13	49.4	51.3	50.4	.6
$FeCO_3$ (mole %)	13	0	.2	.0	.1
$MnCO_3$ (mole %)	13	0	.1	.0	.02
$SrCO_3$ (mole %)	13	0	.0	.0	.01

7) Dolomite-rock texture 7 (coarse- to very coarse-crystalline nonplanar-c dolomite).

	N	Min.	Max.	Mean	Std.Dev.
Fe (ppm)	29	3949	11913	6635	2272
Mn (ppm)	29	30	825	261	192
Sr (ppm)	29	0	125	10	30
Mg (ppm)	29	113780	124644	118348	2744
$CaCO_3$ (mole %)	29	51.1	54.5	52.6	.9
$MgCO_3$ (mole %)	29	43.8	48.0	45.7	1.1
$FeCO_3$ (mole %)	29	0	2.0	1.1	.5
$MnCO_3$ (mole %)	29	0	.1	.0	.03
$SrCO_3$ (mole %)	29	0	.0	.0	.0

8) Dolomite cements (total).

	N	Min.	Max.	Mean	Std.Dev.
Fe (ppm)	391	0	117974	4843	13087
Mn (ppm)	391	0	5784	396	660
Sr (ppm)	391	0	770	50	102
Mg (ppm)	391	61214	136343	123378	9146
$CaCO_3$ (mole %)	392	44.3	55.8	51.4	1.6
$MgCO_3$ (mole %)	392	25.4	50.8	47.3	3.0
$FeCO_3$ (mole %)	392	0	21.3	.8	2.4
$MnCO_3$ (mole %)	392	0	1.0	.1	.1
$SrCO_3$ (mole %)	392	0	2.0	.0	.1

9) Replacive dolomite (total).

	N	Min.	Max.	Mean	Std.Dev.
Fe (ppm)	205	0	4996	448	699
Mn (ppm)	205	0	1121	173	177
Sr (ppm)	205	0	397	66	91
Mg (ppm)	205	105795	136262	126197	5061
$CaCO_3$ (mole %)	205	48.3	55.5	51.3	1.5
$MgCO_3$ (mole %)	205	44.0	51.3	48.2	1.6
$FeCO_3$ (mole %)	205	0	.8	.1	.1
$MnCO_3$ (mole %)	205	0	.3	.0	.04
$SrCO_3$ (mole %)	205	0	.0	0	.01

APPENDIX E

Electron Microprobe Data for Ellenburger Group Dolomites

Listed are 597 electron microprobe analyses. For experimental conditions see descriptions in section on materials and methods. Sample numbers correspond to log depths in feet, from which thin sections were taken for analysis. Individual analyses are reported for iron (Fe), manganese (Mn), strontium (Sr), and magnesium (Mg) in ppm; for carbonates of calcium, magnesium, iron, manganese, and strontium in mole %; for each dolomite type (dol. type); for dolomite cements (C=1), and replacement dolomites (R=2); and for different lithofacies.

Well No.	Sample ft	Fe	Mn	Sr	Mg	$CaCO_3$	$MgCO_3$	$FeCO_3$	$MnCO_3$	$SrCO_3$	Dol. type	C=1 R=2	Litho-Facies
		ppm				mole %							
1	12061	420	475	0	129832	50.11	48.83	.07	.08	0	2	2	1
1	12061	214	562	0	130749	50.63	48.69	.03	.09	0	2	2	1
1	12061	270	317	0	131794	50.55	48.91	.04	.05	0	2	2	1
1	12061	361	671	0	131042	49.92	49.39	.06	.11	0	2	2	1
1	12061	618	556	0	130668	49.88	49.27	.10	.09	0	3	2	1
1	12061	320	456	0	132670	49.62	49.51	.05	.08	0	3	2	1
1	12061	505	354	0	130198	50.11	49.49	.08	.06	0	3	2	1
1	12061	530	443	0	128222	50.32	48.99	.09	.07	0	3	2	1
1	12061	337	451	0	129134	50.44	48.85	.06	.08	0	3	2	1
1	12077	481	342	0	130061	50.14	49.56	.08	.06	0	3	2	1
1	12077	317	637	21	130892	49.96	49.73	.05	.11	0	3	2	1
1	12083	981	317	0	128308	49.68	48.52	.16	.05	0	2	2	1
1	12083	309	101	0	124665	51.03	47.15	.05	.02	0	2	2	1
1	12083	1068	287	0	123719	51.20	46.66	.18	.05	0	2	2	1
1	12083	224	406	0	122395	52.14	46.14	.04	.07	0	2	2	1
1	12083	564	66	0	125333	49.78	47.46	.09	.01	0	2	2	1
1	12083	161	381	0	127846	50.04	47.88	.03	.06	0	2	2	1
1	12094	6310	825	0	116031	51.72	44.24	1.05	.14	0	7	1	6
1	12094	5415	450	0	116073	52.11	44.18	.98	.08	0	7	1	6
1	12094	0	40	0	126461	50.72	47.12	0	.01	0	1	2	6
1	12094	60	209	0	124506	55.12	46.65	.01	.03	0	1	2	6
1	12094	1207	813	0	132540	48.93	50.19	.20	.14	0	4	1	6
1	12094	212	313	122	125560	51.90	47.72	.04	.05	.01	4	2	6
1	12094	995	599	0	130476	48.97	48.76	.16	.10	0	5	1	6
1	12094	323	257	0	129310	49.67	48.07	.05	.04	0	5	2	6
1	12094	105	235	0	127450	50.44	47.74	.02	.04	0	5	2	6
1	12094	142	0	0	126501	50.38	47.70	.02	0	0	5	1	6

Well No.	Sample ft	Fe	Mn	Sr	Mg	$CaCO_3$	$MgCO_3$	$FeCO_3$	$MnCO_3$	$SrCO_3$	Dol. type	C=1 R=2	Litho-Facies
		ppm				mole %							
1	12094	751	364	0	130737	49.30	48.66	.12	.06	0	5	1	6
1	12094	8867	1144	0	113460	52.89	43.70	1.49	.20	0	5	1	6
1	12094	8913	1062	0	113354	52.16	43.24	1.48	.18	0	5	1	6
1	12094	614	218	0	129723	49.41	47.92	.10	.04	0	5	2	6
1	12094	320	320	0	120883	51.71	45.73	.05	.05	0	5	2	6
1	12094	975	409	0	129586	49.53	48.26	.16	.07	0	5	2	6
1	12094	8378	1187	0	118420	51.97	44.07	1.36	.20	0	5	1	6
1	12094	6290	894	0	116264	52.12	43.89	1.03	.15	0	5	1	6
1	12094	6144	659	0	116147	52.40	43.75	1.01	.11	0	7	1	6
1	12094	5779	612	0	116617	53.64	44.97	.97	.10	0	7	1	6
1	12094	6153	612	0	118886	53.16	45.48	1.02	.10	0	7	1	6
1	12094	2855	1387	0	128863	50.73	48.21	.46	.23	0	4	1	6
1	12094	696	156	0	126507	51.85	47.82	.11	.03	.01	4	1	6
1	12094	302	442	0	105795	53.86	45.42	.06	.08	0	4	2	6
1	12094	318	170	0	125673	50.60	48.95	.05	03	0	4	2	6
1	12094	5203	522	0	114394	53.92	44.79	.89	.09	0	4	1	6
1	12094	6724	473	0	114325	53.19	44.71	1.14	.08	0	4	1	6
1	12094	949	688	0	130432	49.96	49.43	.16	.12	0	4	1	6
1	12094	8514	1157	0	114664	53.27	44.71	1.44	.20	0	4	1	6
1	12107	1889	787	0	128498	50.39	48.94	.38	.12	0	5	1	6
1	12107	12315	865	0	115068	52.02	45.10	2.10	.15	0	5	1	6
1	12107	594	501	0	124084	52.60	46.99	.10	.08	0	3	2	6
1	12107	17801	1036	0	111763	51.93	44.48	3.08	.18	0	5	1	6
1	12107	96	0	32	128515	51.18	48.63	.02	0	0	5	1	6
1	12107	148	139	0	127061	51.49	48.17	.02	.02	0	5	1	6
1	12111	152	280	0	130430	51.53	48.26	.02	.05	0	4	2	6
1	12111	8767	854	0	119288	51.40	46.69	1.49	.15	0	4	1	6
1	12111	1209	794	0	128350	50.42	48.92	.20	.13	0	4	1	6
1	12111	407	202	0	126908	51.13	48.50	.07	.03	0	4	2	6
1	12111	8163	852	0	123169	50.41	47.70	1.38	.15	0	4	1	6
1	12111	2363	726	0	135522	49.00	50.19	.39	.12	0	4	1	6
1	12111	2868	238	0	126250	51.72	47.49	.47	.04	0	4	1	6
1	12111	8852	1030	0	118102	51.36	46.61	1.52	.18	0	4	1	6
1	12120	2928	133	0	121474	51.66	47.39	.50	.02	0	4	1	6
1	12120	9264	908	0	118762	51.99	45.94	1.56	.16	0	4	1	6
1	12120	8872	889	0	122802	51.25	46.71	1.47	.15	0	4	1	6
1	12120	622	412	39	131334	50.64	49.06	.10	.07	0	4	1	6
1	12120	501	453	0	132997	50.67	48.99	.08	.07	0	4	1	6
1	12120	341	1415	0	128755	50.47	49.07	.06	.24	0	4	1	6
1	12120	213	275	0	118778	48.86	44.85	.04	.05	0	4	1	6
1	12120	9985	906	0	119489	51.89	45.89	1.67	.15	0	4	1	6
1	12120	952	549	0	129291	49.81	49.70	.16	.09	0	4	1	6
1	12120	965	183	0	130135	50.30	49.27	.16	.03	0	2	2	6
1	12120	668	535	0	134387	49.49	50.12	.11	.09	0	2	2	6
1	12132	2600	494	0	127860	50.74	48.06	.43	.08	0	3	1	6
1	12132	186	156	0	128001	51.23	47.93	.03	.03	0	3	1	6
1	12132	5597	948	0	129051	50.14	48.07	.91	.16	0	3	1	6
1	12132	330	123	0	128008	50.28	48.57	.05	.02	0	3	1	6
1	12132	98	319	0	125140	51.73	47.33	.02	.05	0	3	1	6

Well No.	Sample ft	Fe	Mn	Sr	Mg	$CaCO_3$	$MgCO_3$	$FeCO_3$	$MnCO_3$	$SrCO_3$	Dol. type	C=1 R=2	Litho-Facies
		ppm				mole %							
1	12132	5853	810	0	128238	50.48	47.66	.02	.05	0	3	1	6
1	12132	247	239	0	128974	51.13	47.98	.04	.04	0	3	1	6
1	12132	5488	707	0	126332	50.00	48.18	.90	.12	0	3	1	6
1	12132	5628	913	0	126757	50.15	48.05	.93	.15	0	3	1	6
1	12132	255	97	0	125074	51.71	46.99	.04	.02	0	3	1	6
1	12132	432	204	0	126543	51.87	47.29	.07	.03	0	3	1	6
1	12132	436	317	0	126147	51.63	47.48	.07	.05	0	3	1	6
1	12132	639	421	0	124919	51.39	47.62	.11	.07	0	3	1	6
1	12132	2074	288	0	124954	52.15	46.84	.34	.05	0	3	1	6
1	12161	99	240	40	129187	49.91	49.85	.02	.04	0	3	2	6
1	12161	1672	278	0	119046	48.83	47.70	.29	.05	0	3	1	6
1	12161	62	168	32	127410	51.08	48.76	.01	.03	0	3	2	6
1	12161	837	143	0	128558	50.01	49.55	.14	.02	0	3	1	6
1	12161	1946	29	0	121851	49.42	48.26	.34	.01	0	3	1	6
1	12151	5943	1275	0	130598	50.64	47.18	.93	.20	0	3	1	6
1	12151	1125	620	240	136343	50.39	49.29	.18	.10	.02	3	1	6
1	12151	14466	1013	34	124723	49.92	47.43	2.39	.17	0	3	1	6
1	12151	116	44	0	113705	53.90	45.88	.02	.01	0	3	2	6
1	12151	262	259	187	130440	51.46	48.39	.04	.04	.02	3	2	6
1	12151	455	244	0	136262	50.59	49.20	.07	.04	0	3	2	6
1	12151	134	205	0	126733	52.18	47.65	.02	.03	0	3	2	6
1	12151	156	180	67	128256	51.43	48.48	.03	.03	.01	3	2	6
1	12151	215	190	20	132574	50.32	49.61	.04	.03	0	3	2	6
2	21234	310	276	0	130743	50.64	49.18	.05	.05	0	5	1	3
2	21234	291	135	0	133399	50.02	49.78	.05	.02	0	5	1	3
2	21278	8202	271	169	126396	50.03	48.38	1.37	.05	.02	3	1	3
2	21278	971	176	0	127316	51.44	48.17	.16	.03	0	3	1	3
2	21278	314	215	0	129750	50.47	49.31	.05	.04	0	3	1	3
2	21278	1551	383	0	126584	50.96	48.57	.26	.07	0	3	1	3
2	21278	817	0	0	127914	50.48	49.26	.14	0	0	3	1	3
2	21278	117	43	0	126432	51.83	47.98	.02	.01	0	3	2	3
2	21278	22	0	0	128824	50.73	49.10	0	0	0	3	2	3
2	21278	7984	68	218	125019	51.02	47.50	1.32	.01	.02	3	1	3
2	21278	68	17	0	126553	51.22	48.53	.01	0	0	3	2	3
2	21278	22	47	53	127343	51.75	48.20	0	.01	.01	3	2	3
2	21278	487	47	0	130526	50.15	49.61	.08	.01	0	3	2	3
2	21278	971	163	96	127230	50.64	49.02	.16	.03	.01	3	1	3
2	21278	291	189	105	129966	50.70	49.10	.05	.03	.01	3	2	3
2	21278	–	–	–	–	50.75	49.10	.07	.03	0	3	1	3
2	21278	166	139	0	125255	51.68	48.10	.03	.02	0	3	2	3
2	21278	162	0	0	129909	50.37	49.54	.03	0	0	3	2	3
2	21280	193	254	0	130242	50.52	49.36	.03	.04	0	4	1	3
2	21280	258	112	0	130016	50.97	48.83	.04	.02	0	4	1	3
2	21280	2322	576	183	125009	52.28	47.12	.38	.10	.02	4	1	3
2	21280	204	210	0	127132	51.75	48.02	.03	.04	0	4	1	3
2	21280	87	151	0	126460	50.79	48.99	.01	.03	0	4	2	3
2	21280	127	171	0	125928	52.56	47.15	.02	.03	0	4	2	3
2	21280	0	494	13	128717	50.84	48.94	0	.08	0	4	2	3
2	21280	266	132	0	122247	50.03	46.58	.04	.02	0	4	2	3

Well No.	Sample ft	Fe	Mn	Sr	Mg	$CaCO_3$	$MgCO_3$	$FeCO_3$	$MnCO_3$	$SrCO_3$	Dol. type	C=1 R=2	Litho-Facies
		ppm				mole %							
2	21248	0	109	105	130765	50.25	49.67	0	.02	.01	1	2	3
2	21248	142	234	0	126472	50.77	49.11	.02	.04	0	1	2	3
2	21248	432	0	0	129654	50.49	49.30	.07	0	0	1	2	3
2	21248	406	163	31	114817	53.44	46.36	.07	.03	0	3	1	3
2	21248	543	16	192	126580	51.14	48.67	.09	0	.02	3	1	3
2	21248	5343	96	0	120088	51.51	47.36	.92	.02	0	7	1	3
2	21248	5784	146	0	120150	52.27	46.59	.98	.03	0	7	1	3
2	21248	4639	294	99	123810	51.13	47.98	.78	.05	.01	7	1	3
2	21248	4769	201	0	124644	51.49	47.55	.80	.03	0	7	1	3
2	21248	6353	235	0	118285	52.74	46.12	1.08	.04	0	7	1	3
2	21248	4727	349	125	123308	51.26	47.76	.80	.06	.01	7	1	3
2	21264	3533	270	0	122519	49.19	47.68	.60	.05	0	3	1	1
2	21264	128	227	0	131826	50.30	49.52	.14	.02	0	3	1	1
2	21264	45	233	0	131711	49.72	50.14	.01	.04	0	3	2	1
2	21264	256	51	39	130073	50.57	49.34	.04	.01	0	3	1	1
2	21264	5531	0	0	109104	44.34	41.13	.91	0	0	3	1	1
2	21264	5173	198	0	125069	49.52	48.57	.87	.83	0	3	1	1
2	21264	203	349	0	130285	50.15	49.65	.03	.06	0	3	1	1
2	21272	320	257	148	129146	50.00	49.84	.05	.04	.02	5	1	3
2	21272	592	120	107	129348	50.35	49.50	.10	.02	.01	5	1	3
2	21272	343	89	63	128890	50.46	49.41	.06	.02	.01	5	1	3
2	21272	7132	293	30	125317	50.09	48.62	1.20	.05	0	5	1	3
2	21272	265	177	20	129268	50.58	49.34	.04	.03	0	5	1	3
2	21272	470	102	155	127005	51.37	48.49	.08	.02	.02	3	1	3
2	21272	176	196	0	129636	50.57	50.57	.03	.03	0	5	1	3
2	21272	319	232	0	128577	50.20	49.70	.05	.04	0	5	1	3
2	21191	580	321	0	124578	51.47	48.11	.10	.05	0	2	1	3
2	21191	267	71	0	127194	50.94	48.61	.04	.01	0	2	1	3
2	21191	88	343	0	130251	50.10	49.41	.01	.06	0	2	1	3
2	21191	143	71	0	125323	51.21	48.44	.04	.02	0	2	1	3
2	21191	887	274	0	126537	51.95	47.63	.15	.05	0	2	1	3
2	21191	59	0	0	126274	51.49	48.25	.01	0	0	2	2	3
2	21191	22	98	0	127037	49.60	49.48	0	.02	0	2	2	3
2	21191	285	189	0	128074	50.99	48.87	.05	.03	0	5	1	3
2	21191	293	216	0	132959	50.04	49.69	.05	.04	0	5	1	3
2	21191	1393	285	0	123724	52.16	47.41	.23	.05	0	5	1	3
2	21191	291	285	0	127102	50.63	49.12	.05	.05	0	5	1	3
2	21191	356	179	0	125210	50.43	49.36	.06	.03	0	5	1	3
2	21191	502	183	0	127109	50.68	49.04	.08	.03	0	5	1	3
2	21191	42	0	125	126927	51.46	48.34	.01	0	.01	5	2	3
2	21191	80	0	0	126620	51.27	48.49	.01	0	0	5	2	3
2	21191	5717	140	0	119886	51.97	46.89	1.02	0	0	7	1	3
2	21193	203	0	0	123518	51.42	48.41	.03	0	0	1	2	3
2	21193	234	140	0	125457	51.01	48.85	.04	.02	0	1	2	3
2	21193	196	57	0	125345	50.74	49.05	.03	.01	0	1	2	3
2	21193	315	0	0	129095	50.70	49.20	.05	0	0	1	2	3
2	21193	420	127	74	128645	50.11	49.69	.07	.02	.01	1	2	3
2	21193	997	287	133	123647	52.08	47.63	.17	.05	.01	3	1	3
2	21193	460	75	58	125070	51.05	48.74	.08	.01	.01	3	1	3

Well No.	Sample ft	Fe	Mn	Sr	Mg	$CaCO_3$	$MgCO_3$	$FeCO_3$	$MnCO_3$	$SrCO_3$	Dol. type	C=1 R=2	Litho-Facies
		ppm				mole %							
2	21193	11	17	277	125725	51.16	48.73	0	0	.03	3	2	3
2	21193	0	106	194	124981	52.80	48.07	0	.02	.02	3	2	3
2	21193	0	93	164	128822	50.31	49.61	0	.02	.02	3	2	3
2	21193	596	0	112	126429	50.78	48.65	.07	.02	.01	3	1	3
2	21193	261	222	25	126609	51.51	48.37	.04	.04	0	3	1	3
2	21193	93	84	120	125883	51.09	48.85	.02	.01	.01	3	1	3
2	21193	66	289	15	126187	51.07	48.77	.01	.05	0	3	1	3
2	21193	54	141	81	127538	50.49	49.37	.01	.02	.01	3	1	3
2	21193	119	136	76	127753	50.77	49.10	.02	.02	.01	3	1	3
2	21193	531	17	0	129312	50.63	49.20	.09	0	0	1	2	3
2	21193	38	92	0	125041	51.20	48.69	.01	.02	0	1	2	3
2	21208	223	0	0	125278	51.65	48.12	.04	0	0	5	1	2
2	21208	2032	466	0	121488	51.74	47.66	.35	.08	0	5	1	2
2	21208	334	0	0	126860	51.10	48.67	.06	0	0	5	1	2
2	21208	276	92	0	126818	50.67	49.05	.05	.02	0	5	1	2
2	21208	1497	0	105	125864	50.37	49.17	.25	0	.01	5	1	2
2	21208	369	294	0	125388	50.71	48.96	.06	.05	0	5	1	2
2	21208	3196	307	0	123976	50.95	48.31	.54	.05	0	5	1	2
2	21208	11282	30	0	113783	52.95	44.91	1.94	.01	0	7	1	2
2	21208	11913	135	44	116468	51.59	46.10	2.05	.02	0	7	1	2
2	21208	11630	179	0	113780	53.06	44.71	1.99	.03	0	7	1	2
2	21219	6716	77	0	123380	51.11	47.62	1.13	.01	0	3	1	2
2	21219	294	0	72	130429	50.48	49.76	.05	0	.01	3	1	2
2	21219	359	0	0	127254	50.71	49.15	.06	0	0	3	1	2
2	21219	83	202	242	127094	52.09	47.78	.01	.03	.03	3	2	2
2	21219	5826	230	261	129267	50.88	48.07	.94	.04	.03	3	1	2
2	21219	17	60	0	133199	50.48	49.51	0	.01	0	3	1	2
2	21219	566	0	72	131952	50.86	49.07	.02	.03	.01	3	1	2
2	21219	515	75	0	126528	51.36	48.34	.09	.01	0	3	1	2
2	21219	0	50	0	131972	50.30	49.67	0	.01	0	3	2	2
2	21219	227	0	0	128560	50.12	49.10	.04	0	0	3	2	2
2	21219	355	57	0	124069	50.18	48.25	.06	.01	0	3	2	2
2	21249	1161	202	12	128375	49.98	49.79	.20	.03	0	4	1	2
2	21249	115	0	0	121925	51.82	47.85	.02	0	0	4	2	2
2	21249	1464	144	0	128549	50.00	49.63	.25	.02	0	4	1	2
2	21249	76	70	0	128181	50.78	49.20	.01	.01	0	4	2	2
2	21249	289	167	0	125664	50.80	48.77	.05	.03	0	2	1	2
2	21249	383	215	0	126260	50.68	49.00	.05	.04	0	2	1	2
2	21249	749	157	0	124784	51.44	48.17	.13	.03	0	4	1	2
2	21249	153	78	0	127323	50.91	48.81	.03	.01	0	4	2	2
2	21185	194	299	0	131115	50.51	49.31	.03	.05	0	2	1	4
2	21185	408	98	0	131225	50.11	49.70	.07	.02	0	2	1	4
2	21185	1623	656	0	126579	51.75	47.87	.27	.11	0	2	1	4
2	21185	868	52	0	125707	51.61	48.19	.14	.01	0	2	1	4
2	21185	14	167	0	128859	51.17	48.18	0	.03	0	2	1	4
2	21185	182	47	0	126297	51.76	48.03	.03	.01	0	2	1	4
2	21185	205	105	0	119113	49.68	46.30	.03	.02	0	2	1	4
2	21185	1177	399	0	125787	52.14	47.55	.19	.07	0	4	1	4
2	21185	449	0	0	123628	51.65	47.92	.08	0	0	4	1	4

Well No.	Sample ft	Fe	Mn	Sr	Mg	$CaCO_3$	$MgCO_3$	$FeCO_3$	$MnCO_3$	$SrCO_3$	Dol. type	C=1 R=2	Litho-Facies
		ppm				mole %							
2	21185	722	58	0	128160	50.88	48.92	.12	.01	0	4	1	4
2	21185	285	31	0	130235	49.58	49.95	.05	.01	0	4	1	4
2	21185	413	20	0	126523	51.28	47.89	.07	0	0	2	2	4
2	21185	160	120	0	127572	50.76	48.57	.03	.02	0	2	2	4
2	21185	234	194	0	128286	50.26	49.15	.04	.03	0	2	2	4
2	21185	2086	360	0	129137	50.67	48.65	.34	.06	0	2	2	4
2	21185	3801	612	0	124486	50.55	48.33	.64	.11	0	2	2	4
2	21185	211	219	0	127353	50.93	48.50	.04	.04	0	2	2	4
2	21185	183	0	199	126197	51.91	47.95	.03	0	.02	2	2	4
2	21185	242	160	0	126100	51.33	48.51	.04	.03	0	2	2	4
2	21185	640	353	113	125912	51.61	48.94	.22	.03	.01	2	2	4
2	21185	1242	346	57	126023	51.48	48.16	.21	.06	.01	2	2	4
2	21185	148	104	0	130393	50.34	49.30	.02	.02	0	2	2	4
2	21185	2512	177	0	127163	50.80	48.69	.42	.03	0	2	1	4
2	21185	7111	172	0	121160	51.43	47.20	1.21	.03	0	2	1	4
2	21185	8362	109	24	122146	50.79	47.56	1.42	.02	0	2	1	4
2	21266	6655	381	0	126437	50.86	47.72	1.09	.06	0	5	1	1
2	21266	6491	276	0	125961	50.95	47.76	1.07	.05	0	5	1	1
2	21266	6739	234	0	125251	51.03	47.58	.04	0	0	5	1	1
2	21266	7073	161	0	125347	50.33	48.16	1.18	.03	0	5	1	1
2	21266	7311	386	0	123089	51.52	46.93	1.21	.07	0	5	1	1
2	21266	7392	360	0	123399	51.85	46.57	1.21	.06	0	5	1	1
2	21266	1871	0	0	131054	50.18	49.32	.31	0	0	5	1	1
2	21266	2434	322	0	127606	50.91	48.29	.40	.05	0	5	1	1
2	21266	2268	270	0	128248	50.65	48.73	.38	.05	0	5	1	1
2	21266	2546	114	0	127570	51.04	48.31	.42	.02	0	5	1	1
2	21266	554	140	0	129880	50.81	48.88	.09	.02	0	3	1	1
2	21266	1148	109	0	131799	50.51	49.19	.19	.02	0	3	1	1
2	21266	972	145	0	131996	50.28	49.36	.16	.02	0	3	1	1
2	21266	532	57	0	130746	50.75	49.00	.09	.01	0	3	1	1
2	21266	1938	385	0	130691	50.91	48.46	.31	.06	0	3	1	1
2	21266	328	212	0	132471	50.42	49.40	.05	.04	0	3	2	1
2	21266	273	306	22	119894	52.89	46.98	.05	.05	0	3	2	0
2	21266	229	265	0	132158	50.67	49.19	.04	.04	0	3	2	1
2	21266	180	67	0	130562	51.00	48.90	.03	.01	0	1	2	1
2	21266	332	249	19	130795	50.50	49.30	.05	.04	0	1	2	1
2	21266	162	10	0	129890	50.72	49.00	.03	0	0	1	2	1
2	21268	1053	212	0	129072	51.12	48.46	.17	.04	0	5	1	3
2	21268	1185	103	0	129235	50.87	48.76	.19	.02	0	5	1	3
2	21268	88	239	0	128113	50.98	48.77	.01	.04	0	5	1	3
2	21268	863	368	0	128138	51.28	48.22	.14	.06	0	5	1	3
2	21268	1526	142	0	126753	51.73	47.71	.25	.02	0	5	1	3
2	21268	1986	52	0	126201	50.99	48.32	.33	.01	0	5	1	3
2	21268	2692	211	0	127395	50.83	48.49	.45	.04	0	5	1	3
2	21268	2735	317	0	127257	51.33	47.87	.45	.05	0	5	1	3
2	21268	3634	411	0	126393	51.42	47.74	.60	.07	0	5	1	3
2	21268	4715	353	0	126643	51.05	47.85	.78	.06	0	5	1	3
2	21268	6843	168	0	124233	51.60	46.96	1.13	.03	0	5	1	3
2	21268	7500	153	0	124535	51.39	47.01	1.23	.03	0	5	1	3

Well No.	Sample ft	Fe	Mn	Sr	Mg	$CaCO_3$	$MgCO_3$	$FeCO_3$	$MnCO_3$	$SrCO_3$	Dol. type	C=1 R=2	Litho-Facies
		ppm				mole %							
2	21268	8644	427	0	119288	52.11	49.92	1.45	.07	0	5	1	3
2	21268	67	26	0	130783	50.27	49.56	.01	0	0	5	2	3
2	21268	108	258	0	128998	51.43	48.37	.02	.04	0	5	2	3
2	21268	1536	464	0	127928	51.26	48.32	.25	.08	0	5	1	3
2	21268	270	95	0	132676	50.55	49.23	.04	.02	0	5	1	3
2	21268	889	35	0	125580	50.57	49.13	.15	.01	0	5	1	3
2	21268	1021	159	0	126763	50.76	48.83	.17	.03	0	5	1	3
2	21268	49	175	0	127465	50.66	49.05	.01	.03	0	5	1	3
2	21268	80	56	0	126985	51.23	48.57	.01	.01	0	5	1	3
2	21268	1770	241	0	125542	50.98	48.50	.30	.04	0	5	1	3
2	21268	2448	228	0	125673	50.38	48.94	.41	.04	0	5	1	3
2	21268	8577	122	0	118098	52.23	45.91	1.45	.02	0	7	1	3
2	21268	8847	324	0	116672	51.84	46.02	1.52	.06	0	7	1	3
2	21268	8389	345	0	116800	52.45	45.73	1.43	.06	0	5	1	3
2	21268	9067	213	0	115574	52.45	45.37	1.55	.04	0	7	1	3
2	21268	9117	95	0	115231	52.47	45.18	1.56	.02	0	7	1	3
2	21268	8970	299	0	117578	51.97	46.13	1.53	.05	0	5	1	3
2	21268	6869	272	0	121369	50.98	47.54	1.17	.05	0	5	1	3
2	21268	5933	302	0	122630	50.89	47.77	1.01	.05	0	5	1	3
2	21268	3769	241	0	124513	50.95	48.12	.63	.04	0	5	1	3
2	21268	2321	0	116	125731	50.48	48.97	.39	0	.01	5	1	3
2	21268	1968	168	0	126367	50.45	49.02	.33	.03	0	5	1	3
2	21268	567	134	41	128308	50.42	49.36	.10	.02	0	5	1	3
2	21268	18	160	0	126194	51.19	48.61	0	.03	0	5	1	3
2	21268	0	38	0	128652	49.93	49.85	0	.01	0	5	1	3
2	21268	0	146	0	128962	50.05	49.76	0	.03	0	5	1	3
2	21268	1156	73	0	126173	51.12	48.52	.19	.01	0	5	1	3
2	21268	849	185	0	128557	50.17	49.55	.14	.03	0	5	1	3
2	21268	1034	108	0	127750	49.85	49.84	.18	.02	0	5	1	3
2	21268	932	77	0	127803	50.44	49.26	.16	.01	0	5	1	3
2	21268	489	190	0	129385	49.79	50.00	.07	.03	0	5	1	3
2	21268	345	120	0	128151	50.19	49.55	.06	.02	0	5	1	3
2	21268	364	73	0	127731	50.49	49.28	.06	.01	0	5	1	3
2	21268	289	194	0	127749	50.92	48.88	.05	.03	0	5	1	3
2	21268	913	281	0	127619	50.24	49.40	.15	.05	0	5	1	3
2	21268	199	0	0	128252	50.41	49.41	.03	0	0	5	2	3
2	21268	742	0	0	129146	49.99	49.75	.12	0	0	5	1	3
3	22615	0	0	73	125341	51.47	48.46	0	0	.01	3	2	1
3	22615	0	60	91	126181	51.23	48.71	0	.01	.01	3	2	1
3	22615	33	0	198	124748	52.26	47.71	.01	0	.02	3	2	1
3	22615	150	64	45	125389	51.32	48.63	.03	.01	0	3	2	1
3	22615	686	99	73	126771	51.43	48.42	.11	.02	0	3	1	1
3	22615	476	194	0	126263	51.17	48.68	.08	.03	0	3	1	1
3	22615	1053	271	152	126367	51.58	48.16	.17	.05	.02	3	1	1
3	22615	2057	0	125	126102	50.88	48.75	.35	0	.01	3	1	1
3	22615	1585	125	110	125863	50.96	48.68	.27	.02	.01	3	1	1
3	22615	355	56	0	128356	51.42	48.49	.06	.01	0	3	1	1
3	22615	2185	624	114	123123	52.16	47.34	.37	.11	.01	3	1	1
3	22615	988	684	111	122860	52.05	47.63	.17	.12	.01	3	1	1

Well No.	Sample ft	Fe	Mn	Sr	Mg	$CaCO_3$	$MgCO_3$	$FeCO_3$	$MnCO_3$	$SrCO_3$	Dol. type	C=1 R=2	Litho-Facies
		ppm				mole %							
3	22615	4876	607	0	122391	51.99	47.06	.82	.10	0	3	1	1
3	22615	1584	379	0	123629	52.18	47.46	.26	.06	0	3	1	1
3	22615	905	185	12	125332	51.37	48.45	.15	.03	0	3	1	1
3	22615	1357	103	0	124484	51.87	47.22	.23	.02	0	3	1	1
3	22615	157	180	0	126359	52.13	47.80	.03	.30	0	3	2	1
3	22615	37	146	79	126622	51.20	48.74	.01	.02	.02	3	2	1
3	22615	568	129	0	125264	51.15	48.61	.10	.02	0	1	2	1
3	22615	407	0	0	126048	50.94	48.73	.07	0	0	1	2	1
3	22615	246	172	0	120041	51.48	47.08	.04	.03	0	1	2	1
3	22615	343	137	10	128629	51.21	48.54	.06	.02	.01	2	2	1
3	22615	0	215	0	131135	50.29	49.62	0	.04	0	3	2	1
3	22615	190	159	30	131087	50.26	49.64	.03	.03	0	3	2	1
3	22615	362	197	56	129416	50.84	49.03	.06	.03	.01	3	2	1
3	22615	1922	38	83	128271	51.10	48.51	.32	.01	.01	3	2	1
3	22615	329	356	101	131636	49.85	50.02	.05	.06	.01	3	1	1
3	22615	3488	581	49	125881	51.33	47.99	.58	.10	.01	3	1	1
3	22615	220	279	0	128996	51.52	48.37	.04	.05	0	3	1	1
3	22615	418	73	23	129562	50.34	49.55	.07	.01	0	3	1	1
3	22615	608	231	122	127598	50.70	49.11	.10	.04	.01	3	1	1
3	22615	41	210	73	128422	51.23	48.69	.01	.04	.01	3	1	1
3	22615	4422	279	123	124339	52.34	46.87	.73	.05	.01	3	1	1
3	22615	4704	68	0	121239	53.07	46.09	.78	.01	0	3	1	1
3	22615	6172	330	0	121182	53.62	45.28	1.0	.05	0	3	1	1
3	22615	6199	300	0	117775	53.87	44.98	1.0	.05	0	3	1	1
3	22615	5723	262	0	116444	53.53	45.25	.97	.05	0	7	1	1
3	22615	5780	111	0	118343	53.08	45.79	.97	.02	0	7	1	1
3	22615	5496	244	0	121544	52.47	46.55	.92	.04	0	7	1	1
3	22615	5444	205	0	120031	53.63	45.41	.90	.03	0	7	1	1
3	22635	290	107	0	126185	51.33	48.56	.05	.02	0	3	2	1
3	22635	0	0	134	123428	52.25	47.74	0	0	.01	3	2	1
3	22635	0	261	75	124860	51.93	47.98	0	.04	.01	3	2	1
3	22635	1164	171	0	125152	51.17	48.60	.20	.03	0	3	1	1
3	22635	619	115	0	127621	51.10	48.73	.10	.02	0	3	1	1
3	22635	1837	437	105	123461	51.77	47.83	.31	.07	.01	3	1	1
3	22635	178	85	56	126478	50.63	49.29	.03	.01	.01	3	1	1
3	22635	484	175	46	127512	50.61	49.27	.08	.03	0	3	1	1
3	22635	272	420	91	126035	51.78	48.07	.05	.07	.01	3	1	1
3	22712	605	89	0	126855	51.42	48.10	.10	.01	0	1	2	1
3	22712	79	39	0	128507	51.08	48.64	.01	.01	0	1	2	1
3	22712	807	68	0	126304	51.87	47.81	.13	.01	0	5	1	1
3	22712	92	42	0	126288	52.44	47.38	.02	.01	0	5	1	1
3	22712	657	71	0	126372	52.16	47.59	.11	.01	0	5	1	1
3	22712	1241	205	0	123657	52.87	46.73	.20	.03	0	5	1	1
3	22712	2414	545	0	123778	52.62	46.69	.40	.09	0	5	1	1
3	22712	1110	99	35	124474	52.47	47.20	.18	.02	0	5	1	1
3	22712	244	0	0	129584	51.49	48.31	.04	0	0	5	1	1
3	22712	367	21	0	132999	50.46	49.27	.06	0	0	5	1	1
3	22712	4148	271	0	119487	52.89	46.22	.07	.05	0	7	1	1
3	22712	4274	131	0	120034	53.52	45.57	.71	.02	0	7	1	1

Well No.	Sample ft	Fe	Mn	Sr	Mg	$CaCO_3$	$MgCO_3$	$FeCO_3$	$MnCO_3$	$SrCO_3$	Dol. type	C=1 R=2	Litho-Facies
		ppm				mole %							
3	22712	4584	43	0	119538	53.77	45.36	.76	.01	0	7	1	1
3	22712	3949	182	0	119876	53.88	45.28	.65	.03	0	7	1	1
3	22712	1039	178	0	123005	52.29	47.35	.17	.03	0	5	1	1
3	22712	4882	95	0	116316	52.74	45.13	.82	.02	0	2	1	1
3	22712	6152	30	0	120621	52.28	46.11	1.02	.01	0	2	1	1
3	22712	620	147	0	126256	51.13	48.09	.10	.02	0	1	2	1
3	22712	132	117	0	124566	51.14	47.15	.01	.02	0	2	2	1
3	22712	272	178	0	124383	52.22	47.23	.05	.03	0	1	2	1
3	22712	953	0	0	125000	51.29	47.98	.16	0	0	1	2	1
3	22712	348	152	0	126013	51.09	47.66	.06	.03	0	1	2	1
3	22719	352	226	0	123068	50.72	45.61	.06	.04	0	3	2	1
3	22719	128	6	105	122025	54.17	45.77	.02	.01	.01	3	2	1
3	22719	0	104	136	124087	53.19	46.74	0	.02	.01	3	1	1
3	22719	158	0	172	128044	52.03	47.89	.03	0	.02	3	1	1
3	22719	15	73	63	128418	52.04	47.92	0	.01	.01	3	1	1
3	22719	22	91	149	129919	50.94	48.96	0	.20	.02	3	1	1
3	22719	37	0	13	128520	51.73	48.26	.01	0	0	3	1	1
3	22719	56	0	0	129909	51.18	48.76	.01	0	0	3	1	1
3	22719	831	130	26	127629	51.68	48.15	.14	.02	0	3	1	1
3	22719	1451	60	0	127748	52.29	47.45	.23	.01	0	3	1	1
3	22719	2890	665	110	126221	51.55	47.84	.48	.10	.01	3	1	1
3	22719	760	252	0	128114	51.44	48.36	.12	.04	0	3	1	1
3	22719	328	0	101	130020	51.58	48.32	.05	0	.01	3	1	1
3	22719	303	69	0	130706	49.94	49.98	.05	.01	0	3	1	1
3	22719	328	91	73	130429	51.08	48.82	.05	.02	.01	3	1	1
3	22719	1643	208	93	122271	54.06	45.61	.27	.03	.01	3	1	1
3	22719	1208	317	0	122433	53.35	46.36	.20	.05	0	3	1	1
3	22719	619	143	46	128803	51.24	48.59	.10	.02	0	3	1	1
3	22719	611	273	0	123814	52.92	46.88	.10	.05	0	3	1	1
3	22719	1510	356	108	122424	52.99	46.64	.25	.06	.01	3	1	1
3	22804	173	165	0	124404	51.93	46.82	.03	.03	0	4	1	1
3	22804	135	52	0	130022	49.93	48.51	.02	.01	0	4	1	1
3	22804	279	0	0	121951	52.00	45.74	.05	0	0	4	1	1
3	22804	222	0	0	124349	52.34	46.70	.04	0	0	4	1	1
3	22804	374	117	0	124684	51.81	46.53	.06	.02	0	4	1	1
3	22804	453	0	0	129862	51.29	48.43	.07	0	0	1	2	1
3	22804	339	0	0	128997	51.43	48.33	.06	0	0	1	2	1
3	22805	428	126	0	129576	50.62	49.19	.07	.02	0	5	1	1
3	22607	101	0	0	128194	52.02	47.79	.02	0	0	3	2	1
3	22607	2293	69	0	124079	52.13	47.22	.38	.01	0	3	1	1
3	22607	5805	148	0	117355	54.51	44.30	.95	.02	0	7	1	1
4	14597	7367	1797	429	128165	48.94	49.38	1.24	.31	.05	5	1	1
4	14597	8793	1630	124	126835	49.02	49.15	1.48	.28	.01	5	1	1
4	14597	4393	514	196	123855	50.98	48.16	.74	.09	.02	5	1	1
4	14597	388	161	88	124866	51.58	48.27	.07	.03	.01	5	1	1
4	14597	163	153	181	121201	52.33	47.46	.03	.03	.02	5	2	1
4	14597	0	39	93	125206	51.48	48.44	0	.01	.01	5	2	1
4	14597	4651	870	60	128937	49.63	49.39	.78	.15	.01	3	1	1
4	14597	617	455	109	125299	51.41	48.40	.10	.08	.01	3	1	1

Well No.	Sample ft	Fe	Mn	Sr	Mg	$CaCO_3$	$MgCO_3$	$FeCO_3$	$MnCO_3$	$SrCO_3$	Dol. type	C=1 R=2	Litho-Facies
		ppm				mole %							
4	14597	10571	2646	142	123257	49.79	47.77	1.78	.45	.02	5	1	1
4	14597	397	48	144	129278	50.21	49.63	.07	.01	.02	5	1	1
4	14597	8714	2100	0	121859	50.95	47.10	1.47	.36	0	5	1	1
4	14597	522	139	32	128190	50.18	49.35	.09	.02	0	5	1	1
4	14597	742	83	158	127442	50.73	48.80	.12	.01	.02	5	1	1
4	14597	9749	2010	0	123184	51.01	46.98	1.62	.34	0	5	1	1
4	14597	8579	1673	0	126635	50.63	47.63	1.43	.28	0	5	1	1
4	14597	367	122	0	128138	50.86	49.03	.06	02	0	5	1	1
4	14597	75	17	142	127311	51.26	48.67	.01	0	.02	5	1	1
4	14597	26	313	70	127710	50.88	49.05	.0	.05	.01	5	1	1
4	14597	128	61	59	124690	52.09	47.85	.02	.01	.01	5	1	1
4	14597	2886	354	0	124997	51.10	48.32	.49	.06	0	5	1	1
4	14597	2617	568	115	126669	50.74	48.71	.44	.10	.01	5	1	1
4	14597	4876	512	130	125564	50.78	48.27	.82	.09	.01	5	1	1
4	14597	688	21	124	127418	51.27	48.60	.11	0	.01	5	1	1
4	14597	1454	0	183	127554	50.51	49.22	.24	0	.02	5	1	1
4	14597	113	48	248	125687	50.60	49.34	.02	.01	.03	5	2	1
4	14597	60	109	318	123496	52.16	47.68	.01	.02	.03	5	2	1
4	14597	71	34	96	130231	49.86	50.09	.01	.01	.01	5	2	1
4	14593	282	74	0	130059	49.68	50.26	.05	.01	0	4	1	6
4	14593	109	0	0	133153	49.12	50.78	.02	0	0	4	1	6
4	14593	33	0	97	133840	49.34	50.63	.01	0	.01	4	1	6
4	14593	154	117	77	131190	49.41	50.52	.03	.02	.01	4	1	6
4	14593	810	396	0	129266	49.90	49.88	.14	.07	0	4	1	6
4	14593	1544	540	0	129013	50.03	49.61	.26	.09	0	4	1	6
4	14593	199	91	122	130217	49.67	50.07	.03	.02	.01	4	1	6
4	14593	275	143	83	126535	50.53	49.28	.05	.02	.01	4	1	6
4	14593	354	0	120	131523	49.80	50.07	.06	0	.01	4	1	6
4	14593	2781	427	70	126659	50.57	48.74	.47	.07	.01	4	1	6
4	14593	4369	135	207	120344	52.05	47.15	.75	.02	.02	4	1	6
4	14593	5154	426	97	122210	51.03	48.00	.38	.07	.01	4	1	6
4	14593	5453	243	264	120719	52.10	46.91	.92	.04	.03	4	1	6
4	14593	5404	265	229	122665	51.70	47.32	.91	.05	.02	4	1	6
4	14593	3367	474	199	122408	51.43	47.85	.57	.08	.02	4	1	6
4	14593	5345	356	770	120187	52.30	46.59	.90	.06	.08	4	1	6
4	14593	5128	439	644	120243	52.29	46.68	.87	.06	.07	4	1	6
4	14593	6374	456	733	119968	51.98	46.68	1.08	.08	.08	4	1	6
4	14593	6709	295	645	121592	51.99	46.72	1.12	.05	.07	3	1	6
4	14593	858	104	0	130707	50.20	49.61	.14	.02	0	3	1	6
4	14593	116	87	117	133204	49.39	50.56	.02	.01	.01	3	2	6
4	14593	0	100	0	131129	49.95	50.03	0	.02	0	3	2	6
4	14593	48	69	49	131891	50.10	49.82	.01	.01	.01	3	2	6
4	14593	0	60	15	133222	49.46	50.52	0	.01	0	6	2	6
4	14593	120	113	25	129445	50.39	49.54	.02	.02	0	6	2	6
4	14593	0	69	117	130670	50.57	49.40	0	.01	.01	6	2	6
4	14593	0	143	0	133518	49.49	50.47	0	.02	0	6	2	6
4	14593	0	0	23	132457	49.26	50.73	0	0	0	6	2	6
4	14593	105	78	42	131588	49.68	50.26	.02	.01	0	6	2	6
4	14593	131	17	0	134929	48.28	51.29	.02	0	0	6	2	6

Well No.	Sample ft	Fe	Mn	Sr	Mg	$CaCO_3$	$MgCO_3$	$FeCO_3$	$MnCO_3$	$SrCO_3$	Dol. type	C=1 R=2	Litho-Facies
		ppm				mole %							
4	14533	147	21	164	126734	51.03	48.89	.02	0	.02	3	1	6
4	14533	135	65	80	127972	50.89	49.06	.02	.01	.01	3	2	6
4	14533	0	152	112	127617	50.85	49.11	0	.03	.01	3	2	6
4	14533	82	78	74	126905	51.32	48.62	.01	.01	.01	3	2	6
4	14533	22	39	60	128012	51.34	48.61	0	.01	.01	3	2	6
4	14533	0	213	153	131224	49.20	50.74	0	.04	.02	3	2	6
4	14533	116	335	80	133335	49.38	50.53	.02	.06	.01	3	2	6
4	14533	48	379	71	129022	50.50	49.42	.01	.06	.01	6	2	6
4	14533	587	230	113	131873	49.51	50.24	.10	.04	.01	6	2	6
4	14533	1217	287	168	131722	49.33	50.38	.20	.05	.02	6	2	6
4	14533	154	30	86	133016	48.79	51.16	.03	.01	.01	6	2	6
4	14533	0	0	153	132876	49.35	50.62	0	.02	.01	6	2	6
4	14531	2006	618	0	128701	49.79	49.73	.34	.11	0	3	1	6
4	14531	1613	405	29	129525	49.93	49.58	.27	.07	0	3	1	6
4	14531	384	43	39	127440	50.70	49.19	.06	.01	0	3	1	6
4	14531	56	100	262	128986	50.33	49.57	.01	.02	.03	3	1	6
4	14531	0	21	129	131617	49.62	50.29	0	0	.01	3	1	6
4	14531	1700	409	0	130436	49.87	49.74	.28	.07	0	3	1	6
4	14531	1984	143	37	128274	50.17	49.43	.33	.02	0	3	2	6
4	14531	1539	327	72	130819	49.37	50.27	.26	.06	.01	3	2	6
4	14531	0	444	84	131713	49.45	50.46	0	.08	.01	3	2	6
4	13480	240	0	0	127796	50.71	49.09	.04	0	0	1	2	1
4	13480	116	25	83	129183	50.20	49.63	.02	0	.01	1	2	1
5	5301	207	161	61	129529	51.46	48.45	.03	.03	.01	3	2	2
5	5301	101	0	270	129908	50.97	48.98	.02	0	.03	3	2	2
5	5301	116	0	58	131226	50.55	49.42	.02	0	.01	3	2	2
5	5301	0	183	45	128761	50.83	49.08	0	.03	0	3	2	2
5	5134	2854	804	101	118011	53.86	45.47	.48	.14	.01	1	2	6
5	5134	1298	206	109	115912	53.60	44.76	.22	.04	.01	1	2	6
5	5134	2086	456	0	115883	53.90	45.06	.35	.08	0	1	2	6
5	5134	3673	232	25	111432	54.31	44.63	.62	.04	.03	1	2	6
5	5134	447	176	257	115076	54.22	44.87	.08	.03	.03	1	2	6
5	5134	530	0	313	114098	55.31	44.30	.09	0	.03	1	2	6
5	5134	2088	507	56	118297	53.25	46.23	.36	.09	.01	1	2	6
5	5134	2383	1121	127	116303	54.06	45.24	.40	.19	.01	1	2	6
5	5134	2409	584	214	115076	54.23	44.91	.41	.10	.02	1	2	6
5	5134	78	0	225	121768	54.00	45.66	.01	0	.02	4	2	6
5	5134	338	125	152	114678	55.34	44.11	.06	.02	.02	4	2	6
5	5134	792	21	0	119795	52.32	46.18	.13	0	0	4	2	6
5	5134	2640	189	61	112385	55.74	43.43	.44	.03	.01	4	1	6
5	5134	2379	154	38	114339	54.99	44.38	.40	.03	0	4	1	6
5	5134	1240	253	38	114678	55.09	44.38	.21	.04	0	4	1	6
5	5134	278	90	0	115724	55.04	44.45	.05	.02	0	4	1	6
5	5134	1270	400	56	113174	54.83	44.06	.22	.07	.01	4	1	6
5	5134	40871	3605	0	97076	52.73	38.80	7.11	.64	0	4	1	6
5	5134	41418	3948	0	97759	52.44	39.45	7.27	.70	0	4	1	6
5	5134	86187	1619	144	75373	52.22	31.47	15.66	.30	.02	4	1	6
5	5134	488	0	101	11836	53.38	45.89	.08	0	.01	4	2	6
5	5134	214	0	293	114411	55.47	44.10	.04	.08	.03	4	2	6

Well No.	Sample ft	Fe	Mn	Sr	Mg	$CaCO_3$	$MgCO_3$	$FeCO_3$	$MnCO_3$	$SrCO_3$	Dol. type	C=1 R=2	Litho-Facies
		ppm				mole %							
5	5134	4442	25	0	113370	54.96	43.61	.74	0	0	4	1	6
5	5134	135	60	175	116234	54.56	45.22	.02	.01	.02	4	1	6
5	5134	545	64	0	113500	54.86	44.02	.89	.01	0	4	1	6
5	5134	9165	88	0	113095	52.44	44.51	1.57	.15	0	4	1	6
5	5134	41354	2652	61	98156	52.44	39.37	7.25	.47	.01	4	1	6
5	5134	41354	1789	142	97190	53.38	38.96	7.21	.32	.01	4	1	6
5	5134	79023	1927	0	76832	53.04	32.04	14.34	.36	0	4	1	6
5	5134	82180	1925	0	77851	52.97	31.85	14.63	.35	0	4	1	6
5	5134	1455	397	150	116255	54.16	45.42	.25	.07	.02	4	1	6
5	5134	184	86	37	114226	55.31	44.01	.03	.01	0	4	2	6
5	5134	4996	374	232	116126	54.00	45.05	.84	.06	.03	1	2	6
5	5134	1357	348	349	116685	54.29	45.16	.23	.06	.04	1	2	6
5	5134	2590	512	155	116343	53.66	45.60	.44	.09	.02	1	2	6
5	5134	157	38	310	116184	55.06	44.77	.03	.01	.03	1	2	6
5	5134	1797	476	235	118238	53.76	45.69	.30	.08	.03	1	2	6
5	5134	330	158	126	115701	54.63	44.67	.06	.03	.01	4	2	6
5	5134	142	34	162	123906	52.69	47.24	.02	.01	.02	4	2	6
5	5134	428	34	12	118215	53.97	45.91	.07	.01	0	4	2	6
5	5134	4256	1014	227	115606	53.21	45.41	.73	.18	.02	4	1	6
5	5134	39	4749	24	100491	52.56	39.86	6.68	.83	0	4	1	6
5	5134	43665	2407	0	97385	52.92	38.95	7.60	.43	0	4	1	6
5	5134	361	90	18	125011	51.75	48.05	.06	.02	.02	1	2	6
5	5134	353	0	0	128416	50.38	49.28	.06	0	0	1	2	6
5	5134	117974	1466	120	61214	52.99	25.41	21.31	.27	.01	4	1	6
5	5121	210	34	101	126800	51.23	48.70	.04	.01	.01	4	2	6
5	5121	333	321	112	125673	51.30	48.57	.06	.06	.01	4	2	6
5	5121	1256	30	92	127370	50.96	48.82	.21	.01	.01	4	2	6
5	5121	30	60	124	125064	50.98	48.41	.51	.01	.01	4	2	6
5	5121	49761	5784	0	97382	51.37	38.67	8.60	1.02	0	4	1	6
5	5121	69615	2383	142	85378	52.46	34.70	12.31	.43	.02	4	1	6
5	5121	114770	1748	0	61383	52.15	25.72	20.93	.32	0	4	1	6
5	5121	736	73	85	124951	51.24	48.57	.12	.01	.01	4	2	6
5	5121	54419	1488	53	97838	50.94	39.27	9.51	.26	.01	4	1	6
5	5121	353	60	176	124812	52.19	47.72	.06	.01	.02	4	2	6
5	5121	724	0	105	118151	54.21	45.55	.12	0	.01	4	2	6
5	5121	908	0	26	114899	55.20	44.44	.15	0	0	4	1	6
5	5121	57043	4435	60	90765	51.97	36.93	10.10	0	.01	4	1	6
5	5121	0	163	17	124967	51.75	48.20	0	.03	0	4	2	6
5	5121	191	128	29	124095	51.40	48.38	.03	.02	0	4	2	6
5	5121	52	38	253	116609	54.80	45.13	.01	.01	.03	4	2	6
5	5121	1739	12	105	117676	54.52	45.12	.29	0	.01	4	1	6
5	5121	206	107	365	115709	54.82	44.70	.03	.02	.04	4	1	6
5	5121	14731	3133	0	112215	50.38	44.61	2.55	.55	0	4	1	6
5	5121	416	236	210	117453	54.40	45.45	.07	.04	.02	4	1	6
5	5121	16717	2122	57	110933	52.57	43.60	2.86	.37	.01	4	1	6
5	5121	247	137	397	115321	55.21	44.62	.04	.02	.04	1	2	6
5	5121	168	17	232	121307	53.22	46.63	.03	0	.02	1	2	6
5	5121	386	0	309	121720	53.19	46.62	.06	0	.03	1	2	6
5	5129	101	0	302	115901	55.85	44.81	.02	0	.03	4	1	6

Well No.	Sample ft	Fe	Mn	Sr	Mg	$CaCO_3$	$MgCO_3$	$FeCO_3$	$MnCO_3$	$SrCO_3$	Dol. type	C=1 R=2	Litho-Facies
		ppm				mole %							
5	5129	41	0	404	118408	54.29	45.65	.01	0	.04	4	1	6
5	5129	93	0	329	119508	53.55	45.85	.02	.0	.04	4	1	6
5	5129	0	133	367	117638	54.75	45.06	0	.02	.04	4	1	6
5	5129	26	85	259	117388	54.83	45.11	0	.01	.03	4	1	6
5	5129	1323	55	187	115107	54.49	45.20	.23	.01	.02	4	1	6
5	5129	0	0	486	116940	55.16	44.78	0	0	.05	4	1	6
5	5129	281	184	267	116351	55.19	44.65	.05	.03	.03	4	1	6
5	5129	1223	231	62	117075	54.11	45.55	.21	.04	.01	4	1	6
5	5129	1322	399	60	118379	53.57	46.04	.22	.07	.01	4	1	6
5	5129	2931	146	26	115386	54.92	44.52	.49	.02	0	4	1	6
5	5129	878	171	110	116665	54.45	45.32	.15	.03	.01	4	1	6
5	5129	2051	442	183	116469	54.42	44.97	.34	.08	.02	4	1	6
5	5305	0	240	0	131889	50.25	49.69	0	.04	0	5	1	2
5	5305	808	116	40	129254	50.45	49.36	.13	.02	0	5	1	2
5	5305	127	0	178	129588	50.07	49.86	.02	0	.02	5	1	2
5	5305	60	176	91	126733	50.90	49.03	.01	.03	.01	5	1	2
5	5305	1811	227	114	122619	51.78	47.86	.31	.04	.01	5	1	2
5	5305	3653	270	133	125455	50.57	48.72	.62	.05	.01	5	1	2
5	5305	0	68	346	122786	52.36	47.59	0	.01	.04	3	2	2
5	5305	529	98	318	122497	51.89	47.93	.09	.02	.03	3	2	2
5	5305	1640	146	68	120420	52.04	47.16	.28	.03	.01	1	2	2
5	5305	1719	602	0	121554	52.35	47.14	.29	.10	0	1	2	2

BIBLIOGRAPHY

Adams, J.E., 1965, Stratigraphic development of Delaware Basin: American Association Petroleum Geologists Bulletin, v. 49, 2140 - 2148.

Albee, A.L., and Ray, L., 1970, Correction factors for electron probe microanalysis of silicates, oxides, carbonates, phosphates and sulphates: Analytical chemistry, v. 42, p. 1408 - 1414.

Anderson, G.M., 1983, Some geochemical aspects of sulfide precipitation in carbonate rocks, *in* Kisvarsanyi, G., Grant, S.K., Pratt, W. P., and Koenig, J.W., eds., International conference on Mississippi Valley-type lead - zinc deposits: University of Missouri - Rolla, Rolla, MO, p. 61 - 76.

Anderson, G.M., and Macqueen, R.W., 1982, Ore deposit models - 6. Mississippi-Valley type lead-zinc deposits: Geoscience Canada, v. 9, p. 108 -117.

Amthor, J.E., and Friedman, G.M., 1989 a, Geochemical evidence for basinal fluid migration in Ellenburger dolomites (Lower Ordovician) of West Texas: Geological Society of America Abstracts with Programs, v. 21, p. 219.

Amthor, J.E., and Friedman, G.M., 1989 b, Geochemistry and dolomite textures in the Ellenburger Group (Lower Ordovician), West Texas and southeastern New Mexico indicate multiple episodes of dolomitization (abs.), *in* Cunningham, B.K. & Cromwell, D.W., eds., The Lower Paleozoic of West Texas and Southern New Mexico - Modern exploration concepts: Permian Basin Section Society Economic Paleontologists Mineralogists Publication No. 89-31, p. 111.

Amthor, J.E., and Friedman, G.M., 1989 c, Petrophysical character of Ellenburger karst facies: Stateline (Ellenburger) field, Lea County, New Mexico, *in* Cunningham, B.K. & Cromwell, D.W., eds., The Lower Paleozoic of West Texas and Southern New Mexico - Modern exploration concepts: Permian Basin Section Society Economic Paleontologists Mineralogists Publication No. 89-31, p. 133 - 144.

Amthor, J.E., Kopaska-Merkel, D.C., and Friedman, G.M., 1988, Reservoir characterization, porosity, and recovery efficiency of deeply-buried Paleozoic carbonates: examples from Oklahoma, Texas and New Mexico: Carbonates and Evaporites, v. 3, p. 33 - 52.

Archie, G.E., 1952, Classification of carbonate reservoir rocks and petrophysical considerations: American Association Petroleum Geologists Bulletin, v. 36, p. 278 - 298.

Archie, G.E., 1950, Introduction to petrophysics of reservoir rocks: American Association Petroleum Geologists Bulletin, v. 34, p. 943 - 961.

Ashton, M., 1981, Carbonate tidal rhythmites from the Middle Jurassic of Britan: Sedimentology, v. 28, p. 689 - 698.

Baker, P.A., and Kastner, M., 1981, Constraints on the formation of sedimentary dolomite: Science, v. 213, p. 213 - 216.

Baker , P.A., and Burns, S.J., 1985, Occurrence and formation of dolomite in organic-rich continental sediments: American Association Petroleum Geologists Bulletin, v. 69, p. 1917 - 1930.

Barnes, V.E., 1956, Lead deposits in the Upper Cambrian of central Texas: University of Texas, Bureau of Economic Geology, Report of Investigations 36, p. 1 - 68.

Barnes, V.E., Cloud, P.E., Dixon, L.P., Jr., Folk, R.L., Jonas, E.C., Palmer, A.R., and Tynan, E.J., 1959, Stratigraphy of the pre-Simpson Paleozoic subsurface rocks of Texas and southeast New Mexico: University of Texas, Bureau of Economic Geology, Publication 5924, 2 volumes, 836 pp.

Barnes, V.E., and Dixon, L.P., 1959, Insoluble residues of Ellenburger subsurface rocks, *in* Barnes, V.E., Dixon, L.P., Folk, R.L., Jonas, E.C., Palmer, A.R., and Tynan, E.I., Stratigraphy of pre-Simpson Paleozoic subsurface rocks of Texas and Southeast New Mexico: University of Texas, Bureau of Economic Geology, Publication 5924, p. 191 - 198.

Barnes, V.E., and Bell, W.C., 1977, The Moore Hollow Group of Central Texas: University of Texas, Austin, Bureau of Economic Geology, Report of Investigations No. 88, 169 pp.

Bathurst, R.G.C., 1975, Carbonate sediments and their diagenesis. Elsevier, Amsterdam, 658 pp.

Bein, A., and Land, L.S., 1983, Carbonate sedimentation and diagenesis associated with Mg-Ca-Chloride brines: The Permian San Andres Formation in the Texas Panhandle: Journal of Sedimentary Petrology, v. 53, p. 243 - 260.

Bence, A.E., and Albee, A.L., 1968, Empirical Correction factors for the electron probe microanalysis of silicates and oxides: Journal of Geology, v. 76, p. 382-403.

Berg, R.R., 1975, Capillary-pressures in stratigraphic traps: American Association Petroleum Geologists Bulletin, v. 59, p. 939 - 956.

Berner, R.A., 1970, Sedimentary pyrite formation: American Journal of Science, v. 268, p. 1 - 23.

Berner, R.A., 1984, Sedimentary pyrite formation: an update: Geochimica et Cosmochimica Acta, v. 48, p. 605 - 615.

Bethke, C.M., 1983; Fluid flow and heat transport in compacting sedimentary basins: Geological Society of America Abstracts with Programs, v. 15, p. 526.

Bethke, C.M., 1985, A numerical model of compaction-driven groundwater flow and heat transfer, and its application to the paleohydrology of intracratonic sedimentary basins: Journal Geophysical Research, v. 90, p. 6817 - 6828.

Bethke, C.M., 1986, Hydrologic constraints on the genesis of the Upper Mississippi Valley mineral district from Illinois Basin brines: Economic Geology, v. 81, 33 - 249.

Bethke, C.M., Harrison, W.J., Upson, C., and Altaner, S.P., 1988, Supercomputer analysis of sedimentary basins: Science, v. 239, p. 261 - 267.

Bhattacharyya, A., and Friedman, G.M., 1984, Experimental compaction of ooids under deep burial diagenetic temperatures and pressures: Journal of Sedimentary Petrology, v. 54, p. 362 - 372.

Britt, T.L., 1988, Joy of searching for eroded Ellenburger traps: American Association Petroleum Geologists Bulletin, v. 72, p. 99.

Burns, S.J., and Baker, P.A., 1987, A geochemical study of dolomite in the Monterey Formation, California: Journal of Sedimentary Petrology, v. 57, p. 128 - 139.

Burns, S.J., Baker, P.A., and Showers, W.J., 1988, The factors controlling the formation and chemistry of dolomite in organic-rich sediments: Miocene Drakes Bay Formation, California, *in* Shukla, V., and Baker, P.A., eds., Sedimentology and Geochemistry of Dolostones: Society of Economic Paleontologists and Mineralogists Special Publication, No.. 43, p. 42 - 52.

Cathels, L.M., and Smith, A.T., 1983, Thermal constraints on the formation of Mississippi Valley - type lead - zinc deposits and their applications for episodic basin dewatering and deposit genesis: Economic Geology, v. 78, p. 983 - 1002.

Cebull, S.E., Shurbet, D.H., Keller, G.R., and Russell, L.R., 1976, Possible role of transform faults in the development of apparent offsets in the Ouachita-Southern Appalachian tectonic belt: Journal of Geology, v. 84, p. 107 - 114.

Choquette, P.W., and Pray, L.C., 1970, Geological nomenclature and classification of porosity in sedimentary carbonates: American Association Petroleum Geologists Bulletin, v. 54, p. 207 - 250.

Choquette, P.W., and James, N.P., 1987, Diagenesis in Limestones 3. The deep burial environment: Geoscience Canada, v. 14, p. 3 - 35.

Choquette, P.W., and James, N.P., 1988, Introduction, *in* James, N.P., and Choquette, P.W., eds., Paleokarst: Springer Verlag, p. 1 - 21.

Clemons, E.R., 1989, The Ellenburger - El Paso Connection: Lower Ordovician shelf carbonates, *in* Cunningham, B.K., and Cromwell, D.W., eds., The Lower Paleozoic of West Texas and Southern New Mexico - Modern Exploration concepts: Permian Basin Section Society Economic Paleontologists and Mineralogists Publication No. 89 - 31, p. 85 - 104.

Cloud, P.E. and Barnes, V.E., 1948, The Ellenburger Group of Central Texas: University of Texas Publication 4621, 473 pp.

Cole, C.T., 1942, Subsurface study of Ellenburger formation in West Texas: American Association Petroleum Geologists Bulletin, v. 26, p. 1398 - 1409.

Collins, J.A., and Smith, L., 1975, Zinc deposits related to diagenesis and intrakarstic sedimentation in the Lower Ordovician St. George Formation, Western Newfoundland: Bulletin of Canadian Petroleum Geology, v. 23, p. 393 - 427.

Compton, J.S., 1988 a, Degree of supersaturation and precipitation of organogenic dolomite: Geology, v. 16, p. 318 - 321.

Compton, J.S., 1988 b, Sediment composition and precipitation of dolomite and pyrite in the Neogene Monterey and Sisquoc formations, Santa Maria Basin area, California, *in* Shukla, V., and Baker, P.A., eds., Sedimentology and Geochemistry of Dolostones: Society of Economic Paleontologists and Mineralogists Special Publication, No.. 43, p. 53 - 64.

Compton, J.S., and Siever, R., 1986, Diffusion and mass balance of Mg during early dolomite formation, Monterey Formation: Geochimica et Cosmochimica Acta, v. 50, p. 125 - 136.

Conglio, M., and James, N.P., 1988, Dolomitization of deep-water sediments, Cow Head Group (Cambro-Ordovician), Western Newfoundland: Journal of Sedimentary Petrology, v. 58, p. 1032 - 1045.

Correlation of Stratigraphic Units of North America (COSUNA) Project, 1983, Southwest/Southwest-Mid-Continent Region: American Association Petroleum Geologists.

Crowley, A.J., and Hendricks, L., 1945, Lower Ordovician and Upper Cambrian subsurface subdivision in north-central Texas: American Association Petroleum Geologists Bulletin, v. 29, p. 413 - 425.

Cunningham, B.K., and Cromwell, D.W., eds., 1989, The Lower Paleozoic of West Texas and Southern New Mexico - Modern Exploration concepts: Permian Basin Section Society Economic Paleontologists and Mineralogists, Publication No 89-31, 223 pp.

Dake, C.L., and Bridge, J., 1932, Faunal correlation of the Ellenburger limestone of Texas: Geological Society America Bulletin, v. 43, p. 725 - 741.

Dockal, J.A., 1988, Thermodynamic and kinetic description of dolomitization of calcite and calcitization of dolomite (dedolomitization): Carbonates and Evaporites, v. 3, p. 125 - 141.

Dorobek, S.L., 1987, Petrography, geochemistry, and origin of burial diagenetic facies, Siluro-Devonian Helderberg Group (carbonate rocks), Central Appalachians: American Association Petroleum Geologists Bulletin, v. 71, p. 492 - 514.

Dullien, F.A.L., 1979, Porous Media. Fluid transport and pore structure: Academic Press, 396 pp.

Dunham, R.L., 1962, Classification of carbonate rocks according to their depositional texture, *in* Ham, W.E., ed., Classification of carbonate rocks: American Association Petroleum Geologists Memoir 1, p. 108 - 121.

Ebanks, W.J., Jr., 1987, Geology in enhanced oil recovery, *in* Tillman, R.W., and Weber, K.J., eds., Reservoir sedimentology: Society Economic Paleontologists Mineralogists Special Publication, No. 40, p. 1 - 14.

Elam, J.G., 1985, The Permian basin - past, present, and future: West Texas Geological Society Bulletin, v. 25, p. 4 - 7.

Emery, D., 1987, Trace element source and mobility during limestone burial diagenesis - an example from the Middle Jurassic of eastern England, *in* Marshall, J.D., ed., Diagenesis of sedimentary sequences: Geological Society London Special Publication No. 36, p. 201 - 217.

Enos, P., 1983, Shelf environment, *in* Scholle, P.A., Bebout, D.G., and Moore, C.H., eds., Carbonate depositional environments: American Association Petroleum Geologists Memoir 33, p. 267 - 295.

Esteban, M., and Klappa, C.F., 1983, Subaerial exposure environment, *in* Scholle, P.A., Bebout,. D.G., and Moore, C.M. ,eds., Carbonate depositional environments: American Association Petroleum Geologists Memoir 33, p. 1 - 54.

Etris, E.L., Brumfield, D.S., Ehrlich, R., and Crabtree, S.J., Jr., 1988, Relations between pores, throats and permeability: a petrographic/physical analysis of some carbonate grainstones and packstones: Carbonates and Evaporites, v. 3, p. 17 - 32.

Fairchild, I.J., 1983, Chemical controls of cathodoluminescence of natural dolomites and calcites: new data and review: Sedimentology, v. 30, p. 579 - 583.

Fairchild, I.J., 1980, Stages in a Precambrian dolomitization, Scotland: cementing versus replacement textures: Sedimentology, v. 27, p. 631 - 650.

Farr, M.R., 1989, Compositional zoning characteristics of late dolomite cement in the Cambrian Bonneterre Formation, Missouri: Implications for parent - fluid migration pathways: Carbonate and Evaporites, v. 4, p. 177 - 194.

Folk, R.L., 1962, Spectral subdivision of limestone types, *in* Ham, W.E., ed., Classification of carbonate rocks: American Association Petroleum Geologists Memoir 1, p. 62 - 64.

Folk, R.L., 1959, Thin-section examination of pre-Simpson Paleozoic rocks, *in* Barnes, V.E., Cloud, P.E., Jr., Dixon, L.P., Folk, R.L., Jonas, E.C., Palmer, A.R., Tynan, E.J., Stratigraphy of the pre-Simpson Paleozoic subsurface rocks of Texas and southeast New Mexico: University of Texas, Bureau of Economic Geology Publication No. 5924, p. 95 - 130.

Friedman, G.M., 1959, Identification of carbonate minerals by staining methods: Journal of Sedimentary Petrology, v. 29, p. 87 - 97.

Friedman, G.M., 1965, Terminology of crystallization textures and fabrics in sedimentary rocks: Journal of Sedimentary Petrology, v. 35, p. 643 - 655.

Friedman, G.M., and Lee, Y.II, 1985, Paleokarst and collapse breccia in Tremadocian-Arenigian (Lower Ordovician) facies: the Beekmantown and Ellenburger Groups of the eastern and southeastern U.S.: Society Economic Paleontologists Mineralogists Annual Midyear Meeting Abstracts, p. 32.

Galley, J.E., 1958, Oil and geology in the Permian Basin of Texas and New Mexico, *in* Weeks, L.G., ed., Habitat of oil and gas: American Association Petroleum Geologists Memoir, p. 395 - 446.

Galloway, W.E., Ewing, T.E., Garrett, C.M., Tyler, N., and Bebout, D.G., 1983, Atlas of major Texas oil reservoirs: University of Texas, Bureau of Economic Geology, 139 pp.

Garrison, R.E., Kastner, M., and Zenger, D.H., eds., 1984, Dolomites of the Monterey Formation and other organic - rich units: Society of Economic Paleontologists and Mineralogists Pacific Section Special publication, No., 41, 215 pp.

Garven, G., and Freeze, R.A., 1984, Theoretical analysis of the role of groundwater flow in the genesis of stratabound ore deposits: 2. Quantitative results: American Journal of Science, v. 284, p. 1125 - 1174.

Gawthorpe, R.L., 1987, Burial dolomitization and porosity development in a mixed carbonate-clastic sequence: an example from the Bowland Basin, northern England: Sedimentology, v. 34, p. 533 - 558.

Gieskes, J.M., Elderfield, H., Lawrence, J.R., Johnson, J., Meyers, B., and Campbell, A, 1982, Geochemistry of interstitial waters and sediments, Leg 64, Gulf of California, *in* Curry, J.R., Moore, D.G., et al., Initial Reports of the Deep Sea Drilling Project, v. 64: Washington, D.C., U.S. Government Printing Office, p. 675 - 694.

Given, R.K., and Wilkinson, B.H., 1987, Dolomite abundance and stratigraphic age: constraints on rates and mechanisms of Phanerozoic dolostone formation: Journal of Sedimentary Petrology, v. 57, p. 1060 - 1078.

Ginsburg, R.N., ed., 1975, Tidal deposits: Springer Verlag, New York, 428 pp.

Ghosh, S.K., and Friedman, G.M., 1989, Petrophysics of a dolostone reservoir: San Andres Formation (Permian) of West Texas: Carbonates and Evaporites, V. 4, p. 45 - 119.

Gosh, S.K., Urschel, S.F., and Friedman, G.M., 1987, Substitution of simulated well-cuttings for core plugs in the petrophysical analysis of dolostones: Permian San Andres Formation, Texas: Carbonates and Evaporites, v.2, p. 95 - 100.

Good, R.J. and Mikhail, R.S., 1981, The contact angle in mercury intrusion porosimetry: Powder Technology, v. 29, p. 53 - 62.

Gregg, J.M., 1985, Regional epigenetic dolomitization in the Bonneterre dolomite (Cambrian), southeastern Missouri: Geology, v. 13, p. 503 - 506.

Gregg, J.M., 1988, Origins of dolomite in the offshore of the Bonneterre Formation (Cambrian), southeast Missouri, *in* Shukla, V. & Baker, P.A., eds., Sedimentology and Geochemistry of Dolostones: Society Economic Paleontologists Mineralogists Special Publication, No. 43, p. 67 - 83.

Gregg, J.M., and Sibley, D.F., 1984, Epigenetic dolomitization and the origin of xenotopic dolomite texture: Journal of Sedimentary Petrology, v. 54, p. 908 - 931.

Gregg, J.M., and Shelton, K.L., 1989, Minor- and trace-element distributions in the Bonneterre dolomite (Cambrian), Southeast Missouri: Evidence for possible multiple-basin fluid sources and pathways during lead-zinc mineralization: Geological Society America Bulletin, v. 101, p. 221 - 230.

Grover, G., JR., and Read, J.F., 1983, Paleoaquifer and deep-burial related cements defined by regional cathodoluminescent patterns, Middle Ordovician carbonates, Virginia: American Association Petroleum Geologists Bulletin, v. 67, p. 1275 - 1303.

Hallam, A., 1981, Facies interpretation and the stratigraphic record: Freeman & Co. Ltd., 291 pp.

Hanor, J.S., 1979, The sedimentary genesis of hydrothermal fluids, in Barnes, H.L., ed., Geochemistry of hydrothermal ore deposits: Wiley - Interscciences, New York, p. 137 - 142.

Hanor, J.S., 1987, Origin and migration of subsurface sedimentary brines: Society of Economic Paleontologists and Mineralogists Short Course, No. 21, 247 pp.

Hardie, L.A., 1987, Dolomitization: a critical view of some current views: Journal of Sedimentary Petrology, v. 57, p. 166 - 183.

Hendricks, L., 1940, Subsurface divisions of the Ellenburger Formation in north-central Texas: University of Texas, Austin, Publication 3945, p. 923 - 968.

Hendricks, L., 1952, Correlation between surface and subsurface sections of the Ellenbruger Group of Texas: University of Texas, Austin, Bureau of Economic Geology, Report of Investigations No. 11, 44 pp.

Hill, W.T., Morris, R.G., and Hagegeorge, C.G., 1971, Ore controls and related sedimentary features at the Flat gap Mine, Treadway, Tennessee: Economic Geology., v. 71, p. 748 - 756.

Hills, J.M., 1972, Late Paleozoic sedimentation in West Texas Permian basin: American Association Petroleum Geologists Bulletin, v. 56, p. 2303 - 2322.

Hills, J.M., 1984, Sedimentation, tectonism, and hydrocarbon generation in Delaware basin, West Texas and southeastern New Mexico: American Association Petroleum Geologists Bulletin, v. 68, p. 250 - 267.

Holmquest, H.J., 1965, Deep pays in Delaware and Val Verde basins, *in* Young, A., and Galley, J.E., eds., Fluids in subsurface environments: American Association Petroleum Geologists Memoir 4, p. 257 - 279.

Horak, R.L., 1985, Trans-Pecos tectonism and its effect on the Permian Basin, *in* Dickerson, P.W., and Muehlberger, W.R., eds., Structure and Tectonism of Trans-Pecos Texas: West Texas Geological Society Publication 85 - 81, p. 81 - 87.

Hutcheon, I., and Oldershaw, A., 1985, The effect of hydrothermal reactions on the petrophysical properties of carbonate rocks: Bulletin of Canadian Petroleum Geology, v. 33, p. 359 - 377.

Ijirigho, B.T., 1981, Secondary porosity and hydrocarbon production from the Ordovician Ellenburger Group of the Delaware and Val Verde basins, West Texas: Unpublished Ph.D. Thesis, University of Arizona, 150 pp.

Ijirigho, B.T., 1985, Source, migration and distribution of hydrocarbon in carbonate rocks - A case study from the Ordovician Ellenburger Group, West Texas: Nigerian Journal of Mining and Geology, v. 21, p. 109 - 115.

Ijirigho, B.T., 1989, Tectono-structural development and hydrocarbon distribution in fractured carbonate reservoirs, Permian Basin, West Texas, *in* Cunningham, B.K., and Cromwell, D.W., eds., The Lower Paleozoic of West Texas and Southern New Mexico - Modern Exploration concepts: Permian Basin Section Society Economic Paleontologists and Mineralogists Publication No. 89 - 31, p. 159 - 168.

Ijirigho, B.T. and Schreiber, J.F., Jr., 1986, Origin and classification of fractures and related breccia in the Lower Ordovician Ellenburger Group, West Texas: West Texas Geological Society Bulletin, v. 26, p. 9 - 15.

Ijirigho, B.T., and Schreiber, J.F., 1988, Composite classification of fractured and brecciated carbonate rocks - examples from the Ordovician Ellenburger Group, West Texas: Journal of Petroleum Geology, v. 11, p. 193 - 204.

James, N.P., 1984, Shallowing-upward sequences in carbonates, *in* Walker, R.G., ed., Facies models: Geoscience Canada, p. 162 - 179.

James, N.P., and Choquette, P.W., 1984, Diagenesis 9 - Limestones The meteoric diagenetic environment: Geoscience Canada, v. 11, p. 161 - 194.

Jarosewich, E., and McIntyre, I.G., 1983, Carbonate reference samples for electron microprobe and scanning electron microscope analyses: Journal of Sedimentary Petrology, v. 53, p. 677 - 678.

Jennings, J.B., 1987, Capillary pressure techniques: application to exploration and development geology: American Association Petroleum Geologists Bulletin, v. 71, p. 1196 - 1209.

Kerans, C., 1988 a, Karst-controlled reservoir heterogeneity in Ellenburger Group carbonates of West Texas: American Association Petroleum Geologists Bulletin, v. 72, p. 1160 - 1183.

Kerans, C., 1988 b, Origin of reservoir compartmentalization in Lower Ordovician karstic dolostones, Ellenburger Group, West Texas (abs.): American Association Petroleum Geologists Bulletin, v. 72, p. 205.

Kerans, C., and Lucia, F.J., 1989, Recognition of second, third and fourth/fifth order scale of cyclicity in the El Paso Group and their relationship to genesis and architecture of Ellenburger reservoirs, *in* Cunningham, B.K., and Cromwell, D.W., eds., The Lower Paleozoic of West Texas and Southern New Mexico - Modern Exploration concepts: Permian Basin Section Society Economic Paleontologists and Mineralogists Publication No. 89 - 31, p. 105 - 110.

Kerans, C., Holt, M.H. and Tyler, N., 1989, Contrasting styles of reservoir heterogeneity in Ellenburger Group carbonates, West Texas (abs.), *in* Cunningham, B.K. and Cromwell, D.W., eds., The Lower Paleozoic of West Texas and Southern New Mexico - Modern exploration concepts: Permian Basin Section Society Economic Paleontologists and Mineralogists, Publication No. 89 - 31, p. 131.

King, P.B., 1975, Ancient southern margin of North America: Geology, v. 3, p. 132 - 134.

Kinsman, D.J.J., 1969, Interpretation of Sr^{2+} concentrations in carbonate minerals and rocks: Journal of Sedimentary Petrology, v. 39, p. 486 - 508.

Kluth, C.F., and Coney, P.J., 1981, Plate tectonics of the ancestral Rocky Mountains: Geology, v. 9, p. 10 - 15.

Kopaska-Merkel, D.C., 1988, New applications in the study of porous media: determinations of pore-system characteristics on small fragments (part 1): Northeastern Environmental Science, v. 7, p. 127 - 142.

Kopaska-Merkel, D.C. and Amthor, J.E., 1988, Very high-pressure mercury porosimetry as a tool in reservoir characterization: Carbonates and Evaporites, v. 3, 53 - 63.

Kopaska-Merkel, D.C., and Friedman, G.M., 1989, Petrofacies analysis of carbonate rocks: examples from the Lower Paleozoic Hunton Group of Oklahoma and Texas: American Association Petroleum Geologists Bulletin, v. 11, p. 1289 - 1306.

Kopaska-Merkel, D.C., Amthor, J.E., and Friedman, G.M., 1987, Notes on the use of a mercury porosimeter (Micromeritics Pore Sizer 9305), Northeastern Science Foundation Technical Report No. 1. Troy, Northeastern Science Foundation, 12 pp.

Krause, F.F., Collins, H.N., Nelson, D.A., Machemer, S.D. & French, P.R., 1987, Multiscale anatomy of a reservoir: Geological characterization of Pembina-Cardium Pool, West-Central Alberta, Canada: American Association Petroleum Geologists Bulletin, v. 71, p. 1233-1260.

Kupecz, J.A., 1989, Petrophysical and geochemical characterization of the Lower Ordovician Ellenburger Group, West Texas: Unpublished Ph.D. Dissertation, The University of Texas at Austin, 158 pp.

Kupecz, J.A., and Kerans, C., 1987, Regionally extensive late dolomitization within the Lower Ordovician Ellenburger Group, West Texas: Society Economic Paleontologists Mineralogists Annual MidYear Meeting Abstracts, p. 45.

Kupecz, J.A., and Land, L.S., 1989, Late-stage Ellenburger Group dolomite: an example of rock-water interaction associated with regional tectonics: Geological Society America Abstracts with Programs, v. 21, p. 219.

Kupecz, J.A., Kerans, C., and Land, L.S., 1988, Deep-burial dolomitization in the Ellenburger Group carbonates, West Texas and southeastern New Mexico: Discussion: Journal of Sedimentary Petrology, v. 58, p. 908 - 910.

Kvenvolden, K.A., and Squires, R.M., 1967, Carbon isotopic composition of crude oils from Ellenburger Group (Lower Ordovician) Permian Basin, West Texas, and eastern New Mexico: American Association Petroleum Geologists Bulletin, v. 51, p. 1293 - 1303.

Kyle, J.R., 1983, Economic aspects of subaerial carbonates, *in* Scholle, P.A., Bebout, D.G., and Moore, C.H., eds., Carbonate depositional environments: American Association Petroleum Geologists Memoir 32, p. 73 - 92.

Kyle, J.R., 1976, Brecciation, alteration, and mineralization in the Central Tennessee Zinc district: Economic Geology, v.71, p. 892 - 903.

Land, L.S., 1980, The isotope and trace - element geochemistry of dolomite: the state of the art, in Zenger, D.H., Dunham, J.B., and Ethington, R.L., eds., Concepts and models of dolomitization: Society of Economic Paleontologists and Mineralogists Special Publication, v. 28, p. 87 - 110.

Land, L.S., 1983, Dolomitization: American Association Petroleum Geologists Education Course Note Series, No. 24, 20 pp.

Land, L.S., 1985, The origin of massive dolomites: Journal of Geological Education, v. 33, p. 112 - 125.

Land, L.S., and Prezbindowski, D.R., 1985, Chemical constraints and origins of four groups of Gulf Coast reservoir fluids: discussion: American Association Petroleum Geologists Bulletin, v. 69, p. 119 - 126.

Larson. R.G., and Morrow, N.R., 1981, Effects of sample size on capillary pressures in porous media: *Powder Technology*, v. 30, p. 123 - 138.

Leach, D.L., and Rowan, E.L., 1986, Genetic link between Ouachita fold-belt tectonism and the Mississippi Valley-type lead-zinc deposits of the Ozarks: Geology, v. 14, p. 931 - 935.

Lee, Y.I., and Friedman, G.M., 1987, Deep-burial dolomitization in the Lower Ordovician Ellenburger Group carbonates in West Texas and southeastern New Mexico: Journal of Sedimentary Petrology, v. 57, p. 544 - 557.

Lee, Y.I., and Friedman, G.M., 1988, Deep-burial dolomitization in the Lower Ordovician Ellenburger Group carbonates in West Texas and southeastern New Mexico - Reply: Journal of Sedimentary Petrology, v. 58, p. 910 - 913.

LeMone, D.V., 1988, Early Ordovician El Paso Group of the southern Franklin Mountains, El Paso County, Texas, *in* Franklin Mountains, Tobosa Basin related sequences: El Paso Geological Society and American Association Petroleum Geologists Southwest Section, p. 59 - 74.

Lippmann, F., 1973, Sedimentary carbonate minerals: Springer Verlag, New York, 219 pp.

Li Yu (Y. Li) and Wardlaw, N.C., 1986, The influence of wettability and critical pore-throat size ratio on snap-off: Journal Colloid and Interface Science, v. 109, p. 461 - 472.

Lloyd, R.M., Perkins, R.D., and Kerr, S.D., 1987, Beach and shoreface ooid deposition on shallow interior banks, Turks and Caicos Islands, British West Indies: Journal of Sedimentary Petrology, v. 57, p. 976 - 982.

Lohmann, K.C., 1988, Geochemical patterns of meteoric diagenetic systems and their application to studies of paleokarst, *in* James, N.P., and Choquette, P.W., eds., Paleokarst: Springer Verlag, p. 58 - 80.

Loucks, R.G. and Anderson, J.H., 1980, Depositional facies and porosity development in Lower Ordovician Ellenburger Dolomite, Puckett Field, Pecos County, Texas, *in* Halley, R.B., and Loucks, R.G., eds., Carbonate reservoir rocks: Society Economic Paleontologists Mineralogists Core Workshop No. 1, p. 1 - 31.

Loucks, R.G., and Anderson, J.H., 1985, Depositional facies, diagenetic terranes, and porosity development in Lower Ordovician Ellenburger Dolomite, Puckett Field, West Texas, *in* Roehl, P.O. and Choquette, P.W., eds., Carbonate petroleum reservoirs: Springer-Verlag, New York, p. 1 - 19.

Lucia, F.J., 1968, Sedimentation and paleogeography of the El Paso Group, *in* Stewart, W.J., ed., Delaware Basin exploration: West Texas Geological Society Guidebook 68 - 55, p. 61 - 75.

Lucia, F.J., 1970, Lower Paleozoic history of the western Diablo platform of West Texas and South-Central Mexico, *in* Seewald, K., and Sundeen, D., eds., The geologic framework of the Chihuahua tectonic belt: West Texas Geological Society Field Trip Guidebook, p. 39 - 56.

Lucia, F.J., 1988, Lower Paleozoic collapse brecciation and dolomitization, Franklin Mountains, Texas, *in* Franklin Mountains, Tobosa basin related sequences: El Paso Geological Society and Southwest Section American Association Petroleum Geologists Guidebook, p. 75 - 113.

Lumsden, D.N., and Chimahausky, J.S., 1980, Relationship between dolomite stoichiometry and carbonate-facies parameters, *in* Zenger, D.H., Dunham, J.B., and Ethington, R.L., eds., Concepts and models of dolomitization: Society of Economic Paleontologists and Mineralogists Special Publication 28, p. 123 - 138.

Machel, H. -G., 1988, Fluid - flow direction during dolomite formation as deduced from trace - element trends, *in* Shukla, V., and Baker, P.A., eds., Sedimentology and Geochemistry of Dolostones: Society of Economic Paleontologists and Mineralogists Special Publication, No.. 43, p. 115 - 125.

Machel, H.-G., 1985, Cathodoluminescence in calcite and dolomite and its chemical interpretation: Geoscience Canada, v. 12, p. 139 - 147.

Machel, H.-G., 1987, Saddle dolomite as a by-product of chemical compaction and thermochemical sulfate reduction: Geology, v.15, p. 936 - 940.

Machel, H.-G., and Mountjoy, E.W., 1986, Chemistry and environments of dolomitization: Earth Science Reviews, v. 23, p. 175 - 222.

Machel, H.- G., and Anderson, J.H., 1989, Pervasive subsurface dolomitization of the Nisku Formation of central Alberta: Journal of Sedimentary Petrology, v. 59, p. 891 - 911.

Maliva, R.G., and Siever, R., 1988, Diagenetic replacement controlled by force of crystallization: Geology, v. 16, p. 688 - 691.

Matter, A., 1967, Tidal-flat deposits in the Ordovician of Western Maryland: Journal of Sedimentary Petrology, v. 37, p. 601 - 609.

Mattes, B.W., and Mountjoy, E.W., 1980, Burial dolomitization of the Upper Devonian Miette build-up, Jasper National Park, Alberta, *in* Zenger, D.H., Dunham, J.B., and Ethington, R.L., eds., Concepts and models of dolomitization: Society of Economic and Paleontologists Mineralogists Special Publication 28, p. 259 - 297.

Mazzullo, S.J., 1986, Mississippi Valley - type sulfides in Lower Permian dolomites, Delaware Basin, Texas: implications for basin evolution: American Association Petroleum Geologists Bulletin, v. 70, p. 943 - 952.

Mazzullo, S.J., 1989, Formation and zonal subdivision of the Ellenburger Group (Lower Ordovician), southern Midland Basin, Texas, *in* Cunningham, B.K., and Cromwell, D.W., eds., The Lower Paleozoic of West Texas and Southern New Mexico - Modern Exploration concepts: Permian Basin Section Society Economic Paleontologists and Mineralogists Publication No. 89 - 31, p. 113 - 121.

Mazzullo, S.J., and Gregg, J.M., 1989, Mississippi Valley - type sulfide mineralization and relationships to carbonate diagenesis: Introductory remarks: Carbonates and Evaporites, v. 4, p. 1 - 5.

Mazzullo, S.J., and Harris, P.M., 1989, Porosity formation in the deep-burial environment: a review, with examples, from Permian Basin: American Association Petroleum Geologists Bulletin, v. 73, p. 388.

Mear, C.E., 1989, Ellenburger reservoir development at Midland Farms and Inez fields, Andrews County, Texas, *in* Cunningham, B.K., and Cromwell, D.W., eds., The Lower Paleozoic of West Texas and Southern New Mexico - Modern Exploration concepts: Permian Basin Section Society Economic Paleontologists and Mineralogists Publication No. 89-31, p. 169 - 174.

Micromeritics Instrument Corp., 1983, Instrument manual, Pore Sizer 9305. 1 Micromeritics Drive, Norcross, GA 30 093 USA , (404) 662-3666.

Montanez, I.P., and Read, J.F., 1989, Trace - element and isotope evidence for water - rock interaction during regional dolomitization of Lower Ordovician, Upper Knox carbonates: Geological Society America Abstracts with Programs, v. 21, p. 219.

Moore, C.H., 1985, Upper Jurassic subsurface cements: A case history, *in* Schneidermann, N., and Harris, P.M., eds., Carbonate cements: Society Economic Paleontologists Mineralogists Special Publication, No. 36, p. 291 - 308.

Moore, J., 1982, Stateline, *in* Selected Oil and Gas Fields in West Texas, West Texas Geological Society Publication No. 82 - 75, p. 597 - 600.

Morrow, D.W., 1982 a, Diagenesis I. Dolomite - part I: The chemistry of dolomitization and dolomite precipitation: Geoscience Canada, v. 9, p. 5 - 13.

Morrow, D.W., 1982 b, Diagenesis II. Dolomite - part II: Dolomitization models and ancient dolostones: Geoscience Canada, v. 9, p. 95 - 107.

Morrow, D.W., and Ricketts, B.D., 1988, Experimental investigation of sulfate inhibition of dolomite and its mineral analogues, *in* Shukla, V., and Baker, P.A., eds., Sedimentology and Geochemistry of Dolostones: Society of Economic Paleontologists and Mineralogists Special Publication, No.. 43, p. 25 - 38.

Morton, J.P., 1985, Rb-Sr dating of diagenesis and source age of clays in Upper Devonian black shales of Texas: Geological Society America Bulletin, v. 96, p. 1043 - 1049.

Murray, R.C., and Lucia, F.J., 1967, Cause and control of dolomite distribution by rock selectivity: Geological Society America Bulletin, v. 78, p. 21 - 35.

Mussman, W.J., and Read, J.F., 1986, Sedimentology and development of a passive-to-convergent margin unconformity - Middle Ordovician Knox unconformity, Virginia Appalachians: Geological Society America Bulletin, v. 98, p. 282 - 295.

Mussman, W.J., Montanez, I.P., and Read, J.F., 1988, Ordovician Knox paleokarst unconformity, Appalachians, *in* James, N.P., and Choquette, P.W., eds., Paleokarst: Springer Verlag, p. 211 - 228.

Nicholas, R.L. and Rozendal, R.A., 1975, Subsurface positive elements within the Ouachita foldbelt in Texas and their relation to Paleozoic cratonic margin: American Association Petroleum Geologists Bulletin, v.59, p. 193 - 216.

Neustaedter, R.H., 1968, Log evaluation of deep Ellenburger gas zones: Society Petroleum Engineers of AIME, Reprint No. SPE, 2071, 7 pp.

Ohle, E.L., 1959, Some considerations in determining the origin of ore deposits of the Mississippi-Valley type: Economic Geology, v. 54, p. 769 - 789.

Ohle, E.L., 1980, Some considerations in determining the origin of ore deposits of the Mississippi Valley - type - Part II: Economic Geology, v. 75, p. 161 - 172.

Ohle, E.L., 1985, Breccias in Mississippi Valley - type deposits: Economic Geology, v. 80, p. 1736 - 1752.

Oliver, J., 1986, Fluids expelled tectonically from orogenic belts: Their role in hydrocarbon migration and other phenomena: Geology, v. 14, p. 99 - 102.

Paipe, S., 1911, Mineral resources of the Llano - Burnet region, Texas, with an account of the pre-Cambrian geology: U.S. Geological Survey Bulletin, 450, 103 pp.

Pierson, B.J., 1981, The control of cathodoluminescence in dolomite by iron and manganese: Sedimentology, v. 28, p. 601 - 610.

Pingitore, N.E., Jr., 1982, The role of diffusion during carbonate diagenesis: Journal of Sedimentary Petrology, v. 52, p. 27 - 39.

Purcell, W.R., 1949, Capillary-pressures - their measurement using mercury and the calculation of permeability therefrom: Petroleum Transactions, American Institute of Mining, Metallurgical, and Petroleum Engineers, v. 186, p. 39 - 48.

Radke, B.M., and Mathis, R.L., 1980, On the formation and occurrence of saddle dolomite: Journal of Sedimentary Petrology, v. 50, p. 1149 - 1168.

Reeder, R.J., and Prosky, J.L., 1986, Compositional sector zoning in dolomite: Journal of Sedimetary Petrology, v. 56, p. 237 - 247.

Reeder, R.J., and Paquette, J., 1989, Sector zoning in natural and synthetic calcites, *in* Sellwood, B.W., ed., Zoned carbonate cements: techniques, applications and implications: Sedimentary Geology, v. 65, p. 239 - 247.

Rhodes, D.A., Lantos, E.A., Lantos, J.A., Webb, R.J., and Owens, D.C., 1984, Pine Point orebodies and their relationship to the stratigraphy, structure, dolomitization and karstification of the Middle Devonian barrier complex: Economic Geology, v. 79, p. 991 - 1055.

Richter, D.K., and Zinkernagel, U., 1981, Zur Anwendung der Kathodenlumineszenz in der Karbonatpetrographie: Geologische Rundschau, v. 70, p. 1276 - 1302.

Roehl, P.O., 1967, Stony Mountain (Ordovician) and Interlake (Silurian) facies analogs of Recent low-energy marine and subaerial carbonates, Bahamas: American Association Petroleum Geologists Bulletin, v. 51, p. 1079 - 2032.

Ross, R.J., Jr., 1976, Ordovician sedimentation in the western United States, *in* Bassett, M.G., ed., The Ordovician system: Paleontological Association Symposium Proceedings, P. 73 - 105.

Royse, C.F., Waddell, J.S., and Peterson, L.E., 1971, X- ray determination of calcite - dolomite: an evaluation: Journal of Sedimentary Petrology, v. 41, p. 483 - 488.

Ruppel, S.C., and Cander, H.S., 1988, Dolomitization of shallow - water platform carbonates by seawater and seawater - derived brines: San Andres Formation (Guadalupian), West Texas, *in* Shukla, V., and Baker, P.A., eds., Sedimentology and Geochemistry of Dolostones: Society of Economic Paleontologists and Mineralogists Special Publication, No.. 43, p. 245 - 262.

Sangster, D.F., 1988, Breccia - hosted lead - zinc deposits in carbonate rocks, *in* James, N.P., and Choquette, P.W., eds., Paleokarst: New York, Springer Verlag, p. 102 - 116.

Sarg, J.F., 1988, Carbonate sequence stratigraphy, *in* Wilgus, C.K., Hastings, B.S, Kendall, C.G.St.C., Posamentier, H.W., Ross, C.A., and Van Wagoner, J.C., eds., Sea - level changes: an integrated approach: Society of Economic Paleontologists and Mineralogists special Publication, No. 42, p. 155 - 181.

Sass, E., and Katz, A., 1982, The origin of platform dolomites: American Journal of Science, v. 282, p. 1184 - 1213.

Schofield, K., 1984, Are pressure solution, neomorphism and dolomitisation genetically related?, *in* Stylolites and associated phenomena - relevance to hydrocarbon reservoirs: Abu Dhabi National Reservoir Research Foundation, Special Publication, p. 183 - 201.

Schowalter, T.T., 1979, Mechanisms of secondary hydrocarbon migration and entrapment: American Association Petroleum Geologists Bulletin, v. 63, p. 723 - 760.

Sepkoski, J.J., JR., 1982, Flat-pebble conglomerates, storm deposits and the Cambrian bottom fauna, *in* Einsele, G., and Seilacher, A., eds., Cyclic and event stratification: Springer Verlag Berlin, Heidelberg, p. 371 - 385.

Shinn, E.A., 1983, Tidal flat environments, *in* Scholle, P.A., Bebout, D.G., and Moore, C.H., eds., Carbonate depositional environments: American Association Petroleum Geologists Memoir 33, p. 172 - 210.

Shukla, V., 1988, Sedimentology and geochemistry of a regional dolostone: correlation of trace elements with dolomite fabrics, *in* Shukla, V., and Baker, P.A., eds., Sedimentology and geochemistry of dolostones: Society Economic Mineralogists Paleontologists Special Publication 43, p. 145 - 157.

Shukla, V., 1986, Epigenetic dolomitization and the origin of xenotopic dolomite textures: Discussion: Journal of Sedimentary Petrology, v. 56, p. 733 - 736.

Sibley, D.F., 1982, The origin of common dolomite fabrics, clues from the Pliocene: Journal of Sedimentary Petrology, v. 52, p. 1087 - 1100.

Sibley, D.F. and Gregg, J.M., 1987, Classification of dolomite rock textures: Journal of Sedimentary Petrology, v. 57, p. 967 - 975.

Sibley, D.F., Dedoes, R.E., and Bartlett, T.R., 1987, Kinetics of dolomitization: Geology, v. 15, p. 1112 - 1114.

Sloss, L.L., 1963, Sequences in the cratonic interior of North America: Geological Society America Bulletin, v. 74, p. 93 - 114.

Smith, D.A., 1966, Theoretical considerations of sealing and non-sealing faults: American Association Petroleum Geologists Bulletin, v. 50, p. 363 - 374.

Smith, G.E., 1981, Episodic introduction of Pennsylvanian-age mineralization into Cambrian sediments, Hog Thief Bend, Central Texas: Geological Society America Abstracts with Programs, v. 13, p. 556.

Smith, G.W., 1979, Ellenburger Group, Delaware Basin, West Texas (abs.): American Association Petroleum Geologists Bulletin, v. 63, p. 530.

Sperber, C.M., Wilkinson, B.H., and Peacor, D.R., 1984, Rock composition, dolomite stoichiometry, and rock/water reactions in dolomitic carbonates: Journal of Geology, v. 92, p. 609 - 622.

Spry, A., 1969, Metamorphic textures: Oxford, Pergamon Press, 350 pp.

Stepanek, B.E., 1988, Dolomitization of paleokarst collapse breccias - The Ordovician El Paso Group, Franklin Mountains, West Texas, *in* Franklin Mountains, Tobosa basin related sequences: El Paso Geological Society and Southwest Section American Association Petroleum Geologists Guidebook, p. 114 - 141.

Stewart, W.J., 1983, Delaware basin, column 19, *in* Childs, O.E., Steele, G., and Salvador, A., project. directors, Southwest/Southwest Mid-Continent region: American Association Petroleum Geologists Bulletin Correlation of Stratigraphic Units of North America (COSUNA) Project. 1 sheet.

Stout, J.L., 1964, Pore geometry as related to carbonate stratigraphic traps: American Association Petroleum Geologists Bulletin, v. 48, p. 329 - 337.

Sverjenski, D.A., 1986, Genesis of Mississippi Valley - type lead - zinc deposits: Annual Reviews Earth and Planetary Science Letters, v. 14, p. 177 - 199.

Taylor, T.R., and Sibley, D.F., 1986, Petrographic and geochemical characteristics of dolomite types and the origin of ferroan dolomite in the Trenton Formation, Ordovician, Michigan Basin: Sedimentology, v. 33, p. 61 - 86.

Thomas,, W.A., 1983, Continental margins, orogenic belts and intracratonic structures: Geology, v. 11, p. 270 - 272.

Tobin, R.C., 1985, Reservoir development in Ellenburger Group of West Texas: West Texas Geological Society Bulletin, v. 25, p. 21.

Toomey, D.F., 1970, An unhurried look at the Lower Ordovician mound horizon, southern Franklin Mountains, West Texas: Journal of Sedimentary Petrology, v. 46, p. 1318 - 1334.

Umphress, A.M., 1977, Lithostratigraphic zonation of the Ellenburger Group within the Belco Hickman No. 13 well, Barnhart Field, Reagan Uplift, Texas: Unpublished M.S. thesis, University of Texas at Arlington, 156 pp.

Van Brakel, J., Modry, S. and Svata, M., 1981, Mercury porosimetry: the state of the art: Powder Technology, v. 29, p. 1 - 12.

Veizer, J., 1978, Simulation of limestone diagenesis - a model based on strontium depletion: Discussion: Canadian Journal of Earth Sciences, v. 15, p. 1683 - 1685.

Veizer, J., 1983 a Chemical diagenesis of carbonates: Theory and application of trace element technique, *in* Stable isotopes in sedimentary petrology: Society of Economic Paleontologists and Mineralogists Short Course No. 10, p. 3-1 - 3-100.

Veizer, J., 1983 b, Trace elements and isotopes in sedimentary carbonates: Reviews in Mineralogy, v. 11, p. 265 - 300.

Verseput, T.D., 1989, Depositional setting of the Ellenburger-Langley field, Lea County, New Mexico, *in* Cunningham, B.K., and Cromwell, D.W., eds., The Lower Paleozoic of West Texas and Southern New Mexico - Modern Exploration concepts: Permian Basin Section Society Economic Paleontologists and Mineralogists Publication No. 89 - 31, p. 145 - 157.

Voss, R.L., Hagni, R.D., and Gregg, J.M., 1989, Sequential deposition of zoned dolomite and its relationship to sulfide mineral paragenetic sequence in the Viburnum trend, southest Missouri: Carbonates and Evaporites, v. 4, p. 195 - 209.

Walkden, G.M., 1974, Paleokarstic surfaces in Upper Visean (Carboniferous) limestones of the Derbyshire Block, England: Journal of Sedimentary Petrology, v. 44, p. 1232 - 1247.

Walper, J.L., 1977, Paleozoic tectonics of the southern margin of North America: Transactions of the Gulf Coast Association of Geological Societies, v. 27, p. 230 - 241.

Waples, D.W., 1980, Time and temperature in petroleum exploration: American Association Petroleum Geologists Bulletin, v. 64, p. 916 - 926.

Wardlaw, N.C., 1976, Pore geometry of carbonate rocks as revealed by pore casts and capillary pressure: American Association Petroleum Geologists Bulletin, v. 60, p. 245 -

257.

Wardlaw, N.C., 1979, Pore systems in carbonate rocks and their influence on hydrocarbon recovery efficiency, *in* Geology of Carbonate Porosity: American Association of Petroleum Geologists Education Course Note Series No. 11, p. E1 - E24.

Wardlaw, N.C., 1980, The effects of pore structure on displacement efficiency in reservoir rocks and in glass micromodels: Society Petroleum Engineers AIME, Symposium on Enhanced Oil Recovery, Tulsa, Preprint SPE 8843, p. 345 - 352.

Wardlaw, N.C. and Taylor, R.P., 1976, Mercury capillary pressure curves and the interpretation of pore structure and capillary behavior in reservoir rocks: Bulletin Canadian Petroleum Geologists, v. 24, p. 225 - 262.

Wardlaw, N.C. and McKellar, M., 1981, Mercury porosimetry and the interpretation of pore geometry in sedimentary rocks and artificial models: Powder Technology, v. 29, p. 127 - 143.

Wardlaw, N.C., McKellar, M., and Yu, Li, 1988, Pore and throat size distribution determined by mercury porosimetry and by direct observation: Carbonates and Evaporites, v. 3, p. 1 - 16.

Weber, K.J., 1986, How heterogeneity affects oil recovery, *in* Lake, L.W., and Carroll, H.B., Jr., eds., Reservoir heterogeneity: Academic Press, p. 487-544.

Wilson, J.L., 1980, A review of carbonate reservoirs, *in* Miall, A.D., ed., Facts and principles of world petroleum occurrence: Canadian Society Petroleum Geologists Memoir 6, p. 95 - 115.

Wright, V.P., 1982, The recognition and interpretation of paleokarst: two examples from the Lower Carboniferous of South Wales: Journal of Sedimentary Petrology, v. 52, p. 83 - 94.

Wuellner, D.E., Lehtonen, L.R., and James, W.C., 1986, Sedimentary-tectonic development of the Marathon and Val Verde basins, West Texas, U.S.A.: a Permo-Carboniferous

migrating foredeep, *in* Allen, P.A., and Homewood, A., eds., Foreland basins: International Association of Sedimentologists, Special Publication No. 8, p. 347 - 368.

Yu, Li and Wardlaw, N.C., 1986, The influence of wettability and critical pore-throat size ratio on snap-off: Journal Colloid and Interface Science, v. 109, p. 461 - 472.

Yu, Li and Wardlaw, N.C., 1986, Mechanisms of nonwetting phase trapping during imbibition at slow rates: Journal Colloid and Interface Science, v. 109, p. 473 - 486.

Yu, Li, Laidlaw, W.G., and Wardlaw, N.C., 1986, Sensitivity of drainage and imbibition to pore structures as revealed by computer simulation of displacement process: Advances Colloid and Interface Science, v. 26, p. 1 - 68.

Zenger, D.H., 1983, Burial dolomite in the Lost Burro Formation (Devonian), east-central California, and the significance of late diagenetic dolomitization: Geology, v. 11, p. 519 - 522.

Zenger, D.H., and Dunham, J.B., 1988, Dolomitization of Siluro-Devonian limestones in a deep core (5350 meters), southeastern New Mexico, *in* Shukla, V. and Baker, P.A., eds., Sedimentology and geochemistry of dolostones: Society of Economic Paleontologists and Mineralogists Special Publication , No. 43, p. 161 - 173.